LBL-13327
SAC-53
UC-70

SWEDISH-AMERICAN COOPERATIVE PROGRAM ON RADIOACTIVE WASTE STORAGE IN MINED CAVERNS IN CRYSTALLINE ROCK

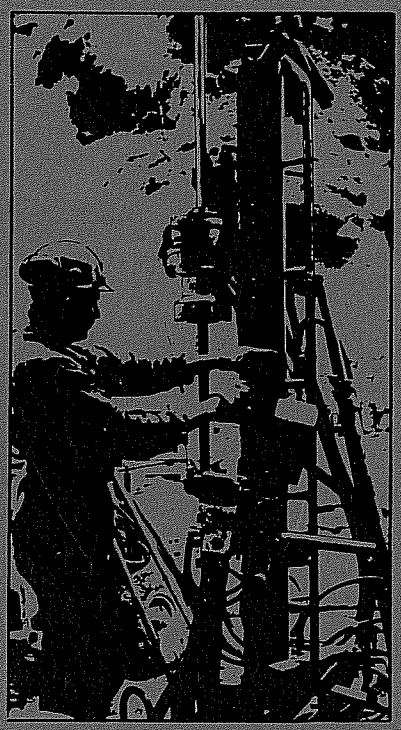

Technical Information Report No. 53

PERFORMANCE OF BOREHOLE DEFORMATION GAUGES AND VIBRATING WIRE STRESSMETERS AT STRIPA

**R. Lingle, P.H. Nelson,
A. DuBois, and H. Sellden**

September 1984

A Joint Project of

Swedish Nuclear Fuel Supply Co.
Fack 10240 Stockholm, Sweden

Operated for the Swedish
Nuclear Power Utility Industry

Lawrence Berkeley Laboratory
Earth Sciences Division
University of California
Berkeley, California 94720, USA

Operated for the U.S. Department of
Energy under Contract DE-AC03-76SF00098

This report was prepared as an account of work sponsored by the United States Government and/or the Swedish Nuclear Fuel Supply Company. Neither the United States nor the U.S. Department of Energy, nor the Swedish Nuclear Fuel Supply Company, nor any of their employees, nor any of their contractors, subcontractors, or their employees, makes any warranty, express or implied or assumes any legal liability or responsibility for the accuracy, completeness or usefulness of any information, apparatus, product or process disclosed, or represents that its use would not infringe privately owned rights.

Printed in the United States of America
Available from
National Technical Information Service
U.S. Department of Commerce
5285 Port Royal Road
Springfield, VA 22161
Price Code: A12

Lawrence Berkeley Laboratory is an equal opportunity employer.

LBL-13327
SAC-53
UC-70

PERFORMANCE OF BOREHOLE DEFORMATION GAUGES AND VIBRATING WIRE STRESSMETERS AT STRIPA

R. Lingle*
Terra Tek, Inc.
400 Wahara Way
Salt Lake City, UT 84108

P.H. Nelson** and A. DuBois
Lawrence Berkeley Laboratory
University of California
Berkeley, California 94720

H. Sellden
Kiruna Mining Company
Kiruna, Sweden

*Presently D&F Consulting
P.O. Box 81211
Salt Lake City, UT 84108

**Presently SOHIO Petroleum Company
100 Pine St.
San Francisco, Ca 94111

September 1984

This work was supported by the Assistant Secretary for Nuclear Energy, Office of Waste Isolation of the U.S. Department of Energy under contract DE-AC03-76SF00098. Funding for this project was administered by the Office of Nuclear Waste Isolation at Battelle Memorial Institute.

PREFACE

This report is one of a series documenting the results of the Swedish-American cooperative research program in which the cooperating scientists explore the geological, geophysical, hydrological, geochemical, and structural effects anticipated from the use of a large crystalline rock mass as a geologic repository for nuclear waste. This program has been sponsored by the Swedish Nuclear Power Utilities through the Swedish Nuclear Fuel Supply Company (SKBF), and the U.S. Department of Energy (DOE) through the Lawrence Berkeley Laboratory.

The principal investigators are L.B. Nilsson and O. Degerman for SKBF, and N.G.W. Cook, P.A. Witherspoon, and J.E. Gale for LBL. Other participants will appear as authors of the individual reports.

Previous technical reports in this series are listed below.

1. Swedish-American Cooperative Program on Radioactive Waste Storage in Mined Caverns by P.A. Witherspoon and O. Degerman. (LBL-7049, SAC-01).

2. Large Scale Permeability Test of the Granite in the Stripa Mine and Thermal Conductivity Test by Lars Lundstrom and Haken Stille. (LBL-7052, SAC-02).

3. The Mechanical Properties of the Stripa Granite by Graham Swan. (LBL-7074, SAC-03).

4. Stress Measurements in the Stripa Granite by Hans Carlsson. (LBL-7078, SAC-04).

5. Borehole Drilling and Related Activities at the Stripa Mine by P.J. Kurfurst, T. Hugo-Persson, and G. Rudolph. (LBL-7080, SAC-05).

6. A Pilot Heater Test in the Stripa Granite by Hans Carlsson. (LBL-7086, SAC-06).

7. An Analysis of Measured Values for the State of Stress in the Earth's Crust by Dennis B. Jamison and Neville G.W. Cook. (LBL-7071, SAC-07).

8. Mining Methods Used in the Underground Tunnels and Test Rooms at Stripa by B. Andersson and P.A. Halen. (LBL-7081, SAC-08).

9. Theoretical Temperature Fields for the Stripa Heater Project by T. Chan, Neville G.W. Cook, and C.F. Tsang. (LBL-7082, SAC-09).

10. Mechanical and Thermal Design Considerations for Radioactive Waste Repositories in Hard Rock. Part I: An Appraisal of Hard Rock for Potential Underground Repositories of Radioactive Waste by N.G.W. Cook; Part II: In Situ Heating Experiments in Hard Rock: Their Objectives and Design by N.G.W. Cook and P.A. Witherspoon. (LBL-7073, SAC-10).

11. Full-Scale and Time-Scale Heating Experiments at Stripa: Preliminary Results by N.G.W. Cook and M. Hood. (LBL-7072, SAC-11).

12. Geochemistry and Isotope Hydrology of Groundwaters in the Stripa Granite: Results and Preliminary Interpretation by P. Fritz, J.F. Barker, and J.E. Gale. (LBL-8285, SAC-12).

13. Electrical Heaters for Thermo-Mechanical Tests at the Stripa Mine by R.H. Burleigh, E.P. Binnall, A.O. DuBois, D.O. Norgren, and A.R. Ortiz. (LBL-7063, SAC-13).

14. Data Acquisition, Handling, and Display for the Heater Experiments at Stripa by Maurice B. McEvoy. (LBL-7063, SAC-14).

15. An Approach to the Fracture Hydrology at Stripa: Preliminary Results by J.E. Gale and P.A. Witherspoon. (LBL-7079, SAC-15).

16. Preliminary Report on Geophysical and Mechanical Borehole Measurements at Stripa by P. Nelson, B. Paulsson, R. Rachiele, L. Andersson, T. Schrauf, W. Hustrulid, O. Duran, and K.A. Magnussen. (LBL-8280, SAC-16).

17. Observations of a Potential Size-Effect in Experimental Determination of the Hydraulic Properties of Fractures by P.A. Witherspoon, C.H. Amick, J.E. Gale, and K. Iwai. (LBL-8571, SAC-17).

18. Rock Mass Characterization for Storage in Nucler Waste in Granite by P.A. Witherspoon, P. Nelson, T. Doe, R. Thorpe, B. Paulsson, J.E. Gale, and C. Forster. (LBL-8570, SAC-18).

19. Fracture Detection in Crystalline Rock Using Ultrasonic Shear Waves by K.H. Waters, S.P. Palmer, and W.F. Farrell. (LBL-7051, SAC-19).

20. Characterization of Discontinuities in the Stripa Granite--Time Scale Heater Experiment by R. Thorpe. (LBL-7083, SAC-20).

21. Geology and Fracture System at Stripa by A. Okliewicz, J.E. Gale, R. Thorpe, and B. Paulsson. (LBL-8907, SAC-21).

22. Calculated Thermally Induced Displacements and Stresses for Heater Experiements at Stripa by T. Chan and N.G.W. Cook. (LBL-7061, SAC-22).

23. Validity of Cubic Law for Fluid Flow in a Deformable Rock Fracture by P.A. Witherspoon, J. Wang, K. Iwai, and J.E. Gale. (LBL-9557, SAC-23).

24. Determination of In-Situ Thermal Properties of Stripa Granite from Temperature Measurements in the Full-Scale Heater Experiments: Methods and Primary Results by J. Jeffry, T. Chan, N.G.W. Cook and P.A. Witherspoon. (LBL-8424, SAC-24).

25. Instrumentation Evaluation, Calibration, and Installation for Heater Tests Simulating Nuclear Waste in Crystalline Rock, Sweden by T. Schrauf, H. Pratt, E. Simonson, W. Hustrulid, P. Nelson, A. DuBois, E. Binnall, and R. Haught. (LBL-8313, SAC-25)

26. Part I: Some Results From a Field Investigation of Thermo-Mechanical Loading of a Rock Mass When Heater Canisters are Emplaced in the Rock by M. Hood. Part II: The Application of Field Data from Heater Experiments Conducted at Stripa, Sweden for Repository Design by M. Hood, H. Carlsson, and P.H. Nelson. (LBL-9392, SAC-26).

27. Progress with Field Investigations at Stripa by P.A. Witherspoon, N.G.W. Cook, and J.E. Gale (LBL-10559, SAC-27).

28. A Laboratory Assessment of the Use of Borehole Pressure Transients to Measure the Permeability of Fractured Rock Masses by C.B. Forster and J.E. Gale. (LBL-8674, SAC-28).

29. Thermal and Thermomechanical Data for In Situ Heater Experiments at Stripa, Sweden by T. Chan, E. Binnall, P. Nelson, O. Wan, C. Weaver, K. Ang, J. Braley, and M. McEvoy. (LBL-11477, SAC-29).

30. The Effect of Radon Transport in Groundwater Upon Gamma Ray Borehole Logs by P.H. Nelson, R. Rachiele, and A. Smith. (LBL-11180, SAC-30).

31. Strength and Permeability Tests on Ultra-Large Stripa Granite Core by R. Thorpe, D.J. Watkins, W.E. Ralph, R. Hsu, and S. Flexser. (LBL-11203, SAC-31).

32. Ultrasonic and Acoustic Emission Results from the Stripa Heater Experiments. Part I: A Cross-Hole Investigation of a Rock Mass Subjected to Heating by B.N.P. Paulsson and M.S. King. Part II: Acoustic Emission Monitoring During Cool-Down of the Stripa Heater Experiment by R. Rachiele. (LBL-10975, SAC-32).

33. Numerical Modeling to Assess Possible Influence of the Mine Openings on Far-Field In Situ Stress Measurements at Stripa by T. Chan, V. Guvanasen, and N. Littlestone (LBL-12469, SAC-33).

34. A Field Assessment of the Use of Borehole Pressure Transients to Measure the Permeability of Fractured Rock Masses by C.B. Forster and J.E. Gale. (LBL-11829, SAC-34).

35. Water Inflow into Boreholes During the Stripa Experiments by P.H. Nelson, R. Rachiele, J.S. Remer and H.S. Carlsson. (LBL-12574, SAC-35).

36. Petrology and Radiogeology of the Stripa Pluton by H. Wollenberg, S. Flexser, and L. Andersson. (LBL-11654, SAC-36).

37. Geohydrological Data from the Macopermeability Experiment at Stripa, Sweden by C.R. Wilson, J.C.S. Long, R.M. Galbraith, K. Karasaki, H.K. Endo, A.O. DuBois, M.J. McPherson, and G. Ramqvist. (LBL-12520, SAC-37).

38. Characterization of Discontinuities in the Stripa Granite--Full-Scale Heater Experiments by B.N.P. Paulsson, P.H. Nelson, and P.J. Kurfurst. (LBL-9063, SAC-38).

39. Application of Borehole Geophysics at an Experimental Waste Storage Site by P.H. Nelson, K.A. Magnusson, and R. Rachiele. (LBL-11982, SAC-39).

40. Laboratory Investigations of Thermomechanical Properties of Stripa Granite by L. Myer and R. Rachiele. (LBL-13435, SAC-40)

41. Petrologic Changes and Damage in the Stripa Quartz Monzonite in Response to Heater Tests by S. Flexser, H. Wollenberg, and D.E. Wedge. (LBL-14929, SAC-41).

42. Fracture Mapping in the Ventilation Drift at Stripa: Procedures and Results by A. Rouleau, J.E. Gale, and J. Baleshta. (LBL-13071, SAC-42).

43. Thermal Analysis of the Stripa Heater Test Data from the Full Scale Drift by I. Javandel and P.A. Witherspoon. (LBL-13217, SAC-43).

44. In Situ Stress Measurements at the Stripa Mine, Sweden by T.W. Doe, K. Ingevald, L. Strindell, B. Leijon, W. Hustrulid, E. Majer, and H. Carlsson. (LBL-15009, SAC-44).

45. Fracture Detection in Crystalline Rock Using Ultrasonic Reflection Techniques by S.P. Palmer. (LBL-16347, SAC-45).

46. Fracture and Hydrology Data from Field Studies at Stripa, Sweden by J.E. Gale. (LBL-13101, SAC-46).

47. Equipment Design, Installation, and Operation for the Macropermeability Experiment at Stripa, Sweden by R.M. Galbraith, C.R. Wilson, A.O. DuBois, S.A. Lundgren, M.J. McPherson and G.W. West. (LBL-13392, SAC-47).

48. Effects of Sample Size on the Stress Permeability Relationship for Natural Fractures by J.E. Gale and K.G. Raven. (LBL-11865, SAC-48).

49. Progress with Hydrogeological Characterization of the Stripa Site by J.E. Gale, A. Rouleau, P.A. Witherspoon and C.R. Wilson. (LBL-14878, SAC-49).

50. Extensometer Performance During Heater Experiments at Stripa by A.O. DuBois, M. Hood, E.P. Binnall and L. Andersson. (LBL-13531, SAC-50).

51. Seismic Velocities and Attenuation in a Heated Underground Granitic Repository by B.N.P. Paulsson (LBL-16346 1/2, SAC-51).

52. Characterization of the Fracture System at Stripa with Emphasis on the Ventilation Drift by A. Rouleau and J. E. Gale. (LBL-14875, SAC-52).

TABLE OF CONTENTS

Page

LIST OF FIGURES ix

LIST OF TABLES xiii

ABSTRACT xv

1. INTRODUCTION 1

1.1 Background 1
1.2 Data Acquisition and Processing 6
1.3 Experience with Gauge Calibration and Operation 8

2. VIBRATING WIRE STRESSMETERS 11

2.1 Response Equation of the VWS 11
2.2 Operating History of Vibrating Wire Stressmeters 16
2.2.1 Calibration and Operation Sequence 16
2.2.2 Gauge Failures 22
2.2.3 Changes in Unloaded Period (R_0) 27
2.2.4 Gaps and Noise in the VWS Data Records 27
2.2.4.1 Noise Due to Instrumentation Problems . . 27
2.2.4.2 Misplacement of Data Due to Gauge Interchange 33
2.2.4.3 Omission of Data at Start of Experiments. 34
2.2.4.4 Reversal of Radial and Tangential Gauges 35
2.3 Calibration of the VWS 35
2.3.1 Calibration Procedures 35
2.3.2 Calibration Facilities 38
2.3.3 VWS Calibration Results 50
2.3.3.1 End-Loaded Cylinder Calibration 50
2.3.3.2 Calibrations in 15-inch Block at Stripa . 53
2.3.3.3 Calibrations at Elevated Temperatures . . 55
2.3.3.4 12-Inch Block Calibrations 58
2.3.3.5 Ambient Temperature Calibration 60
2.3.3.6 Calibrations with Different ΔR Values . . 60
2.3.3.7 Triaxial Load Test 67
2.3.3.8 Calibration at Elevated Temperatures . . . 67
2.3.3.9 Radially-Loaded Cylinder Calibrations . . 70
2.4 Effects of Temperature on Unloaded Gauges 73
2.5 Analysis of VWS Performance 76
2.5.1 Dependence of C_1 on Preload 76
2.5.2 Effect of Loading and Unloading 79
2.5.3 Variation of C_1 with Temperature 83
2.5.4 Variation of R_s with Temperature 85
2.5.5 Evidence for the Seating Effect 85
2.5.6 Dependence of C_1 on Rock Modulus 87

2.5.7 Long-Term Drift in Unloaded Gauge Period 89
2.5.8 Evaluation of C_1 89
2.6 Error Analysis 94
2.7 Summary 99

3. USBM BOREHOLE DEFORMATION GAUGE 101

3.1 Introduction 101
3.2 Calibration 105
3.2.1 Pre- and Post-Experiment Calibrations 106
3.2.2 Change in Calibration Factor vs. Temperature . . . 106
3.3 Operating History 112
3.4 Gauge Repair and Modification 121
2.4.1 Gauge Repairs 121
2.4.2 Gauge Modification 122
3.5 Error Analysis 124
3.5.1 Voltage Reading Errors 125
3.5.2 Errors in Temperature Measurement 126
3.5.3 Calibration Factor Error 126
3.5.4 Error Due to Temperature Effects on Measured Voltage 127
3.5.5 Error Due to Temperature Effects on Calibration Factor 128
3.5.6 Error Due to Uncertainty in Gauge Coefficient of Thermal Expansion 128
3.5.7 Combined Errors 129
3.6 Special Tests 130
3.6.1 Leak Tests 130
3.6.1.1 Test Apparatus. 130
3.2.1.2 Test Procedure. 133
3.6.2 Test to Detemine the Expansion Coefficient of the USBM Gauge 133

4. SAMPLE STRESS CALCULATIONS 147

4.1 Stress Change Calculations from USBM Gauge Measurements . 147
4.2 Stress-Change Calculations from VWS Measurements 148
4.3 Comparison of Stress Data 151

5. SUMMARY AND CONCLUSIONS 157

5.1 Summary 157
5.1.1 Vibrating Wire Stressmeters 157
5.1.2 USBM Gauges 157
5.2 Conclusions 158

6. ACKNOWLEDGMENTS 161

7. REFERENCES 163

APPENDIX A. IRAD GAUGE (VWS) FIELD RECORDS 167

APPENDIX B. USBM GAUGE FIELD RECORDS 205

APPENDIX C. INTERCHANGES OF GAUGES IN BOREHOLES 259

LIST OF FIGURES

		Page
1-1	Plan view of experimental areas 340 m underground at Stripa, showing location of instrument boreholes	2
1-2	Location of virating wire stressmeters in full-scale experimental areas, projected to horizontal surface	3
1-3	Location of USBM borehole deformation gauges	4
2-1	Exploded sectional view of vibrating wire stressmeter	12
2-2	Relationship between gauge calibration factor C_1 and gauge sensitivity factor α	15
2-3	Barre granite data from Hawkes and Bailey	17
2-4	Example of VWS field record	21
2-5	Plot of VWS- failure	24
2-6	End view of gauge-wedge-platen assembly after heater experiment, showing corrosion and pitting	25
2-7	Head of extraction tool mounted on a gauge-wedge-platen assembly	26
2-8	Twenty days of detailed record gauge C6Z	29
2-9	Forty days of detailed record gauge C40	30
2-10	Calibration data and plot for gauge C11Z at 106°C	37
2-11	End-loaded cylinder setup for VWS calibrations	39
2-12	Fifteen-inch block cut in floor of full-scale drift at Stripa	42
2-13	Twelve-inch block of Stripa granite with biaxial loading and heating capabilities	45
2-14	Configuration for triaxial loading of 12-inch block	46
2-15	Radially loaded cylinder calibration setup	49
2-16	Imprints of wedge and gauge seating made with carbon paper on paper	65
2-17	VWS calibrations as function of setting pressure done in thin slab of Climax granite	78

Page

2-18 Distribution of VWS installation period readings at Stripa, plotted on scale proportional to setting pressure 80

2-19 Calibrations done in 12-inch block, plotted against scale proportional to setting pressure 81

2-20 Calculated C_1 and R values from 3 tests on gauge C10Z (3-45) in the 12-inch block 82

2-21 Calibration factor (C_1) as a function of temperature for eight gauges 84

2-22 Change of VWS period R_s with temperature, while hydrostatic confining pressure was held constant on radially loaded cylinder 86

2-23 Dependence of VWS calibration factor on modulus of test medium 88

2-24 Histogram of change in period of unloaded gauges recovered from Stripa heater experiments 90

2-25 Distibution of C_1 values from calibrations in 12-inch and 15-inch blocks 92

2-26 Stress change as function of $1/R^2$ for range of C_1 values . . 96

2-27 Stress-change error due to uncertainty in R_s 98

3-1 USBM borehole deformation gauge 102

3-2 Calibration factor (C_1) as a function of temperature for gauge #405 (6/81) 114

3-3 Calibration factor (C_1) as a function of temperature for gauge #416 (6/81) 114

3-4 Calibration factor (C_1) as a function of temperature for gauge #452 (6/81) 115

3-5 Operating history of USBM gauges 117

3-6a Example of USBM gauge field record (U1) 119

3-6b Example of USBM gauge field record (U2) 120

3-7 USBM gauge modifications. 123

3-8 Uncertainty in borehole deformation measurements as a function of temperature 131

3-9 Schematic showing sectional view of leak test apparatus . . . 132

Page

3-10 Leak test record 134

3-11 Response of components 1 & 3, gauge #428 as leaking occurred 135

3-12 Strain gauge arrangement for stainless steel and aluminum cylinders 139

3-13 Stainless steel cylinder strains as a function of temperature 141

3-14 Aluminum cylinder strains as a function of temperature . . . 142

3-15 Borehole deformation vs. temperature for stainless steel cylinder 143

3-16 Borehole displacement vs. temperature for aluminum cylinder . 144

3-17 Calculated αg from stainless steel and aluminum cylinder test 146

4-1 Comparison of stress change from measurements with predicted results from Chan and Cook (1979) 153

LIST OF TABLES

		Page
1-1	Guide to reports on instrumentation and data acquisition for Stripa heater experiments	5
1-2	Flow chart of data acquisition and processing at Stripa and LBL for USBM and VWS data	7
2-1	History of VWS calibration and usage	18
2-2	Period R_0 of unloaded gauges, measured before and after Stripa heater experiments, and again after return air shipment	28
2-3	Young's modulus of end-loaded cylinder of Stripa granite	41
2-4	Elastic properties measured on cores from the 12-inch block	47
2-5	VWS gauge calibration results in end-loaded cylinder	51
2-6	Calibrations of gauge C10Z (ser. #3-45) at elevated temperature in end-loaded cylinder	52
2-7	Calibration of gauge C10Z in end-loaded steel cylinder, parallel and perpendicular to uniaxial load	54
2-8	Calibration of 26 gauges in 15-inch block at Stripa	56
2-9	Calibrations of VWS gauge $C5_\Theta$ and C5R at elevated temperatures in 15-inch block at Stripa	59
2-10	Calibration of 27 gauges in 12-inch block of Stripa granite at Terra Tek	61
2-11	Calibration of four gauges at different preset values, performed in the 12-inch block	63
2-12	Calibration of two gauges at four preset values, performed in the 12-inch block	66
2-13	Calibration of gauge C11Z in 12-inch block under triaxial load	68
2-14	Calibration of two VWS gauges at different temperatures in the 12-inch block	71
2-15	Calibration of two gauges installed in radially-loaded cylinder at different temperatures	72
2-16	Observed period of two gauges installed in radially-loaded cylinder at different temperatures and constant confining pressure	74

Page

2-17 Measured period of unloaded gauges at room and elevated temperatures 75

2-18 Mean and standard deviation of C_1 for 25 VWSs measured at room temperature 93

3-1 USBM gauge calibrations, H9 107

3-2 USBM gauge calibrations, H10 109

3-3 Comparison of repeat calibration data 112

3-4 USBM gauge calibration factor vs temperature (6/81) 113

3-5 Summary of calibration factors vs temperature 116

3-6 USBM gauge leak test summary 136

3-7 Dimensions of test cylinders used for the gauge thermal expansion measurements 137

3-8 Gauge #405 calibration information 138

4-1 Calculated stress changes in USBM gauges for H9 experiment . . 149

4-2 Calculated stress changes in USBM gauges for H10 experiment . 150

4-3 Stress change calculated from VWS reading from the H9 and H10 experiments 152

4-4 Input data for stress calculations 154

ABSTRACT

Vibrating wire stressmeters and borehole deformation gauges were deployed in two full-scale heater experiments at Stripa to determine the thermally induced stress changes in the rock mass. The heater experiments ran for 18 months, including a six-month cool-down period after the heaters were turned off. During the course of the experiments, vibrating wire stressmeters (VWSs) were installed in a total of 15 boreholes (two per borehole), and borehole deformation (USBM) gauges were installed in 30 boreholes (one per borehole). Gauges were installed in both horizontal and vertical boreholes and were subjected to temperatures ranging from 10°C to 120°C, depending upon the distance of a gauge from the central heater. Most gauges operated in a moist environment because groundwater flowed into many of the instrument boreholes during the experiments.

Of the 36 VWSs installed at Stripa, six failed. The rest operated satisfactorily, although not all were installed for the full experimental period. Failures were attributed to corrosion of the vibrating wire due to moisture entering the gauge body. Despite corrosion of some gauge bodies and wedges, long-term stability was quite good. By contrast, of the 30 borehole deformation gauges installed at the beginning of the experiments, 22 failed, also as the result of water entering the gauge body. Modification and reinstallation of gauges eliminated the problem of water infiltration, but much data from early stages of the experiments were not recorded due to gauge failures, particularly those in vertical boreholes.

Calibration of the VWSs in blocks of Stripa granite showed a lack of repeatability unless extreme care was used in installing the gauge.

Variability in calibration results is attributed to seating effects which are closely coupled to variations in the elastic modulus of the rock and to changes in temperature. These three effects combined to produce an uncertainty judged to be approximately $\pm$ 33% of the stress changes measured at Stripa. On the other hand, the major source of error in determining stress with the USBM gauge appears to be the uncertainty in rock modulus and thermal expansion coefficient. Sample calculations based on data acquired near the end of the experiments yield stress-change values and radial distance dependency of stress which are in reasonable accord with theoretical values.

Off-the-shelf VWSs and USBM gauges installed at Stripa did not function reliably enough to provide good data on stress changes. Further effort is required to provide stress monitoring instrumentation that can function adequately in the environment of a nuclear-waste repository.

1. INTRODUCTION

1.1 Background

Thermomechanical experiments driven by large electrical heaters emplaced in boreholes in an underground granitic site at Stripa, Sweden were completed in late February, 1980. Surrounding the electrical heaters were arrays of thermocouples, rod extensometers, borehole deformation (USBM) gauges, and vibrating wire stressmeters (VWS). The heaters simulated the thermal load imposed on the rock mass by canisters of radioactive waste, while the instrumentation detected the ensuing thermal and mechanical changes in the surrounding rock mass during the 1 1/2-year duration of the experiments.

The experiments were located some 340 m below the surface in drifts, as depicted in Fig. 1-1. The time-scaled experiment is not addressed in this report because USBM gauges and VWSs were installed only in the full-scale experiments. Details on the installations in the full-scale experiments are shown in Figs. 1-2 and 1-3. Each USBM installation produced three outputs in response to borehole diametral changes at 120° intervals. A thermocouple was attached to each gauge to determine the gauge temperature. Each VWS installation consisted of two orthogonally mounted gauges and a thermocouple. The VWSs were oriented vertically and horizontally in horizontal boreholes, and radially and azimuthally to the central heater in vertical boreholes. All gauges were located within $\pm$ one meter vertically from the midplane of the heaters. More information on the installation and a tabulation of gauge coordinates are given by Schrauf et al. (1979).

Table 1-1 lists the reports that deal with various aspects of the instrumentation and data processing. Three reports on the installation of the

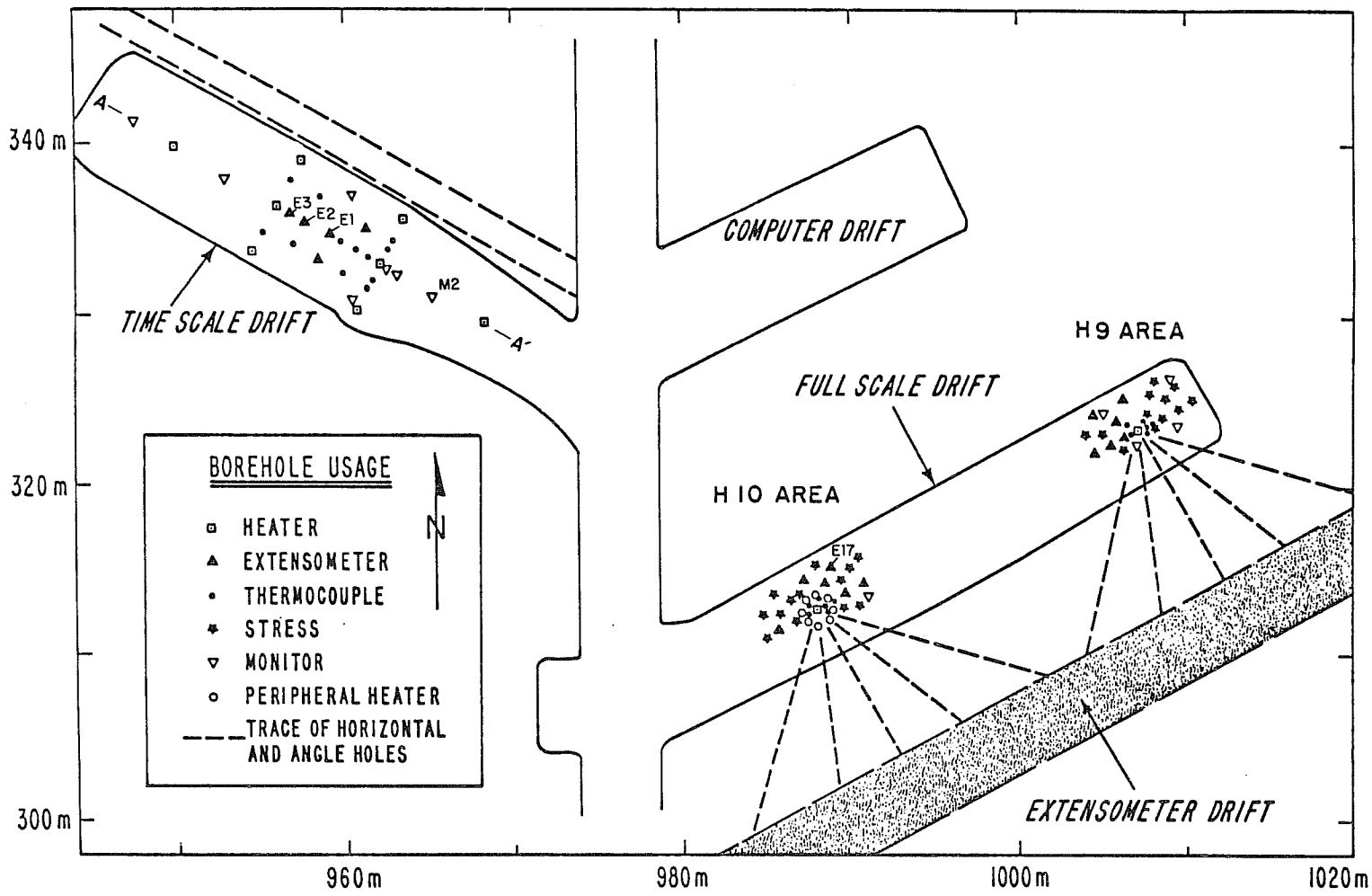

Fig. 1-1. Plan view of experimental areas 340 m underground at Stripa, showing location of instrument boreholes.

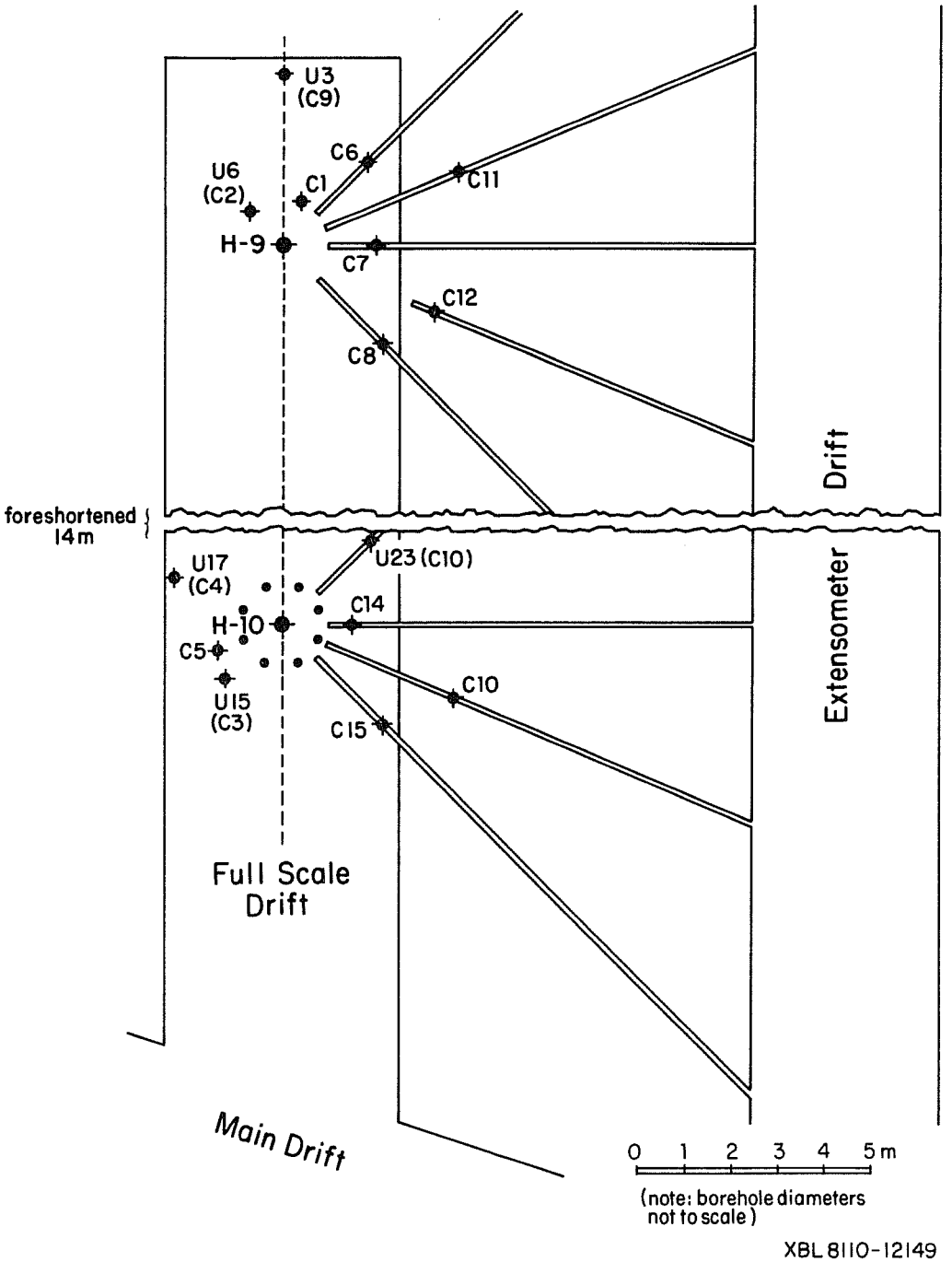

Fig. 1-2. Location of vibrating wire stressmeters in full-scale experimental areas, projected to horizontal surface. Eight dots around the H10 heater hole designate the peripheral heaters.

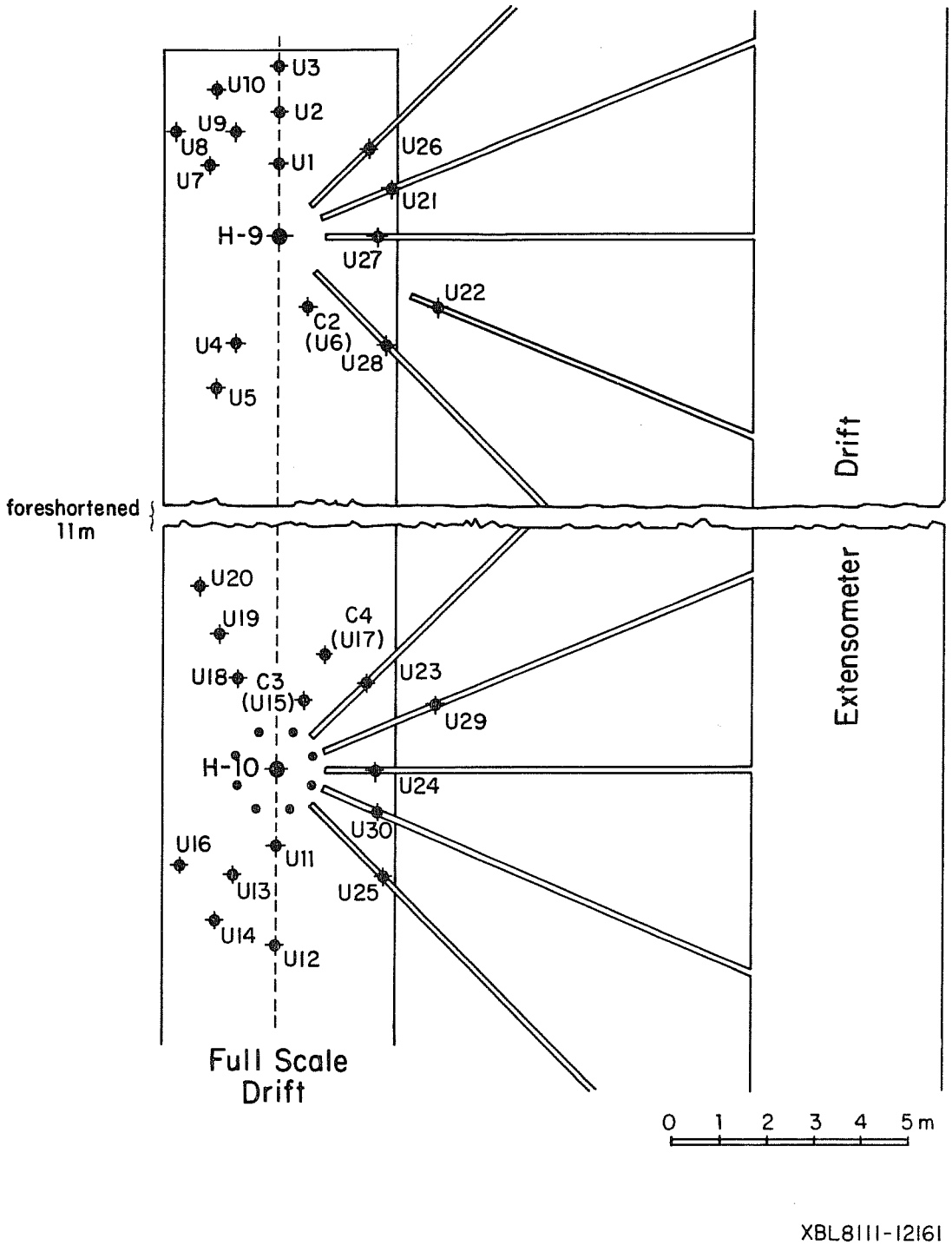

Fig. 1-3. Location of USBM borehole deformation gauges.

Table 1-1. Guide to reports on instrumentation and data acquisition for Stripa heater experiments.

Type	Installation	Performance
Heaters	Burleigh et al. (1978; SAC-13)	no report
Thermocouples	Schrauf et al. (1979, SAC-25)	Binnall & McEvoy (1981; SAC-53)
Extensometers	"	DuBois et al, (1981; SAC-50)
VWS and USBM gauges	"	this report
Dewatering system	"	Nelson et al. (1981; SAC-35)
Data acquisition	McEvoy (1978; SAC-14)	Chan et al. (1980; SAC-29)

heater experiments have been issued. Five more, including this one, describe the operation of the experiments, the status of the data base, and the performance and final calibration of the instruments. A major goal of this report and the companion reports by Binnall and McEvoy (1981) and DuBois et al. (1981) is to establish for each type of instrument an error estimate that will be valid for the conditions encountered at Stripa. A secondary purpose is to recount the successes and problems encountered while operating and calibrating the instruments, so that our experience will be of use in future experiments and in underground waste repository applications.

1.2 Data Acquisition and Processing

Table 1-2 depicts the sequence of hardware and software operations which brought the measurements from VWS and USBM gauges to their organized, accessible form on computer-written magnetic tape at the Lawrence Berkeley Laboratory (LBL). Data processing is discussed by Chan et al. (1981), concluding with a description of the data tapes and instructions on how to access them. The mainline sequence of operations in Table 1-2 begins with the borehole instrumentation and ends with the compilation of time-averaged engineering data on magnetic tape (item e). Intermediate compilations and storage of data are useful for checking the validity of the time-averaged data base and for examining specific details that are lost in the time averaging. For future analysis of the data base, however, it is assumed that the tapes and microfiche (item e) will be the most useful. Plots of the time-averaged data were also made and stored on microfiche, as indicated by item f. These plots are reproduced in Appendices A and B in summary sheets for each VWS and USBM gauge.

Table 1-2. Flow chart of data acquisition and processing at Stripa and LBL for USBM and VWS data.

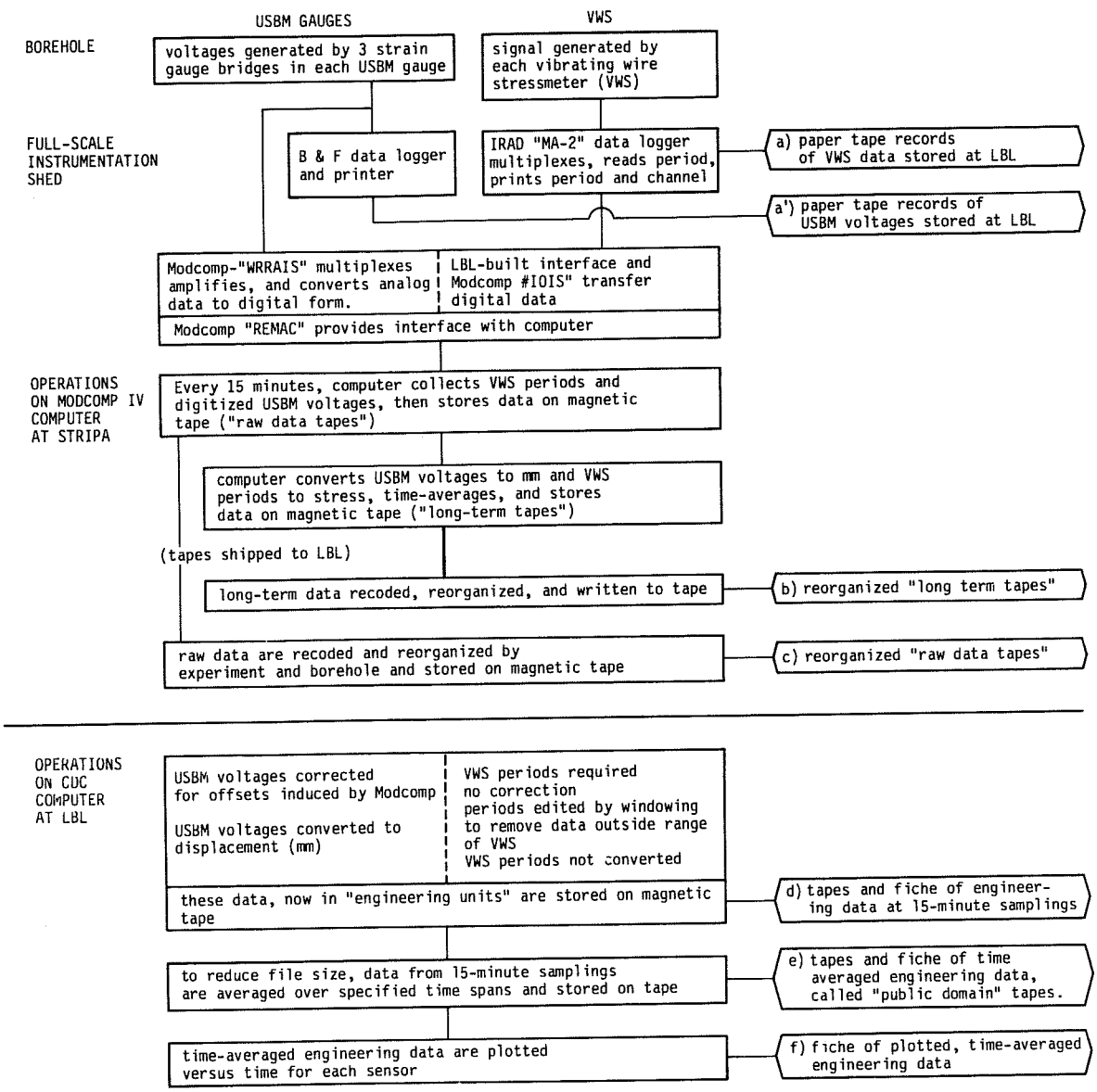

Data loggers provided back-up to the computer acquisition by printing the output of each gauge on paper tapes. These data were subsequently used to remove offsets in the computer-based raw data as described by Chan et al. (1979). The offsets were not removed from the reorganized "raw" data (item c). Hence this data base should not be used unless the corrections are made.

The reorganized "long-term" tapes (item b) contain the unwanted offsets as well as other inherent errors. On these tapes the USBM and VWS data were converted to diametral displacement in millimeters (mm) and to stress (MPa), respectively, based on preliminary calibration work done prior to installation and start-up of the experiments in the summer of 1978 (Schrauf et al., 1979). Subsequent calibration work to be described in this report has shown that the algorithms and coefficients used to convert the VWS data are invalid. Minor problems also exist in the USBM data. For these reasons, this data base (item b) should not be used as it stands to interpret the rock mass response.

1.3 Experience with Gauge Calibration and Operation

The Stripa experiments were unusual in that the instruments were required to operate at sustained temperatures higher than normally attained in most rock mechanics applications. The temperature problem was addressed at the outset by modifying the USBM gauges in an attempt to extend their operating range to 200°C (Schrauf et al., 1979). A response equation for the gauge was established which incorporated temperature-dependent terms. Calibration data at ambient and elevated temperatures were acquired to supply the coefficients for converting strain-gauge voltages to borehole displacement. This report adds post-experiment calibration results at both ambient and elevated temperatures to the earlier work, and discusses the shifts observed in the coefficients in terms of the errors induced in the measurements.

Preliminary calibrations of the VWSs were also done in a block of Stripa granite at ambient and elevated temperatures. However, the work was incomplete at the time of installation because of the pressing schedule. At the conclusion of the experiments, an extensive effort was made to calibrate all surviving VWSs. As this effort proceeded, it became apparent that there were serious inconsistencies in the calibration data. These problems, including the reliability with which a gauge can be repeatedly installed and calibrated in a block, are described, and their impact on the error in computed stress is discussed.

Because early reports from Sweden indicated that the test site would be dry, little effort was devoted to improving the water immunity of the gauges. This report proved to be false; almost all of the boreholes had a continuous inflow of water, and even with the implementation of a dewatering system (Schrauf et al., 1979), water infiltration into the USBM gauges resulted in failure of 17 of the 20 mounted in vertical boreholes and 5 of the 10 in horizontal holes. Field rework and subsequent modifications were undertaken in an attempt to overcome the problems caused, for the most part, by moisture infiltration. Some of the VWSs also failed because of similar infiltration of moisture. These failures are discussed further in the sections dealing with VWS and USBM gauges.

The USBM gauge data have been converted to values of borehole deformation sensed by the gauge and are available as indicated in Table 1-2 (item e). The calibration results in this report permit an assessment of the errors in those values. Final conversion of measured displacement to stress requires a knowledge of the thermal expansion coefficient and of the elastic properties of

the rock. Laboratory data acquired to date (Myer and Rachiele, 1981) indicate a large uncertainty in the values for these properties; in this report, we hazard an estimate of the final error in the measured stress change based on estimated values. An error assessment for the VWSs would appear to be more straightforward from inspection of the response equation. However, the calibration problems led to error bounds that are quite broad. An error analysis for each gauge type, along with a few trial conversions of measured data to stress, are presented and discussed in the concluding section of this report.

2. VIBRATING WIRE STRESSMETERS

2.1 Response Equation of the VWS

The vibrating wire stressmeter (VWS) consists of a hollow steel cylinder set into position in a borehole by means of a sliding wedge and platen assembly (Fig. 2-1). The sensing element is a highly stressed steel wire, stretched across the diameter of the hollow cylinder. A small electromagnet both excites and senses the natural vibration of the wire. A change of stress in the rock deforms the gauge body slightly, changing the stress on the wire and shifting the fundamental vibratory period. More detail on the design and operation of the gauge was given by Hawkes and Bailey (1973).

The gauges used in the Stripa heater experiments were manufactured by Irad Gage, Inc. of Lebanon, New Hampshire and were the type designated VBS-1HT with the hard rock (HR) platen. The change in wire stress was read either by the IRAD MA-2 data logger or the MB-6 hand-held unit, both also manufactured by Irad Gage, Inc. (IRAD, 1977).

Hawkes and Bailey (1973) developed a response equation for the gauge that defines the sensitivity factor, α, as the ratio of the change in wire stress to change in rock stress. A version of this response equation given by Schrauf et al. (1979) defined the gauge calibration factor differently by relating the change in rock stress directly to the vibratory period. In the following paragraphs, these two formulations are linked, and the nomenclature adopted in this report is established. Equations originally given by Hawkes and Bailey (with some nomenclature changes) are designated parenthetically (HB--).

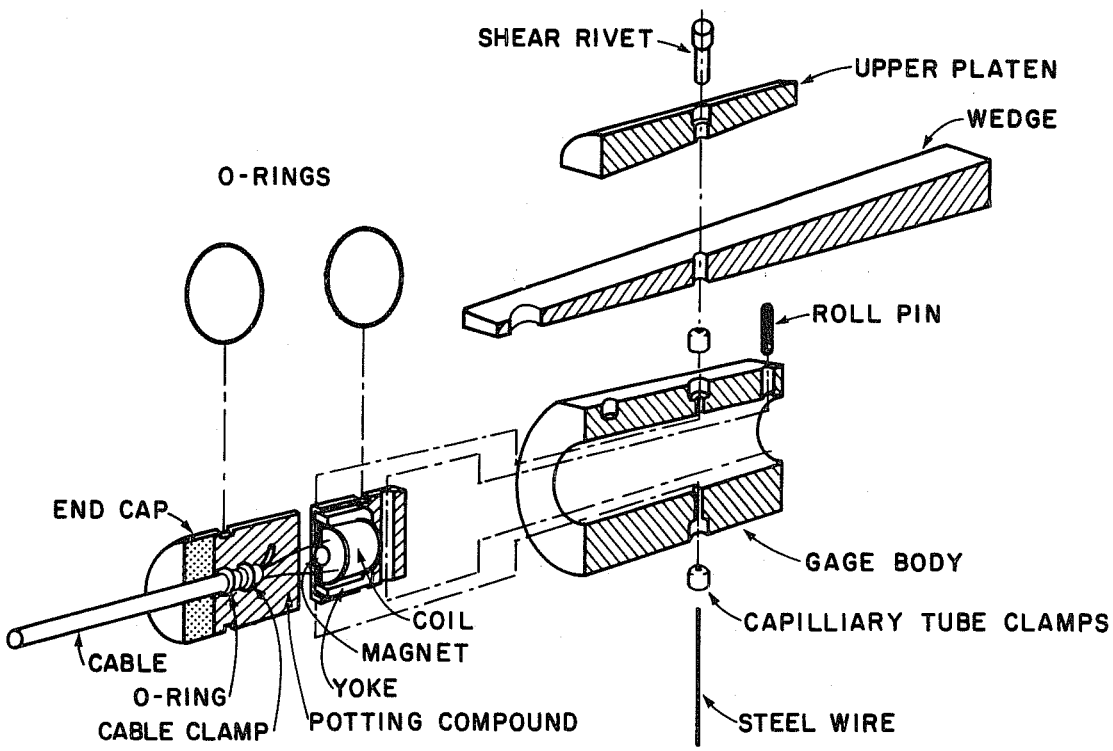

Fig. 2-1. Exploded sectional view of vibrating wire stressmeter.

Reserving T to designate temperature, we use R to designate the period of the vibrating wire, which is determined by

$$R = 2\ell \sqrt{\frac{\rho}{\sigma_w g}}, \qquad \text{(HB1)} \qquad (2\text{-}1)$$

where the wire length ℓ = 0.0198 meters, the wire density ρ = 0.283 lb/m^3 and gravitational acceleration g = 9.8 m/sec^2. Substituting these values gives:

$$R\ (\text{sec}) = \frac{0.04224}{\sqrt{\sigma_w}}, \qquad \text{(HB3)} \qquad (2\text{-}2)$$

if the wire tension σ_w is given in psi. Assuming a linear relation between the change in wire stress and the change in rock stress, we can write:

$$\Delta\sigma_w = \sigma_{wo} - \alpha\Delta\sigma_r, \qquad \text{(HB14)} \qquad (2\text{-}3)$$

where $\Delta\sigma_r$ is the change in rock stress from the stress existing when the gauge is first set and σ_{wo} is the wire tension when the gauge is first set. The sensitivity factor α relates $\Delta\sigma_w$ to $\Delta\sigma_r$. Combining (2-2) and (2-3), and expressing the period R in 10^{-7} seconds, which are the units displayed on the readout meter, we get:

$$R = \frac{422400}{\sqrt{\sigma_{wo} - \alpha\Delta\sigma_r}}$$

$$= \frac{422400}{\sqrt{\sigma_{wo}(1 - \alpha\Delta\sigma_r/\sigma_{wo})}} \qquad \text{(HB15)} \qquad (2\text{-}4)$$

Equation (2-4) can be rewritten as

$$\Delta\sigma_r = \frac{1}{\alpha}\left[\sigma_{wo} - \left(\frac{422400}{R}\right)^2\right] \qquad (2\text{-}5)$$

The starting period, or period of vibration when the gauge is first set, is designated R_s, which is equal to $422400/\sqrt{\sigma_{wo}}$, so that:

$$\Delta\sigma_r \text{ (psi)} = \frac{422400^2}{\alpha}\left(\frac{1}{R_s^2} - \frac{1}{R^2}\right). \qquad (2\text{-}6)$$

Converting to metric units where 1 psi = 6895 Pa,

$$\Delta\sigma_r \text{ (MPa)} = \frac{1.23 \times 10^9}{\alpha}\left(\frac{1}{R_s^2} - \frac{1}{R^2}\right). \qquad (2\text{-}7)$$

The calibration data for Stripa gauges were given in terms of C_1 (slope) and C_2 (intercept) by Schrauf et al. (1979). The equation for stress change is:

$$\Delta\sigma_r \text{ (MPa)} = \frac{C_1}{R^2} + C_2. \qquad (2\text{-}8)$$

Therefore, the relationship between Eq. (2-7) and (2-8) is $C_1 = -1.23 \times 10^9/\alpha$, and $C_2 = 1.23 \times 10^9/(\alpha R_s^2)$.

Some of the tabulated calibration data list the parameter C_2, which combines the starting period R_s and the slope C_1 as $-C_1/R_s^2$. However, we will use the relationship

$$\Delta\sigma_r \text{ (MPa)} = C_1\left(\frac{1}{R^2} - \frac{1}{R_s^2}\right) \qquad (2\text{-}9)$$

to discuss the calibration results. The periods R and R_s are always given in meter reading units, which are equivalent to 10^{-7} seconds. The intercept C_2 is given in units of MPa and C_1, which has the dimensions of stress times the square of time, is given in MPa times the square of the meter reading. The relationship between C_1 and the reciprocal value of gauge sensitivity factor (α) is plotted in Fig. 2-2.

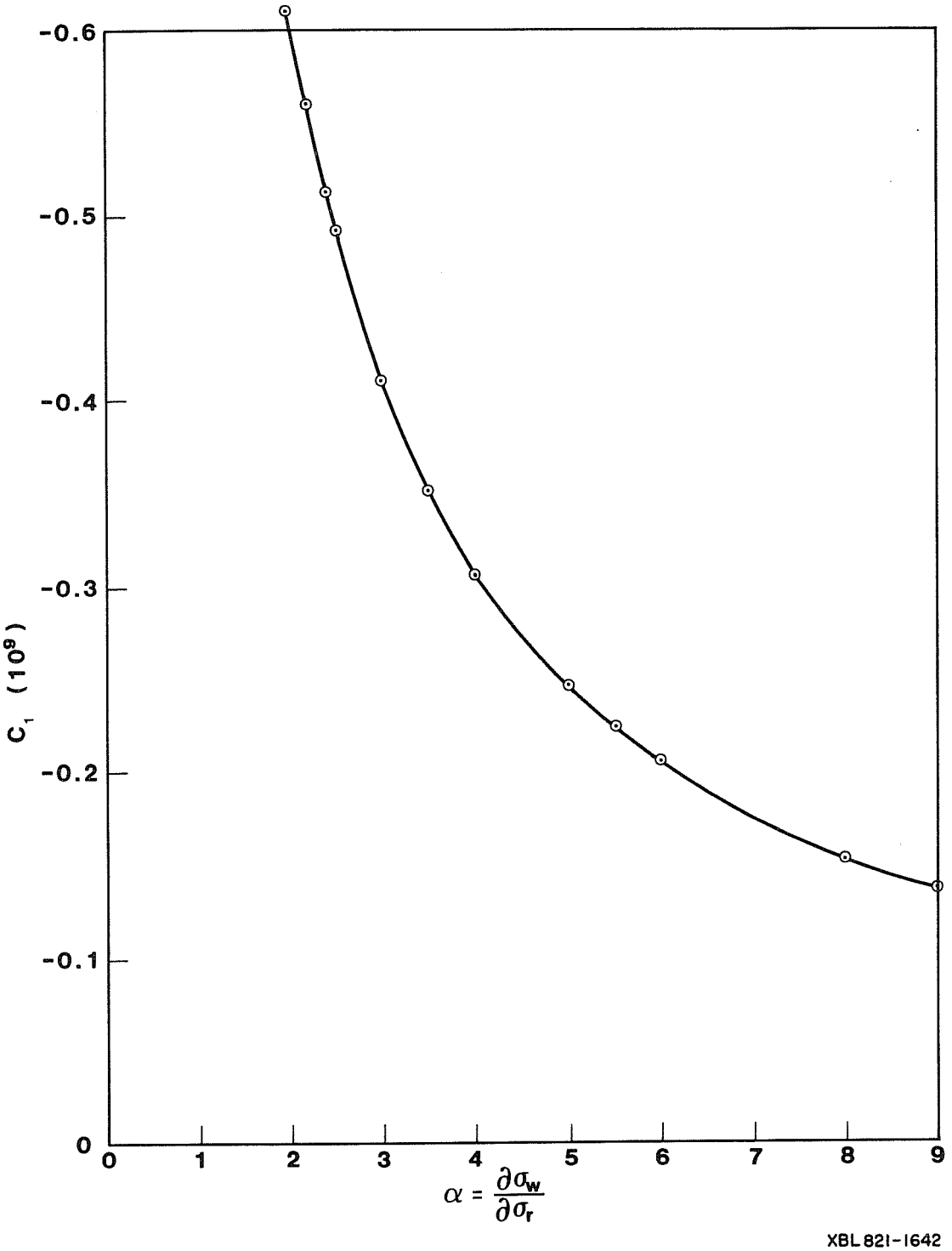

Fig. 2-2. Relationship between gauge calibration factor C_1 and gauge sensitivity factor α.

Data points from Fig. 13 of Hawkes and Bailey for calibration in a slab of Barre granite have been replotted in Fig. 2-3 as a function of $1/R^2$ instead of R as originally plotted. The resulting straight-line fit through the data gives a C_1 value of -0.196×10^9. The value obtained for α by Hawkes and Bailey was 6.1, which, according to the conversion given in Eq. (2-8), corresponds to a C_1 value of -0.21×10^9. The 7% difference is attributed to the use of graphical rather than numerical data.

Besides serving as a check on the equivalence between nomenclatures, Fig. 2-3 also serves to introduce the graphical format and units that will be used in presenting results in this report. Values of the calibration factor C_1 can be readily compared and computed from calibration data plotted in this format. Since the $1/R^2$ axis is directly proportional to the stress change on the vibrating wire, our format is similar to plots of $\Delta\sigma_w$ (ordinate) vs $\Delta\sigma_r$ (abscissa) presented by Dutta et al. (1980).

2.2 Operating History of Vibrating Wire Stressmeters

2.2.1 Calibration and Operation Sequence

Table 2-1 shows the calibration and operational history of each vibrating wire stressmeter (VWS) used in the Stripa experiments. The first three columns identify the gauge, first by its label, second by the borehole in which the gauge was installed, and third by the gauge serial number. The gauge labels were assigned during the experimental design phase and usually, but not always, correspond to the borehole identification. The labels are not unique to an individual gauge; if a gauge failed and was replaced by another, the replacement was assigned the same label as the original. Historically, it was

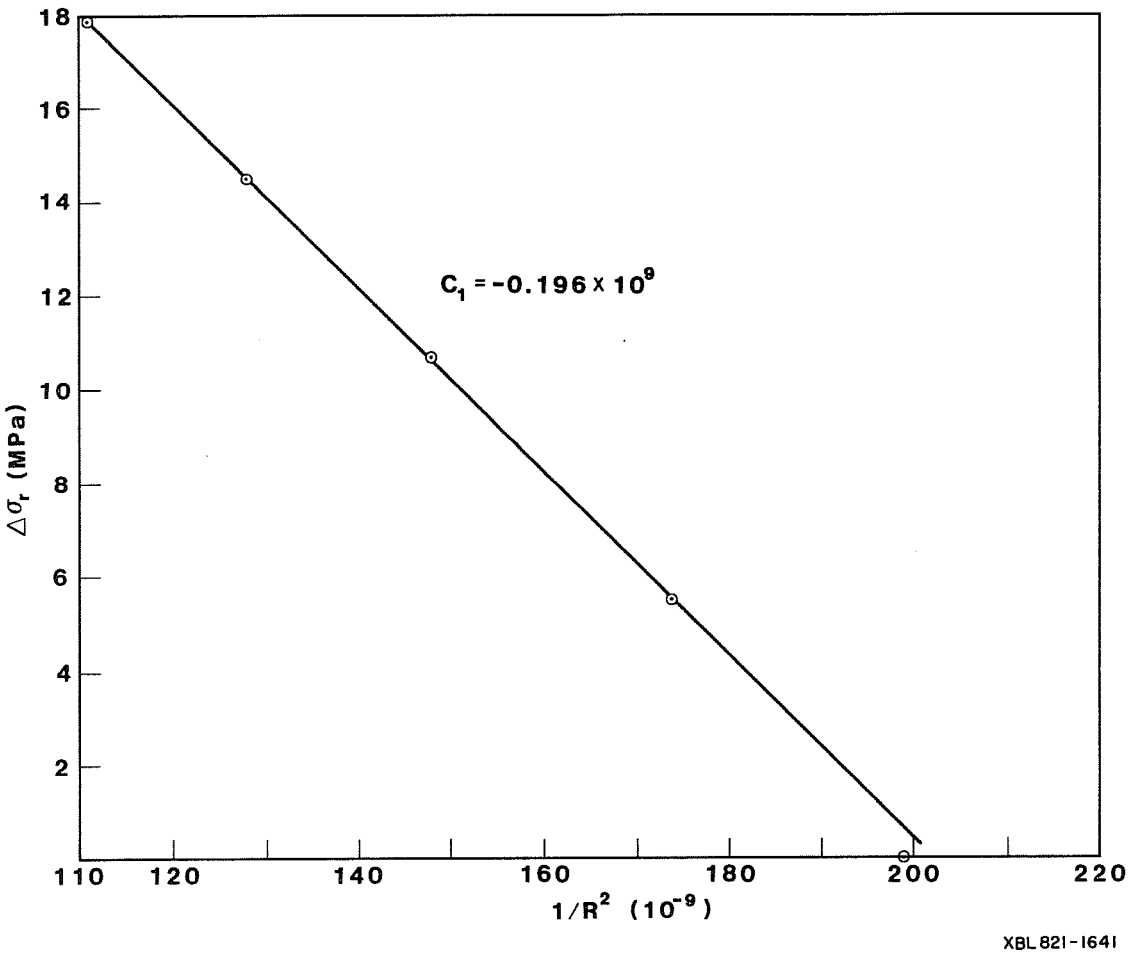

Fig. 2-3. Barre granite data from Hawkes and Bailey (1973) Gauge sensitivity factor = 6.1, unloaded gauge period R_0 = 1996.

Table 2-1. History of VWS calibration and usage.

Label	Hole	Serial No.	Calib (1977)	Calib (1980)	Calib (1980)	Calib (1981)
Installed-H9						
C1⊖	C1	3-22		B	C	
C1R	C1	3-20		B	C	
C2⊖	U6	3-18	A(T)			
C2R	U6	3-16	A			
C6⊖	C6	3-55		B	C	
C6Z	C6	3-68	A	B	C	
C7⊖	C7	3-92	A	B	C(Rs)	C(Rs,T), D(T)
C7Z	C7	3-74	A	B	C	
C8	C8	3-90	A	B	C	
C8Z	C8	3-58		B	C	
C11⊖	C11	3-01		B	C	
C11Z	C11	3-37	A	B	C(Rs)	C(Rs, Z,T), D(T)
C12⊖	C12	3-48		B	C	
C12Z	C12	3-43		B	C	
C9⊖	U3	K-2	A	B	C(Rs)	
C9R	U3	J-40	A	B	C	
Installed - H10						
C3⊖	U15	3-77	A			
C3⊖	U15	E-56		B	C	
C3R	U15	3-73	A(T)			
C3R	U15	E-73		B	C(Rs)	
C4⊖	U17	3-08				
C4⊖	U17	E-58		B	C	
C4R	U17	3-63				
C4R	U17	E-62		B	C	
C5⊖	C5	3-82				
C5⊖	C5	E-51		B(T)	C	
C5R	C5	3-35				
C5R	C5	E-50		B(T)	C	
C10⊖	C10	3-14				
C10⊖	U23	E-69		B	C	
C10Z	C10	3-45	A(T),S		C	
C10Z	U23	3-42	A(T)	B	C	
C14⊖	C14	3-09		B	A,C(Rs)	
C14Z	C14	3-29		B	C	
C15⊖	C15	3-50	A	B	C	
C15Z	C15	3-36	A	B	C	
Damaged						
		3-62	A			
		3-71	A			
		3-80	A			
		3-54	A			
Not used						
		3-04				
		3-05				

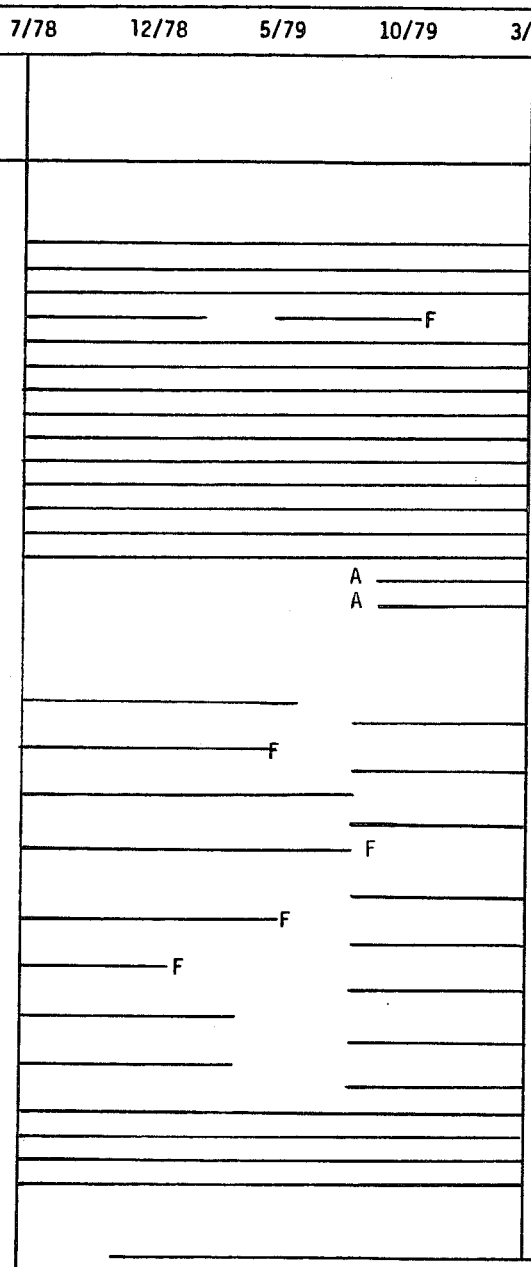

Calibration Techniques

Facilities
A - end-loaded cylinder
B - 15-inch block
C - 12-inch block
D - radially loaded cylinder
S - steel cylinder

Conditions
Rs - variable setting periods
T - temperature
Z - triaxial

F - failed

preferable to use the gauge label when discussing performance and results, but multiple assignments have caused ambiguity in some cases. The R, Θ, or Z included in the label identification signify the orientation of the gauge. The "R" was used only for gauges in vertical boreholes and means the axis of the gauge was aligned along a radial path from the centerline of the main heater to the gauge location; "Θ" was used for gauges in both horizontal and vertical boreholes where the orientation was in the horizontal plane and perpendicular to the radial axis. The "Z" signifies that the gauge was in a horizontal borehole aligned in a vertical direction. These identifiers were not used in the report by Chan et al. (1980). In the computer listing in Table A-3 of that report, the letter "A" was used in place of "Θ," and "B" in place of both "R" and "Z". In this report, VWS gauges with non-unique labels are identified by the gauge serial number or by a (1) or (2) indicating the first or second installation in a borehole.

Calibrations, discussed in Section 2.3, are identified by calibration block (see legend of Table 2-1), and by the year in which they were done. A parenthetical letter indicates those calibrations in which temperature or setting period was varied. Otherwise, a calibration entry indicates the determination of C_1 at room temperature. Only 13 of the installed gauges were calibrated before installation. However, all but 3 were calibrated either before or after the heater experiments. In all, 36 VWSs were purchased, of which 16 were installed in 8 boreholes in the H9 experiment, and 20 were installed at various times in 7 boreholes in the H10 experiment.

The operating time of each gauge is indicated schematically by horizontal line segments in Table 2-1. The line simply indicates the time over which data were acquired; it does not indicate whether the data are valid. The exchange of one gauge for another in a borehole is shown by the termination of a line and the beginning of a line segment of a different gauge which has the same label in the first column. Gauge failure and replacement are discussed further in a later section.

Field records for the gauges are given in Appendix A. For discussion purposes, the field record for the first gauge assigned label C4Θ is reproduced as Fig. 2-4. The upper left-hand box indicates the duration for which data were acquired from the gauge. The upper right-hand box gives the gauge coordinates in meters relative to the heater midplane (see Appendix A of Schrauf et al. (1979) for a description of the coordinate systems used at Stripa). The top of the plan map is oriented towards the rear of the full-scale drift and shows the position of the gauge with respect to the heater. Figure 1-2 shows the relative position of all VWSs. Specific information for the gauge and its corresponding thermocouple is given in the third box of Fig. 2-4. The third box also gives the sensor number used to identify a record on the computer disk file and the channel number used to identify a record on the data logger.

The plot at the bottom of Fig. 2-4 is a replica of the time-averaged data records produced by Chan et al. (1980). The time axis is given accurately in experiment days and approximately in calendar months. Temperature measured by the associated thermocouple is labeled "T" and the recorded period for the VWS is labeled "I". The VWS period is the value recorded in the field,

IRAD GAUGE FIELD RECORD

Full Scale Experiment H-10

Gauge C4θ (1st)
Hole U17

Term of Gauge Usage	
Entire Experiment ☐	Partial Experiment including... (calendar dates) 78/7/2 - 79/7/7 (y) (m) (d) (experiment days) 0 - 369

[X] vert. [ ] horiz.

r= 2.46
θ= 292.7
z= -.65

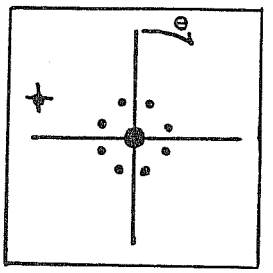

	Label	Mfg. Serial No.	Sensor No. (on disc file)	Logger Channel	R_o (pre-exp.)	R_o (post-exp.)	R_s (set)	ΔR_s (R_s-R_o)		
IRAD Gauge	C4A	3-8	863	6	1868		2047	179		
Corresponding Thermocouple	TC4		503	103						

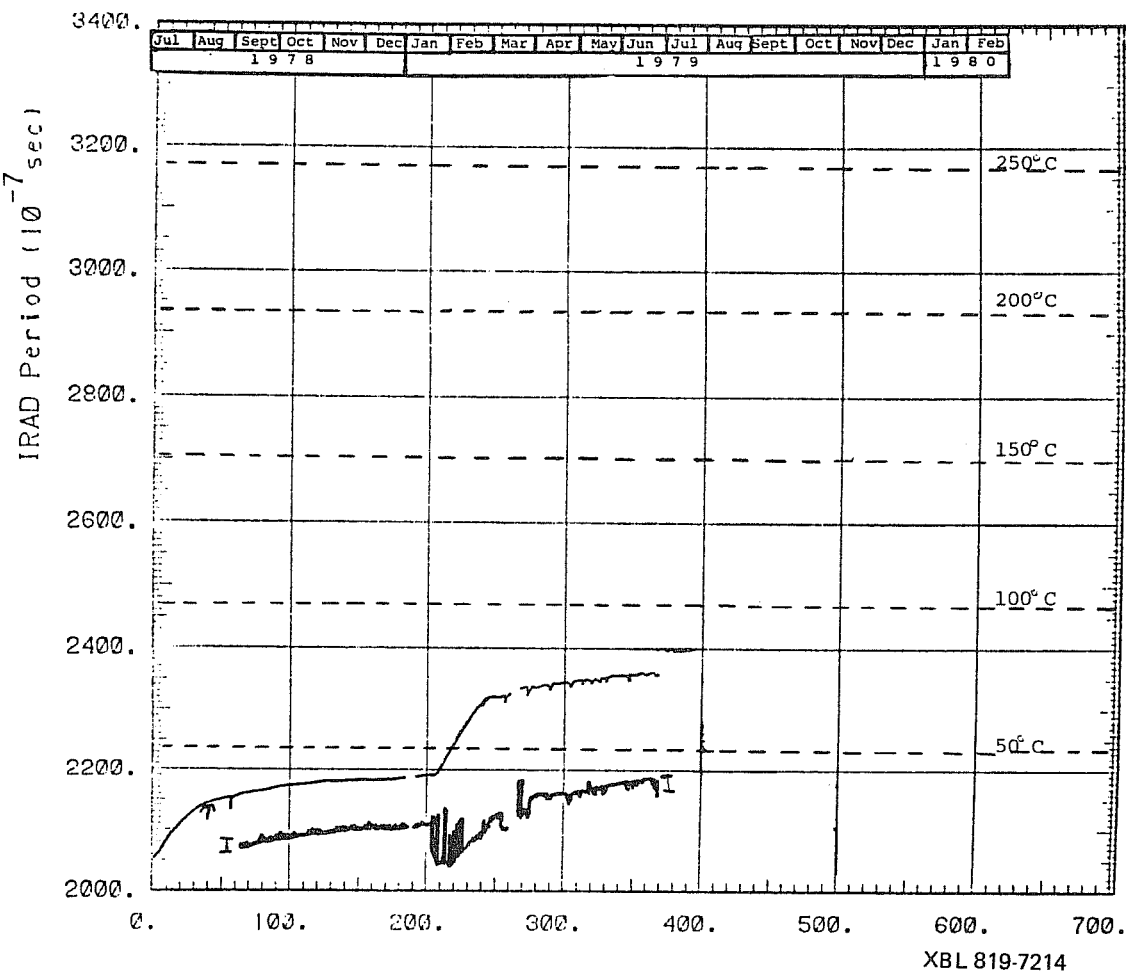

Fig. 2-4. Example of VWS field record.

unaltered except for time-averaging and some minor editing, as described later.

There were some changes in the location and labels of gauges during the course of the heating experiments, the details of which are given in Appendix C.

2.2.2 Gauge Failures

Five gauges failed during operation of the heater experiments as indicated by the "F" in Table 2-1. Another gauge (C2θ) appeared to operate to the end of the experiment but was not operating after removal. The record for C2R is erratic and the gauge was inoperative upon removal from the borehole at the end of the experiment. The four other failures referred to in Table 2-1 can be readily observed on the plots in Appendix A. Gauges C3R, C4R, C5θ, and C5R were all located within the H10 experiment area, all were in vertical boreholes, and all failed after the peripheral heaters were turned on at experiment day 204. Gauge temperatures at the time of failure were in the range of 50 to 110°C. Failure cannot be directly attributed to high sustained temperatures because gauges in borehole C14, for example, operated at a maximum temperature of 120°C with no failures. As shown in Table 2-1, there is little or no calibration data for the failed gauges.

Table 2-1 could be somewhat misleading as far as total gauge failure is concerned, because if one of a pair of gauges failed, both were subsequently removed and replaced. Initially, 26 gauges were installed in 13 boreholes; however, replacement of failed or removed gauges and installation of gauges in two other boreholes brought the total count up to 36. To analyze the failures, the total population of operational gauges is taken to be 36, and failures and removals without failure are tallied separately (Fig. 2-5). Gauge removals and

failures are plotted against time in service rather than experiment time. The failure percentage is then calculated excluding the gauges removed for reasons other than failure. It can be seen in Fig. 2-5 that failures were less than 20% until a few weeks before the end of the experiment when failures climbed to 27%.

In summary, 6 gauges failed, 16 operated throughout the 550-day experiment, and another 14 operated satisfactorily, but for less than the full 550-day period. The VWS failures have been attributed to corrosion of the vibrating wire as a result of water getting inside the gauge housing. All gauges showed exterior corrosion when removed from the boreholes, with the greatest amount occurring on those experiencing the highest temperatures. Figure 2-6 shows the corrosion on failed gauge C5R, which reached a temperature in excess of 100°C.

Considerable difficulty was encountered in attempting to remove failed gauges before heater turn-off. The anchor wedges were highly corroded and bent very easily during the dislodging process, making it necessary to drill out some of the gauges. To solve this problem, a special tool was built that would fit over the wedge, so as to prevent bending.

This extraction tool, attached to a steel pipe, was placed into the position shown in Fig. 2-7, and the end of the pipe was rapped sharply to dislodge the wedge. The gauge was then pulled out by its cable. The wedge and platen were removed using a magnet lowered into the borehole. Using this tool, all gauges were removed from the boreholes without damage after the termination of the experiment.

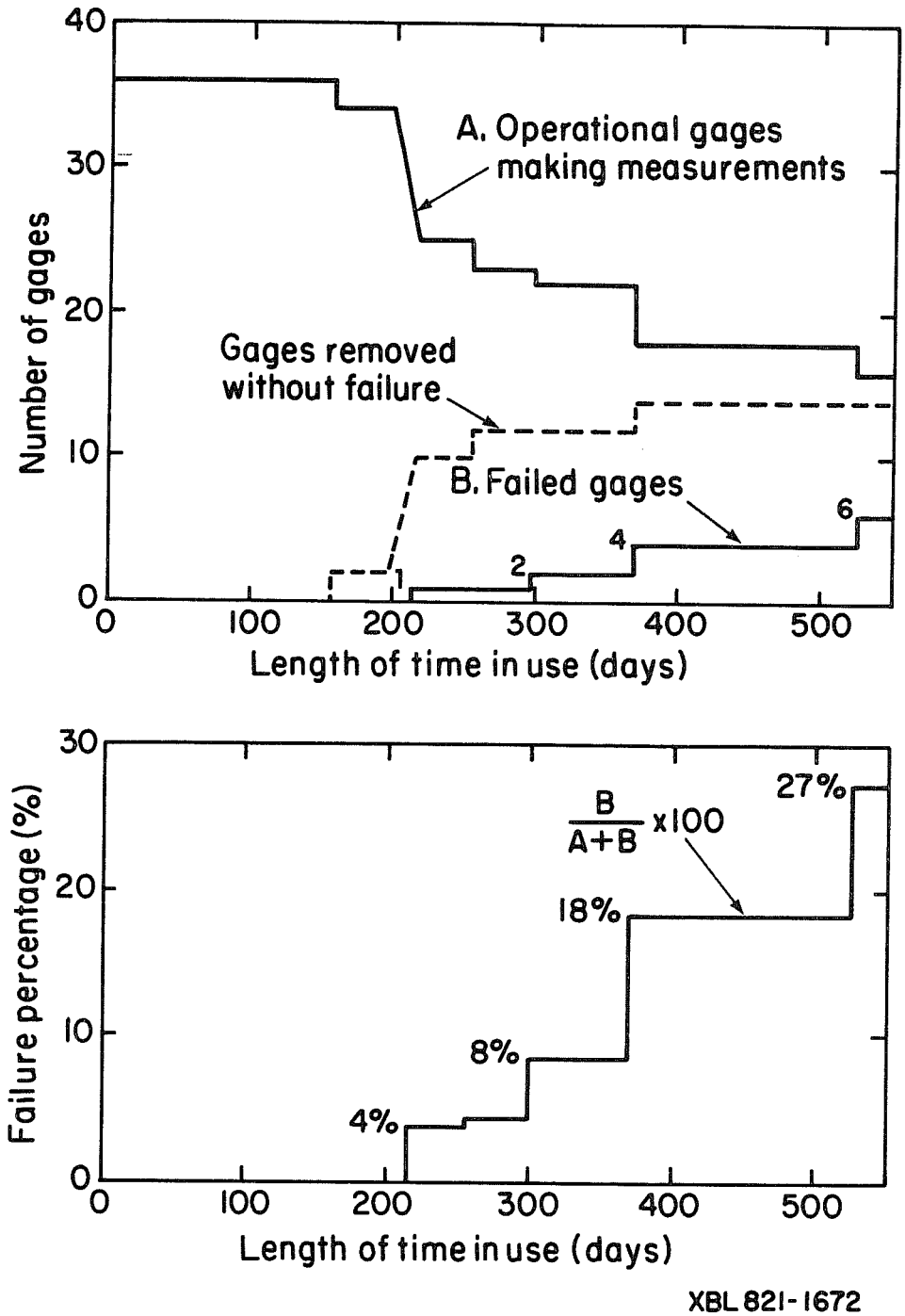

Fig. 2-5. Plot of VWS- failure.

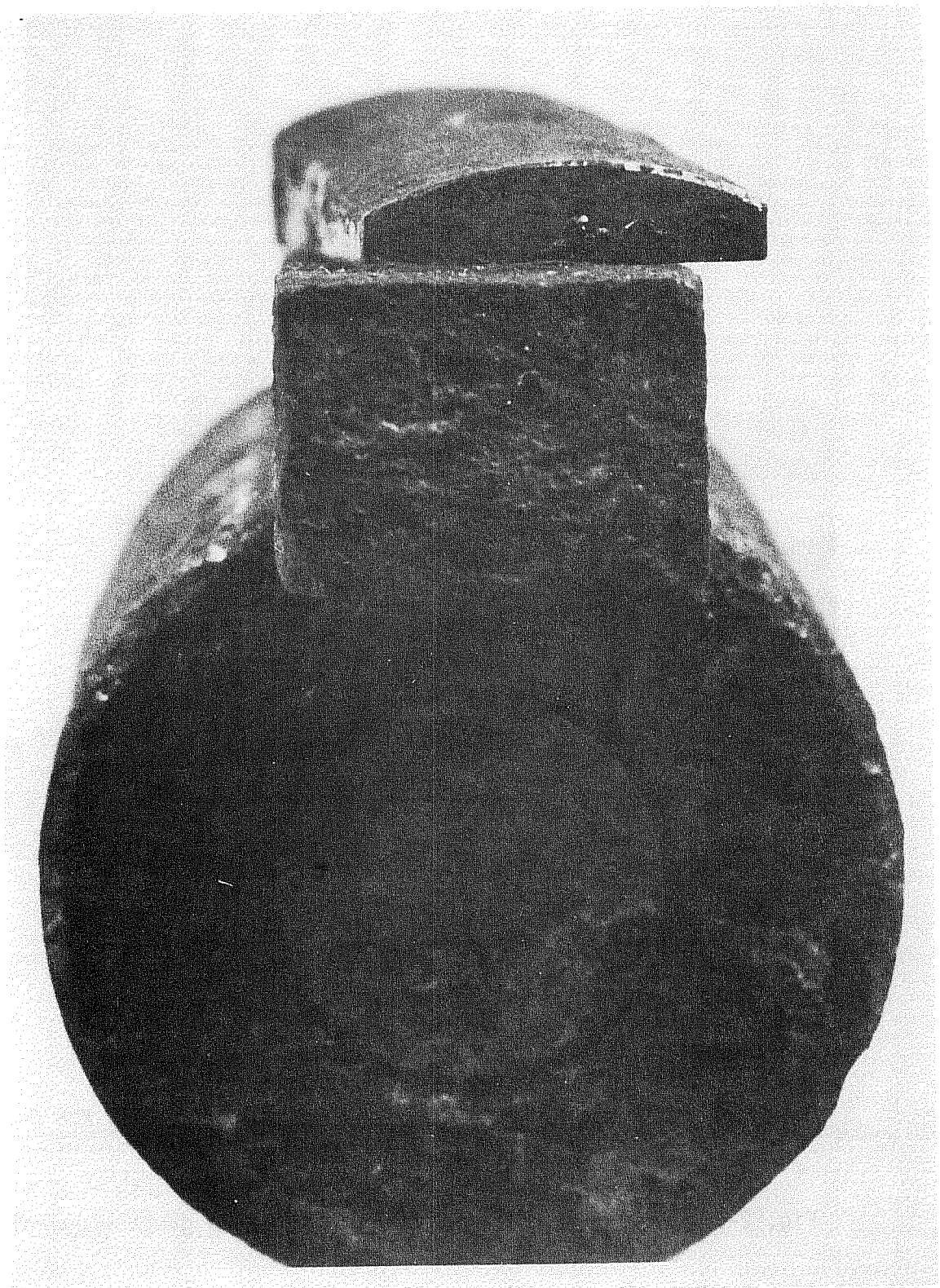

XBB 847-5185

Fig. 2-6. End view of gauge-wedge-platen assembly after heater experiment, showing corrosion and pitting.

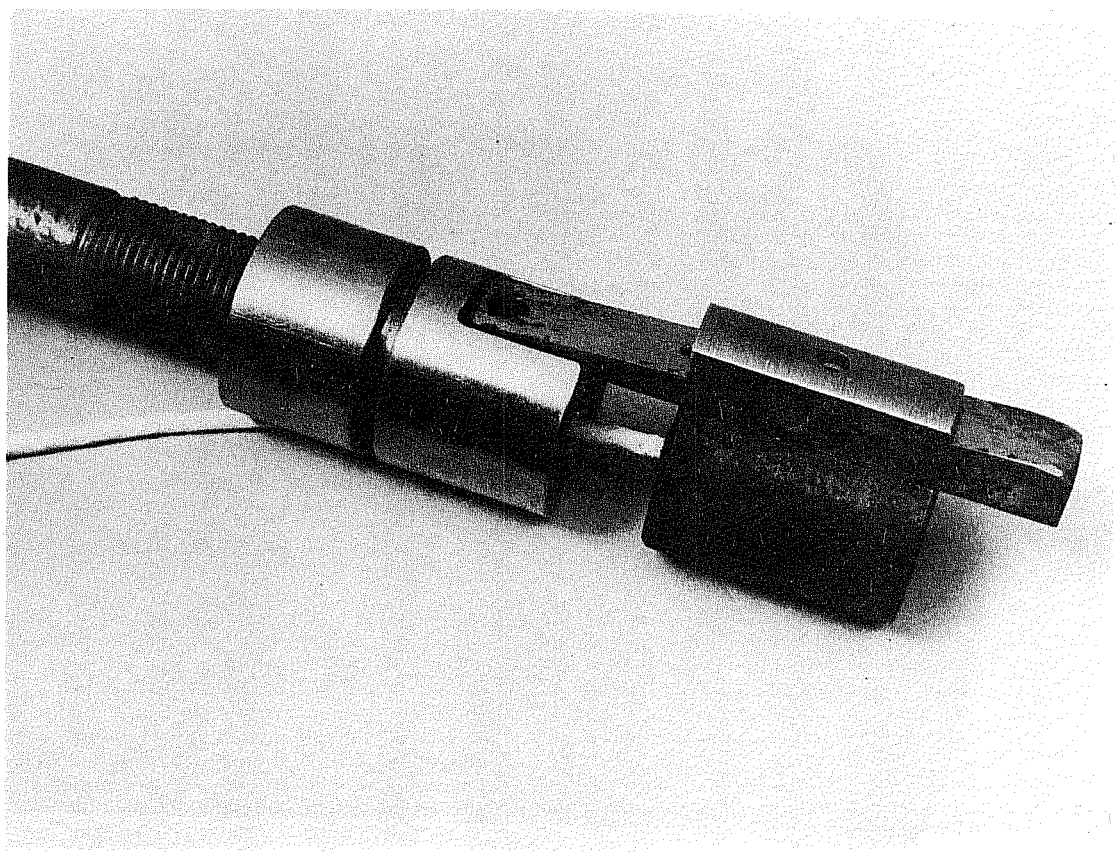

XBB 847-5184

Fig. 2-7. Head of extraction tool mounted on a gauge-wedge-platen assembly.

2.2.3 Changes in Unloaded Period (R_o)

The gauges that were operational when removed from the boreholes are listed in Table 2-2. The unloaded period of vibration (R_o) is listed for each gauge prior to installation and after removal. Four gauges showed a much greater shift in R_o than the average. The data from these gauges (C14Z, C15Θ, C15Z, and C10Z ser. #3-42) should be suspect since there is no way of knowing when the shift occurred. The value for R_o was recorded again on each gauge after they were sent by air from Sweden to Salt Lake City, Utah, as shown in the rightmost column in Table 2-2. The leads were inadvertently damaged on gauge C10Θ, ser. #3-14; so the reading could not be taken. The only significant change was the R_o value for C15Θ, which was one of the gauges that had undergone a large change previously.

2.2.4 Gaps and Noise in the VWS Data Records

2.2.4.1 Noise Due to Instrumentation Problems. Inspection of field records in Appendix A shows that many time-averaged records of gauge readings are cluttered with noise-like deviations from the more slowly varying trends attributed to the effect of heating. To try to gain a better understanding of the noise-like clutter, portions of gauge time-averaged records and hand-plotted data from the IRAD data logger paper tapes along with data from microfiche copy of the "raw data" tapes were plotted together as shown in Figs. 2-8 and 2-9. Every point recorded by the data loggers (one point every four hours) is shown. However, the computer-based raw data were acquired every 15 minutes, so only those acquired every fourth hour are plotted. All intervening points were scanned for deviations from average, and these deviations are shown as vertical lines terminating with a symbol

Table 2-2. Period R_0 of unloaded gauges, measured before and after Stripa heater experiments, and again after return air shipment.

ID	Ser. #	Period of unloaded gauge, R_0 Pre-experiment	Post-experiment	Difference	Post-shipment
C1Θ	3-22	1926	1940	+14	1942
C1R	3-20	1926	1909	-17	1915
C3Θ	E-56	2151	2160	+9	2159
C3R	E-73	2143	2143	0	2146
C4Θ	E-58	2025	2021	-4	2021
C4R	E-62	2178	2163	15	2168
C5Θ	E-51	2137	2131	-6	2133
C5R	E-50	2097	2088	-9	2093
C6Θ	3-55	2044	2028	-16	2035
C6Z	3-68	2044	2027	-17	2028
C7Θ	3-92	1974	1975	+1	1977
C7Z	3-74	1985	1979	-6	1986
C8Θ	3-90	2051	2053	+2	2051
C8Z	3-58	2072	2056	-16	2054
C9Θ	K-2	2009	2007	-2	2010
C9R	J-40	1907	1901	-6	1902
C10Θ	3-14	2244	2231	-13	----
C10Z	3-45	2204	2198	-6	2198
C11Θ	3-1	2139	2137	-2	2134
C11Z	3-37	2131	2127	-4	2136
C12Θ	3-48	2285	2299	+14	2295
C12Z	3-43	2195	2182	-13	2184
C14Θ	3-9	2005	2004	-1	2013
C14Z	3-29	2010	1980	-30	1984
C15Θ	3-50	2161	2116	-45	2131
C15Z	3-56	2165	2129	-36	2132
C10Θ	E-69	----	2218	---	2223
C10Z	3-42	2444	2417	-27	2421

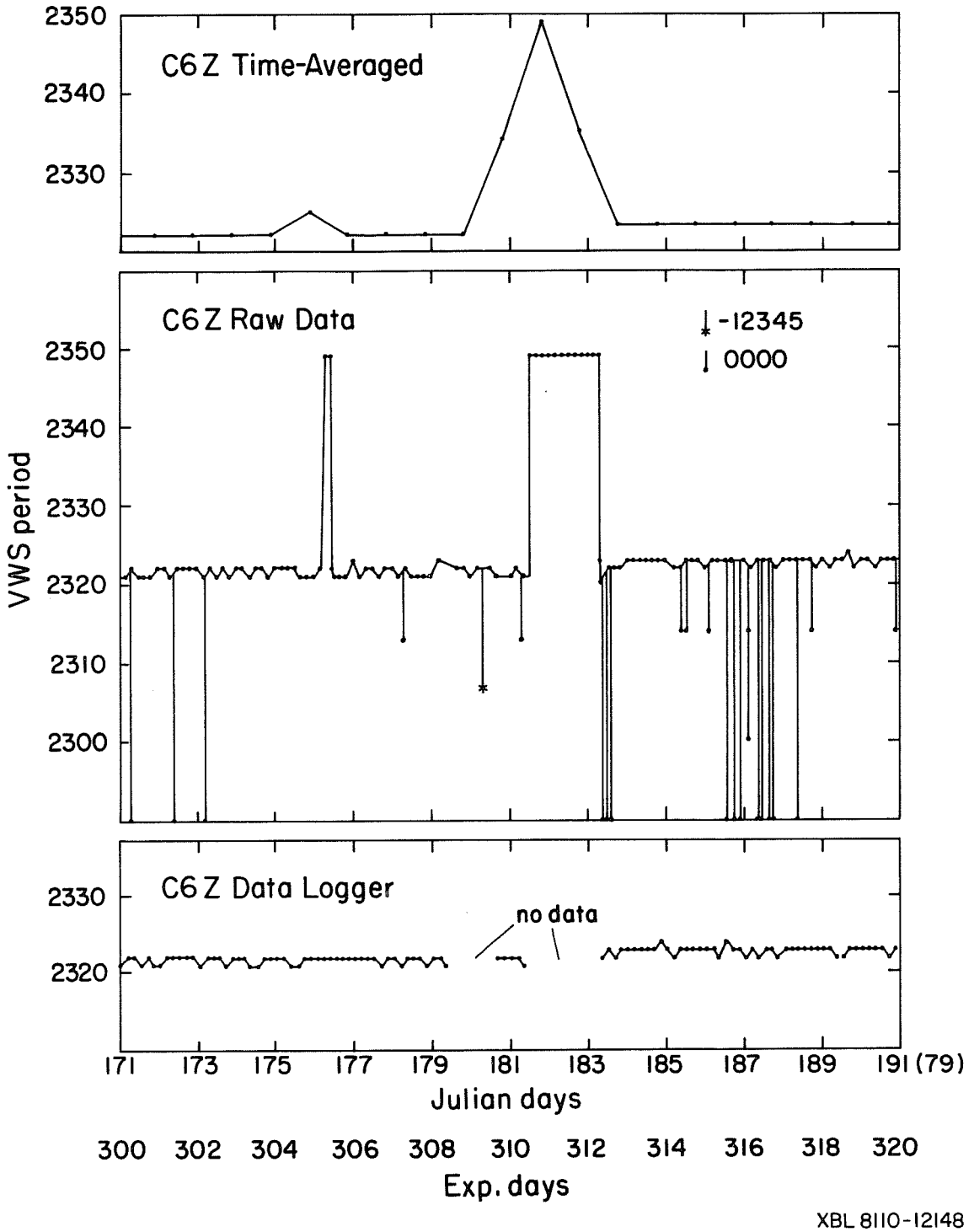

Fig. 2-8. Twenty days of detailed record gauge C6Z.

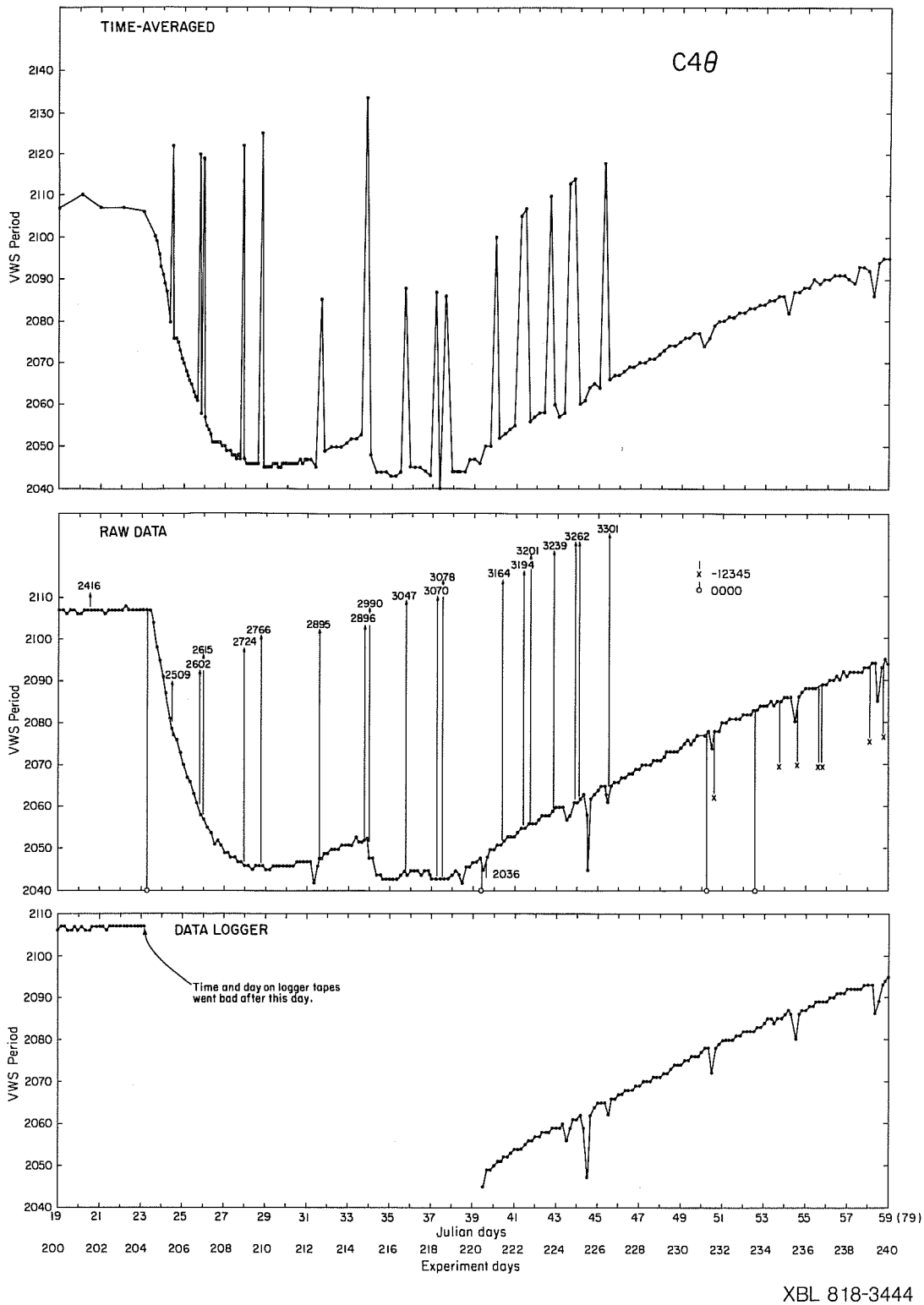

Fig. 2-9. Forty days of detailed record gauge C4θ.

to indicate the nature of the deviation. The time-averaging intervals varied throughout the experiment: in the upper graph of Fig. 2-8 the data density is one per 24 hours, while in the upper graph of Fig. 2-9 it was increased to provide more detail during the time immediately following turn-on of the peripheral heaters on day 204.

Inspection of the data logger record, computer-based raw data, and time-averaged data has led to the following diagnosis of data acquisition problems.

a) Least Count Ripple: A direct overlay of the data logger record onto the raw data shows that the average trends agree to within one count of the least significant digit. Acquisition times of the data logger and computer were not synchronized, so the two devices generally acquired data at times several minutes apart. The one-count discrepancy accords with the normal flutter observed on the read-out of the IRAD data logger.

b) Hair: Much of the noise in the time-averaged records in Appendix A appears as low-amplitude (10 to 30 counts) "hair" of both positive and negative polarity riding on the slowly varying average. An expanded graph of gauge C4Θ from experiment days 204 to 227 is shown in the upper part of Fig. 2-9. Its cause is shown to be the individual deviations in the raw data shown in the center part of Fig. 2-9. Such deviations are found only in the computer-based raw data, never in the data logger record. These data points are 500 to 1300 counts above the average and they show a monotonic increase. It was discovered

that they are samples of the preceding channel of the IRAD data logger. Occasionally the computer acquisition system failed to advance to the next data logger channel when a channel was read. The improper sequencing did not propagate through the scan; only one channel was affected at a time. Hence the hair-like events are uncorrelated from channel to channel. Because the hair events are isolated and obvious, there seems to be no need to remove them from the data records as long as they are avoided in computing stress changes.

c) Spikes: A few spikes occur on records such as C6Z and C8Θ which are otherwise free of hair. One prominent spike appears at day 310 in the time-averaged data on 10 of the 13 working gauges in the H9 experiment, and another on 4 of 6 working gauges on H10 experiment at day 362. The expanded plot of C6Z in Fig. 2-8 shows a 28-count increase for a two-day period beginning just after day 310. The log books from Stripa revealed that the sharp increase in counts was coincident with a power failure during an electrical storm. Data are missing from the IRAD data logger record because the data logger failed to record the time during this interval, although it kept printing data. It is also seen in Fig. 2.9 that the data logger malfunction is coincident with the raw data increase for this particular spike. It is surmised that a problem with the data logger developed with the onset of the power failure which continued over the weekend until the logger was reset on the following Monday morning. Fortunately, such events occurred infrequently.

d) 0000 and -12345: Figures 2-8 and 2-9 both contain several negative-going single drop-outs in the raw data which have numerical values of either zero or -12345. A zero value was output by the IRAD data logger if the return voltage from a gauge was too low to be decoded. The code -12345 was supplied by the computer and signifies that a sensor was deactivated. Neither of these codes occurred frequently enough to cause gaps on the data base, and the time-averaging algorithm rejected these points before averaging, as can be seen in Fig. 2-8.

e) Invalid Data on Failed Gauge Channels: Close inspection of the records from the first installation of gauges C3R, C4R, C5R, and C5R shows some isolated data points in the computer-based record which could be misconstrued as reasonable values, except for the fact that they occur after the gauge has produced very erratic values. These isolated points are actually taken from the preceding data logger channel as described above in (b). Their origin is the same as that of the "hair," although they appear as semi-continuous data because no valid data were produced by the failed gauges. Such points should not be included when converting the computer-based data records to stress.

2.2.4.2 Misplacement of Data Due to Gauge Interchange. In most cases, gauge labels remained the same before and after reinstallation of a repaired or replacement gauge. However, in four boreholes (U3, C3, C10, and U23), USBM and VWS gauges were interchanged. These changes are discussed in detail in Appendix C. The interchanges of VWS and USBM gauges have caused one omission

and one labeling error in the computer-based experimental data described by Chan et al. (1980):

1) Plots and data for the C9 gauges installed in borehole U3 after 9/22/79 (sensor nos. 286 and 285) have been omitted from the computer-based data file. Gauges with these sensor numbers were also omitted from the sensor list in Appendix A of the Chan report.
2) Plots and data for VWS pair C10 (sensor nos. 869 and 870) labeled this pair as being located in borehole C10 throughout the life of the experiment; in fact, they were located in borehole U23 (not (not C10) after 2/20/79.

The raw data exists, so both problems can be cured. The field records in Appendix A of this report contain the correct information with regard to the above omission and labeling error.

2.2.4.3 Omission of Data at Start of Experiments. As the records in Appendix A show, neither the H9 nor the H10 VWS data commence with heater turn-on at experiment day zero. Gauges were installed prior to day zero, but data were not properly acquired by the computer system because of a software problem in the data acquisition routine. This problem was corrected on September 5, 1978 (day 12 for the H9 experiment, day 64 for the H10 experiment), and valid data collection commenced at 1715 hours. The computer-based raw data files contain numbers acquired before that time, but they do not appear to be valid. Data printed on the data logger tapes for this early period are valid however, and could be entered manually into the computer file.

2.2.4.4 Reversal of Radial and Tangential Gauges. The tangential (R) component gauge was assigned the smaller of the two disk file numbers associated with boreholes and was designated by "A" in the CDC-based computer files (items d, e, and f on Table 1-2). A gauge mounted in the radial or vertical direction was assigned the larger disk file number and the letter "B". This convention was reversed for five installations: C1, C2, and C9 (installed in hole U3), all in the H9 area; and the second installation of C4 and C5 in the H10 area. Labeling for these gauges have been corrected in the field records presented in Appendix A but is incorrect in Table 2-1 and in the computer file discussed by Chan et al. (1980). The five reversals are in vertical boreholes; gauges installed in horizontal boreholes were connected properly according to convention.

The orientation of gauges in vertical boreholes can be distinguished on the basis of their records. At heater turn-on (or turn-off), the radial gauge responds by increasing (or decreasing) sharply and monotonically, while the tangential gauge exhibits a pulse-like transient spike. These spikes can be observed in the field records at peripheral turn-on and at main heater turn-off.

2.3 Calibration of the VWS

2.3.1 Calibration procedures

Calibrations were conducted in four different test facilities, some at room temperature and some at elevated temperatures. The VWSs were calibrated by installing them in a borehole in a cylinder or block and applying a known stress to the exterior of the sample. The period of vibration of the wire was recorded at increments of increasing or decreasing stress.

The nomenclature used throughout the sections on calibrations is as follows.

R = gauge period,

R_0 = period of unloaded gauge,

R_s = period of gauge after installation,

R_f = gauge period after a load-unload cycle,

ΔR = $R_s - R_0$,

ΔR = change of gauge period upon installation (R_s-R_0),

C_1 = slope of straight-line fit of $1/R^2$ vs stress data,

C_2 = ordinate of straight-line fit at $1/R^2$ equal to zero,

T = temperature (°C),

r = correlation coefficient of least-squares fit to data, and

E = Young's modulus of calibration sample.

Figure 2-10 shows a typical calibration run where the inverse square of the gauge readings are plotted as a function of stress change. The gauge calibration factor is determined as the slope of a straight-line fit to the data using the least-squares technique. The correlation coefficients (r) were close to 1.0, indicating nearly perfect fits for both the loading and unloading runs. This was true for most of the calibrations; that is, the gauge response was very linear over the ranges of stress applied to the calibration blocks. The failure of the gauge reading to return to the initial R_s value is believed to be due to seating of the gauge into the host material.

The VWS calibrations prior to the installation were all conducted in an end-loaded cylinder. Post-experiment calibrations were done in a flatjack-loaded block in situ at Stripa, in a flatjack-loaded block in the laboratory,

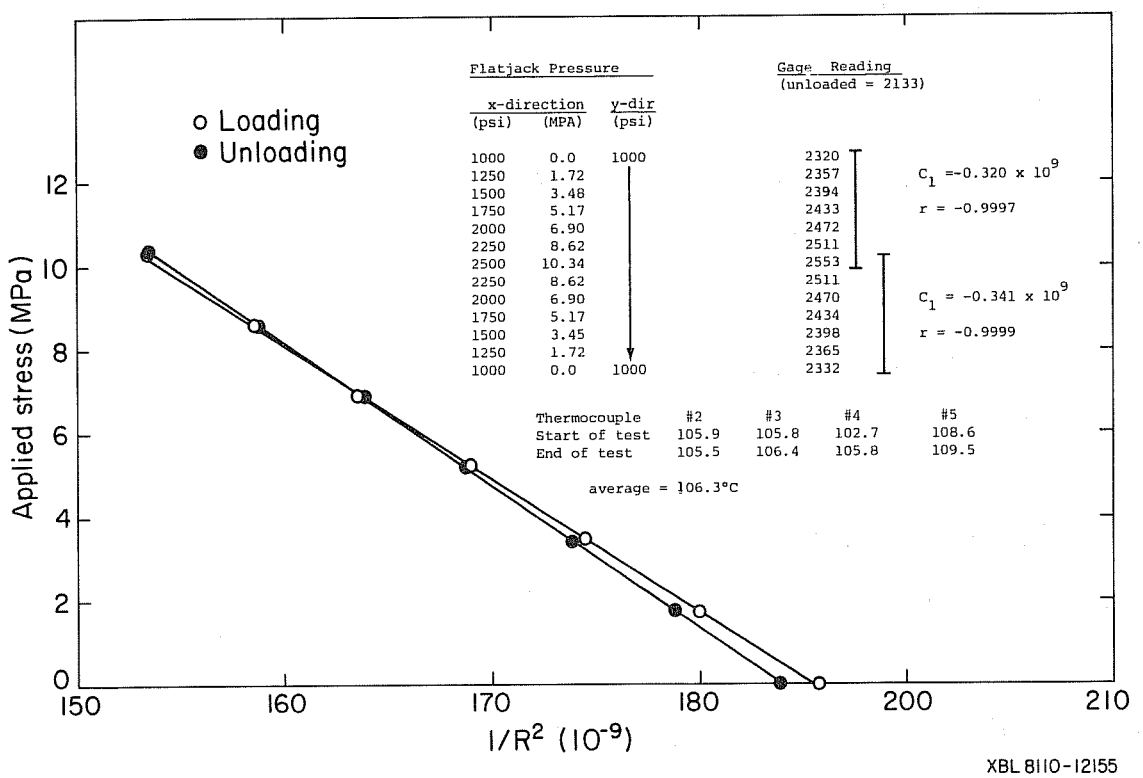

Fig. 2-10. Calibration data and plot for gauge C11Z at 106°C. Gauge aligned along x-axis of 12-inch block, 9 inches below surface. Both x and y axes of block pre-loaded to 1000 psi.

and in a radially-loaded cylinder also in the laboratory. Refer to Table 2-1 for the calibration history of each gauge.

All four calibration samples were prepared such that the hole in which the gauge was installed was much longer than the gauge body. In this respect, the calibrations described in this report differ from those obtained by Hawkes and Bailey (1973) and by Dutta et al. (1980), who performed most of their tests in slabs of thickness comparable to the gauge body length.

The four calibration facilities are described in Section 2.3.2. Even though the rock for each facility was obtained from the same underground site in the Stripa pluton, there was a variation in the elastic properties of the four samples as will be discussed. The calibration results and special test will also be presented in the following sections.

2.3.2 Calibration Facilities

End-Loaded Cylinder: Prior to shipment and installation of the VWSs at Stripa, 18 gauges were calibrated in a cylinder of Stripa granite 24 cm in diameter, as described by Schrauf et al. (1979) and shown in Fig. 2-11. The load was applied by means of a hydraulic actuator mounted to the upper platen of a large four-column load frame (not shown). The uniaxial load applied to the test sample was measured by a calibrated load cell mounted in the load string, above the upper granite endcap.

The endcaps provided thermal isolation, thus minimizing the temperature gradient in the granite sample during the calibrations at elevated temperatures. The entire granite sample, with the VWS installed, was heated by means of electrical heating tape in contact with the circumference of the cylinder.

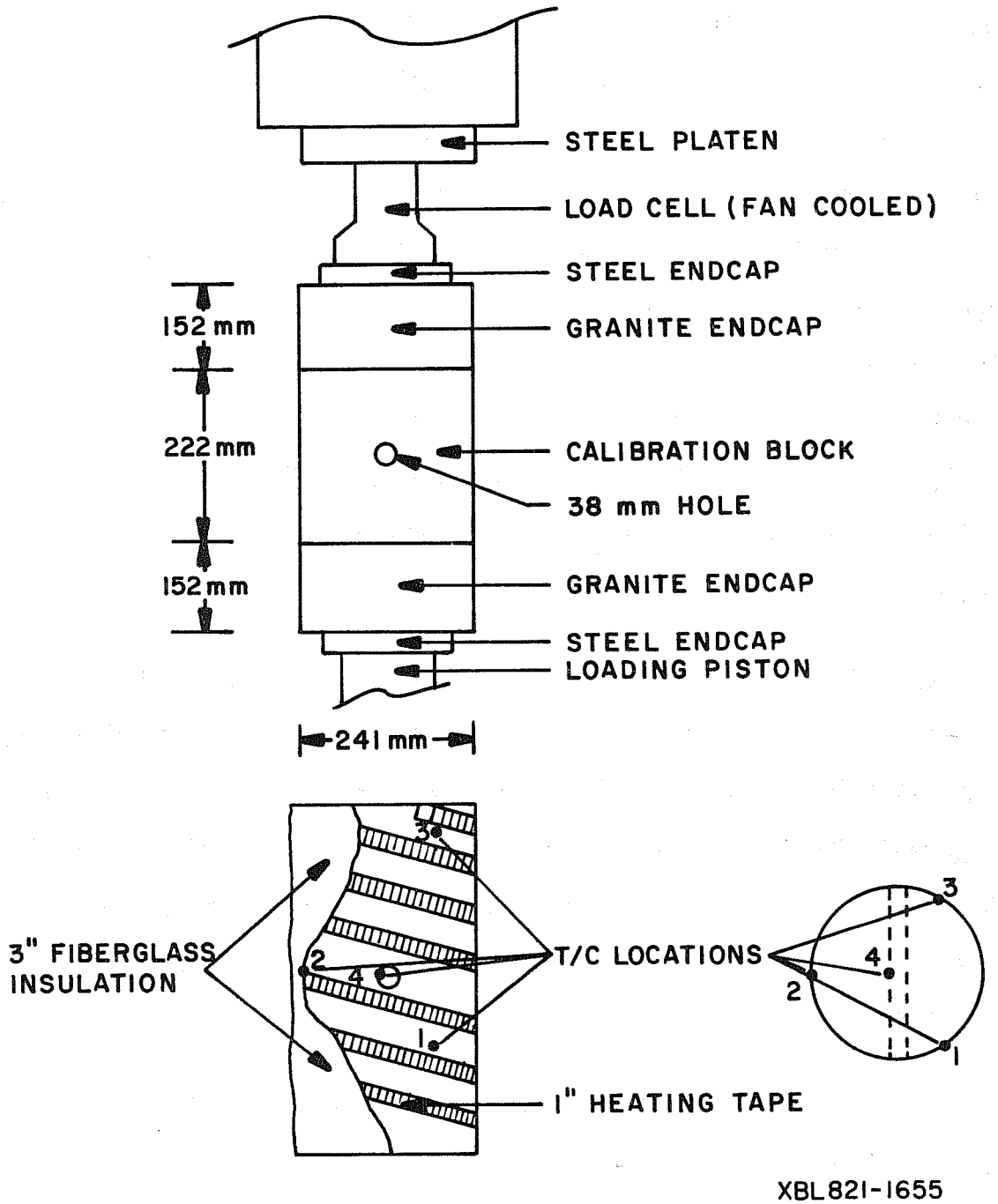

Fig. 2-11. End-loaded cylinder setup for VWS calibrations.

Two methods were used to determine the elastic modulus of the end-loaded cylinder of Stripa granite. One was from deformation measurements made with strain gauges mounted on the surface of the cylinder; the other was from deformation measurements made with a USBM gauge installed in the borehole. The cylinder-surface strain measurements indicate a Young's modulus of 64.8 GPa at room temperature, decreasing to 59.3 GPa at 88°C. These values are consistent with other measurements made on Stripa granite (Swan, 1978). However, the borehole deformation measurements show a very different characteristic. These measurements, as can be seen in Table 2-3, indicate a much lower value at comparable temperatures, a value that diminishes further with time, or more appropriately with increasing numbers of load cycles on the rock.

15-inch block at Stripa. At the conclusion of the heating experiments in Sweden, a calibration facility was constructed at a location approximately midway between the two full-scale heating experiments. The site was carefully selected to minimize the number of natural fractures intersecting the test block. Calibration at the field site has the advantage that an in situ block should be more representative of the intact rock mass than a sample that has been removed and transported.

The calibration facility at Stripa consisted of a 38-cm cube of granite loaded on opposite sides by means of flatjacks grouted in drilled slots as shown in Fig. 2-12. To determine the integrity of the selected location, the gauge borehole was cored and the core examined prior to line-drilling the slots. The block remained attached at the bottom; to prevent distortions

Table 2-3. Young's modulus of end-loaded cylinder of Stripa granite.

Measurement Technique	Measurements Taken in	Temperature °C	Young's Modulus E (GPa)
2	1977	22	37.2
1	1979	23	64.8
1	1979	88	59.3
2	1979	26	31.2
2	1979	28	31.0
2	1979	22	33.2
2	1979	22	33.3
2	1981	23	28.6
2	1981	23	29.0
2	1981	23	28.4
2	1981	23	28.0

1. Strain gauge bonded to surface of rock cylinder.

2. Calculated from borehole deformation measurements using the equation given by Obert and Duvall (1967).

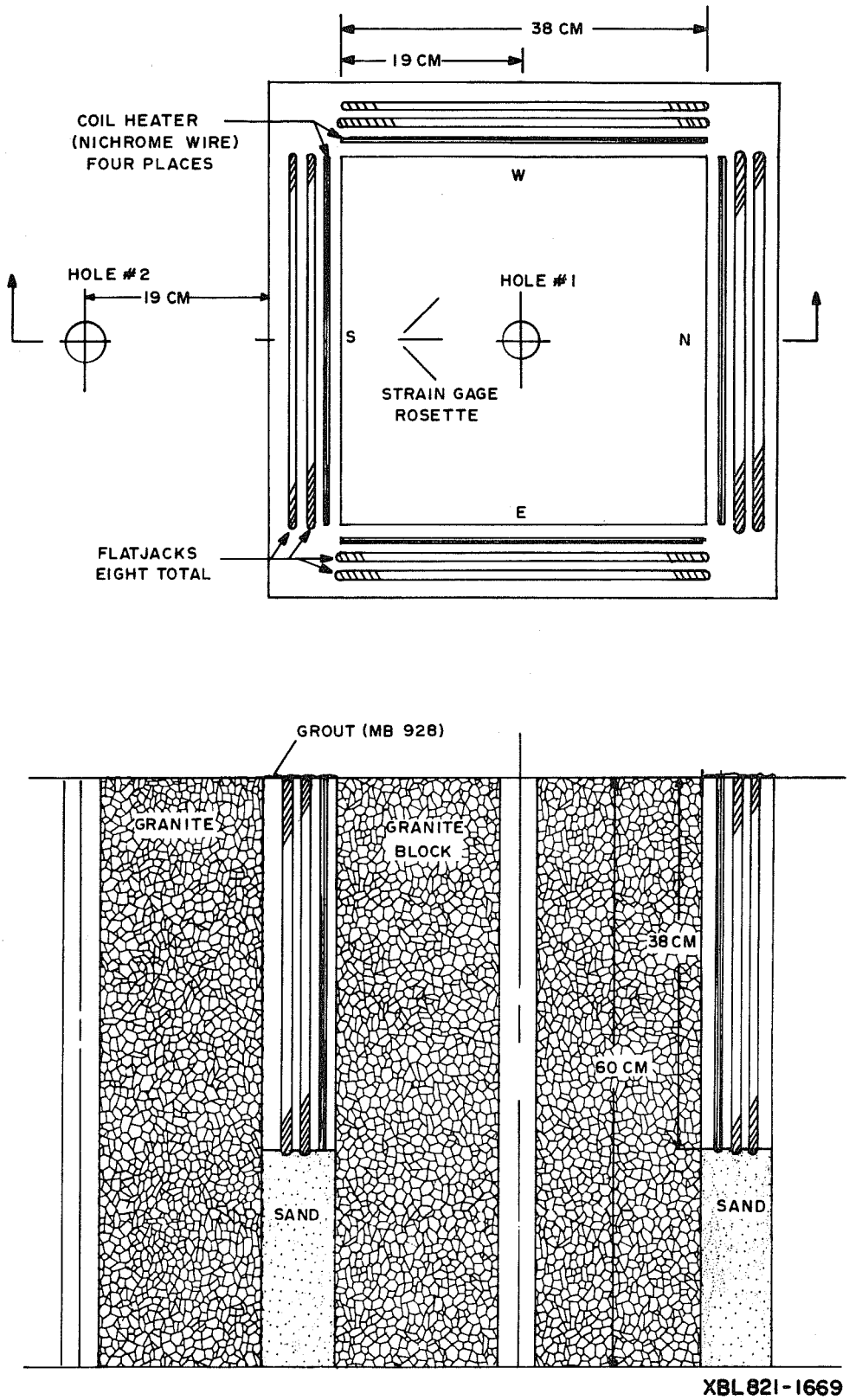

Fig. 2-12. Fifteen-inch block cut in floor of full-scale drift at Stripa. Gauges were calibrated by installing them in the center 38-mm borehole and pressurizing the flatjacks.

in the stress field, the slots were made deeper than the flatjacks and the excess filled with loosely packed sand prior to grouting. A high-modulus grout (83 GPa after a 28-day cure), Master Builders MB-928, was used. The four slots were labeled N, S, E, and W.

Heating capability was provided by Nichrome wire heating coils grouted into the slots as shown in Fig. 2-12. The first attempt to heat the block was hampered by a conductive path in the grout. This problem was self correcting as the grout cured.

Hole #2 (Fig. 2-12) was cored in order to do simultaneous gauge evaluations and stress-field studies; however, the allotted time elapsed before this work could be undertaken.

Very early in the calibration program, both flatjacks in the "E" slot failed. This somewhat limited the overall usefulness of the facility, but posed no problem for the VWS calibrations, which required uniaxial loading only.

Early attempts to obtain in situ stress and modulus data with measurements from strain-gauge rosettes bonded to the surface of the block were unsuccessful. This failure was attributed to the dislodging of a surface slab (about 2 cm) during the percussion drilling of the slots.

Elastic modulus measurements were made on the block using the USBM gauge at two different depths in the borehole. At 13 cm below the surface, Young's modulus was determined to be 63 GPa and, at 25 cm, 70 GPa. These values fall within the range measured by Swan (1978).

12-inch block. During the summer of 1980, VWS gauges were again calibrated at Terra Tek in a block of Stripa granite of dimensions 30.5 x 30.5 x 45.7 cm (12 x 12 x 18 inches). Figure 2-13 shows the biaxial test configuration which utilized flatjacks set within a steel retaining ring. For triaxial testing, the biaxial system was mounted in a frame where the load was applied along the axis of the borehole (Fig. 2-14).

The facility was equipped with heating coils to facilitate calibrations at elevated temperatures. The heating coil consisted of Nichrome wire wrapped around the outside of the slightly undersized block. Hydrostone grout was cast around the wire; this held the heating coil in place while providing electrical insulation from the flatjacks. The voltage to the heating coil was controlled by a variable transformer connected to the AC house power. To minimize the temperature gradient within the block, heating tape was wrapped around the retaining ring. The entire assembly was insulated with fiber glass. Four thermocouples were used to determine the thermal gradient in the block, one in the borehole (attached to the gauge being tested), and three others located in shallow drillholes (approximately 6 mm) across the top of the block. Gauges were tested one at a time in this facility.

Elastic properties were measured on core samples from the center borehole. Values for Young's modulus and Poisson's ratio were obtained at different confining pressures, as shown in Table 2-4.

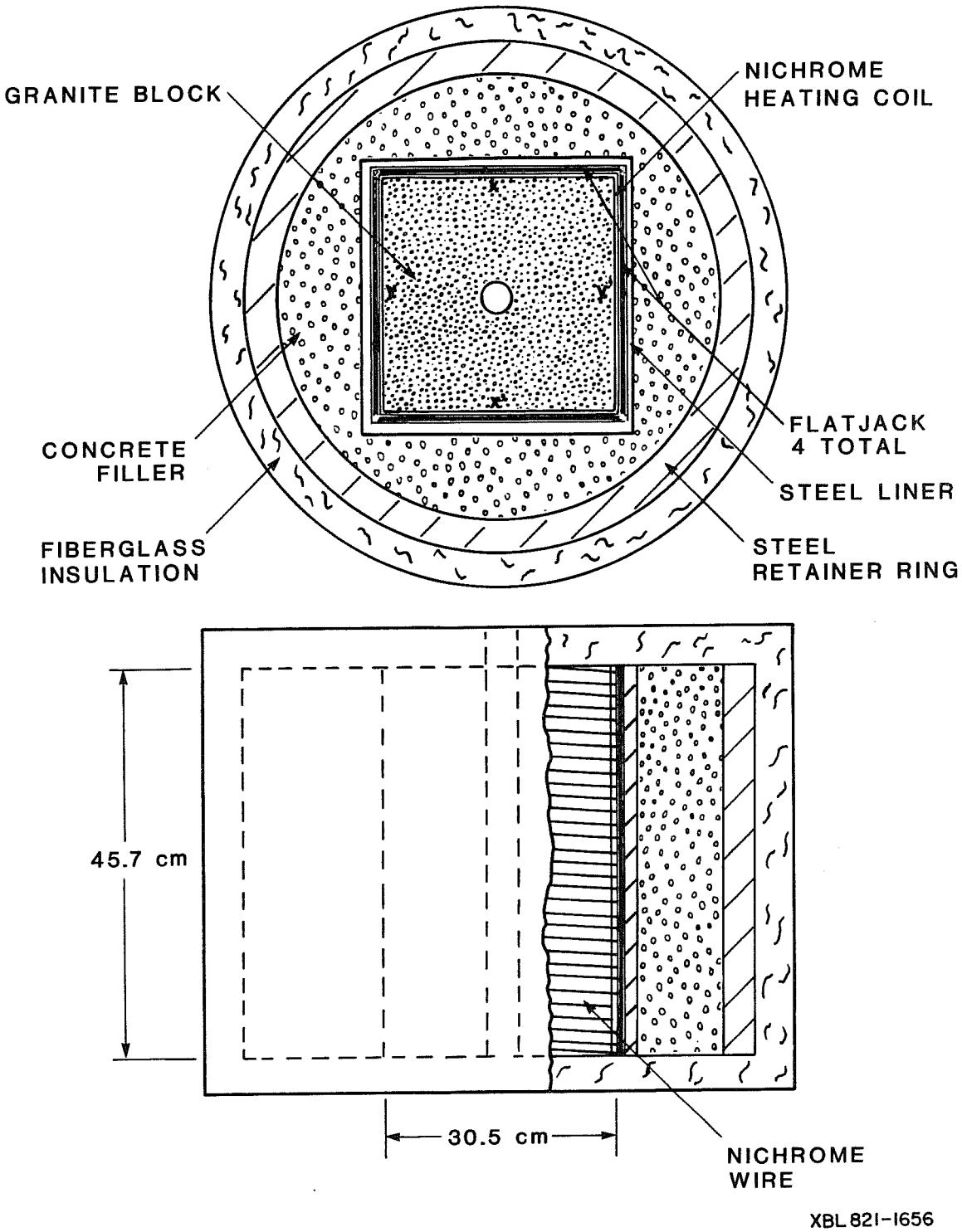

Fig. 2-13. Twelve-inch block of Stripa granite with biaxial loading and heating capabilities.

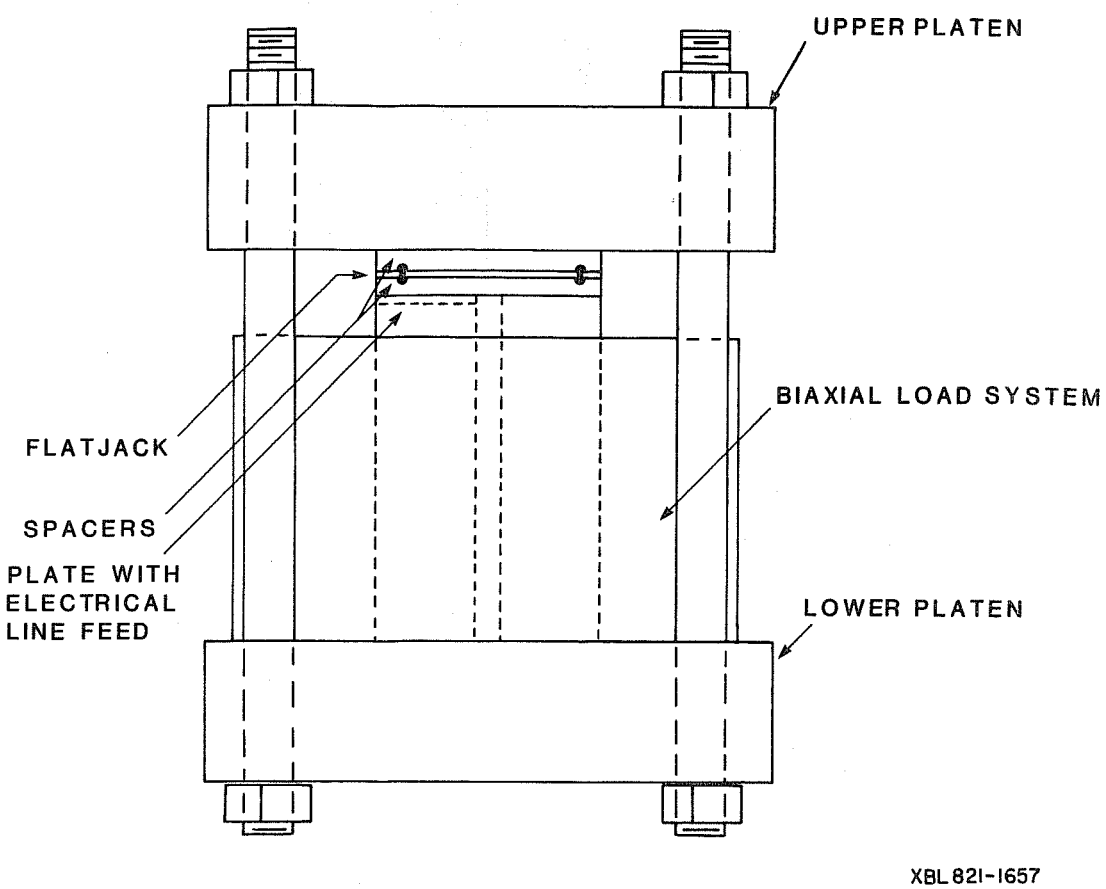

Fig. 2-14. Configuration for triaxial loading of 12-inch block.

Table 2-4. Elastic properties measured on cores from the 12-inch block.

Confining pressure		Young's modulus		Poisson's ratio
MPa	PSI	GPa	PSI x 10^6	
0	0	31.7	4.6	0.12
6.9	1000	60.7	8.8	0.21
20.7	3000	66.9	9.7	0.22

Borehole deformation measurements made on the 12-inch block using the USBM gauge revealed a large modulus anisotropy. The block was much stiffer (higher modulus of elasticity) when loaded along the x - x' axis than it was along the y - y' axis.

A method for deriving the anisotropic elastic properties from deformation measurements was reported by Becker (1968) and Becker and Hooker (1969). For a transversely isotropic (orthotropic) material, a measure of five elastic constants are required for a solution. Unfortunately, in the case of the calibration block, too few measurements were taken to characterize the anisotropy. However, from the standpoint of a gauge calibration facility, the apparent modulus as calculated from the equation given by Obert and Duvall (1967) is valid as far as uniaxial loading is concerned. It is only in the interpretation of biaxial or triaxial loading response that anisotropy causes a problem.

The values for Young's modulus were calculated from seven sets of deformation mesurements in each direction in the block. The average value obtained for the x-direction was 52.2 GPa with a standard deviation of 1.7 GPa. In the y-direction, the average was 36.9 GPa with a standard deviation of 2.67 GPa.

Radially Loaded Cylinder. The radially loaded cylinder calibration setup shown in Fig. 2-15 consists of a biaxial loading chamber (housing and bladder), pressure gauge, hand-actuated hydraulic pump, and associated plumbing. The system was manufactured by Rogers Arms and Machine Company, Inc. A cylinder of Stripa granite containing a borehole through its entire length was installed in the assembly. Gauges to be calibrated were installed one at a time in the borehole, and the rock was loaded hydrostatically by pressurizing the bladder. The entire assembly, excluding pressure gauge and pump, was installed in a controlled-temperature chamber for elevated temperature calibrations.

The three calibration facilities described in earlier sections, the end-loaded cylinder, the 15-inch block, and the 12-inch block were all uniaxial loading devices, whereas the radially loaded cylinder is a hydrostatic biaxial loading system. In order to convert the load to an equivalent uniaxial stress, the applied pressure was multiplied by a factor of 0.72 (Dutta et al., 1980).

A value of Young's modulus for the cylinder was obtained using measured borehole deformation data. The average value for seven measurements was 36.9 GPa, with a standard deviation of 2.3 GPa.

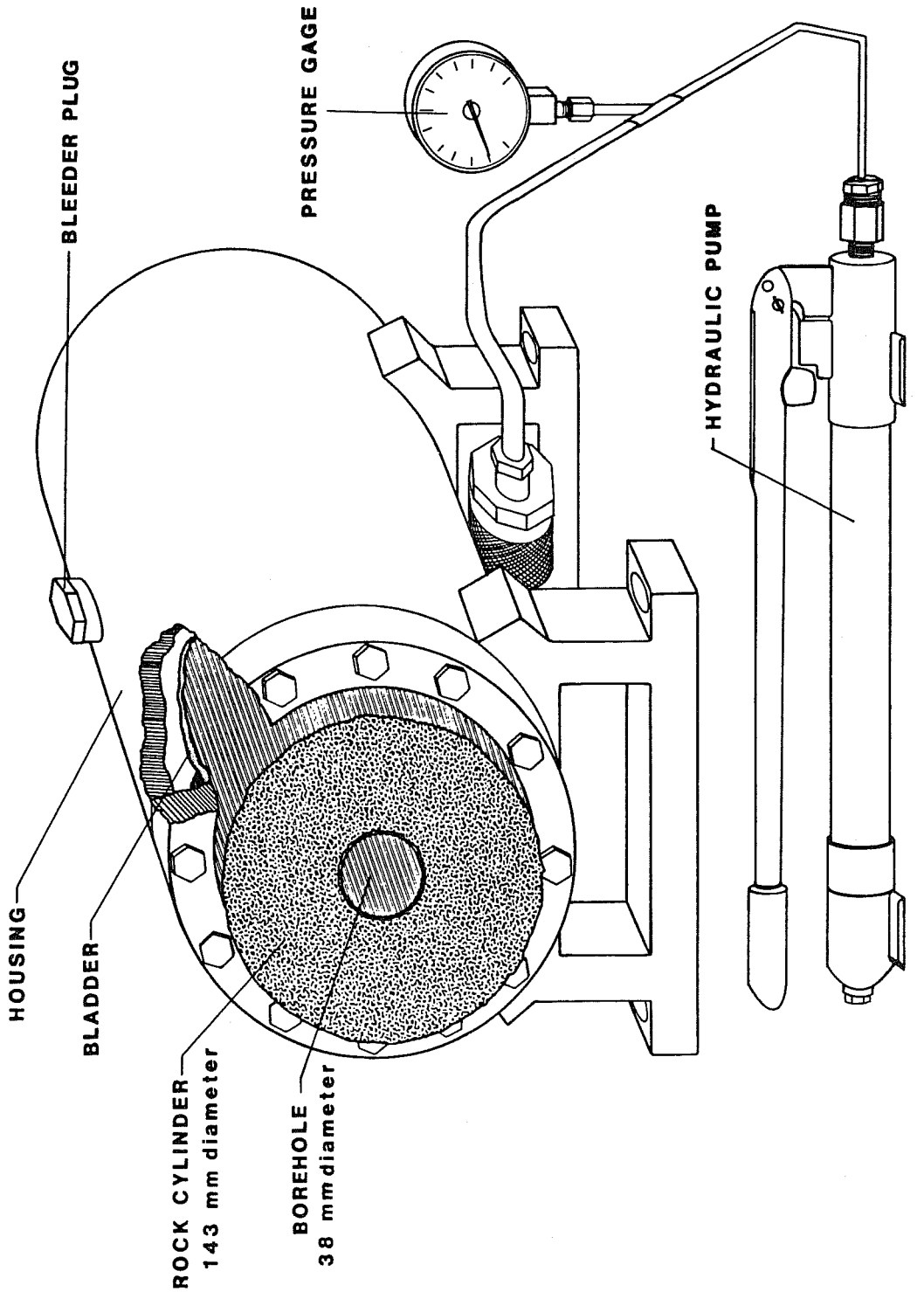

Fig. 2-15. Radially loaded cylinder calibration setup.

2.3.3 VWS Calibration Results

2.3.3.1. End-Loaded Cylinder Calibrations. Before installation at Stripa, 18 VWS gauges were calibrated in the end-loaded cylinder, including four runs at elevated temperature. The results presented and discussed by Schrauf et al. (1979), are reproduced here in Table 2-5 along with the calibration of two other gauges, J-40 and K-2, performed before their installation at mid-experiment.

The algorithm described by Schrauf et al. (1979) for reducing the VWS measurements to stress was based on the calibration data of Table 2-5. This algorithm, including the method for temperature compensation, is no longer considered valid for reducing the Stripa data. The main reasons are the low modulus of the cylinder, the scatter of the calibration data, and the incompleteness of the calibrations.

As an interim check on VWS performance and reliability, gauge C10Z (serial #3-45) was removed from operation during the experiment and returned for calibration at elevated temperatures (Table 2-6). Once installed in the end-loaded calibration cylinder, the gauge was never removed throughout the sequence of temperature changes and loading cycles. At each temperature, the block was loaded incrementally from 0 to 13.6 MPa; C_1 values were determined over the range 6.5 to 13.6 MPa. A "bedding-in" or seating effect is indicated by the change in periods recorded after the first installation, shown in the lower portion of Table 2-6.

Table 2-5. VWS gauge calibration results in end-loaded cylinder (Schrauf et al., 1979). Except as indicated under comments, each test included loading to 14 MPa and unloading to zero.

Gauge no.	Temp (°C)	ΔR	C_2	C_1 ($\times 10^9$)	Standard error (MPa)	Comments
3-18	23	107	60.03	-0.256	0.12	Max. load 7 MPa, load only
3-18	23	94	54.00	-0.226	0.08	Max. load 7 MPa, unload only
3-18	23	94	51.15	-0.213	0.19	
3-18	200	116	39.90	-0.170	0.14	Cool before unloading cycle
3-42	23	108	47.16	-0.305	0.18	Max. load 7 MPa
3-42	23	97	41.00	-0.260	0.24	
3-42	195	59	30.49	-0.190	0.03	
3-42	23	51	41.68	-0.253	0.32	
3-42	108	85	32.42	-0.205	0.12	
3-42	76	82	34.83	-0.219	0.16	
3-42	23	56	42.78	-0.262	0.34	
3-45	23	107	77.42	-0.414	0.13	Max. load 7 MPa
3-45	23	69	62.18	-0.321	0.12	
3-45	182	53	44.84	-0.228	0.06	
3-37	23	116	54.40	-0.234	0.03	Max. load 7 MPa
3-73	23	109	54.53	-0.234	0.11	Strain gauged for modulus erratic servo
3-73	23	105	54.69	-0.233	0.04	" "
3-73	88	122	45.70	-0.198	0.09	" "
3-73	120	119	44.33	-0.193	0.12	Strain gauge failed
3-73	155	109	45.90	-0.196	0.02	
3-73	190	100	46.84	-0.198	0.03	
3-77	23	92	71.51	-0.300	0.20	
3-74	23	91	68.53	-0.293	0.19	
3-62	23	76	71.78	-0.383	0.22	
3-71	23	79	68.88	-0.306	0.19	
3-92	23	108	45.72	-0.194	0.20	
3-80	23	-	92.01	-0.396	0.49	
3-82	23	81	72.18	-0.305	0.15	
3-90	23	94	84.40	-0.393	0.21	
3-71	23	86	63.26	-0.281	0.26	
3-50	23	75	67.17	-0.338	0.17	
3-68	23	98	58.62	-0.267	0.17	
3-16	23	92	67.86	-0.279	0.19	
3-37	23	97	58.38	-0.289	0.21	
3-36	23	98	67.17	-0.338	0.22	
3-54	23	89	66.90	-0.344	0.23	
J-40	23	162	56.48	-0.233		
K-2	23	200	53.04	-0.257		

Table 2-6. Calibrations of gauge C10Z (ser. #3-45) at elevated temperatures in end-loaded cylinder.

T(°C)	R_s	R_f	$C_1(10^9)$ Load Increasing	$C_1(10^9)$ Load Decreasing
23	2289	2266	-0.310	-0.289
81	2290	2289	-0.265	-0.254
142	2294	2297	-0.246	-0.229
110	2277	2283	-0.260	-0.232
81	2265	2273	-0.273	-0.248
51	2253	2259	-0.287	-0.263
21	2241	2245	-0.332	-0.294

Unloaded period (R_0)	2198
After first installation	2301
5 minutes after installation	2296
12 hours after installation	2289

Gauge C10Z was calibrated in a steel cylinder with the same configuration and dimensions as the granite cylinder. The Young's modulus calculated from borehole deformation measurements made at 26°C was 177 GPa. Gauge C10Z was calibrated with the transducer aligned with the load in the usual fashion, and repeated with the transducer aligned orthogonally to the load (Table 2-7). It is suspected that the gauge wedge slipped slightly during the load-unload cycle because the data form a piecewise linear curve when plotted as stress vs $1/R^2$.

The C_1 values shown in Table 2-7 are computed over intervals where the data are linear. Note that even in the steel cylinder the gauge reading changes 6 counts over a 3-1/2 hour period after installation and prior to loading.

2.3.3.2 Calibrations in 15-Inch Block at Stripa. Numerous problems were encountered during the initial calibration attempts. For example, totally erratic results were obtained when the gauges were installed with a preload to produce a change in the period of vibration of 100 units. (This was the value used for all laboratory calibrations in the end-loaded cylinder). All calibrations were subsequently carried out with a higher preload of approximately 150 units or above.

Another problem was "cross talk" between gauges, i.e., a change in reading of a gauge when the second gauge was installed in the hole. The cross talk was eliminated when the gauge spacing was increased to 12 cm, 6 cm above and below the center line of the flatjacks (the spacing between gauges installed in the heating experiments was approximately 11.5 cm).

Table 2-7. Calibration of gauge C10Z in end-loaded steel cylinder, parallel and perpendicular to uniaxial load.

Gauge C10Z aligned with load			Gauge C10Z perpendicular to load	
Unloaded	2198		Unloaded	2197
Installed	2380		Installed	2391
Installed + 1.5 hrs	2375		Installed + 15 hrs	2388
Installed + 3.5 hrs	2374			
Load (MPa)*	R	$C_1(10^9)$	Load (MPa)*	R
0	2374		0	2388
1.6	2384		1.7	2385
3.0	2399		3.0	2381
4.6	2413		4.6	2378
6.1	2427		6.1	2375
7.7	2240		7.7	2371
9.1	2452	-0.863	9.0	2368
10.7	2465		10.5	2366
12.1	2478		12.1	2363
13.7	2491		13.7	2360
12.2	2472		12.2	2363
10.6	2454		10.6	2366
9.1	2439		9.1	2369
7.6	2423		7.4	2372
6.1	2409	-0.735	6.1	2375
4.5	2394		4.5	2378
3.0	2381		3.0	2381
1.6	2368		1.5	2385
0	2357		0	2388

* Stress on gauge assumed to be equal to applied load.

A total of 26 gauges were calibrated in the block at an ambient temperature of about 12°C. Generally gauges were calibrated two at a time, with both aligned to sense the stress applied by the N-S flatjacks. Because of the observed change in the installed period (R_s) after the first load cycle (as much as 40 counts), all gauges were cycled once before data were recorded. The applied stress was taken to be equal to the measured pressure in the flatjacks, i.e., the efficiency of the flatjacks was assumed to be 100%.

The C_1 and C_2 values were calculated and are listed in Table 2-8. The first value listed for each gauge is the slope for increasing load and the second value is for decreasing load. Only the portion of the data between 6.9 MPa and 20.69 MPa was used to calculate C_1 and C_2. The repeats are from reinstalled gauges except as noted.

As mentioned previously, the calibration factors (C_1) obtained from these measurements differed substantially from those obtained using the end-loaded cylinder, as can be seen by comparing Tables 2-5 and 2-8. The average value of C_1 obtained in the 15-inch block at Stripa is -0.439×10^9, while the average from the cylindrical block is -0.281×10^9. This discrepancy led to another round of calibrations using the 12-inch block in the laboratory and will be discussed later.

2.3.3.3 Calibrations at Elevated Temperatures. The 15-inch block was heated by Nichrome wire embedded in the grout in each slot (Fig. 2-12). The wires were distributed uniformly across the width of the block and extended to a depth of 38 cm. These heater elements, connected in parallel, were hooked up to one of the controllers for the peripheral heaters in the H10 experiment.

Table 2-8. Calibration of 26 gauges in 15-inch block at Stripa. Entries on first line of each gauge are for increasing load, entries on second line are for decreasing load.

Gauge ID	Gauge Ser.#	Preset (ΔR)	C_1 (10^9)	C_2	Repeats: Preset (ΔR)	Repeats: C_1 (10^9)	Repeats: C_2
C1R	3-20	76	-.504	129.5	139	-.783(1)	187.8
C1R	3-20	76	-.485	125.9	139	-.783(1)	187.8
C1θ	3-22	134	-.406	95.3	149	- 776(1)	178.5
C1θ	3-22	134	-.388	92.1	149	-.769(1)	177.1
C3R	E-73	169	-.498	94.3	----	-----	-----
C3R	E-73	169	-.493	93.6	----	-----	-----
C3θ	E-56	209	-.508	93.0	----	-----	-----
C3θ	E-56	209	-.494	91.0	----	-----	-----
C4θ	E-62	184	-.623	114.0	----	-----	-----
C4R	E-62	184	-.609	111.9	----	-----	-----
C4θ	E-58	217	-.421	85.3	----	-----	-----
C4θ	E-58	217	-.415	84.5	----	-----	-----
C5R	E-50	170	-.481	95.0	162	-.474	94.5
C5R	E-50	170	-.478	94.7	162	-.486	96.3
C5θ	E-51	211	-.496	91.4	198	-.501	93.2
C5θ	E-51	211	-.491	90.8	198	-.514	95.0
C6Z	3-68	160	-.536	113.2	----	-----	-----
C6Z	3-68	160	-.550	115.5	----	-----	-----
C6θ	3-55	190	-.372	76.5	----	-----	-----
C6θ	3-55	190	-.366	75.8	----	-----	-----
C7Z	3-74	153	-.361	80.4	----	-----	-----
C7Z	3-74	153	-.362	80.7	----	-----	-----
C7θ	3-92	175	-.322	70.8	----	-----	-----
C7θ	3-92	175	-.325	71.2	----	-----	-----
C8Z	3-58	164	-.417	86.3	*159	-.415	86.2
C8Z	3-58	164	-.413	85.6	159	-.413	85.9
C8θ	3-90	171	-.475	98.0	161	-.468	97.3
C8θ	3-90	171	-.462	95.9	161	-.466	97.0

Continued on next page

Table 2-8. Continued

Gauge ID	Gauge Ser.#	Preset (ΔR)	C_1 (10^9)	C_2	Repeats Preset (ΔR)	Repeats C_1 (10^9)	Repeats C_2
C9R	J-40	172	-.402	94.5	119	-.405	100.7
C9R	J-40	172	-.392	92.5	119	-.401	99.0
C9Θ	K-2	193	-.353	73.5	169	-.344	73.8
C9Θ	K-2	193	-.353	73.4	169	-.331	71.8
C10Z	3-42	214	-.437	64.9	----	----	----
C10Z	3-42	214	-.439	65.1	----	----	----
C10Θ	E-69	186	-.349	61.0	----	----	----
C10Θ	E-69	186	-.345	60.7	----	----	----
C11Z	3-37	229	-.403	73.6	221	-.398	73.4
C11Z	3-37	229	-.398	72.9	221	-.401	73.8
C11Θ	3-1	164	-.408	78.1	146	-.395	76.7
C11Θ	3-1	164	-.393	76.1	146	-.397	77.0
C12Z	3-43	367	-.355	55.7	151	-.674	127.7
C12Z	3-43	367	-.356	55.7	151	-.663	123.2
C12Θ	3-48	160	-.489	82.5	160	-.404	68.7
C12Θ	3-48	160	-.482	81.6	160	-.400	68.2
C14Z	3-29	181	-.394	85.4	187	-.485	104.0
C14Z	3-29	181	-.398	86.1	187	-.485	104.0
C14Θ	3-9	108	-1.190(1)	267.0	222	-.436	88.6
C14Θ	3-9	108	-1.043(1)	236.0	222	-.434	88.5
C15Z	3-36	215	-.454	83.9	211	-.452	83.7
C15Z	3-36	215	-.456	84.2	211	-.456	84.3
C15Θ	3-50	190	-.478	91.1	424	-.401	63.4
C15Θ	3-50	190	-.475	90.6	424	-.386	61.8

*Repeat without reinstallation
(1) Excluded from average

Unfortunately, a leakage path to the ground through the grout reduced the current that could be supplied to the wires, so that only a 26°C temperature increase could be attained. Temperature was monitored by a thermocouple at the midplane in the gauge borehole.

Two gauges were calibrated at elevated temperatures in the 15-inch block. Gauges C5Θ and C5R were installed 13 and 25 cm below the surface of the block and calibrated at three temperatures above ambient (Table 2-9). The gauges were installed twice; once for the first calibration at 12.5°C and again for the second 12.5°C run. After this they were left in position for all subsequent calibrations. As in the other calibrations, both gauges were aligned in the NS direction and loaded with the NS flatjacks. For the elevated temperature calibrations, a low pressure (0.7 MPa) was maintained on the W flatjack to improve the thermal conductivity from the heater coil to the block.

2.3.3.4 12-Inch Block Calibrations. Four types of measurements were made on on VWSs using the 12-inch block facililty at Terra Tek.

1. The calibration coefficients C_1 and C_2 were determined at ambient temperature with the starting period R_S set as close as possible to the values when the gauges were installed in the heating experiments at Stripa.
2. The effect of different installation periods (R_S) on the slope C_1 was studied by reinserting the same gauge at different setting pressures.
3. Triaxial load tests were performed.
4. Calibrations were made at temperatures above ambient.

Each of these tests is discussed below.

Table 2-9. Calibrations of VWS gauges C5Θ and C5R at elevated temperatures in 15-inch block at Stripa.

Gauge	T(°C)	R_s	R_f	C_1 (10^9) Load Increasing	C_1 (10^9) Load Decreasing
C5Θ	12.5	2342	2332	-0.496	-0.491
C5R	12.5	2258	2254	-0.481	-0.478
C5Θ	12.5	2329	-	-0.514	-0.509
C5R	12.5	2250	-	-0.474	-0.486
C5Θ	19.3	2370	2375	-0.509	-0.523
C5R	19.3	2290	2293	-0.481	-0.495
C5Θ	28.9	2393	2393	-0.507	-0.515
C5R	28.9	2309	2310	-0.478	-0.486
C5Θ	38.5	2410	2410	-0.509	-0.504
C5R	38.5	2325	2325	-0.478	-0.475

Unloaded period (Ro) C5Θ (E-51): 2131
C5R (E-50): 2088

2.3.3.5 Ambient temperature calibration. Calibrations were done one gauge at a time in the 12-inch block. The block was preloaded uniaxially in the x-direction with the flatjacks pressurized to 6.9 MPa (1000 psi). The gauge was then aligned in the x-direction and installed in the center of the block. The set period (R_S) was made as close as possible to the value established in the Stripa experiments. The period R was recorded as the load increased to 20.7 MPa (3000 psi) and decreased back to 6.9 MPa in steps of 3.45 MPa (500 psi). With a least-squares curve-fitting routine, a line was fit to the stress vs $1/R^2$ data over the stress range 6.9 MPa to 20.7 MPa. The fit of the line was generally excellent, with correlation coefficient (r) never less than 0.99.

These data are tabulated in Table 2-10. Each entry represents a complete calibration, with the gauge removed and reinstalled between runs. The calibration of each gauge was repeated one or more times.

2.3.3.6 Calibrations with different ΔR values. Previous calibrations had indicated that C_1 was not totally independent of the stress applied to the gauge during wedge seating, which is indicated by the value of ΔR ($R_S - R_O$), the change in gauge period. Tests were run in the 12-inch block during the summer of 1980 to examine this possible dependence. Four gauges were tested by sequentially installing, loading, removing, and reinstalling them at different preset values. Data were recorded for both increasing and decreasing load after insertion into the block, which was prestressed uniaxially in the x-direction to 6.9 MPa. Almost all calibrations were repeated, giving two calibrations at comparable preset levels, as shown in Table 2-11. The initial periods for each gauge are given at the top of the table.

Table 2-10. Calibration of 27 gauges in 12-inch block of Stripa granite at Terra Tek. First line entries for each gauge are for increasing load, second line for decreasing load.

Gauge Label	Gauge Ser.#	ΔR		C_1	C_2	Repeats					
		Exp.	Calib.	(10^9)		ΔR Calib.	C_1 ($x10^9$)	C_2	ΔR Calib.	C_1 (10^9)	C_2
C1R	3-20	156	157	-.434	101.3	155	-.415	96.9	----	-----	-----
C1R	"	"	"	-.400	94.5	"	-.383	90.5	----	-----	-----
C1θ	3-22	127	129	-.501	117.0	127	-.525	123.2	----	-----	-----
C1θ	"	"	"	-.453	107.3	"	-.466	110.8	----	-----	-----
C3R	E-73	216	217	-.476	85.2	215	-.476	85.3	----	-----	-----
C3R	"	"	"	-.430	78.5	"	-.436	79.7	----	-----	-----
C3θ	E-56	373	373	-.418	65.3	375	-.433	67.6	----	-----	-----
C3θ	"	"	"	-.383	61.0	"	-.392	62.6	----	-----	-----
C4R	E-62	130	133	-.753	142.2	131	-.686	129.8	----	-----	-----
C4R	"	"	"	-.651	125.1	"	-.607	116.7	----	-----	-----
C4θ	E-58	373	373	-.351	61.3	368	-.341	59.9	----	-----	-----
C4θ	"	"	"	-.318	57.0	"	-.318	56.9	----	-----	-----
C5R	E-50	277	276	-.435	77.5	277	-.410	73.0	----	-----	-----
C5R	"	"	"	-.396	71.9	"	-.376	68.2	----	-----	-----
C5θ	E-51	208	207	-.546	99.8	208	-.530	96.8	----	-----	-----
C5θ	"	"	"	-.484	90.3	"	-.483	89.7	----	-----	-----
C6Z	3-68	233	233	-.385	75.3	232	-.497	97.2	232	-.451	88.5
C6Z	"	"	"	-.352	70.3	"	-.443	88.4	"	-.407	81.3
C6θ	3-55	232	223	-.398	78.2	233	-.386	75.0	----	-----	-----
C6θ	"	"	"	-.367	73.3	"	-.355	70.3	----	-----	-----
C7Z	3-74	210	209	-.418	86.9	209	-.412	85.5	----	-----	-----
C7Z	"	"	"	-.382	80.6	"	-.381	80.4	----	-----	-----
C7θ	3-92	188	187	-.416	89.0	186	-.412	88.1	----	-----	-----
C7θ	"	"	"	-.380	82.6	"	-.386	83.7	----	-----	-----
C8Z	3-58	198	197	-.450	88.8	197	-.467	92.3	----	-----	-----
C8Z	"	"	"	-.418	83.6	"	-.435	87.2	----	-----	-----
C8θ	3-90	204	204	-.439	86.4	204	-.485	95.5	----	-----	-----
C8θ	"	"	"	-.407	81.2	"	-.441	88.2	----	-----	-----
C9θ	J-40	154	154	-.491	115.9	155	-.508	119.9	----	-----	-----
C9R	"	"	"	-.441	105.6	"	-.452	108.3	----	-----	-----
C9θ	K-2	"	"	-.414	84.7	197	-.428	88.0	----	-----	-----
C9θ	"	"	"	-.388	80.4	"	-.401	83.4	----	-----	-----

Table 2-10. Continued

Gauge Label	Gauge Ser.#	ΔR Exp.	ΔR Calib.	C_1 (10^9)	C_2	Repeats ΔR Calib.	Repeats C_1 ($x10^9$)	Repeats C_2	Repeats ΔR Calib.	Repeats C_1 (10^9)	Repeats C_2
C10Z	3-42	218	217	-.483	69.5	216	-.501	72.2	----	-----	-----
C10Z	"	"	"	-.452	66.1	"	-.465	68.2	----	-----	-----
C10Θ	E-69	262	262	-.527	85.3	262	-.488	79.1	----	-----	-----
C10Θ	"	"	"	-.485	79.8	"	-.447	73.7	----	-----	-----
C11Z	3-37	185	182	-.509	94.7	186	-.526	97.6	----	-----	-----
C11Z	"	"	"	-.478	89.8	"	-.483	90.9	----	-----	-----
C11Θ	3-1	187	189	-.527	97.7	187	-.519	96.5	----	-----	-----
C11Θ	"	"	"	-.488	91.7	"	-.481	90.4	----	-----	-----
C12Z	3-43	181	182	-.444	79.4	180	-.455	81.5	----	-----	-----
C12Z	"	"	"	-.409	74.4	"	-.430	78.0	----	-----	-----
C12Θ	3-48	225	221	-.433	68.4	229	-.467	73.5	226	-.513	80.7
C12Θ	"	"	"	-.393	63.6	"	-.429	68.8	"	-.464	74.5
C12Θ	3-48	225	--	----	----	222	-.601	94.9	223	-.663	104.6
C12Θ	"	"	--	----	----	"	-.547	87.8	"	-.574	92.6
C14R	3-29	156	156	-.456	100.0	156	-.507	110.9	----	-----	-----
C14R	"	"	"	- 421	93.3	"	-.459	102.0	----	-----	-----
C14Θ	3-9	189	192	-.467	96.3	185	-.433	96.6	184	-.429	95.9
C14Θ	"	"	"	-.460	95.2	"	-.408	92.4	"	-.395	90.0
C14Θ	3-9	189	--	----	----	186	-.400	89.7	192	-.402	89.8
C14Θ	"	"	--	----	----	"	-.375	85.5	"	-.377	85.7
C14Θ	3-9	189	--	----	----	186	-.516	106.9	187	-.592	122.3
C14Θ	"	"	--	----	----	"	-.456	96.0	"	-.546	114.1
C14Θ	3-9	189	--	----	----	183	-.456	94.7	188	-.443	91.5
C14Θ	"	"	--	----	----	"	-.421	88.8	"	-.410	85.9
C14Θ	3-9	189	--	----	----	187	-.443	91.8	---	-----	----
C14Θ	"	"	--	----	----	"	-.406	85.3	---	-----	----
C15Z	3-36	185	186	-.475	88.5	182	-.481	90.0	----	-----	-----
C15Z	"	"	"	-.445	84.0	"	-.446	84.6	----	-----	-----
C15Θ	3-50	210	209	-.535	97.8	211	-.526	96.0	----	-----	-----
C15Θ	"	"	"	-.480	89.5	"	-.473	88.0	----	-----	-----
--	3-42	227	226	-.479	81.5	227	-.442	71.9	225	-.384	65.8
	"	"	"	-.440	76.2	"	-.396	68.4	"	-.366	63.5

Table 2-11. Calibrations of four gauges at different preset values, performed in the 12-inch block. The first line for each preset entry is for increasing load, the second for decreasing load.

Gauge C3R (E-73) Ro - 2143			Gauge C7Θ Ro = 1975			Gauge C9Θ Ro = 2008			Gauge C14Θ Ro = 2004		
ΔR	C_1 (10^9)	C_2	ΔR	C_1 (10^9)	C_2	ΔR	C_1 (10^9)	C_2	ΔR	C_1 (10^9)	C_2
151	-.515	97.6	150	-.495	109.7	151	-.447	95.7	151	-502	107.4
"	-.479	92.0	"	-.464	103.9	"	-.422	91.4	"	-.428	93.6
147	-.511	97.2	150	-.465	103.0	149	-.439	94.1	185	-.434	90.0
"	-.464	89.3	"	-.436	97.7	"	-.416	90.0	"	-.409	85.7
176	-.474	87.9	175	-.412	89.0	173	-.503	105.5	184	-.429	89.9
"	-.435	82.1	"	-.386	84.4	"	-.450	95.8	"	-.394	83.0
176	-.497	92.1	170	-.390	84.8	175	-.384	80.3	186	-.399	82.5
"	-.463	87.0	"	-.366	80.6	"	-.356	75.6	"	-.374	79.4
199	-.502	91.2	199	-.372	78.6	199	-.393	80.5	188	-.443	91.5
"	-.453	83.9	"	-.345	74.2	"	-.369	76.5	"	-.410	85.9
199	-.438	79.7	199	-.431	91.1	203	-.423	86.4	187	-.443	91.8
"	-.411	75.9	"	-.396	84.7	"	-.392	81.3	"	-.406	85.3
221	-.493	88.0	227	-.406	83.7	222	-.422	84.5	192	-.467	96.3
"	-.448	81.4	"	-.377	78.8	"	-.388	79.1	"	-.460	95.2
225	-.409	72.8	225	-.371	76.6	221	-.363	73.0	192	-.403	83.0
"	-.386	69.7	"	-.349	73.1	"	-.343	69.7	"	-.376	78.5
249	-.408	71.0	249	-.398	80.6	250	-.326	63.8	223	-.334	67.5
"	-.376	66.8	"	-.369	75.8	"	-.309	61.3	"	-.298	61.8
249	-.403	70.2	250	-.356	72.0	250	-.372	72.9	260	-.318	61.6
"	-.366	65.2	"	-.331	67.9	"	-.344	68.5	"	-.308	60.0
274	-.386	65.7	275	-.380	75.1	276	-.342	65.3			
"	-.350	61.2	"	-.354	71.0	"	-.322	62.5			
272	-.387	66.2	275	-.374	73.8	273	-.360	69.1			
"	-.353	61.8	"	-.346	69.6	"	-.334	65.3			
296	-.369	61.8	300	-.380	73.4	299	-.324	61.0			
"	-.336	57.7	"	-.353	69.2	"	-.305	58.1			
296	-.416	69.7	298	-.351	67.9	301	-.364	68.0			
"	-.376	64.6	"	-.327	64.3	"	-.340	64.6			

Table 2-11 shows that C_1 decreases (gauge sensitivity increases) with increasing values of ΔR, or setting pressure. In searching for the cause of this dependence, imprints were made of the contact between the gauge and the borehole wall by placing a sandwich of carbon paper and paper between the gauge and rock. The gauge was set and released and the imprints retrieved. (Calibrations were not run with the carbon paper in place because the wedge tended to slip.) An example of the imprints is shown in Fig. 2-16. For this gauge, contact area increases gradually as ΔR increases up to 150, after which little change is seen. This change in contact could easily influence the sensitivity of the gauge.

As the work with imprints progressed, more care was taken when setting the gauge to assure proper alignment and contact. Two gauges were tested again to see if the dependence on setting pressure persisted. The results, shown in Table 2-12, are inconclusive. Gauge C11Z still shows the dependence while C7Θ shows somewhat erratic behavior, but the scatter in the value for C_1 was less than in the previous test (Table 2-11), indicating better seating. The difference between the period after (R_f) and before (R_s) during the load cycle is also given in Table 2-12. Since these differences are all small, it is surmised that there was little "settling in" of the gauge during the load cycle. However, there is a definite trend toward a bigger change with increasing ΔR (increase in installation preload), which might be an indication of increased localized rock damage. The only known difference between the conditions for these measurements and those made earlier, besides extra care in setting, was that the block was preloaded biaxially instead of uniaxially.

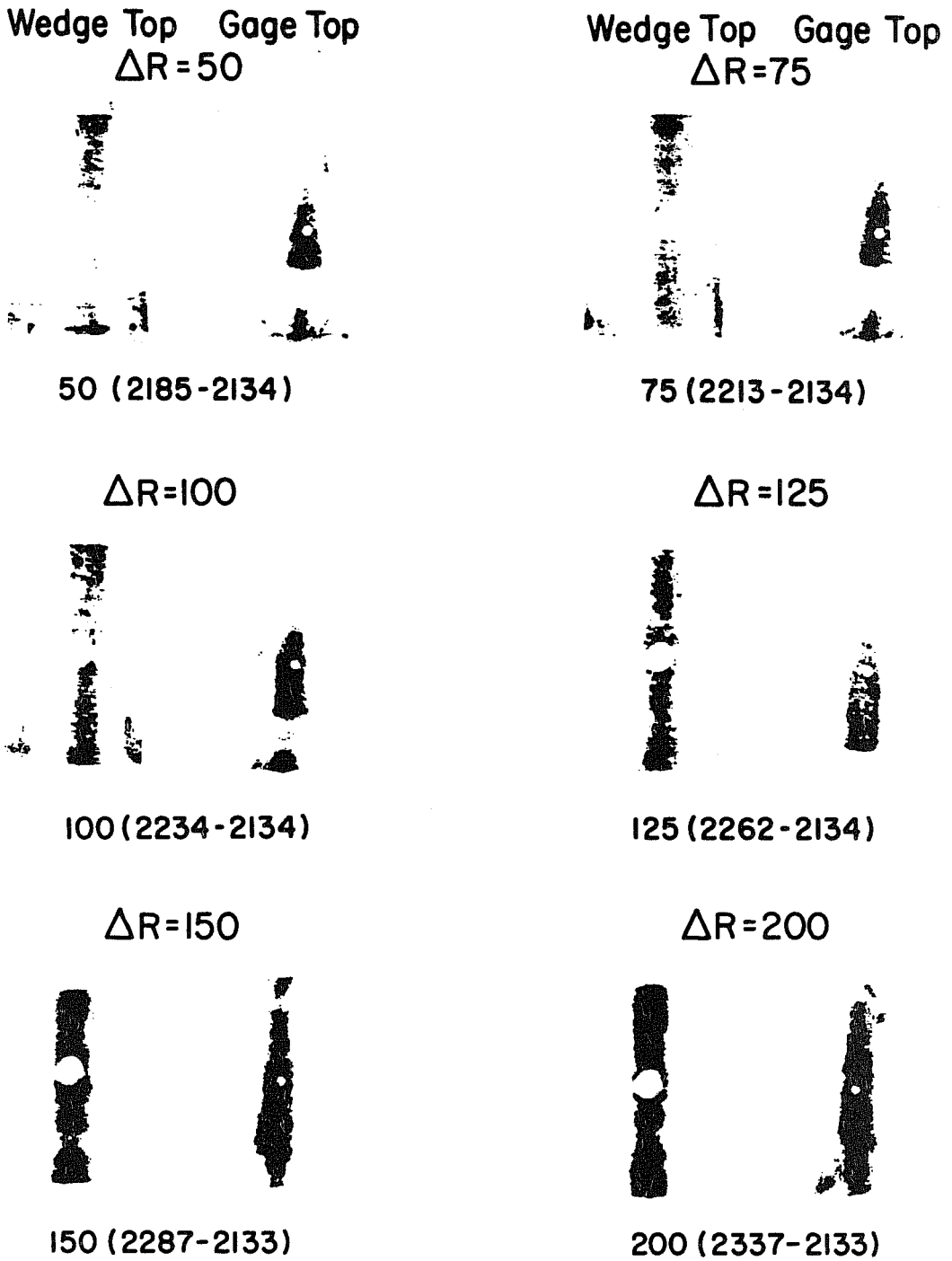

Fig. 2-16. Imprints of wedge and gauge seating made with carbon paper on paper. Gauge C11Z was installed in the x-direction of the 12-inch block. ΔR values are the difference between setting period and initial period.

Table 2-12. Calibrations of two gauges at four preset values, performed in the 12-inch block. Calibrations were preceded by carbon paper imprints to indicate contact area. Gauges were oriented in the x-direction in the block.

Gauge	R_o counts	ΔR counts	$(R_f - R_s)$ counts	$(R_o^{-2} - R_s^{-2})$ (10^{-9})	C1 (10^9) Load increasing	C1 (10^9) Load decreasing
C11Z	2134	100	-5	19.2	-0.724	-0.684
		151	-6	28.1	-0.430	-0.411
		193	-8	34.9	-0.393	-0.376
		253	-13	44.1	-0.337	-0.318
C7Θ	1976	102	-5	24.5	-0.363	-0.347
		150	-10	34.9	-0.368	-0.346
		202	-9	45.3	-0.392	-0.367
		255	-13	55.2	-0.302	-0.284

2.3.3.7 Triaxial load test. To evaluate the response of a gauge under triaxial load conditions, the 12-inch block with its retaining ring and orthogonal flatjacks was placed in the loading frame shown in Fig. 2-14. The data obtained is given in Table 2-13. Gauge C11Z was first installed in the x-plane and the block was sequentially loaded in the x, y, and z planes. It was reinstalled in the y-plane and the block was sequentially loaded in the y, x, and z planes. The table indicates the order in which the load-unload cycles were performed in each of the three orthogonal directions. The gauge remained in place throughout each three-cycle sequence. The C_1 coefficient is computed only for the data acquired with the gauge aligned with the direction of applied stress. When the load is increased from 0 to 17.2 MPa in the z-direction, the period increased 10 counts with the x-alignment, but decreased 24 counts with the y-alignment, clearly indicating the block anistropy discussed earlier.

2.3.3.8 Calibration at elevated temperatures. Two gauges were calibrated at elevated temperatures in the 12-inch block. The block was initially loaded with flatjack pressures of 6.9 MPa (1000 psi) in both the x and y directions. After the block was heated to the desired test temperature, the gauge was installed in the x-direction. Stress along the x-direction was increased to 17.2 MPa in steps of 1.72 MPa, while stress in the y-direction was held constant at 6.9 MPa by bleeding or pressurizing the y-direction flatjacks as required. After each run, the gauge was removed, the block heated or cooled to another temperature, and the gauge reinstalled.

Table 2-13. Calibration of gauge C11Z in 12-inch block under triaxial load.

Aligned in x-direction
R_o = 2133

Pressure (MPa) x	y	z	R	C_1	Pressure (MPa) x	y	z	R
6.90	6.90	0	2318		6.90	6.90	0	2313
8.63	↓	↓	2342		↓	↓	1.73	2317
10.35			2370				3.45	2319
12.08			2401	-0.390×10^9			5.18	2320
13.80			2433				6.90	2321
15.53			2467				8.63	2321
17.25			2501				10.35	2322
15.53			2465				12.08	2322
13.80			2431				13.80	2322
12.08			2398	-0.384×10^9			15.53	2323
10.35			2368				17.25	2323
8.63			2339				15.53	2323
6.90	6.90	0	2315				13.80	2322
↓	8.63	↓	2302				12.08	2322
	10.35		2291				10.35	2322
	12.08		2281				8.63	2321
	13.80		2272				6.90	2320
	15.53		2264				5.18	2319
	17.25		2257				3.45	2319
	15.53		2264				1.73	2318
	13.80		2271		6.90	6.90	0	2318
	12.08		2279					
	10.35		2290					
	8.63		2301					
6.90	6.90	0	2313					

Continued on next page

Aligned in y-direction
R_o = 2134

Pressure (MPa) x	y	z	R	C_1	Pressure (MPa) x	y	z	R
6.90	6.90	0	2326		6.90	6.90	6.90	2310
	8.63		2368				1.73	2305
	10.35		2417				3.45	2303
	12.08		2470	-0.243×10^9			5.18	2301
	13.80		2524				6.90	2299
	15.53		2586				8.63	2297
	17.25		2648				10.35	2296
	15.53		--				12.08	2294
	13.80		2520				13.80	2292
	12.08		2468				15.53	2289
	10.35		2410	-0.234×10^9			17.25	2286
	8.63		2360				15.53	2287
6.90	6.90	0	2315				13.80	2288
8.63			2300				12.08	2288
10.35			2289				10.35	2289
12.08			2278				8.63	2290
13.80			2265				6.90	2291
15.53			2254				5.18	2292
17.25			2245				3.45	2293
15.53			2253				1.73	--
13.80			2263		6.90	6.90	6.90	2301
12.08			2274					
10.35			2285					
8.63			2297					
6.90	6.90	0	2310					

On the sixth temperature run, when gauge C11Z was under test at 127°C, one of the flatjacks in the x-direction failed. As a result, the entire sequence of temperature calibration runs was repeated with the gauge oriented in the y-direction. Because of the failed flatjack, the block could not be confined in the x-direction. The data are given in Table 2-14 with the load conditions noted.

As noted above, the gauge was installed after the block temperature had equilibrated at the specified temperatures. An attempt was also made to allow the gauge to come to the same temperature before installation. However, some temperature changes probably occurred during the load cycle, as indicated by the increase in the $(R_f - R_s)$ value (this value usually decreased during room temperature tests). This increase in apparent stress is probably due to the difference in coefficient of thermal expansion of the gauge and the rock. The increase in the gauge reading after (and probably during) the load cycle accounts for the increase in the C_1 value for the decreasing load, compared to the value for increasing load. All room temperature calibrations show the opposite effect.

There was also a trend toward decreasing C_1 with increasing temperature. This is consistent with the trend reported by Schrauf et al. (1979) and is probably due to the decreasing Young's modulus with temperature (Swan, 1978).

2.3.3.9 Radially-Loaded Cylinder Calibrations. Two gauges, C7Θ and C11Z, were calibrated in the radially-loaded cylinder as a function of temperature. These data are summarized in Table 2-15. Each gauge was reinstalled in the cylinder at the indicated temperature, prior to the load cycle. A constant

Table 2-14. Calibration of two VWS gauges at different temperatures in the 12-inch block.

Gauge	Gauge orientation in block	Load in perp. dir. (MPa)	T(°C)	ΔR	R_f-R_s counts	$C_1(10^9)$ Load increasing	$C_1(10^9)$ Load decreasing
C7Θ	x	6.9	81	192	+10	-0.317	-0.339
		6.9	113	177	+29	-0.254	-0.298
		6.9	126	187	+20	-0.278	-0.309
C11Z	x	6.9	82	187	+2	-0.384	-0.390
		6.9	106	187	+12	-0.320	-0.340
		6.9[a]	127	186	-	-0.260	[a]
C7Θ	y	0	24	188	+8	-0.246	-0.253
		0	48	189	+11	-0.239	-0.250
		0	94	190	+18	-0.236	-0.252
		0	126	194	+21	-0.212	-0.231
		0	131	190	+32	-0.216	-0.252
C11Z	y	0	24	188	-3	-0.301	-0.294
		0	46	186	+2	-0.259	-0.258
		0	95	187	+32	-0.277	-0.284
		0	133	189	+25	-0.264	-0.291
		0	127	187	+19	-0.255	-0.276

[a]X-oriented flatjack failed during this test.

Table 2-15. Calibration of two gauges installed in radially-loaded cylinder at different temperatures.

Gauge and (Ro)	Preload (MPa)	T(°C)	R_s	$(R_f - R_s)$	C_1 (10^9) Increasing load	C_1 (10^9) Decreasing load
C11Z (2134)	3.45	50	2306	+5	-0.320	-0.335
		50	2330	-4	-0.369	-0.358
		100	2330	+2	-0.321	-0.329
		130	2330	-3	-0.324	-0.321
		50	2331	+16	-0.260	-0.286
		50	2329	+8	-0.292	-0.308
		18	2331	+6	-0.274	-0.288
C7Θ (1976)	3.45	19	2168	+8	-0.253	-0.269
		50	2166	+1	-0.286	-0.289
		100	2165	+2	-0.311	-0.316
		130	2169	+3	-0.266	-0.274
		19	2169	+7	-0.259	-0.273

pre-load of 3.45 MPa (500 psi) was maintained on the rock during the heating and gauge installation. The load cycle was superimposed on the pre-load.

An additional set of temperature tests was run on the same two gauges. These were individually installed in the cylinder at room temperature and, as described above, the temperature of the assembly was raised slowly while the period of the gauge was being recorded. The first test was run without pressurizing the bladder and the second with the pressure held constant at 3.45 MPa (500 psi). The data from these tests are listed in Table 2-16.

The change in gauge reading as the temperature changes should be related in some manner to the difference in thermal expansion of the gauge and rock. However, the results are probably influenced by the change in elastic modulus of the rock as well, as indicated by the marked difference in the confined and unconfined data.

2.4 Effects of Temperature on Unloaded Gauges

Prior to installation at Stripa, two gauges had been placed in an oven and heated to 200°C (Schrauf et al., 1979). After thermal equilibrium was attained, the high-temperature gauge readings were within 5 units of the room-temperature readings as shown on Table 2-16. The natural vibratory period of the gauges was little affected by temperature.

After completion of the heater experiments, a similar test was conducted on ten gauges. Five were placed in an oven with their axes vertical, and five with their axes horizontal. Oven temperature was held constant for one hour before the gauge readings were recorded to allow thermal equilibration within the gauges. After the first temperature cycle, the gauge positions were

Table 2-16. Observed period of two gauges installed in radially-loaded cylinder at different temperatures and constant confining pressure.

Confining Pressure (MPa)	T(°C)	C7Θ (R_0 = 1976) Equilibration time (hr)	R	C11Z (R_0 = 2134) Equilibration time (hr)	R
0	20	--	2177	--	2321
0	50	1.5	2186	1.5	2324
0	100	1.75	2185	1.25	2319
0	150	1.75	2181	1.75	2307
0	200	2.0	2139	1.5	2278
0	20	15.0	2124	16.0	2311
3.45	22	--	2167	--	2323
3.45	50	2	2172	2	2325
3.45	100	2	2193	2	2349
3.45	130	2	2205	2	2351
3.45	22	20	2140	20	2294

Table 2-17. Measured period of unloaded gauges at room and elevated temperatures. Gauges mounted in both horizontal and vertical positions in oven.

Gauge label	RT (22°C)	50°C	75°C	100°C	75°C	50°C	RT(28°C)
			Vertical				
C3R	2146	2146	2144	2141	2143	2144	2146
C5Θ	2132	2132	2131	2129	2131	2132	2132
C9Θ	2011	2013	2015	2016	2015	2013	2012
C10Z	2195	2195	2194	2193	2193	2194	2195
C14Z	1984	1987	1989	1987	1987	1986	1984
			Horizontal				
C1Θ	1941	1944	1946	1946	1946	1944	1942
C1R	1915	1923	1925	1926	1924	1921	1917
C7Θ	1977	1982	1984	1985	1983	1981	1978
C7Z	1986	1990	1991	1992	1992	1990	1987
C12Z	2185	2186	2185	2182	2183	2185	2185
			Reversed Orientations				
			Horizontal				
C3R	2146	2146	2144	2142	2143	2144	2145
C5Θ	2132	2132	2131	2129	2131	2132	2132
C9Θ	2011	2014	2015	2016	2015	2013	2012
C10Z	2195	2195	2194	2193	2194	2194	2195
C14Z	1984	1987	1988	1988	1987	1986	1984
			Vertical				
C1Θ	1941	1943	1945	1946	1945	1943	1941
C1R	1915	1921	1924	1926	1923	1921	1918
C7Θ	1977	1981	1983	1984	1982	1980	1978
C7Z	1986	1991	1992	1991	1992	1991	1988
C12Z	2185	2186	2184	2180	2183	2185	2185

reversed and the temperature cycle repeated. As can be seen from the data in Table 2-17, the largest change from room temperature to 200°C was 11 units on gauge C1R. The largest change registered at room temperature before and after the two temperature cycles was 3 units.

2.5 Analysis of VWS Performance

Drawing upon the operating and calibration results described in the preceding sections, the uncertainties in the determination of C_1 and R_s are now summarized. These uncertainties in measurement are then used to estimate the error in stress determination.

2.5.1 Dependence of C_1 on preload

During the calibration work it was observed that the calibration factor C_1 varied with the amount of gauge preload (ΔR). As the wedge was set with higher pressure, ΔR increased and C_1 decreased, i.e., the gauge became more sensitive. This effect has also been noted by Dutta et al. (1980).

Although the ΔR term is convenient for field use, it is not a good indicator of preload. The load sensed by the gauge is proportional not to ΔR but to $(R_o^{-2} - R_s^{-2})$. It can be shown from Eqn. 2-9 that ΔR is approximately equal to $0.5\ R_o^3\ (R_o^3 - R_s^{-2})$, so ΔR, a product of the preload times R_o^3, is useful as an indicator of preload only in referring to one gauge or to a set of gauges with nearly equal R_o values. For that reason, in the following discussion the term $(R_o^{-2} - R_s^{-2})$ will be used as the measure of gauge preload.

The sequence of runs done with four gauges installed at different preloads in the 12-inch block, given in Table 2-11, shows this decrease in C_1 with increasing ΔR. These data are plotted in Fig. 2-17 using $(R_o^{-2} - R_s^{-2})$ as abscissa. The preload ranges of the four gauges overlap one another as a result of their different R_o values. Two representative ΔR scales are given at the top of the figure for reference. Four data points measured by Dutta et al. (1980) in a thin slab of Climax granite are also plotted in Fig. 2-17. Their preload values also overlap with the sequence of runs from the four gauges in the 12-inch block.

After the work with gauge imprints revealed the variations in wedge positioning, two gauges were installed with varying ΔR while using special care in the alignment of the gauge and wedge (refer to Section 2.3). The C_1 values from these two gauges, C7Θ and C11Z, are plotted in Fig. 2-17 as open squares and open circles. These C_1 values plot below the trend established by the other tests, indicating that careful wedge placement reduces the dependence of gauge sensitivity on preload.

The scatter of data points in Fig. 2-17 indicates that the relationship between preload and C_1 is statistical in nature. The exact value obtained for any gauge on any installation depends on the details of the seating for that particular installation.

At the time of installation at Stripa, the effect of preload and gauge alignment were not appreciated. Many of the gauges were set with ΔR of around 200 counts, but, as shown above, this does not assure that they were set with an equivalent preload. Figure 2-18 shows that most gauges were set between

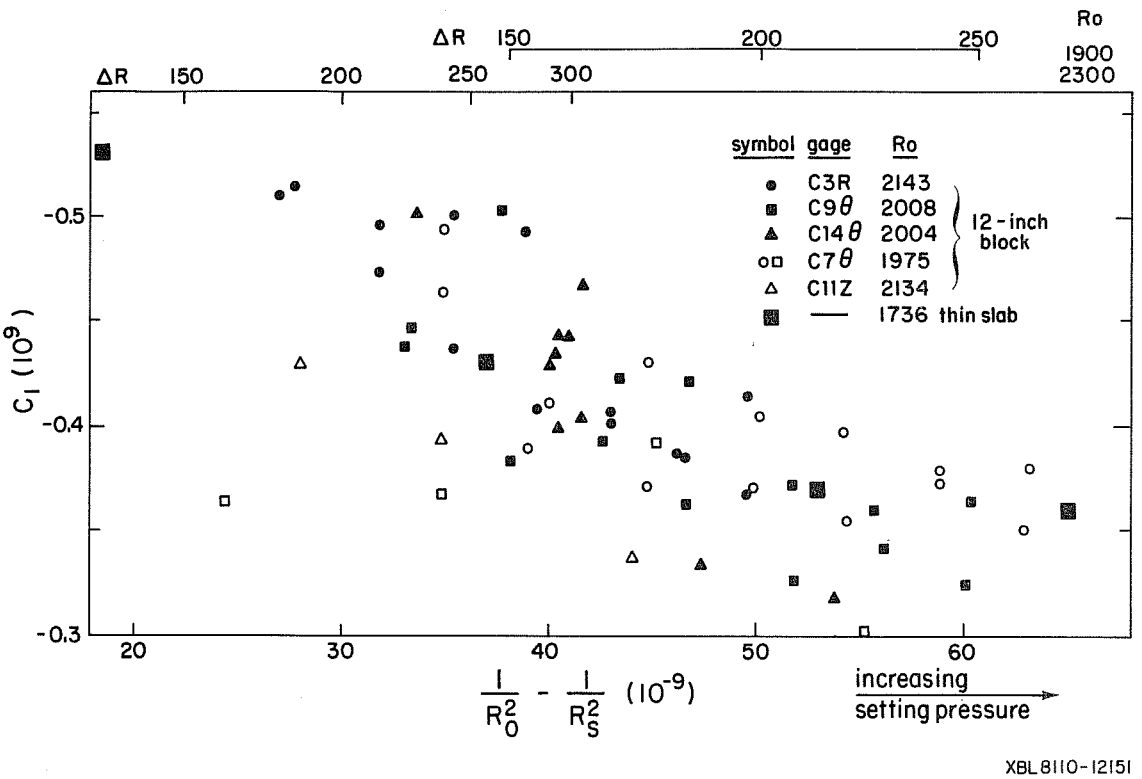

Fig. 2-17. VWS calibrations as function of setting pressure done in thin slab of Climax granite (Dutta et al., 1980).

30 and 50 x 10^{-9} in $1/R_o^2 - 1/R_s^2$ units, with a few above and below this range. Unfortunately, this range corresponds to the region where C_1 varies with preload, as shown in Fig. 2-17.

The gauges calibrated in the 12-inch block were installed so as to mimic the ΔR used for each gauge in the Stripa heater experiments (Table 2-10). They are plotted in Fig. 2-19 in the same format as Fig. 2-17. Not all of the gauges installed at Stripa are represented in Fig. 2-19 because some failed in service and could not be recalibrated. The trend in Fig. 2-19 is marred by the high scatter, but it is more or less similar to the one in Fig. 2-17: C_1 values decline with increasing values of $1/R_o^2 - 1/R_s^2$ reaching a plateau at 50 x 10^{-9} and greater.

2.5.2 Effect of Loading and Unloading

The calibration factors C_1 determined in the 15-inch and 12-inch blocks are given in Tables 2-7 and 2-10 for both increasing and decreasing load cycles. Invariably, the magnitude of C_1 was less when the calibration blocks are being unloaded, that is, the gauge sensitivity increases after the block has once been loaded. A graphical example is given in Fig. 2-20, which shows reduced slopes from three sequential load cycles. The gauge was removed and reinstalled between each load cycle with the R_s value duplicated as closely as possible. The reason for the slope change is assumed to be an increase in contact area between the gauge and rock as a result of a small amount of creep in the rock. This change in calibration factor between loading and unloading is very small in comparison to the overall scatter in the C_1 value. Therefore, no attempt has been made to correct for this effect.

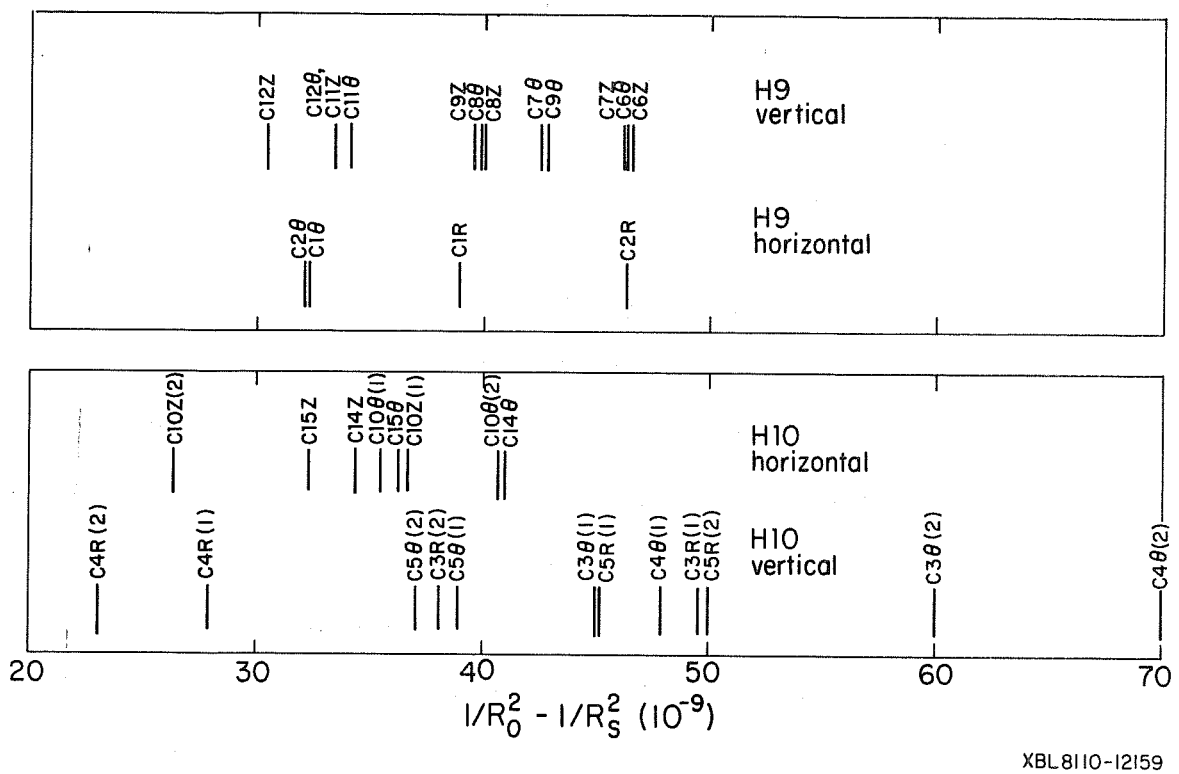

Fig. 2-18. Distribution of VWS installation period readings at Stripa, plotted on scale proportional to setting pressure. Parenthetical number indicates first or second installation.

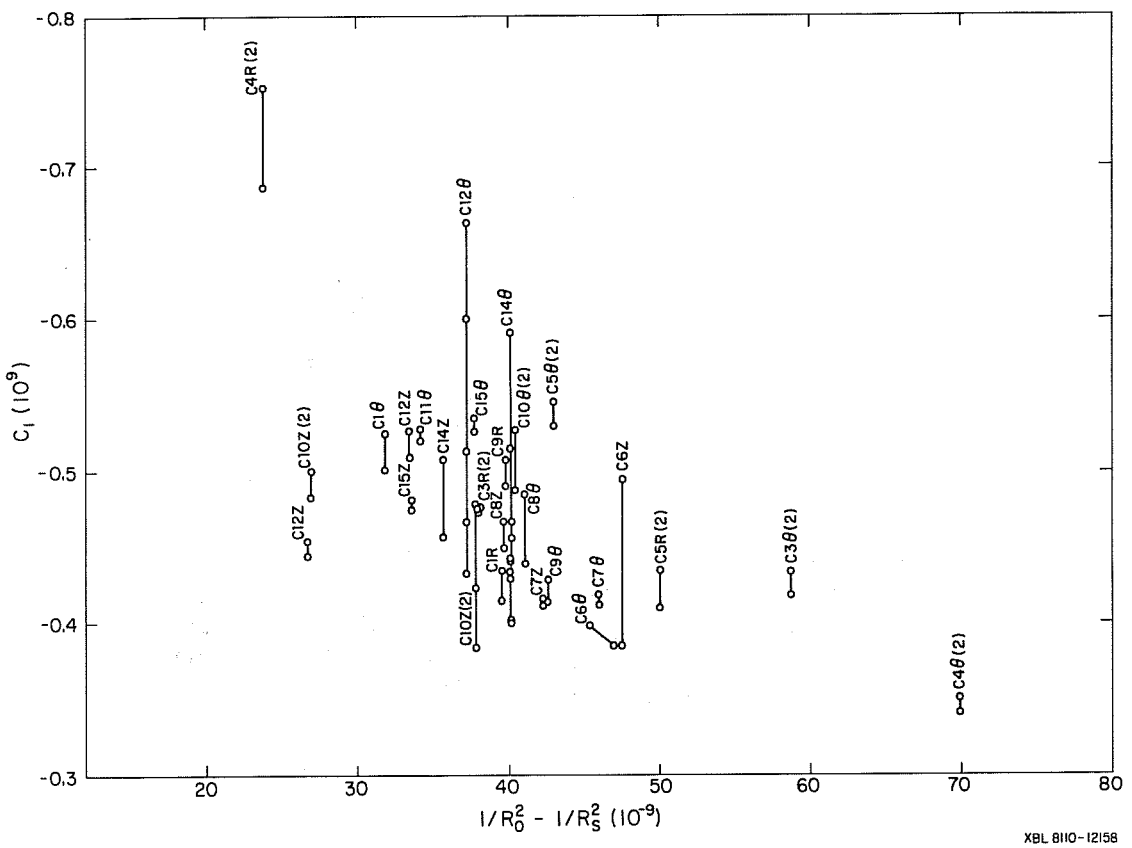

Fig. 2-19. Calibrations done in 12-inch block, plotted against scale proportional to setting pressure. All points are loading cycle only.

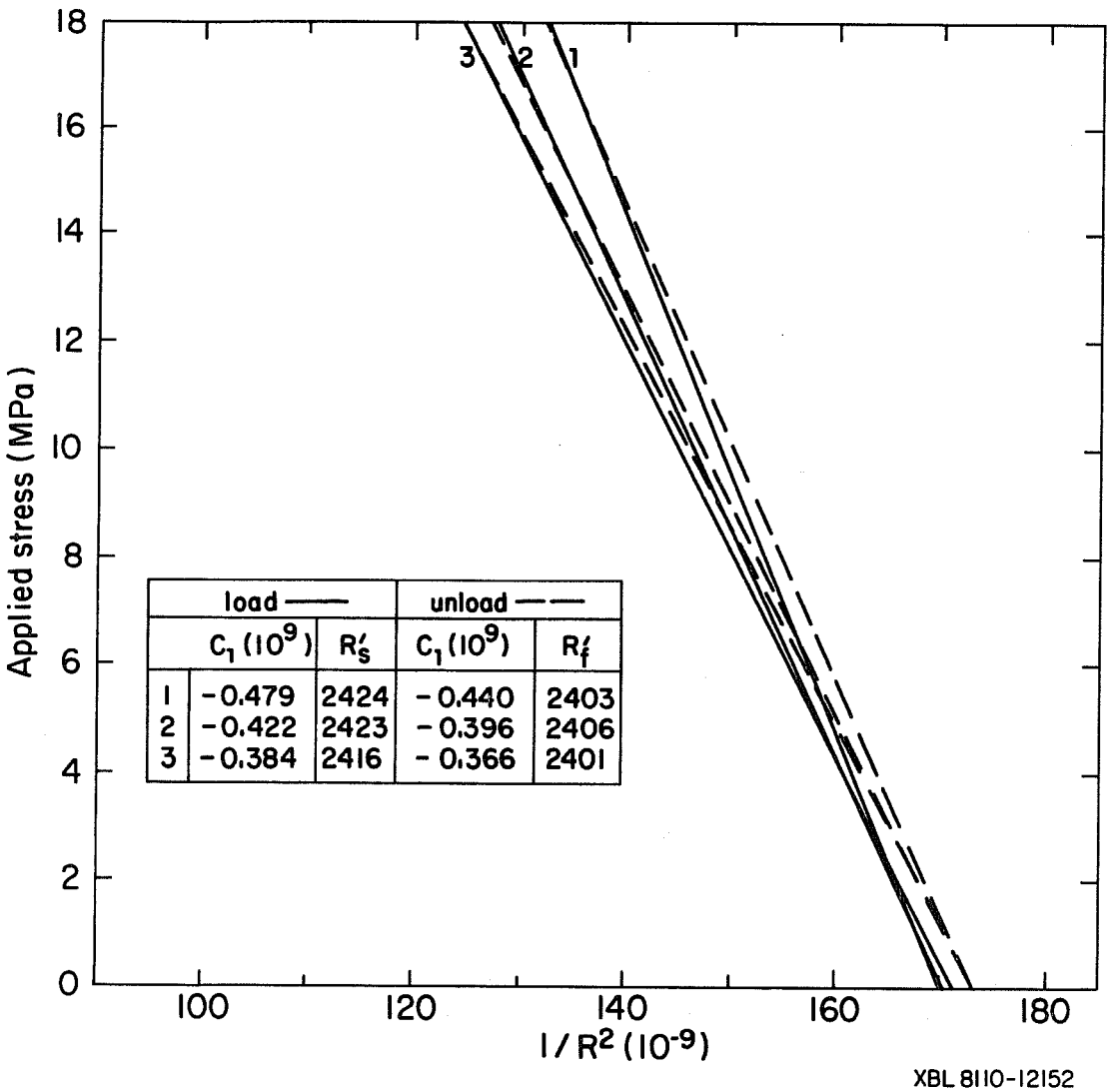

Fig. 2-20. Calculated C_1 and R values from 3 tests on gauge C10Z (3-45) in the 12-inch block. Each test is a separate installation.

2.5.3 Variation of C_1 with Temperature

The calibrations done as a function of temperature are summarized in Fig. 2-21a. At least one temperature test was done in each of the four calibration facilities. Load-unload cycles were done sequentially without reinstallation between temperature increases in the end-loaded cylinder and the 15-inch block. However, in the radially-loaded cylinder and 12-inch block, the gauges were reinstalled at the test temperature before each load-unload cycle.

Results in the end-loaded cylinder were consistent one with another and also consistent in the sense that gauge C10Z (3-45) produced virtually the same dependence of C_1 on T when measured before and after its use at Stripa (Fig. 2-21b). However, temperature calibrations in the end-loaded cylinder may not be representative because the modulus of the cylinder was low compared to that in situ (as measured in the borehole) and the gauges were installed at a very low preload.

The two gauges calibrated in the 12-inch block also showed a decline of C_1 over the temperature range 23-130°C of as much as 37% (Fig. 2-21f). However, values obtained in the y-direction of the 12-inch block (Fig. 2-21e) and in the 15-inch block (Fig. 2-21d) show little temperature dependence. The results from the radially-loaded cylinder appear erratic: the four tests at 50°C on gauge C11Z varied from -0.26 to -0.38 x 10^9. This scatter is presumed to be due to lack of consistent seating on reinstallation rather than to temperature.

The temperature tests conducted on VWSs used at Stripa are inadequate to assess the change of gauge characteristic with temperature. Some of the results indicate that C_1 is affected very little by temperature change,

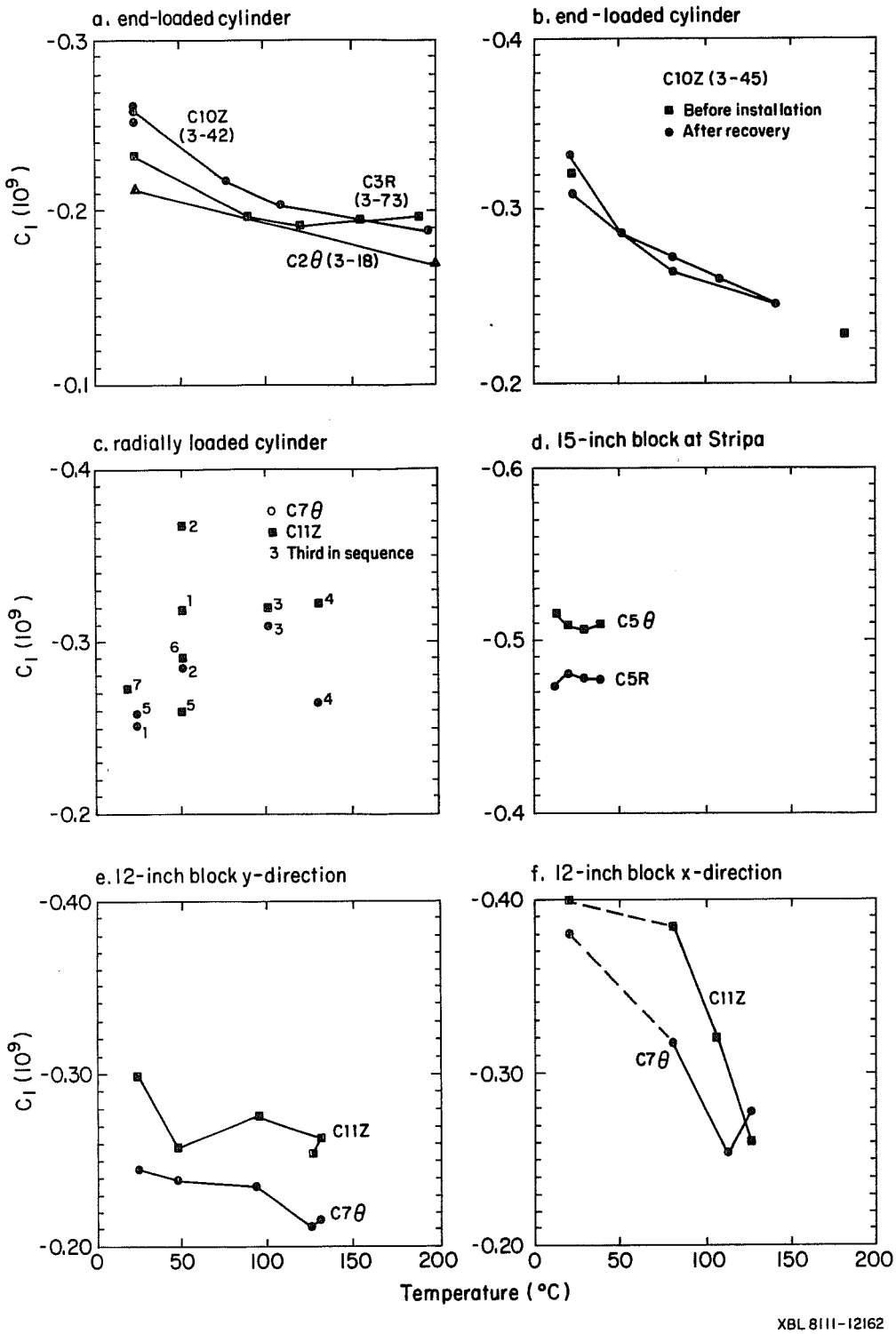

Fig. 2-21. Calibration factor (C_1) as a function of temperature for eight gauges.

while other results indicate a decrease in the value of C_1 by more than one-third over the temperature range 23° to 130°C. It is suspected that the observed change in C_1 is another manifestation of the bedding-in (seating effect), rather than a true temperature effect.

2.5.4 Variation of R_s with Temperature

Tests were performed in the radially loaded cylinder without varying the load to assess the effect of temperature on R_s alone (Table 2-16). The results show a marked difference in the response when the maintained confining pressure was increased. Results with confining pressure held constant at 3.45 MPa, plotted in Fig. 2-22, show that R_s increases by about 30 units over the range 23° to 130°C.

2.5.5 Evidence for the Seating Effect

The several variations in C_1 pointed out in the preceding paragraphs are ascribed to a seating or "bedding-in" effect. The pertinent observations are as follows:

a) When the gauge is first set, the period changes with time. The change is noticeable within the first 10 minutes after setting and then declines with increasing time. Examples can be found in Tables 2-6 and 2-7.

b) The value for C_1 is greater for increasing load than for decreasing load, as shown by the data of Tables 2-8 through 2-11. In addition, in tests where the gauge was cycled more than once without removal from the calibration block, the C_1 value obtained on the first load path was generally higher than all subsequent values, whether obtained on load or unload runs.

c) The value of C_1 either is unaffected by or declines with increasing temperature, as shown in Fig. 2-21.

d) C_1 is generally higher for low values of seating pressure $(R_o^{-2} - R_s^{-2})$ than it is for high values (Fig. 2-17). As seating pressure increases, C_1 declines until reaching a plateau value.

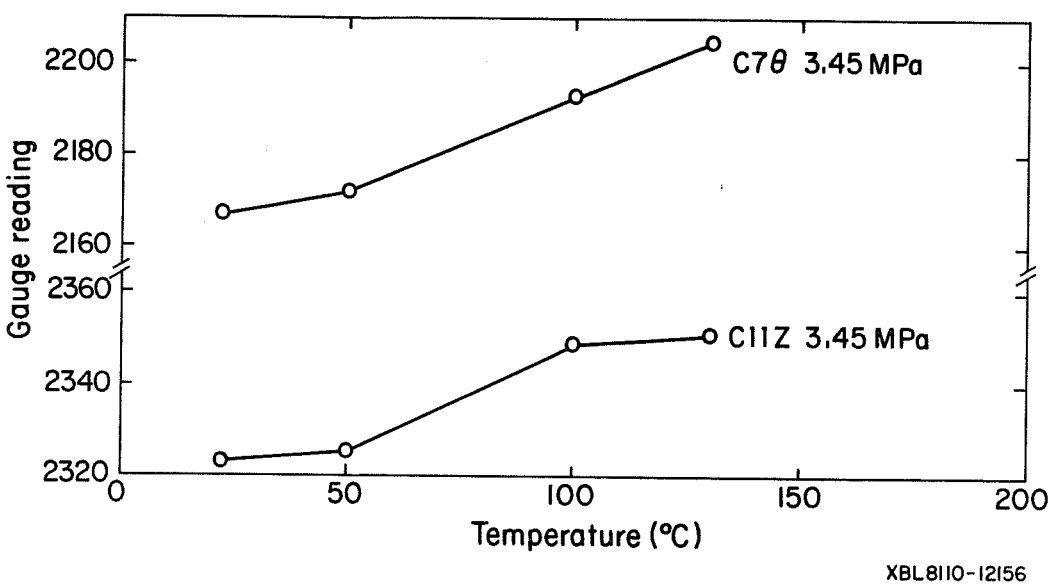

Fig. 2-22. Change of VWS period R_S with temperature, while hydrostatic confining pressure was held constant on radially loaded cylinder.

e) C_1 tended to decrease when more care was taken installing the gauge. Carbon-paper imprints showed the wedge to be off-center when high C_1 values were obtained.

All of the above can be ascribed to seating effects. If a gauge is poorly seated, whether due to improper orientation, insufficient setting pressure, or asperities in the rock, the result is to increase the value of C_1, that is, to decrease gauge sensitivity.

2.5.6 Dependence of C_1 on Rock Modulus

The sensitivity (calibration factor) of the VWS is dependent on the elastic modulus of the host material. This has been reported by Hawkes and Bailey (1973) and by Fossum et al. (1977); it also became evident during the course of the various gauge calibrations on the VWSs used at Stripa.

Values of C_1 and rock modulus determined as described in Section 2-3 are plotted in Fig. 2-23. The clusters (e-h) were from the four facilities used to calibrate Stripa gauges. Two measurements made in a steel cylinder are shown on the expanded scale of the inset. The error brackets denote standard deviations except for cases where only a few measurements were made, in which case the range is indicated.

The values of C_1 measured in blocks and cylinders of Stripa granite are higher than the thin-slab tests by Hawkes and Bailey (1973), some by more than a factor of two in material of comparable modulus. No explanation is offered for this discrepancy, although there may be an effect related to the ratio of block thickness to gauge length. In this regard, it should be noted that the steel cylinder results (j) lie above the trend established by the thin-slab results.

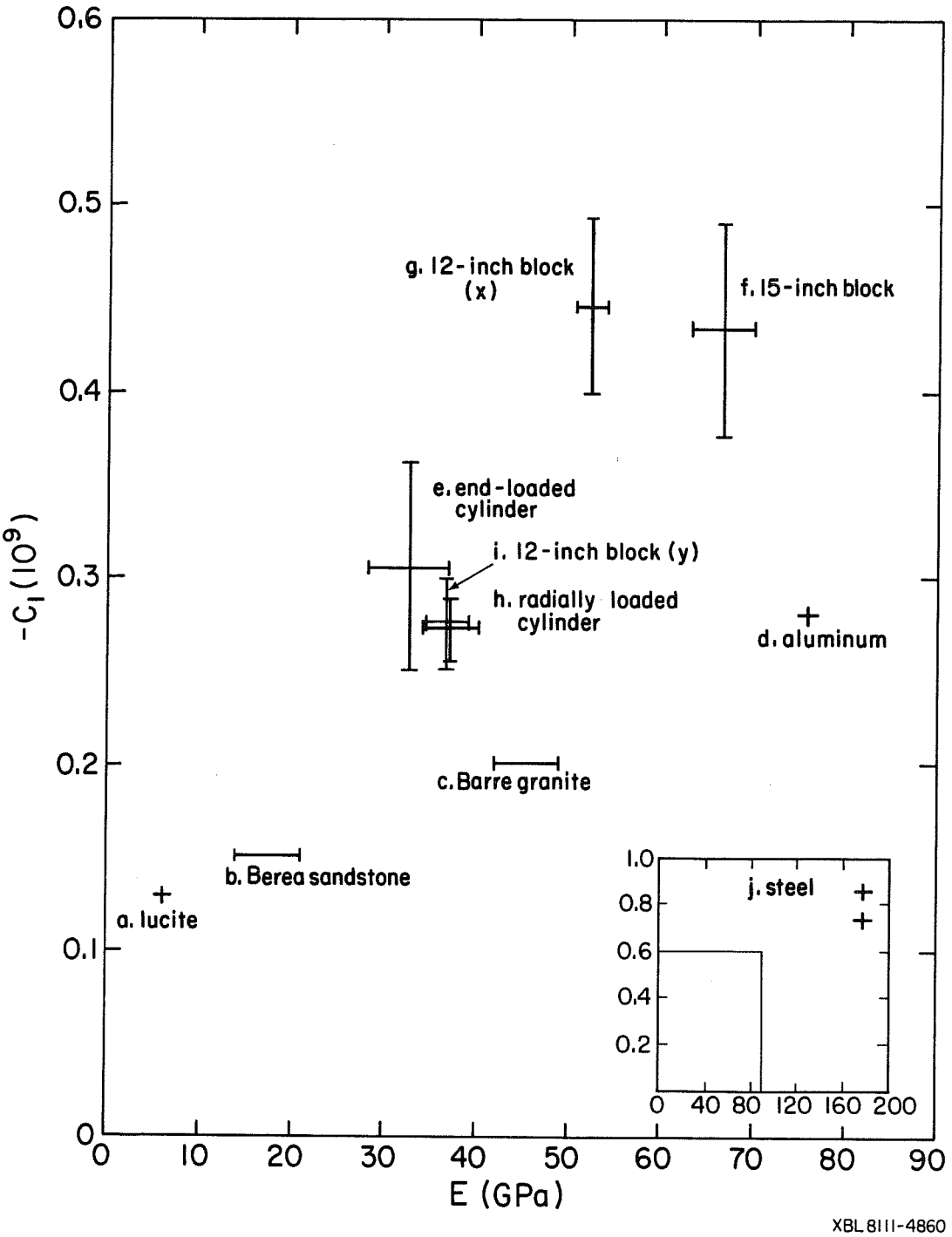

Fig. 2-23. Dependence of VWS calibration factor on modulus of test medium. Points a through d from Hawkes and Bailey (1973).

It is evident from the data in Fig. 2-23 that the VWS calibration factor is influenced by the elastic modulus of the host material, but, because of the large scatter in the data, it is not possible to derive a mathematical relationship for this dependency. Without the ability to adjust the C_1 value for changes in the elastic properties of the host material, the calibration data from the 15-inch block is probably the most reliable. This is true because the block is more representative of the in situ rock properties.

2.5.7 Long-Term Drift in Unloaded Gauge Period

The period of each gauge measured in its unloaded state after retrieval from the experiment, less its unloaded period prior to installation, was given in Table 2.2. These same values are presented as histograms in Fig. 2-24. Of the 28 gauges recovered, 7 had higher periods after the experiment than before. The period of four gauges decreased by more than 20 counts.

It is not known at this time exactly what caused these changes in the period of vibration of the wire in the gauges, nor it is known exactly when the change occurred. The increased values could be accounted for by slippage of the crimp on the wire, thus lessening the tension. Oxidation of the wire might either increase or decrease the period, depending upon whether the oxide particles adhere to the wire.

2.5.8 Evaluation of C_1

Before stress can be computed from VWS measurements, a value for C_1 must be assigned. However, it was observed that repeated calibrations on a single gauge produced scatter in C_1 values as great as $\pm$20% from the mean. It was also observed that C_1 is not independent of R_s, as shown in Fig. 2-17. These

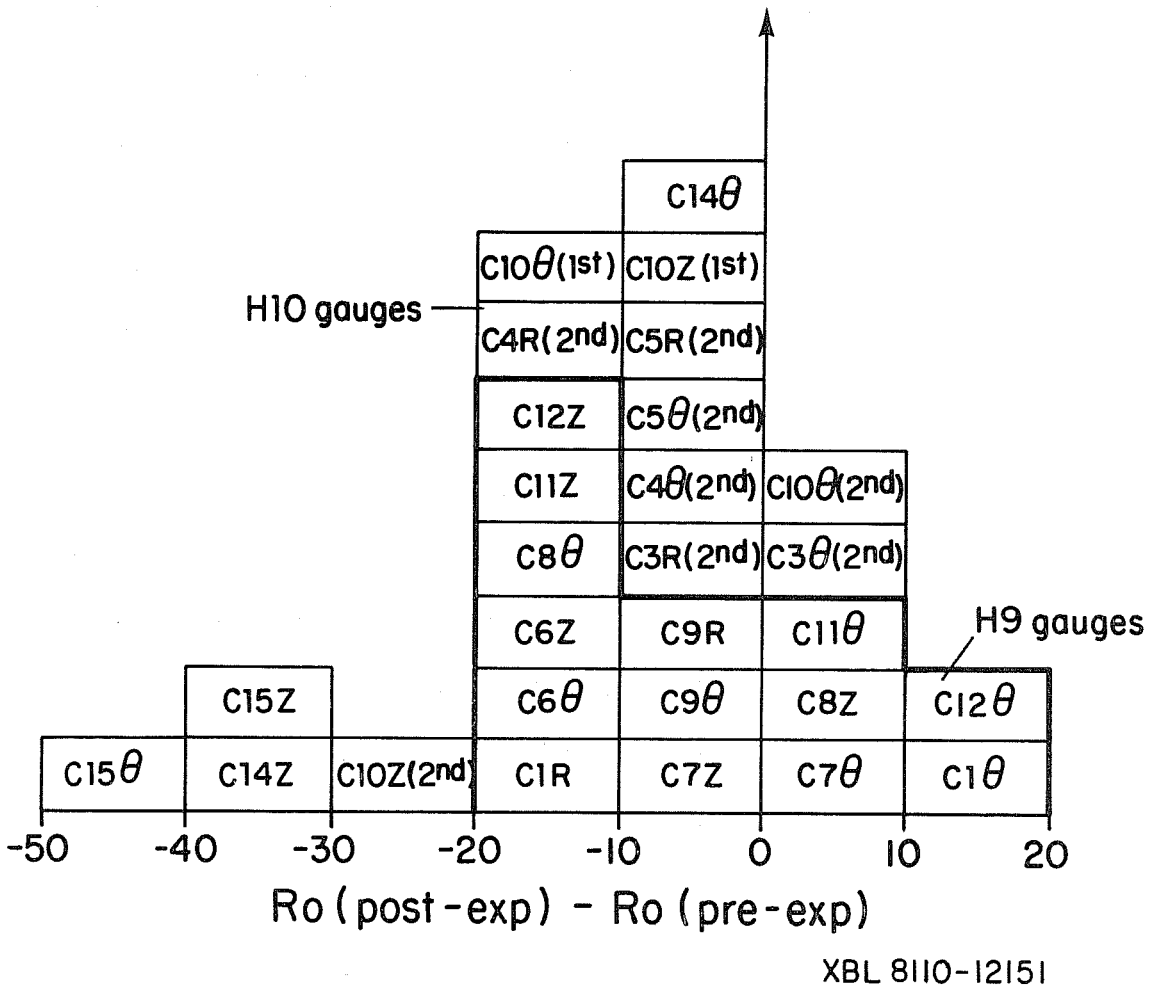

Fig. 2-24. Histogram of change in period of unloaded gauges recovered from Stripa heater experiments.

problems preclude assigning unique values of C_1 to each gauge.

How consistently did the gauges perform as a class? Figure 2-25 is a gauge-by-gauge plot of the calibration factors obtained in the 12-inch and 15-inch blocks. Only one calibration run from each block is plotted; repeat calibrations have been omitted. The scatter in C_1 obtained on any individual gauge is probably representative of the repeatability of setting a gauge in the field, since the results were obtained in different blocks (of comparable moduli) at different times by different operators. In general, it can be seen that the scatter for individual gauges is just as great as the scatter for the gauges as a class. It thus seems reasonable to compute the mean and standard deviation values for C_1; these are presented in Table 2-18. To compile the averages all calibrations for each gauge in each calibration facility were first averaged so that no one gauge was weighted more than any other. The resulting values for each of the 26 gauges were then averaged to produce the results shown in Table 2-18. It can be seen that differences between the two calibration blocks are well within one standard deviation, as are the differences between load and unload cycles. Hence, we adopt a value of -0.44×10^9 for C_1. Omitted from this overall average is gauge C4R, which is assigned a C_1 value of -0.65×10^9.

If the scatter obtained from repetitive calibrations at room temperature were the only significant source of error, then the standard deviations quoted for C_1 in Table 2-18 would suffice. However, the other uncertainties already discussed add to the error in a manner that can only be estimated. For example, although the data were inconsistent, C_1 was found to decrease

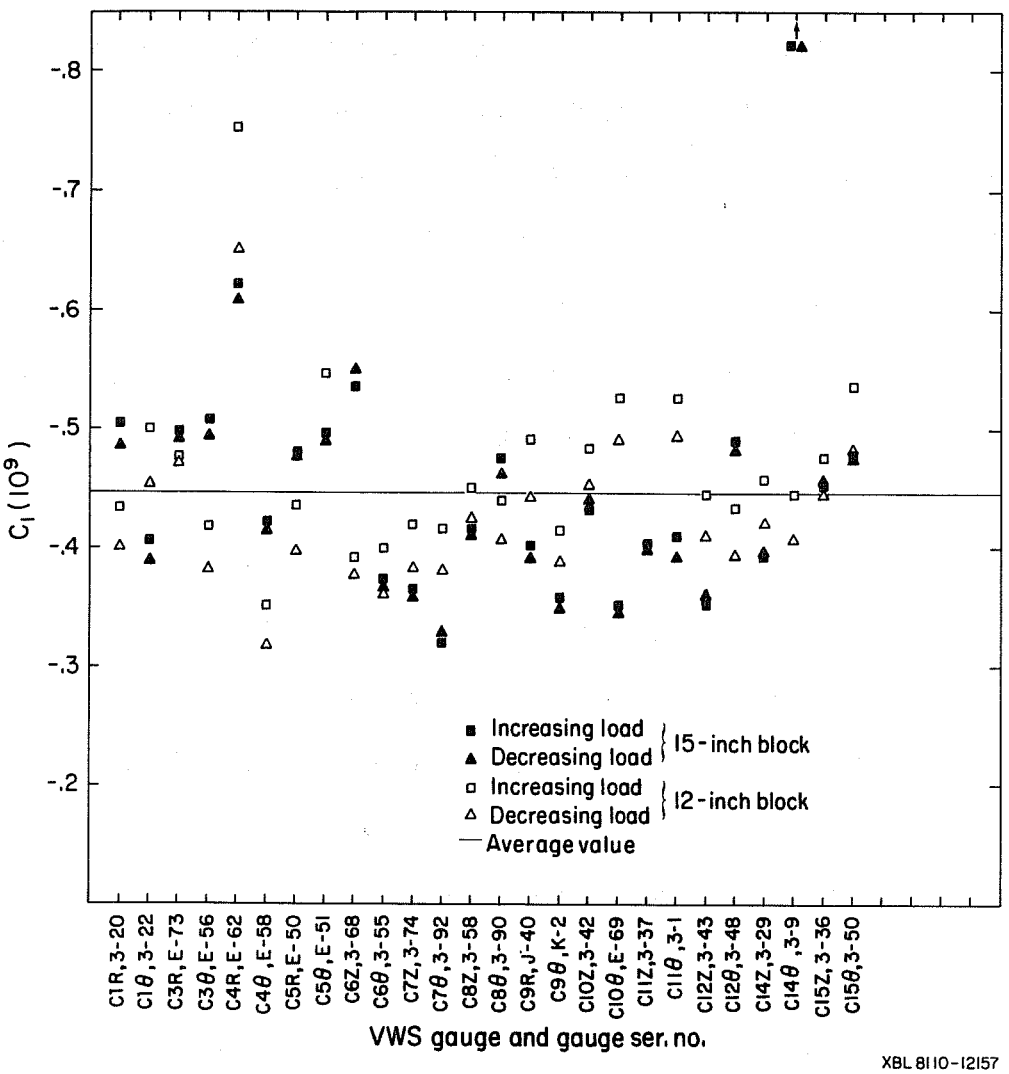

Fig. 2-25. Distribution of C_1 values from calibrations in 12-inch and 15-inch blocks. Repeat calibrations not shown.

Table 2-18. Mean and standard deviation of C_1 for 25 VWSs measured at room temperature.[a]

Calibration facility	Calibration Factor $C_1 \times 10^9$	
	Increasing load	Decreasing load
15-inch block	-0.435 ± 0.0578	-0.431 ± 0.0582
12-inch block	-0.465 ± 0.0498	-0.426 ± 0.0437

[a] One gauge, C4R, has been omitted; it has been assigned a C_1 value of -0.65×10^9.

with increasing temperature by as much as one third. If this decrease is real, gauges with low values of C_1 operating to high temperatures would extend the range of uncertainty in C_1 to even lower values. It is somewhat fortunate that most gauges that reached temperatures of 80°C or more had C_1 values equal to the average or higher. On inspection, it appears that most of the uncertainty due to temperature can be encompassed by a lower bound to C_1 of about -0.3×10^9. The effect of variations in Young's modulus upon C_1 are equally difficult to quantify, but the available data indicate that these variations are less than ±20%. With these considerations, values of

$$C_1 = -0.44 \pm 0.14 \times 10^9 \text{ for all gauges except C4R, and}$$

$$C_1 = -0.65 \pm 0.21 \times 10^9 \text{ for gauge C4R,}$$

were adopted as the average and the bound. The bounds are about 2.5 times greater than the standard deviation computed from installation scatter and shown in Table 2-18, but no statistical statements can be made regarding these bounds because of the other, rather subjective, factors that were considered.

2.6 Error Analysis

From the gauge response equation presented in Section 2.1 and the gauge calibration data presented above, the error bounds have been estimated for the measurements made with the VWS at Stripa. The response equation (2-9), rewritten here as:

$$\Delta\sigma \text{ (MPa)} = C_1 \left(\frac{1}{R^2} - \frac{1}{R_s^2}\right) , \qquad (2\text{-}9)$$

has been established as an acceptable means of calculating stress change from the VWS data. To calculate errors in stress change, the effects of errors in C_1, R, and R_s, must be separately assessed.

Errors due to C_1 are examined by differentiating Eq. (2-9) with respect to C_1, giving

$$\delta\Delta\sigma = \delta C_1 \left(\frac{1}{R^2} - \frac{1}{R_s^2} \right) \qquad (2\text{-}10)$$

$$= \delta C_1 \, (\Delta\sigma / C_1),$$

so fractioned errors in C_1 produce equivalent fractional errors in stress:

$$\delta\Delta\sigma/\Delta\sigma = \delta C_1 / C_1 \; ; \qquad (2\text{-}11)$$

that is, a 25% uncertainty in C_1 causes a 25% uncertainty in stress change. For example, if the rock stress changed by 10 MPa, and the gauge calibration factor were $(-0.40 \pm 0.10) \times 10^9$, then the uncertainty in stress change would be ± 2.5 MPa. Figure 2-26 illustrates this point for six hypothetical gauges, each of different C_1 values and each with the same initial setting period R_s of 200 units. Using the adopted values for C_1, Eq. (2-10) shows that the fractional error in C_1 is 0.14/44 or 0.32, so the uncertainty in $\Delta\sigma$ will be $\pm 0.32\Delta\sigma$.

Errors in R can be ignored because the error in reading a given value by the data logger, which is only ± 1 count, is negligible compared to the change in R_s value after the initial setting.

Errors due to R_s are accounted for by differentiating Eq. 2-9 with respect to R_s, giving:

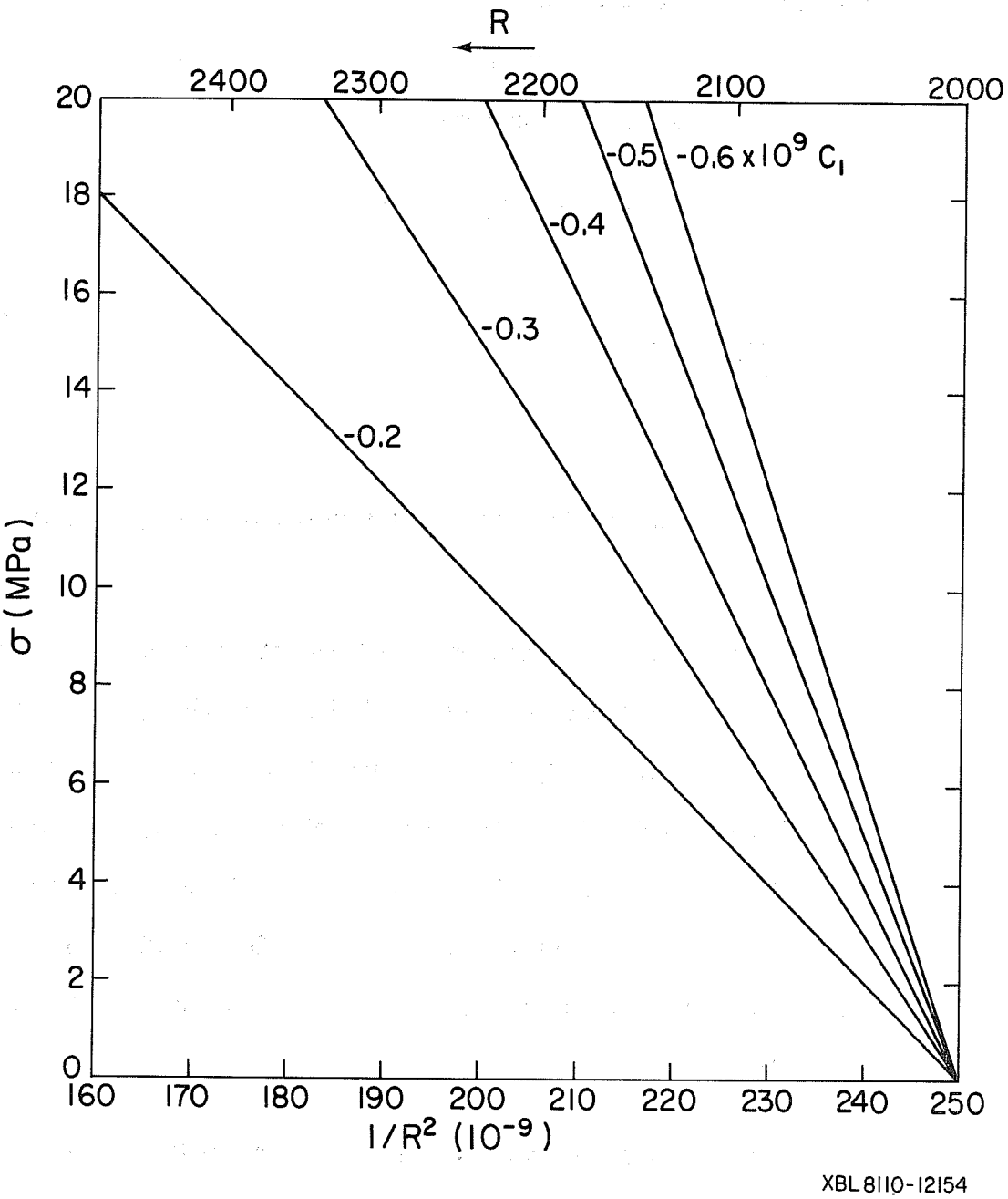

Fig. 2-26. Stress change as function of $1/R^2$ for range of C_1 values.

$$\delta\Delta\sigma = 2C_1, (\delta R_s/R_s^3), \qquad (2\text{-}12)$$

a result which shows that the stress errors due to the uncertainty in R_s will be quite sensitive to the magnitude of R_s. This is illustrated in Fig. 2-27, which shows that a gauge set at 2600 counts will induce less than one-half the stress-change error of a gauge set at 2000 counts, for a given uncertainty in R_s.

A statistical value for δR_s is difficult to obtain because so many factors contribute to the seating effects, as summarized earlier. Cycling the load at constant temperature produced a change as much as + 32 counts (Table 2-14), and Fig. 2-20 shows a change in the opposite direction; thus a value of ± 30 counts will be used in the error analysis. The data of Appendix A show that R_s values at Stripa range from 2053 to 2662; a value of 2100 will be used to estimate the error. Substituting these values into Eq. (2-12) gives

$$\delta\Delta\sigma = 2(-0.44 \times 10^9)\ (\pm 30)/(2100)^3$$

$$= \pm\ 2.8\ \text{MPa}\ . \qquad (2\text{-}13)$$

As can be seen in Fig. 2-27, this value reduces to approximately ±1.5 MPa if an R_s value of 2600 is used.

Although a change in R_s is presumed to occur during a loading (heating) cycle, there is no way to assess when or whether such a shift occurred during the experiment. It is accounted for as an additive constant to the uncertainty produced by C_1. These effects combine to give:

$$\delta\Delta\sigma(\text{MPa}) = \pm\ 0.32\Delta\sigma\ \pm 2.8 \qquad (2\text{-}14)$$

for the error on stress change determined with the VWS at Stripa. This assessment of the overall error in measured stress change is conservative in that

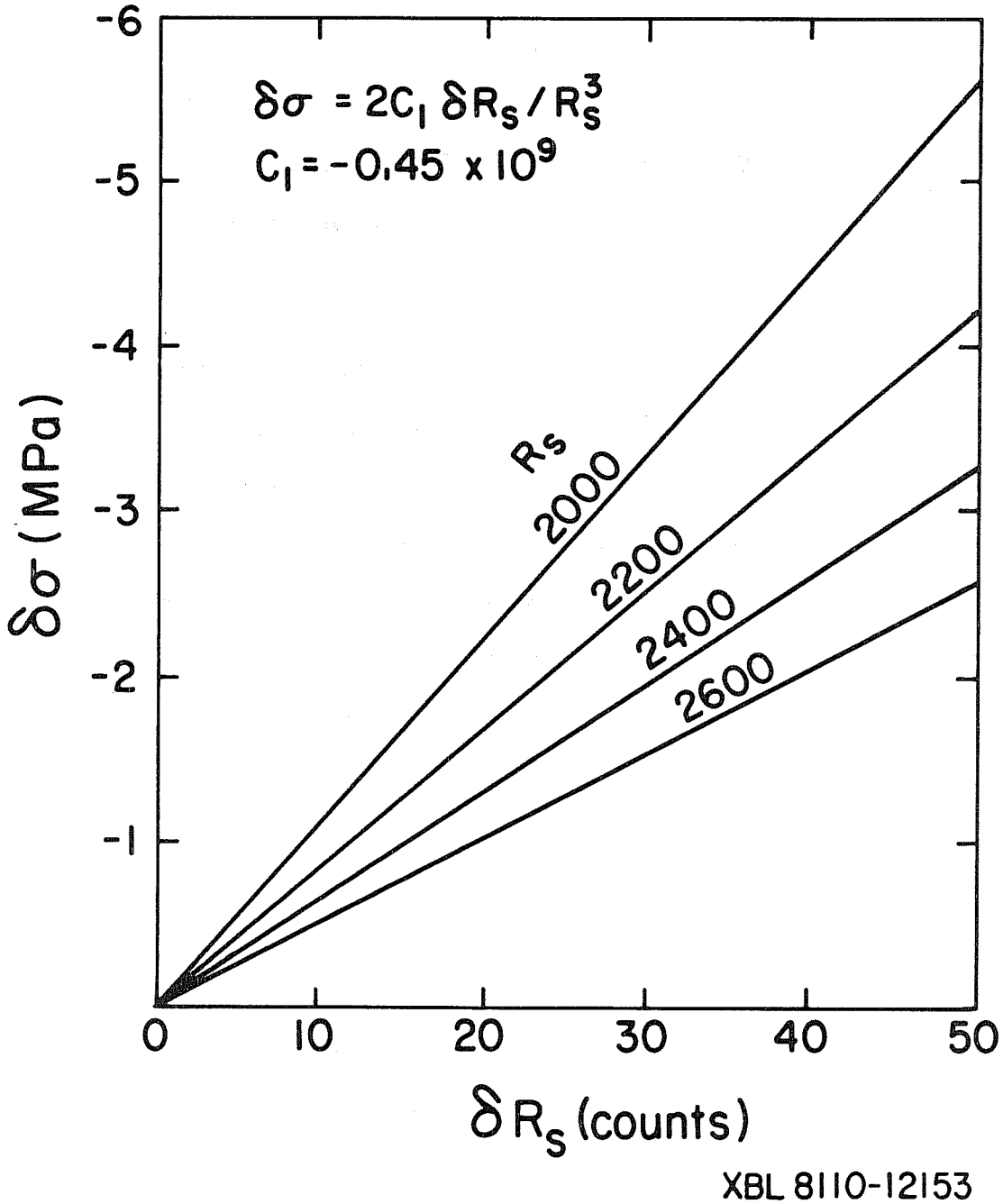

Fig. 2-27. Stress-change error due to uncertainty in R_s.

a crude attempt was made to account for effects of temperature and seating. Because these effects are not well understood, the error bounds can only be regarded as estimates.

2.7 Summary

Three problem areas were encountered in calibrating the VWSs used in the Stripa heater experiments:

1) Seating Effects. Without using extreme care when installing the VWS in a calibration block, the calibration factor C_1 obtained from a series of installations and loading exhibited a scatter as great as $\pm$20% from the mean. A systematic variation in C_1 with setting pressure was also found, which means that C_1 is not independent of the setting period R_s. A lesser problem was a change in C_1 following the first loading of the gauge. Although these observations are based on gauge calibration in a granite block, the same problems would be expected to occur when the gauge is installed in a borehole in any material.

2) Rock Modulus Dependence. On the basis of the Stripa experience and the reports of others, it is concluded that the calibration factor C_1 depends on the Young's modulus of the host rock. While it is always possible to use the proper rock type for calibration, it is not easy to guarantee that its modulus is representative of the rock modulus in situ. It appears that the modulus dependence is masked by the variations in C_1 attributed to seating effects.

3) Temperature Dependence. The dependence of C_1 and R_S upon temperature has not been adequately assessed. Insufficient testing was done on temperature-related effects because most efforts were directed at sorting out the C_1 variations that occurred at ambient temperature.

The performance of the VWSs used on the heating experiments at Stripa, other than the calibration problems, is summarized as follows:

1. The VWS was more reliable than the USBM borehole deformation gauge. Midway through the heater experiments, only 4% of the VWSs had failed, although the number of failures increased to 27% by the end of the 550-day experiments.
2. Data quality appears to be good overall. Most flaws in the data record are attributed to the computer-based data acquisition problems, not to the gauges.
3. Long-term stability is quite good. Only four gauges had an unloaded period change before and after the experiment of more than 20 counts.

3. USBM BOREHOLE DEFORMATION GAUGE

3.1 Introduction

The borehole deformation gauge developed by the U.S. Bureau of Mines (USBM) was selected along with the IRAD vibrating wire stressmeter for determining the stress changes induced in the granitic rock mass during the full-scale heating experiments at Stripa, Sweden. The USBM gauge supplier was Rogers Arms and Machine Company, Inc.

The USBM gauge shown in Fig. 3-1 is comprised of three identical strain-gauged cantilever sets. The three components are positioned 120° apart to sense the diametral change of the borehole at three positions. Each component was sized to the borehole to insure that the cantilever arms were initially deflected to near midrange so that both expansion and contraction of the borehole could be detected.

The gauges were installed in the borehole with a rigid tool that permitted accurate alignment. In all cases, component A (#1) was aligned in the Θ direction, i.e., perpendicular to the vertical plane extending from the gauge location to the center line of the main heater borehole.

The algorithm used to convert the measured USBM gauge output voltages to borehole deformations (Chan et al., 1980) is as follows:

$$\Delta U_i = C_i(V_i - V_{oi}) - C_s(V_{ss} - V_{os}) \qquad (3\text{-}1)$$

where

ΔU_i = borehole diametral change,

C_i = gauge calibration factor at temperature T_i,

V_i = gauge output voltage at temperature T_i,

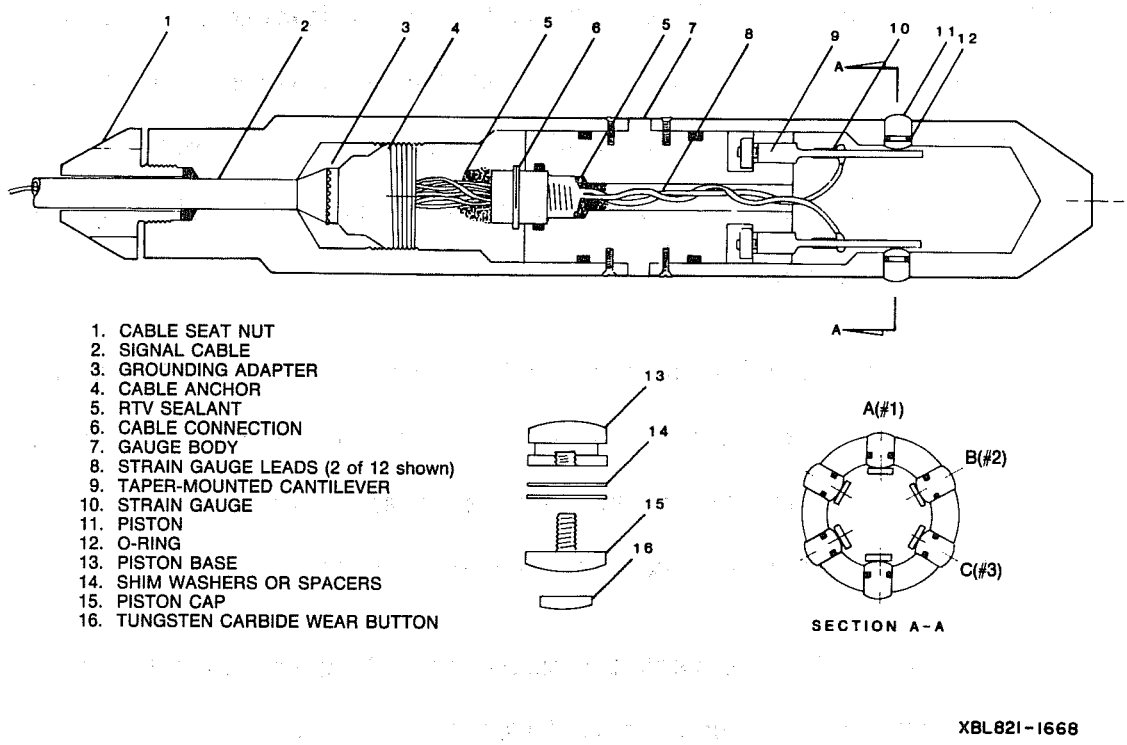

Fig. 3-1. USBM borehole deformation gauge.

V_{oi} = gauge output voltage with zero cantilever displacement (pistons removed) at temperature T_i,

C_s = gauge calibration factor at temperature T_s, where s denotes starting/installation value,

V_{ss} = gauge output voltage when positioned in borehole, and

V_{os} = gauge output voltage with zero cantilever displacement (pistons removed) at temperature T_s.

The values for C_i and C_s are obtained from (Schraut et al., 1979):

$$C_i = C_o \left[1 + \left(\frac{C_1 - C_o}{C_o}\right)\left(\frac{T_i - T_o}{T_i - T_o}\right)\right] \text{ , and} \qquad (3\text{-}2)$$

$$C_s = C_o \left[1 + \left(\frac{C_1 - C_o}{C_o}\right)\left(\frac{T_s - T_o}{T_1 - T_o}\right)\right] . \qquad (3\text{-}3)$$

C_o is the gauge calibration factor at temperature T_o and is derived from

$$C_o = C_c \left[1 + \left(\frac{C_1 - C_o}{C_o}\right)\left(\frac{T_c - T_o}{T_1 - T_o}\right)\right] . \qquad (3\text{-}4)$$

The other terms are defined as follows:

C_c = gauge calibration factor at temperature T_c,

T_c = temperature at which voltage output vs displacement calibrations were performed (14°C for the Stripa experiment),

T_o = lower reference temperature for zero cantilever displacement voltage (11°C for the Stripa experiment),

T_1 = upper reference temperature for no cantilever displacement voltage (200°C for the Stripa experiment),

T_s = starting temperature (gauge temperature when positioned in borehole), and

T_i = temperature at any time a voltage reading (V_i) is taken.

The voltages V_{oi} and V_{os} are not measured quantities; instead, they must be derived as follows:

$$V_{oi} = V_{oo} + (V_{o1} - V_{oo}) \left(\frac{T_i - T_o}{T_1 - T_o}\right), \text{ and} \tag{3-5}$$

$$V_{os} = V_{oo} + (V_{o1} - V_{oo}) \left(\frac{T_s - T_o}{T_1 - T_o}\right), \tag{3-6}$$

where

V_{oo} = gauge output voltage with zero cantilever displacement at temperature T_o (11°C)

V_{o1} = gauge output voltage with zero cantilever displacement at temperature T_1 (200°C)

Earlier calibration results indicated that $\frac{C_1 - C_o}{C_o}$ was approximately equal to 0.06. However, more recent calibrations (detailed in Section 3.2) show that this quantity varies considerably from gauge to gauge. The uncertainty in this value has a pronounced effect on the overall error in the corrected diametral change as discussed in Section 3.5.

The diametral change (ΔU_i) as obtained from solving Eq. (3-1) is the displacement sensed by the cantilever deflection. This value was corrected (Chan et al., 1980) to remove the increment of displacement resulting from the thermal expansion of the gauge (α_g) and that of the rock (α_r). The true borehole deformation (diametral change) is obtained from:

$$\Delta U = \Delta U_i - \alpha_g \, d(T_i - T_s) \tag{3-7}$$

where d is the starting borehole diameter.

It should be pointed out that the borehole deformation (ΔU) in Eq. (3-7) is the result of the change in stress field and of the thermal expansion of the rock. In order to determine stress changes only, the deformation due to thermal expansion of the rock must be removed.

All available information on the USBM gauges used during the Stripa heating experiments has been reviewed, including calibrations at the conclusion of the tests, and an error analysis has been conducted to establish error bounds that should be associated with the recorded data.

No attempt has been made to convert all borehole deformation data to stress, primarily because of the uncertainty in the values for the in situ modulus of elasticity and the coefficient of thermal expansion of the rock. However, for the purpose of comparing vibrating wire stressmeter data and USBM gauge-derived data, sample conversions are presented in Section 3.7.

3.2 Calibration

At the outset of the Stripa program, laboratory tests were conducted to determine if the USBM gauge response could be used for long-term operation at high temperatures (Schrauf et al., 1979). It was determined that the gauge response was reproducible and that temperature effects could be determined. A knowledge of three gauge parameters plus gauge temperature are required in order to correctly convert the gauge output voltage to borehole deformation. These parameters are:

1. Change in gauge output as a function of temperature with no displacement of the cantilevers (pistons removed), giving a value for $(V_{oi} - V_{ol})$;
2. Gauge calibration factor C_o at ambient temperature;
3. Change in calibration factor as a function of temperature, given by $(C_i - C_o)/C_o$.

The first two parameters are gauge dependent and must be measured for each gauge. The third is a function of the strain gauge used on the cantilevers, and was initially considered constant for all the gauges used at Stripa.

3.2.1 Pre- and Post-Experiment Calibrations

The calibration factor at ambient temperature (C_C) and change in output vs temperature ($V_{Oi} - V_{OO}$) were measured for each USBM gauge, before being installed at Stripa. The procedures were identical to those reported by Schrauf et al. (1979). All gauges that were operational at the conclusion of the heating experiments were recalibrated. The calibration data for the gauges used on experiment H9 and H10 are listed in Table 3-1 and 3-2 respectively.

Of the 22 gauges recalibrated, three showed excessive shift with recalibration, i.e., a change greater than the standard deviation of the average. These three gauges (U8, U26, and U27) should be given special consideration when assigning error bars to the recorded data. The average value and standard deviation were calculated for V_{OO}, $(V_{O1} - V_{OO})$, and C_C and are shown in Table 3-3.

3.2.2 Change in Calibration Factor vs Temperature

The temperature-dependent change in calibration factor of the strain-gauge cantilever system is a result of contributions from various elements of the system. Some factors that can change with temperature and thus alter the gauge sensitivity are: gauge alloy, elastic modulus of the cantilever arms, elastic modulus of the gauge backing material, and elastic modulus of the bonding material.

At the beginning of this program, the change in calibration factor with temperature was believed to be the same for all gauges (Schrauf et al., 1979). However, subsequent tests on three additional gauges indicated that this is not the case. The additional gauges tested were #405, which had been installed, failed, and rebuilt; #416 which had been installed in borehole

Table 3-1. USBM gauge calibrations, H9.

Gauge	Record No.	Pre-Experiment				Post-Experiment			
		Date	V_{oo} (mV)	Calib. Factor (mm/mV)	$V_{o1} - V_{oo}$ (mV)	Date	V_{oo} (mV)	Calib. Factor (mm/mV)	$V_{o1} - V_{oo}$ (mV)
U1-1	201	8/78	.106	.0686	-.320	3/80	.071	.0688	-.317
U1-2	202	8/78	-.038	.0665	-.140	3/80	.063	.0661	-.155
U1-3	203	8/78	2.445	.0662	.090	3/80	NG	.0658	NG
U2-1	204	8/78	.207	.0658	.012	--	--	--	--
U2-2	205	8/78	.188	.0657	-.054	--	--	--	--
U2-3	206	8/78	.445	.0649	.012	--	--	--	--
U2-1	204	9/79	-.109	.0647	-.172	3/80	-.054	.0646	-.200
U2-2	205	9/79	-.028	.0645	.013	3/80	.036	.0638	-.030
U2-3	206	9/79	-.275	.0656	.085	3/80	-.269	.0635	.128
U3-1	207	8/78	-.110	.0645	.076	--	--	--	--
U3-2	208	8/78	2.140	.0656	-.047	--	--	--	--
U3-3	209	8/78	-.264	.0646	-.067	--	--	--	--
U4-1	210	8/78	.197	.0642	.242	3/80	.243	.0642	.183
U4-2	211	8/78	-.252	.0659	.231	3/80	-.219	.0658	.177
U4-3	212	8/78	.397	.0655	000	3/80	.356	.0658	.004
U5-1	213	8/78	.299	.0651	.006	--	--	--	--
U5-2	214	8/78	-.235	.0658	.042	--	--	--	--
U5-3	215	8/78	2.750	.0637	.043	--	--	--	--
U5-1	213	9/79	.539	.0678	-.221	3/80	.546	.0681	-.215
U5-2	214	9/79	-.641	.0672	-.142	3/80	-.590	.0659	-.181
U5-3	215	9/79	-.083	.0653	-.065	3/80	-.054	.0639	-.045
U6-1	216	8/78	.046	.0682	.029	--	--	--	--
U6-2	217	8/78	.362	.0661	-.017	--	--	--	--
U6-3	218	8/78	.304	.0653	.165	--	--	--	--
U6-1	216	8/79	1.111	.0658	.022	3/80	1.144	.0657	.057
U6-2	217	8/79	-.043	.0648	-.060	3/80	-.046	.0648	-.029
U6-3	218	8/79	-.068	.0646	.011	3/80	000	.0640	.018
U7-1	219	8/78	-.233	.0697	-.124	--	--	--	--
U7-2	220	8/78	-.038	.0632	-.208	--	--	--	--
U7-3	221	8/78	.631	.0668	-.039	--	--	--	--
U7-1	219	8/79	-.221	.0621	-.028	3/80	-.225	.0626	.001
U7-2	220	8/79	-.049	.0650	-.122	3/80	-.027	.0651	-.128
U7-3	221	8/79	.636	.0677	.071	3/80	.598	.0665	-.048

XBL821-1658

Table 3-1 continued. USBM gauge calibrations, H9.

Gauge	Record No.	Pre-Experiment				Post-Experiment			
		Date	V_{00} (mV)	Calib. Factor (mm/mV)	$V_{01} - V_{00}$ (mV)	Date	V_{00} (mV)	Calib. Factor (mm/mV)	$V_{01} - V_{00}$ (mV)
U8-1	222	8/78	.073	.0649	-.061	--	--	--	--
U8-2	223	8/78	.216	.0641	.058	--	--	--	--
U8-3	224	8/78	-.040	.0639	.048	--	--	--	--
U8-1	222	9/79	-.517	.0650	.090	3/80	-.495	.0678	.090
U8-2	223	9/79	-.562	.0654	.003	3/80	-.528	.0650	.007
U8-3	224	9/79	-1.617	.0647	.033	3/80	-1.590	.0644	.037
U9-1	225	8/78	-.463	.0581	.200	--	--	--	--
U9-2	226	8/78	-.033	.0695	.008	--	--	--	--
U9-3	227	8/78	.630	.0671	.093	--	--	--	--
U9-1	225	8/79	.421	.0570	.039	3/80	.447	.0564	.061
U9-2	226	8/79	-.230	.0646	-.130	3/80	-.246	.0638	-.062
U9-3	227	8/79	.049	.0655	.102	3/80	.092	.0648	.094
U10-1	228	8/78	.057	.0651	-.026	3/80	-.025	.0653	-.016
U10-2	229	8/78	-.154	.0662	.091	3/80	-.080	.0660	.079
U10-3	230	8/78	.097	.0658	000	3/80	.271	.0658	-.043
U21-1	231	8/78	-.003	.0713	-.054	--	--	--	--
U21-2	232	8/78	-.258	.0694	-.074	--	--	--	--
U21-3	233	8/78	.003	.0667	-.252	--	--	--	--
U22-1	234	8/78	-.166	.0661	-.085	3/80	-.092	.0662	-.112
U22-2	235	8/78	-.418	.0673	.042	3/80	-.358	.0675	.055
U22-3	236	8/78	-1.530	.0666	-.066	3/80	-1.537	.0668	-.071
U26-1	237	8/78	.290	.0641	.055	3/80	.370	.0662	-.022
U26-2	238	8/78	.763	.0655	-.006	3/80	.386	.0662	-.128
U26-3	239	8/78	.242	.0643	.020	3/80	.311	.0648	-.140
U27-1	240	8/78	.518	.0626	-.139	3/80	-.216	.0644	-.322
U27-2	241	8/78	.454	.0631	.026	3/80	-.223	.0660	-.101
U27-3	242	8/78	-.141	.0650	.130	3/80	-.137	.0663	.135
U28-1	243	8/78	.079	.0625	-.158	3/80	-.468	.0638	-.169
U28-2	244	8/78	-1.580	.0663	-.113	3/80	-1.905	.0657	-.098
U28-3	245	8/78	-.589	.0666	000	3/80	-.509	.0668	-.090

XBL821-1659

Table 3-2. USBM gauge calibrations, H10.

Gauge	Record No.	Pre-Experiment				Post-Experiment			
		Date	V_{00} (mV)	Calib. Factor (mm/mV)	$V_{01} - V_{00}$ (mV)	Date	V_{00} (mV)	Calib. Factor (mm/mV)	$V_{01} - V_{00}$ (mV)
U11-1	711	7/78	.177	.0645	.033	--	--	--	--
U11-2	712	7/78	.262	.0656	-.058	--	--	--	--
U11-3	713	7/78	1.765	.0657	-.070	--	--	--	--
U11-1	711	6/79	-1.178	.0638	.059	3/80	-1.130	.0630	.058
U11-2	712	6/79	1.146	.0652	-.038	3/80	1.072	.0655	-.003
U11-3	713	6/79	.906	.0639	-.113	3/80	.761	.0625	-.086
U12-1	714	7/78	-.040	.0666	.057	--	--	--	--
U12-2	715	7/78	.118	.0650	-.214	--	--	--	--
U12-3	716	7/78	.021	.0675	-.171	--	--	--	--
U12-1	714	1/79	.075	.0676	.075	--	--	--	--
U12-2	715	1/79	.275	.0653	-.150	--	--	--	--
U12-3	716	1/79	.075	.0690	-.175	--	--	--	--
U12-1	714	7/79	.109	.0643	-.018	3/80	.164	.0648	-.044
U12-2	715	7/79	-.595	.0653	.153	3/80	-.531	.0649	.132
U12-3	716	7/79	-.308	.0696	-.114	3/80	-.305	.0691	-.089
U13-1	717	9/78	.113	.0650	.146	--	--	--	--
U13-2	718	9/78	-.010	.0645	-.650	--	--	--	--
U13-3	719	9/78	-.183	.0638	-.045	--	--	--	--
U13-1	717	1/79	.100	.0622	-.075	--	--	--	--
U13-2	718	1/79	-1.250	.0650	000	--	--	--	--
U13-3	719	1/79	-1.250	.0647	-.125	--	--	--	--
U13-1	717	7/79	.032	.0676	-.098	3/80	.426	.0677	-.171
U13-2	718	7/79	1.113	.0641	-.022	3/80	.901	.0645	-.012
U13-3	719	7/79	-1.107	.0657	.096	3/80	-1.657	.0654	.094
U14-1	720	6/78	.128	.0645	.136	--	--	--	--
U14-2	721	6/78	-.152	.0644	-.183	--	--	--	--
U14-3	722	6/78	-.190	.0643	-.025	--	--	--	--
U14-1	720	8/78	.405	.0629	-.156	--	--	--	--
U14-2	721	8/78	1.538	.0627	.087	--	--	--	--
U14-3	722	8/78	.237	.0638	-.042	--	--	--	--
U14-1	720	1/79	.110	.0643	-.160	--	--	--	--
U14-2	721	1/79	-.010	.0631	.060	--	--	--	--
U14-3	722	1/79	-.020	.0641	.150	--	--	--	--

XBL 821-1660

Table 3.2 (continued). USBM gauge calibrations, H10.

Gauge	Record No.	Pre-Experiment				Post-Experiment			
		Date	V_{00} (mV)	Calib. Factor (mm/mV)	$V_{01} - V_{00}$ (mV)	Date	V_{00} (mV)	Calib. Factor (mm/mV)	$V_{01} - V_{00}$ (mV)
U14-1	720	7/79	-.411	.0675	-.043	3/80	-.425	.0675	-.034
U14-2	721	7/79	-.496	.0645	.193	3/80	-.404	.0646	.188
U14-3	722	7/79	.429	.0670	-.064	3/80	.487	.0670	-.062
U15-1	723	6/78	-.190	.0666	-.086	--	--	--	--
U15-2	724	6/78	.105	.0683	.022	--	--	--	--
U15-3	725	6/78	.081	.0692	.208	--	--	--	--
U15-1	723	6/79	.158	.0647	-.050	3/80	.147	.0653	-.047
U15-2	724	6/79	.070	.0648	.035	3/80	.046	.0636	.024
U15-3	725	6/79	-.001	.0616	-.037	3/80	-.022	.0613	-.011
U16-1	726	6/78	-1.354	.0657	-.146	--	--	--	--
U16-2	727	6/78	.066	.0691	.034	--	--	--	--
U16-3	728	6/78	.327	.0659	-.261	--	--	--	--
U16-1	726	9/78	.113	.0633	.146	--	--	--	--
U16-2	727	9/78	-.010	.0633	-.650	--	--	--	--
U16-3	728	9/78	-.183	.0634	-.045	--	--	--	--
U16-1	726	7/79	.402	.0672	.088	--	--	--	--
U16-2	727	7/79	.100	.0653	-.090	--	--	--	--
U16-3	728	7/79	.114	.0682	.112	--	--	--	--
U17-1	729	7/78	-.221	.0645	.038	--	--	--	--
U17-2	730	7/78	.117	.0655	.038	--	--	--	--
U17-3	731	7/78	-.079	.0635	-.117	--	--	--	--
U17-1	729	1/79	000	.0666	000	--	--	--	--
U17-2	730	1/79	.075	.0649	.050	--	--	--	--
U17-3	731	1/79	-.820	.0642	-.105	--	--	--	--
U17-1	729	7/79	.171	.0673	-.087	3/80	.142	.0684	-.072
U17-2	730	7/79	.607	.0644	.076	3/80	.627	.0648	.086
U17-3	731	7/79	.215	.0677	.144	3/80	.168	.0668	.139
U18-1	732	7/78	.008	.0640	-.165	--	--	--	--
U18-2	733	7/78	.049	.0647	-.151	--	--	--	--
U18-3	734	7/78	-.485	.0645	-.120	--	--	--	--
U18-1	732	1/79	.040	.0693	-.115	--	--	--	--
U18-2	733	1/79	.110	.0645	-.135	--	--	--	--
U18-3	734	1/79	-.200	.0647	-.125	--	--	--	--

XBL821-1661

Table 3-2 (continued). USBM gauge calibrations, H10.

Gauge	Record No.	Pre-Experiment				Post-Experiment			
		Date	V_{00} (mV)	Calib. Factor (mm/mV)	$V_{01} - V_{00}$ (mV)	Date	V_{00} (mV)	Calib. Factor (mm/mV)	$V_{01} - V_{00}$ (mV)
*U18-1	732	7/79	.001	.1757	-.007	--	--	--	--
U18-2	733	7/79	.120	.1764	.014	--	--	--	--
U18-3	734	7/79	.389	.1742	.006	--	--	--	--
U19-1	735	6/78	-.100	.0637	-.049	--	--	--	--
U19-2	736	6/78	.331	.0656	-.149	--	--	--	--
U19-3	737	6/78	-.698	.0655	-.175	--	--	--	--
U19-1	735	7/79	-1.069	.0681	.008	3/80	-1.065	.0682	-.002
U19-2	736	7/79	-.446	.0681	.297	3/80	-.371	.0675	.245
U19-3	737	7/79	-.025	.0652	.008	3/80	.003	.0656	.002
U20-1	738	6/78	.065	.0655	.008	--	--	--	--
U20-2	739	6/78	.522	.0643	000	--	--	--	--
U20-3	740	6/78	-.052	.0666	.087	--	--	--	--
U20-1	738	1/79	-.050	.0655	-.300	--	--	--	--
U20-2	739	1/79	.100	.0698	.175	--	--	--	--
U20-3	740	1/79	.700	.0666	-.350	--	--	--	--
U23-1	741	7/79	-.015	.0680	-.195	--	--	--	--
U23-2	742	7/79	1.560	.0667	.114	--	--	--	--
U23-3	743	7/79	.007	.0678	.020	--	--	--	--
U24-1	744	7/79	1.714	.0631	-.065	3/80	1.856	.0635	-.073
U24-2	745	7/79	-.283	.0638	-.186	3/80	-.148	.0646	-.178
U24-3	746	7/79	-.298	.0655	.101	3/80	-.166	.0661	.112
U25-1	747	7/79	-.344	.0641	-.100	--	--	--	--
U25-2	748	7/79	.153	.0642	-.019	--	--	--	--
U25-3	749	7/79	-.898	.0648	-.032	--	--	--	--
U29-1	750	7/79	.369	.0674	-.024	--	--	--	--
U29-2	751	7/79	-.237	.0687	-.374	--	--	--	--
U29-3	752	7/79	.061	.0660	.205	--	--	--	--
U30-1	753	7/79	-.308	.0668	.128	3/80	-.302	.0668	.123
U30-2	754	7/79	-.085	.0661	-.069	3/80	-.036	.0681	-.046
U30-3	755	7/79	-.347	.0687	.219	3/80	-.330	.0693	.241

*Gage output terminated with a 300 ohm resistor to reduce noise problem.

XBL821-1662

Table 3-3. Comparison of repeat calibration data.

	V_{oo} (mV)		$V_{o1} - V_{oo}$ (mV)		Calibration factor C_c (mm/mV)	
	Before	After	Before	After	Before	After
Average, 22 gauges	-.056	-.079	-.003	-.017	.06539	.06548
Standard Deviation	.623	.637	.117	.121	.0019	.0020

U22 throughout the course of the heating experiment; and #452, which had been rebuilt and reinstalled in borehole U2. The calibration factors obtained at different temperatures for these three gauges are given in Table 3-4. These data are also plotted in Figs. 3-2 through 3-4.

The results of the calibration as a function of temperature are summarized in Table 3-5. The large and variable change in calibration factor is probably due to a change in the thickness or uniformity of the material used to bond the strain gauges to the cantilever arms. The significance of the uncertainty in the temperature effects on the calibration factor for the USBM gauge is evaluated in Section 3.5.

3.3 Operating History

The failure rate of the USBM gauges used during the heater experiments at Stripa was extremely high, as can be seen in Fig. 3-5 (shaded areas are periods of successful operation). At the end of 11 months, 57% (17 of 30) of the gauges originally installed were inoperative, and at the end of the experiments (approximately 19 months), 22 (73%) of the original gauges had failed. More failures occurred in vertical than in horizontal boreholes: 17

Table 3-4. USBM gauge calibration factor vs temperature (6/81).

Temp. (°C)	Comp. #1 (inches/strain)	Comp. #2 (inches/strain)	Comp. #3 (inches/strain)
	Gauge #405		
22.5	0.9724	0.9880	0.9974
74.5	0.9900	0.9996	1.0038
100.5	0.9950	1.0090	1.0150
150.0	1.0243	1.0282	1.0449
	Gauge #416		
27.8	0.9985	0.9942	0.9842
50.3	1.0300	1.0250	1.0194
100.2	1.0720	1.0475	1.0249
150.4	1.0828	1.0508	1.0558
	Gauge #452		
27.3	0.9893	0.9793	0.9639
50.5	1.0096	0.9898	1.0080
100.2	1.0360	1.0086	1.0165
150.7	1.0575	1.0232	1.0260

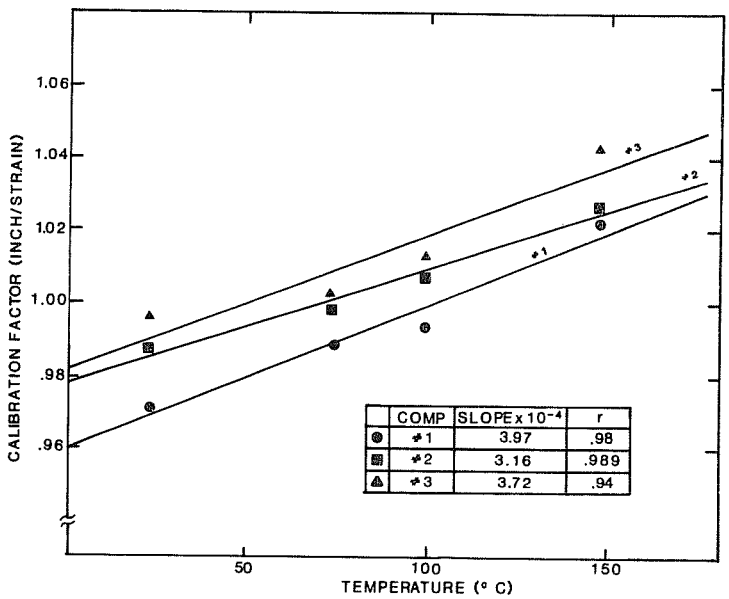

Fig. 3-2. Calibration factor (C_1) as a function of temperature for gauge #405 (6/81).

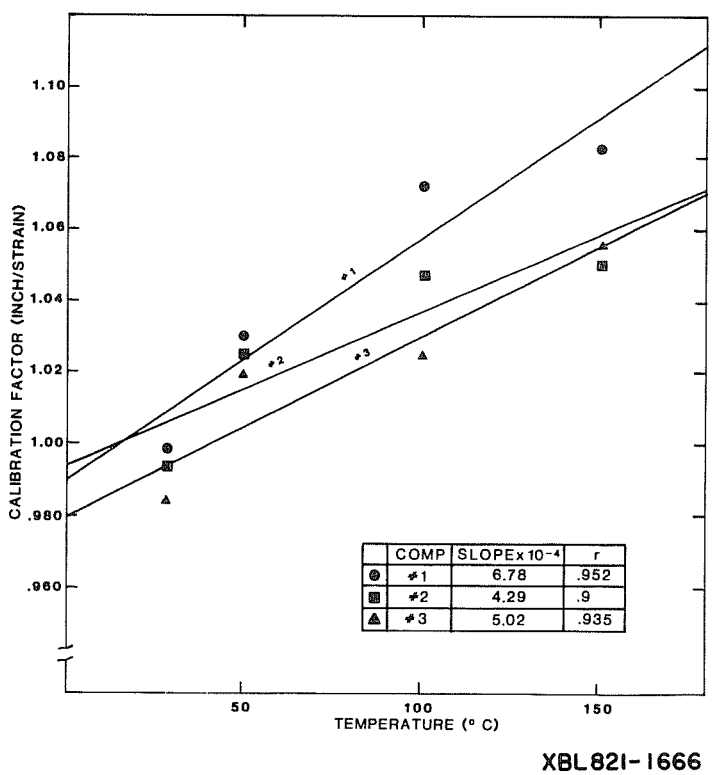

Fig. 3-3. Calibration factor (C_1) as a function of temperature for gauge #416 (6/81).

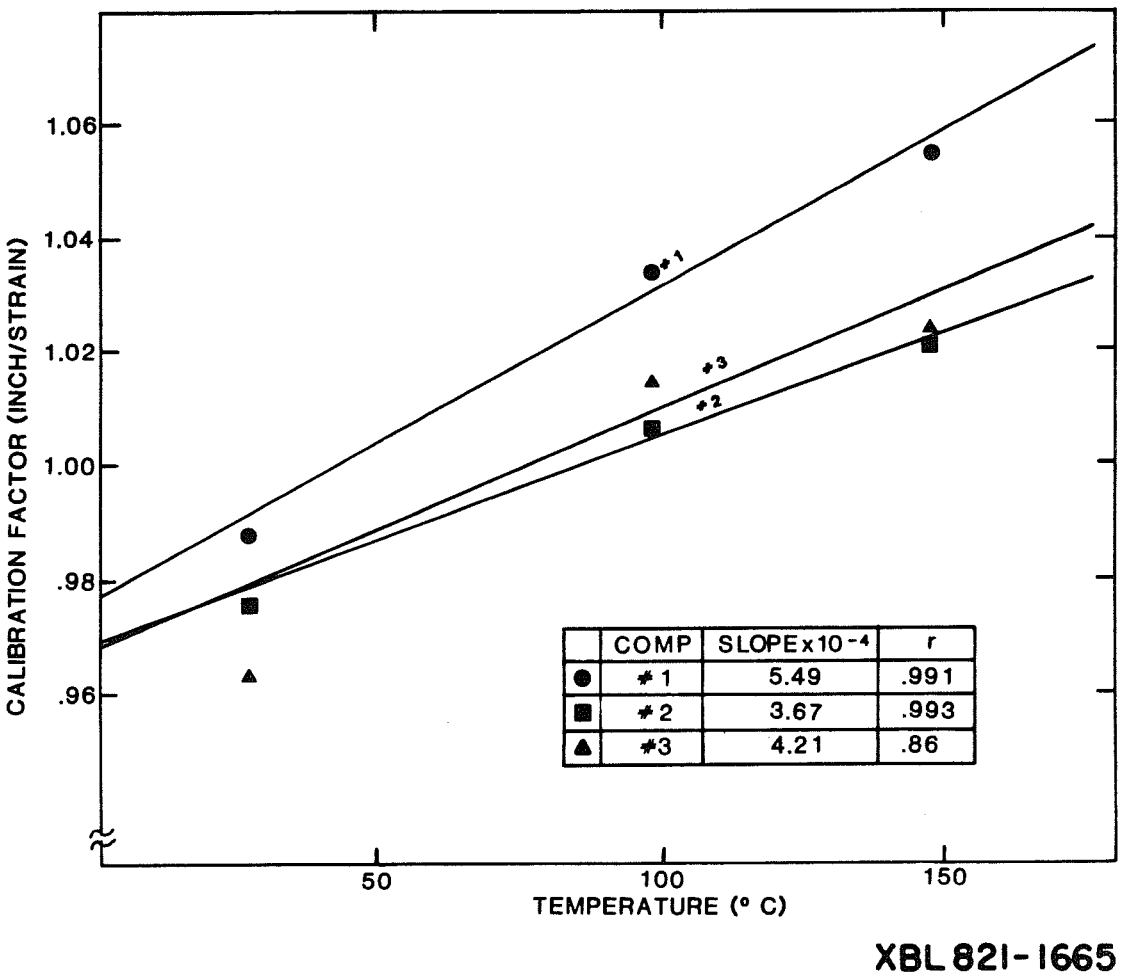

Fig. 3-4. Calibration factor (C_1) as a function of temperature for gauge #452 (6/81).

Table 3-5. Summary of calibration factors vs temperature.

Gauge #	Date	Component #	Average % change (20°C - 200°C)
*401A	6/79	1	6.15
*401B	6/79	2	6.15
*401C	6/79	3	5.10
*405A	6/79	1	8.36
*405B	6/79	2	6.50
*405C	6/79	3	8.00
405A	6/81	1	7.4
405B	6/81	2	5.8
405C	6/81	3	6.8
416A	6/81	1	12.2
416B	6/81	2	7.7
416C	6/81	3	9.1
452A	6/81	1	9.99
452B	6/81	2	6.76
452C	6/81	3	8.65
		Average =	7.04
		Standard deviation =	1.84

*After Schrauf et al., 1979

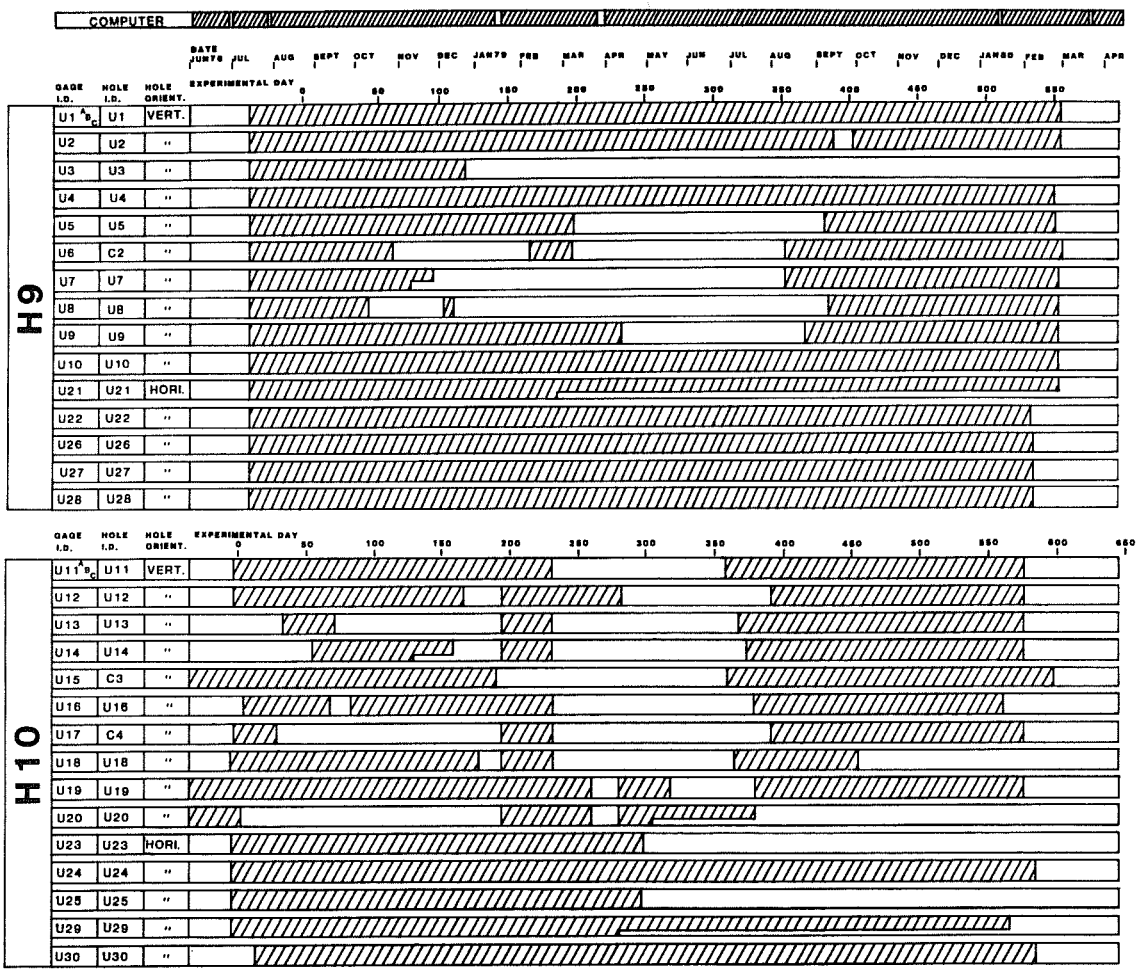

XBL 847-3046

Fig. 3-5. Operating history of USBM gauges.

of the 20 gauges (85%) mounted in vertical boreholes failed. Figure 3-5 shows that many of the failed gauges were repaired, reinstalled, and again failed.

In all cases, the failures were attributed to corrosion problems associated with water infiltration into the gauge body. Prior to turning off the heaters, all available gauges were modified in an attempt to eliminate the water problem. Of the 15 modified gauges reinstalled after July 1980, 6 failed (40%), but water infiltration was not a factor. These failures were all traced to breakage in electrical leads. The gauge modifications and repairs are discussed in more detail in Section 3.4.

Figure 3-5 also indicates that, in a few cases (shown by fractional shading of bars), one component of a gauge failed but the gauge continued to be operational. The reason is that if the gauge is aligned properly, components B (#2) and C (#3) produce redundant data. In vertical holes, component A (#1) was always aligned perpendicular to the plane extending from the hole through the center of the heater hole (in the $\sigma\Theta$ plane); thus components B and C were offset equally from the maximum principal stress plane (σ_r). In the case of a horizontal borehole, component A was aligned in the horizontal plane and components B and C were offset equally from the vertical component of stress (σ_z). The loss of either component B or C would preclude the calculation of the offset angle resulting from misalignment, but the principal stresses could be computed assuming that they were perpendicular and the rock was isotropic and homogeneous.

Figure 3-6a and b shows examples of the field records for the USBM gauges. Records for all gauges are found in Appendix B. A new record was made for each gauge installation even though it may have been the same gauge after repair and reinstallation. In all cases, V_{oo}, $(V_{o1} - V_{oo})$, and C_c were determined before the installation. The field record lists all pertinent

USBM GAUGE FIELD RECORD

Full Scale Experiment H9 Gauge U1 Hole U1

	Label	Sensor No.	Logger Channel	V_{ss} Voltage	V_{oo} Rezero	C_o Slope	$V_{oi}-V_{oo}$ Temp. Const.	T_s Start Temp.	
USBM Gauge	U1A	201	0	7.471	0.106	0.0686	-0.320	11.12	
USBM Gauge	U1B	202	1	7.578	-0.038	0.0665	-0.140	11.12	
USBM Gauge	U1C	203	2	10.732	2.445	0.0662	0.090	11.12	
Corresponding Thermocouple		2	115						

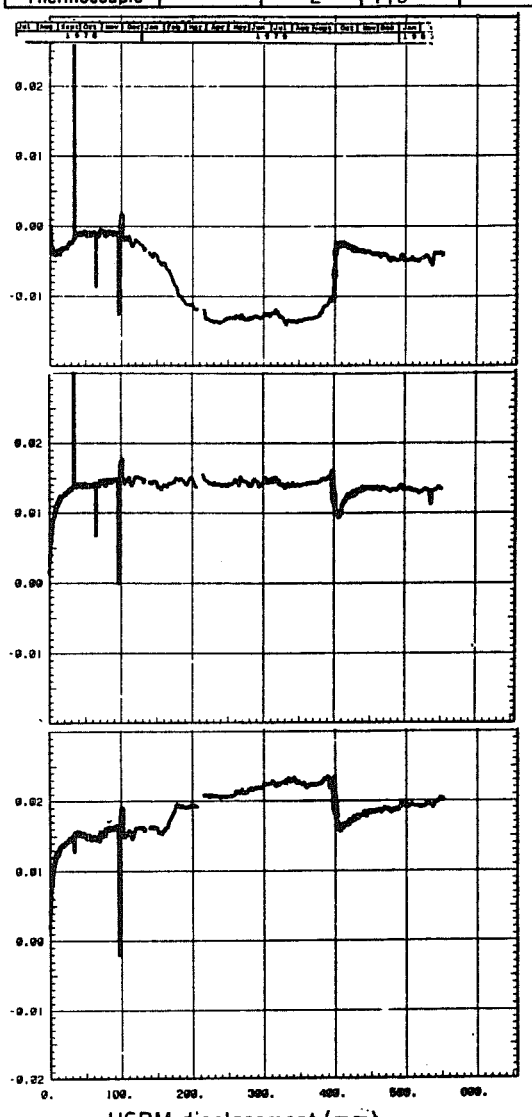

USBM displacement (mm)

[X] vert. [ ] horiz.

r = 1.51

θ = 0

z = 0.85

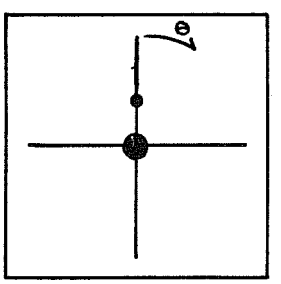

Entire Experiment [X]

Partial Experiment Including
(Calendar dates)

_____ – _____

(Experiment days)

_____ – _____

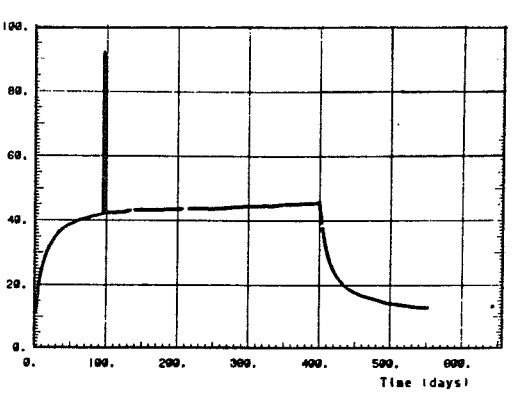

Temp (°C)

XBL 819-7453

Fig. 3-6a. Example of USBM gauge field record (U1).

USBM GAUGE FIELD RECORD

Full Scale Experiment H9 Gauge U2 (1st) Hole U2

	Label	Sensor No.	Logger Channel	V_{ss} Voltage	V_{oo} Rezero	C_o Slope	V_{oi}-V_{oo} Temp. Const.	T_s Start Temp.	
USBM Gauge	U2A	204	3	5.571	0.207	0.0658	0.012	10.44	
USBM Gauge	U2B	205	4	5.947	0.188	0.0657	-0.054	10.44	
USBM Gauge	U2C	206	5	6.772	0.445	0.0649	0.012	10.44	
Corresponding Thermocouple		3	116						

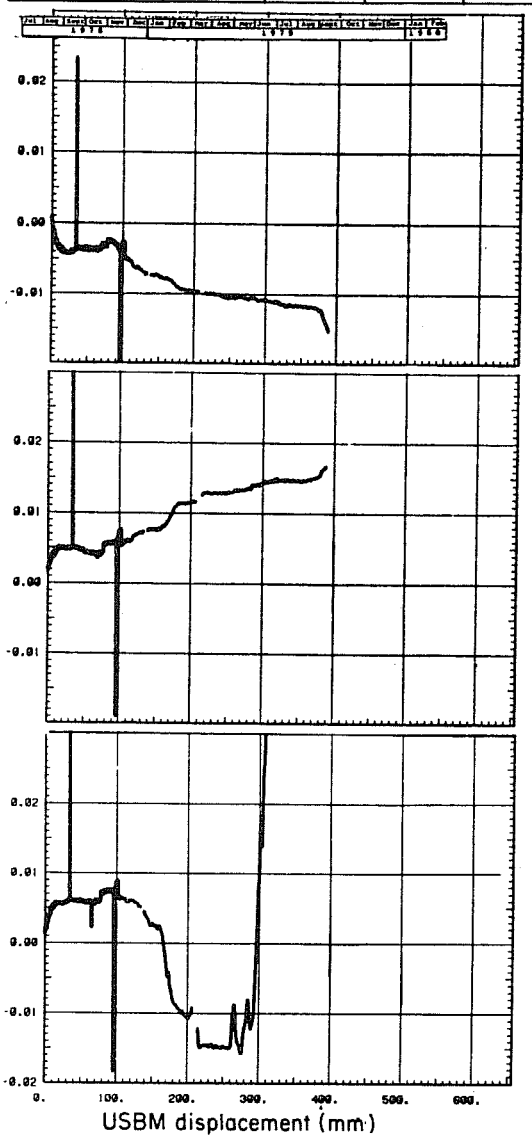

[X] vert. [ ] horiz.

r = 2.49

θ = 0

z = -0.65

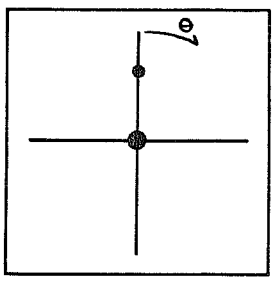

Entire Experiment [ ]

Partial Experiment Including (Calendar dates)

8/24/78 – 9/17/79

(Experiment days)

0 – 389

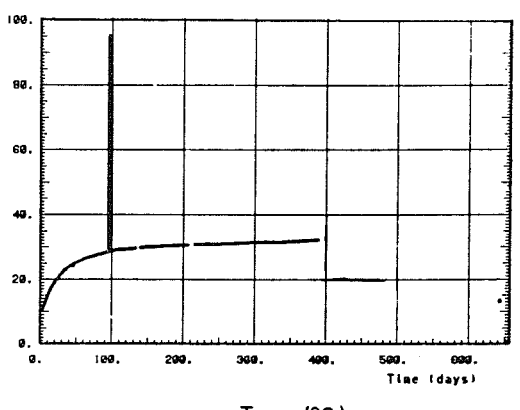

XBL 819-7454

Fig. 3-6b. Example of USBM gauge field record (U2).

information regarding an installed gauge, including its location, duration of operation, and information necessary to calculate the borehole displacement changes, including temperature. All voltages are given in millivolts, C_c is in mm/ mv, and temperature is in °C. To keep track of the many gauge changes, it is recommended that these records be consulted when attempting to interpret the raw data (item c, Table 1-2) recorded at Stripa (Chan et al., 1980).

3.4 Gauge Repair and Modification

As discussed in Section 3.3, there were many USBM gauge failures. The failures were for the most part a direct consequence of water entering the gauge assembly. A concerted effort was put forth on two occasions to try to get as many of the gauges as possible back in operation. The first occasion was prior to turning on the peripheral heaters on experiment H10 (January 23, 1979), and the second was prior to turning off the heaters on both full-scale experiments. On the first occasion, the gauges were repaired either in the field or by the manufacturer (four were returned to the manufacturer for repairs). On the latter occasion, all available gauges were returned to the manufacturer for more extensive modifications in an attempt to eliminate the water infiltration problem.

3.4.1 Gauge Repairs

There were six USBM gauges out of operation on experiment H10 prior to turn-on of the peripheral heaters. The failure of these gauges were all a result of moisture inside the gauge body. All failed gauges had corroded pins on the connector (item 6 in Fig. 3-1), and some had failed because of corrosion at the strain gauges. Four with strain-gauge problems were

returned to the manufacturer for rework, and the other two were repaired in the field. The manufacturer's rework consisted of replacing all strain gauges and replacing both male and female connectors. The field repairs included replacing corroded connectors, removing a damaged section of the cable near the gauge, and wrapping all damaged cable insulation with Teflon tape.

3.4.2 Gauge Modification

In addition to the repairs described above, it was decided to further modify the failed USBM gauges in an attempt to improve reliability. A total of 15 gauges were modified by the manufacturers and reinstalled prior to heater turn-off. The gauge modifications are illustrated in Fig. 3-7 and are as follows:

1. The seal around the electrical cable was improved by the addition of the Teflon bushing.

2. A grounding adaptor and locking screw were provided to insure a more positive connection of the cable shield to the gauge body.

3. The electrical connector was replaced with electrical feed-through pins. This required soldering to both ends of the feed-through, but with the use of higher temperature solder on the strain-gauge side (first attached).

4. The gauge was also modified to make it possible to fill the body with fluid. The fluid was injected through one of the piston holes (Fig. 3-1) by means of an adaptor with a feed-through tube attached to a hand-held syringe. With the bleed plug removed (see Fig. 3-7) and the gauge in the vertical position (cable up) the fluid was forced into the body, up through the vent tubes and into the upper section until it flowed out the bleed hole. Air was left in the space above the bleed hole to allow the fluid to expand as the temperature increased.

5. The end of the electrical cable that extends into the gauge body was vacuum impregnated with a silicone elastomer (Dow Corning Sylgard 182) to provide a better seat for the cable seal and to block water that might get inside the cable insulation.

6. After the solder connection had been made to the feed-through pins, all uninsulated surfaces were coated with a high-temperature (260°C)

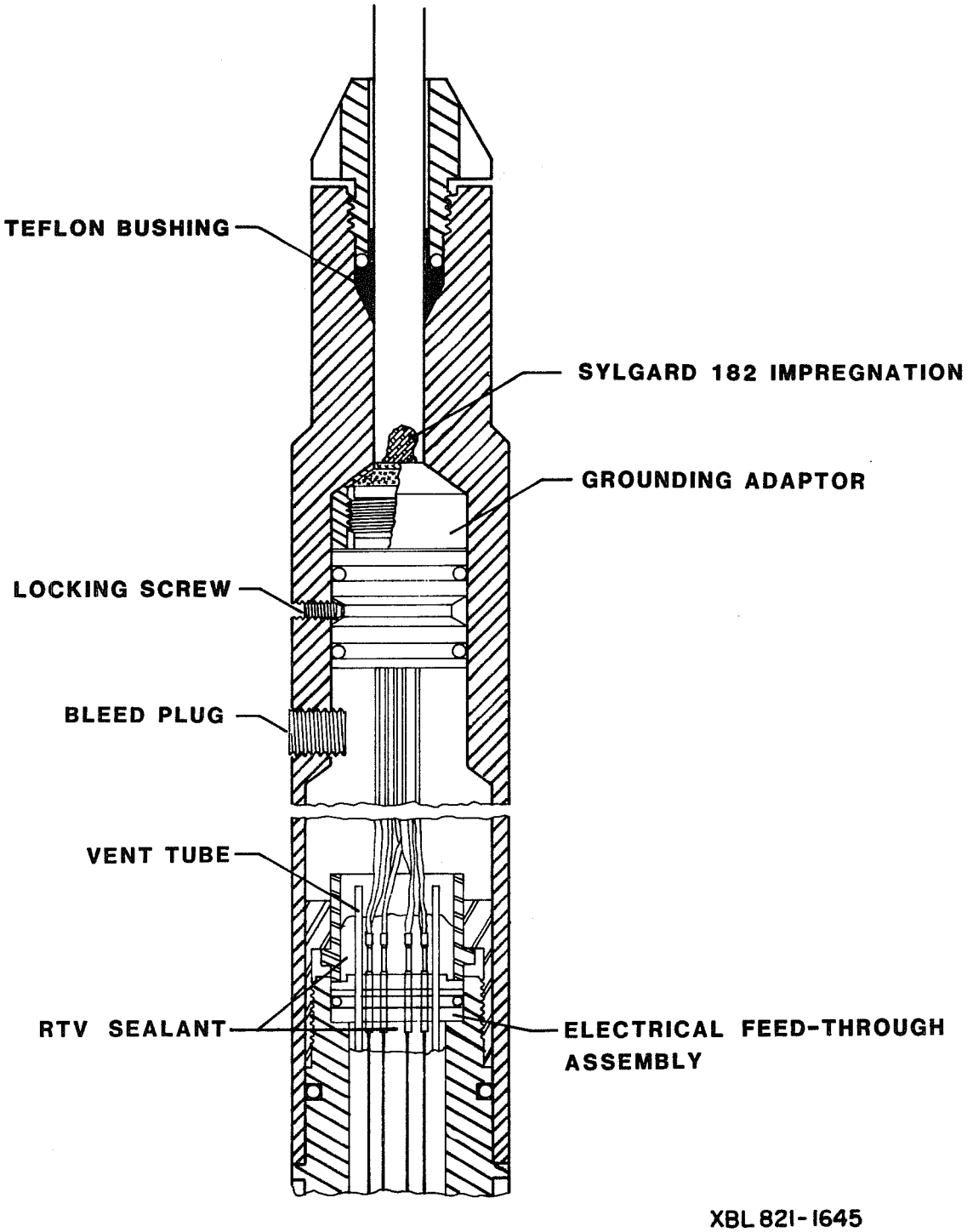

Fig. 3-7. USBM gauge modifications.

fluorosilicone sealant (Dow Corning, RTV 730) to insure the best possible adherence to the Teflon insulation on the electrical lead. A Teflon etch (Tetra-Etch) was used before applying the RTV sealant.

After the gauges were reconnected to the recording system at Stripa, they were temperature-cycled to 200°C before making temperature-offset measurements and calibrations. They were filled with silicone fluid (Dow Corning 550) immediately prior to installation.

3.5 Error Analysis

The following measured quantities are required in order to calculate changes in borehole deformation using the USBM gauge.

1. Voltages (V_i)
2. Temperatures (T_i)
3. Calibration factor (C)
4. Temperature correction for voltage
5. Temperature correction for the calibration factor.

In order to do a comprehensive error analysis, the uncertainty in each measured quantity must be considered. Equation (3-1) was used to calculate the change in borehole diameter; for convenience, it is repeated here:

$$\Delta U_i = C_i (V_i - V_{oi}) - C_s(V_{ss} - V_{os}) . \qquad (3\text{-}1)$$

Assuming $T_1 = 200°C$ and $T_s \simeq T_c \simeq T_o \simeq 11°C$, i.e., the starting temperature, the lower temperature offset, and the calibration temperatures were all the same (they were within about 4°C for the initial installation), then

$$C_s \simeq C_o \simeq C_c \text{ and } V_{os} \simeq V_{oo}.$$

This results in

$$\Delta U_i \simeq C_c \left[1 + \left(\frac{C_1 - C_o}{C_o}\right)\left(\frac{T_i - 11}{189}\right)\right] \left\{V_i - \left[V_{oo} + \left(V_{oi} - V_{oo}\right)\left(\frac{T_i - 11}{189}\right)\right]\right\}$$

$$- C_c \left(V_{ss} - V_{oo}\right) \qquad (3\text{-}9)$$

Since V_{oo} is small compared to V_i and V_{ss} (on the average, less than 10%), this equation simplifies to

$$\Delta U_i \simeq C_c \left[1 + \left(\frac{C_1 - C_o}{C_o}\right)\left(\frac{T_i - 11}{189}\right)\right] V_i - C_c V_{ss} \quad . \qquad (3\text{-}10)$$

3.5.1 Voltage Reading Errors

There were three main sources of error in the USBM gauge voltage reading at Stripa as discussed by Schrauf et al. (1979). They include drift in the gauge output (± 10 microvolts), drift in the bridge excitation voltage (± 7 μV), and A/D converter stability (± 30 μV) from Chan et al., 1980). The root-mean-square of these values (± 32.4 μV) is taken as the best estimate of the true random error. The effect of the uncertainty in the voltage measurements on the calculated borehole deformation can be evaluated by differentiating Eq. (3-10) with respect to the voltage, keeping in mind that the V_{ss} value would be subject to the same uncertainty as V_i; therefore:

$$\delta\Delta U_i \simeq \pm\delta V C_c \left[1 + \left(\frac{C_i - C_o}{C_o}\right)\left(\frac{T_i - 11}{189}\right)\right] \pm \delta V C_c \qquad (3\text{-}11)$$

Taking the average values for all gauges of $C_c = 0.0654 \mu m/\mu V$, $\frac{C_i - C_o}{C_o} = 0.0764$, then for $T_i = 30°C$, we get:

$$\delta\Delta U_i \simeq (\pm 32.4)(0.0654)\left[1 + (0.0764)\left(\frac{30-11}{189}\right)\right] \pm (32.4)(0.0654)$$

$$\simeq \pm 4.25 \times 10^{-6} \text{ meters (the worst case).}$$

For $T_i = 60°C$,

$$\delta\Delta U_i \simeq \pm 4.28 \times 10^{-6} \text{ meters},$$

and for $T_i = 130°C$,

$$\delta\Delta U_i \simeq \pm 4.34 \times 10^{-6} \text{ meters}.$$

3.5.2. Errors in Temperature Measurement

The uncertainty in the measured temperature (T_i) at the Stripa experiments has been determined to be ± 1°C (Binnall and McEvoy 1981). By differentiating Eq. (3-10) with respect to T_i, the effect of the temperature uncertainty on the calculated borehole deformation can be evaluated as follows:

$$\delta\Delta U_i \simeq V_i \, C_c \left(\frac{C_i - C_o}{C_o}\right) \left(\frac{\delta T_i}{189}\right) . \tag{3-12}$$

With the values of C_c and $\frac{C_i - C_o}{C_o}$ as defined above, and for $V_i = 8000$ μV, this becomes:

$$\delta\Delta U_i \simeq 8000 \; (0.0654) \; (0.0764) \pm \frac{1}{189}$$

$$\simeq \pm 0.21 \times 10^{-6} \text{ meters}$$

This error is constant with temperature.

3.5.3 Calibration Factor Error

To evaluate the significance of the uncertainty in the calibration factor, it is necessary to differentiate Eq. (3-10) with respect to C_c. This becomes:

$$\delta\Delta U_i \simeq \delta C_c \left\{\left[1 + \left(\frac{C_i - C_o}{C_o}\right)\left(\frac{T_i - 11}{189}\right)\right] V_i - V_{ss}\right\} . \tag{3-13}$$

Taking $\delta C_c = 6.5 \times 10^{-4}$ (average difference in the pre- and post-experiment calibrations), $V_i = 8000$ μV, $V_{ss} = 7000$ μV,

$$\frac{C_i - C_o}{C_o} = 0.0764, \text{ then for } T_i = 30°C:$$

$$\delta\Delta U_i \simeq 6.5 \times 10^{-4} \left\{\left[1 + (0.0764) \left(\frac{30-11}{189}\right)\right] \quad 8000 - 7000\right\}$$

$$\simeq 0.69 \times 10^{-6} \text{ meters}$$

with $T_i = 60°C$

$$\delta\Delta U_i \simeq 0.75 \times 10^{-6} \text{ meters}$$

and with $T_i = 130°C$

$$\delta\Delta U_i \simeq 0.90 \times 10^{-6} \text{ meters.}$$

3.5.4 Error Due to Temperature Effects on Measured Voltage

The measured voltage at any temperature other than the temperature at which the gauge was installed has undergone a change due to temperature only. The temperature offset measurements (gauge output as a function of temperature with no deflection of the cantilevers) are used to correct for this change; the quantity V_{oo} corrected for temperature is subtracted from the gauge output. To evaluate the effect of the uncertainty in this quantity, Eq. (3-9) is differentiated with respect to V_{oo} to obtain

$$\delta\Delta U_i \simeq \delta V_{oo} \; C_c \left\{\left[\left(\frac{T_i - 11}{189}\right) - 1\right] \left[1 + \left(\frac{C_1 - C_o}{C_o}\right)\left(\frac{T_i - 11}{189}\right)\right] + 1\right\}. \qquad (3\text{-}14)$$

The uncertainty in V_{oo} was found by averaging the difference in the initial and repeat values from Tables 3-1 and 3-2, which is equal to 102 μV. For $T_i = 30°C$ and the other constants as defined previously,

$$\delta\Delta U_i \simeq (102)\ (0.0654) \left\{\left[\left(\frac{30 - 11}{189}\right) - 1\right] \left[1 + (0.0764)\left(\frac{30 - 11}{189}\right)\right] + 1\right\}$$

$$\delta\Delta U_i \simeq 0.62 \times 10^{-6} \text{ meters}$$

with $T_i = 60°C$

$$\delta\Delta U_i \simeq 1.6 \times 10^{-6}$$

and with $T_i = 130°C$

$$\delta\Delta U_i \simeq 4.1 \times 10^{-6} \text{ meters}$$

3.5.5 Error Due to Temperature Effects on Calibration Factor

The calibration factor for any given temperature was determined by scaling the laboratory measured change in the factor over the temperature range of 20°C to 200°C. The average change in the calibration factor $(C_i - C_o)/C_o$ was determined to be 7.64% with a standard deviation of 1.84% (Table 3-4). The effect of this uncertainty is evaluated by differentiating Eq. (3-10) with respect to $(C_i - C_o)/C_o$, which becomes

$$\delta\Delta U_i = C_c V_i \left(\frac{T_i - 11}{189}\right) \delta \left(\frac{C_i - C_o}{C_o}\right) \qquad (3\text{-}15)$$

with $C_c = 0.0654$ μm/μv, $V_i = 8000$ μV, and $T_i = 30°C$

$$\delta\Delta U_i \simeq 0.0654\ (8000) \left(\frac{30 - 11}{189}\right) \quad (0.0184)$$

$$\simeq 0.97 \times 10^{-6} \text{ meters}$$

with $T_i = 60°C$

$$\delta\Delta U_i \simeq 2.5 \times 10^{-6} \text{ meters}$$

and with $T_i = 130°C$

$$\delta\Delta U_i \simeq 6.1 \times 10^{-6} \text{ meters.}$$

3.5.6 Error Due to Uncertainty in Gauge Coefficient of Thermal Expansion

The previously discussed errors are those associated with the measurements taken in the borehole. In addition to these errors, the error associated with the value used for the expansion of the gauge as it is heated must be considered. This is done by differentiating Eq. (3-7) as a function of

α_g (coefficient of thermal expansion of the gauge), which gives

$$\delta\Delta U = \delta\alpha_g \, d(T_i - T_s) \; . \qquad (3\text{-}16)$$

Taking the standard deviation value of $0.99 \times 10^{-6}/°C$ from the average value for $\delta\alpha_g$ (Section 3.6) and with d = 38 mm, $T_s = 11°C$, and $T_i = 30°C$, then:

$$\delta\Delta U = (-0.99 \times 10^{-6}) \; 38 \; (30\text{-}11)$$

$$= -0.7 \times 10^{-6} \text{ meters;}$$

with $T_i = 60°C$,

$$\delta\Delta U = -1.8 \times 10^{-6} \text{ meters,}$$

and with $T_i = 130°C$

$$\delta\Delta U = -4.5 \times 10^{-6} \text{ meters.}$$

3.5.7 Combined Errors

The total error associated with the borehole deformation changes as measured by the USBM gauges used during the Stripa heating experiments can be obtained by the following equation:

$$\delta U_t = \sqrt{(\delta U_1)^2 + \text{----------} (\delta U_N)^2} \qquad (3\text{-}17)$$

where δU_t is the total error and δU_1 through δU_N are the individual contributing errors.

When considering the error resulting from the borehole deformation gauge measurements only, the results obtained in Sections 3.5.1 through 3.5.5 would be used. For example, the total gauge error at a temperature of 60°C (which approximates the average maximum temperature of the USBM gauges) is

$$\delta U_t = \sqrt{(4.28 \times 10^{-6})^2 + (.21 \times 10^{-6})^2 + (.75 \times 10^{-6})^2 + (1.6 \times 10^{-6})^2 + (2.5 \times 10^{-6})^2}$$

$$= 5.3 \times 10^{-6} \text{ meters.}$$

However, this is not the total error to be associated with the data made available by Chan et al. (1980) (item e in Table 1-2). These data also contain the

uncertainty related to the measurement of the coefficient of thermal expansion for the gauge (Section 3.5.6) and is determined (at 60°C as follows:

$$\delta U_t = \sqrt{(4.28 \times 10^{-6})^2 + (.21 \times 10^{-6})^2 + (.75 \times 10^{-6})^2 + (1.6 \times 10^{-6})^2 + (2.5 \times 10^{-6})^2 + (1.8 \times 10^{-6})^2} = 5.6 \times 10^{-6} \text{ meters.}$$

The uncertainty (error) associated with the borehole deformation measurements increase with temperature. The three sample calculations (plotted in Fig. 3-8) show this relationship. This uncertainty in the indicated change in borehole deformation would produce a significant uncertainty in calculated stresses. For the value of voltage change assumed (1000 μV) in the sample calculations, this corresponds to about a ±10% error, and it would be even higher for smaller deformation changes.

3.6 Special Tests

Two special test series were conducted on USBM gauges. This work included leak testing the modified gauges prior to reinstallation before heater turnoff, and the determination of the linear coefficient of expansion of the gauge assembly in the plane of the measured borehole deformation.

3.6.1 Leak Tests

After the USBM gauges were modified by the manufacturer (see Section 3.4) they were shipped to Terra Tek to be checked out and leak tested prior to reinstallation.

3.6.1.1 Test Apparatus. The apparatus used to leak test the USBM gauges is shown in Fig. 3-9. It was made from 1-1/2 inch inside diameter stainless steel pipe with threaded endcaps containing pressure fittings to seal around the electrical cables. A pressure transducer was mounted in the wall of the pipe to monitor pressure applied to the exterior of the gauges. The entire fixture

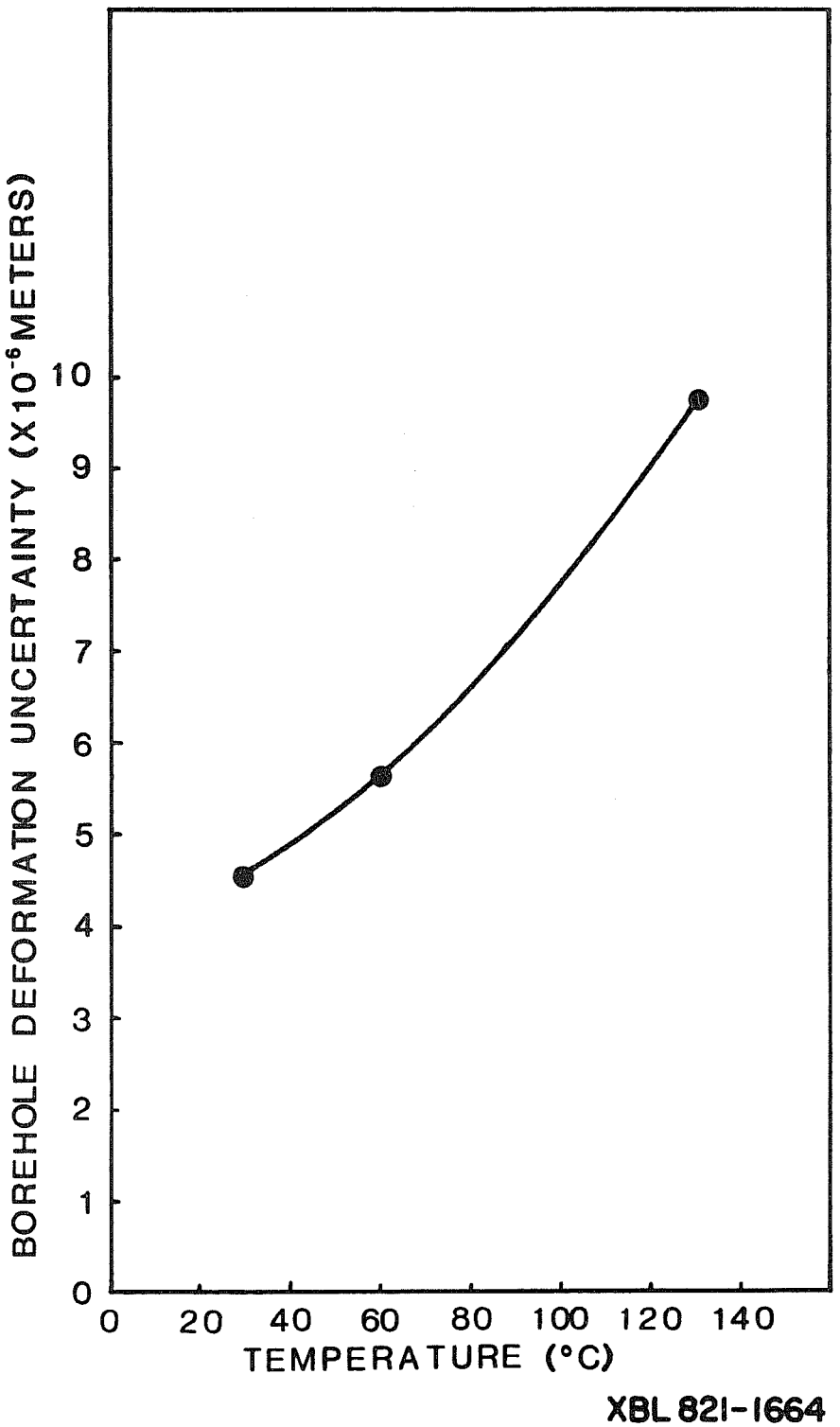

Fig. 3-8. Uncertainty in borehole deformation measurements as a function of temperature.

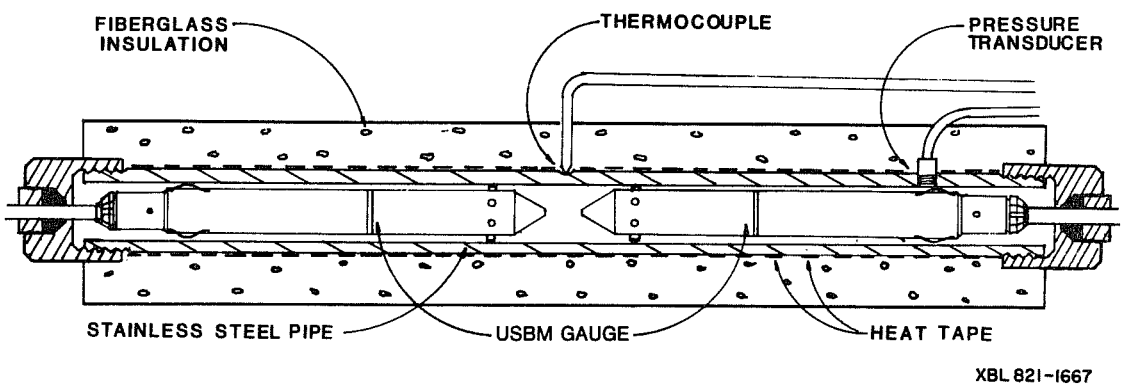

Fig. 3-9. Schematic showing sectional view of leak test apparatus.

was heated by heating tape wrapped around the pipe. Fiber glass insulation was placed over the heat tape to prevent heat loss. The temperature was maintained at equilibrium to within ± 3°C by means of a timer switch in the power line to the heater tape. The three gauge outputs, the temperature, and the pipe internal pressure were automatically recorded by a datalogger.

3.6.1.2 Test Procedure. All gauges were temperature-cycled to 200°C at least once to insure proper operation before the start of the leak test. The pistons were then sized to deflect the cantilevers to midrange when installed in the test apparatus. With two gauges installed and sealed with pressure fittings around the cables, the pipe was filled with water through the pressure transducer mounting hole. Once the gauges were found to be operating properly, the pressure transducer was installed and the power applied to the heating tape. Figure 3-10 shows the temperature and pressure as a function of time for a typical test.

The occurrence of a gauge leak was readily detectable by observing the gauge output, as illustrated in Fig. 3-11. The gauges that developed problems were all returned to the manufacturer for repair and were subsequently successfully leak tested, as shown in Table 3-6. At the conclusion of each leak test, the gauges were disassembled to inspect for signs of water infiltration. Gauges designated "OK" on Table 3-6 contained no sign of moisture inside.

3.6.2 Test to Determine the Expansion Coefficient of the USBM Gauge

The decision was made to experimentally determine the coefficient of expansion (α) for the USBM gauge because of the discrepancy observed between the stress calculated from the USBM gauges, the VWSs, and the model. It was

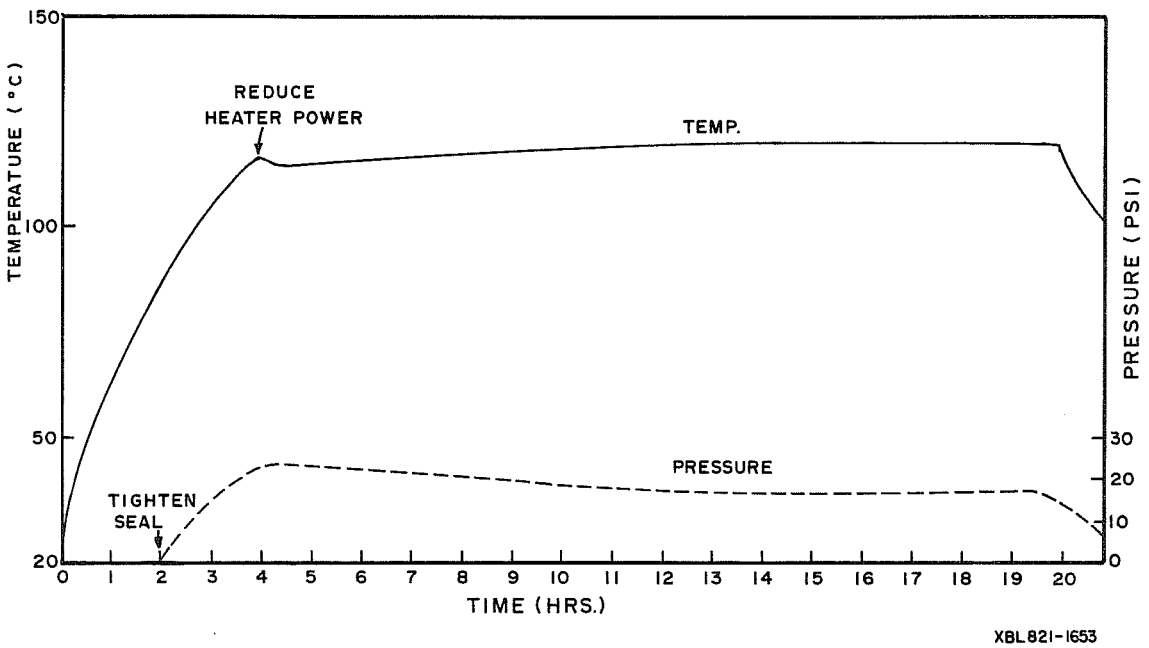

Fig. 3-10. Leak test record.

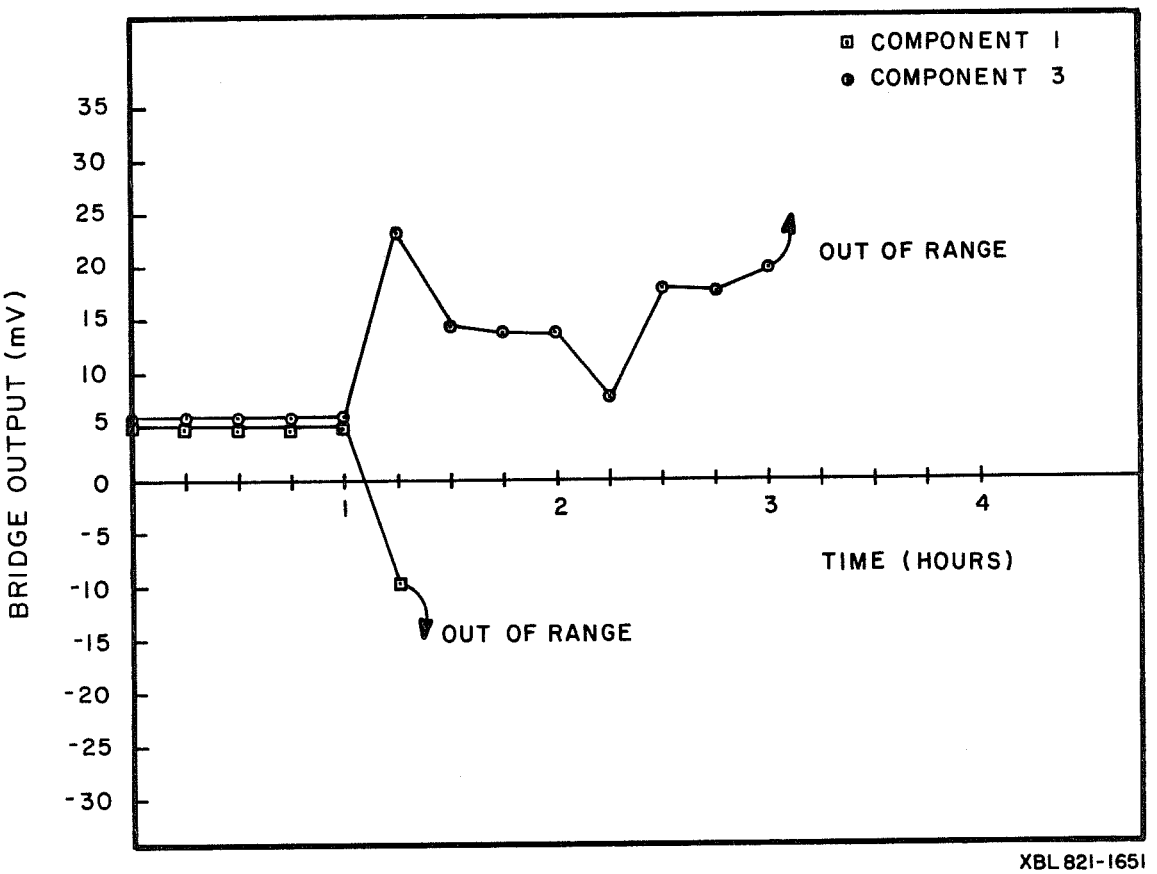

Fig. 3-11. Response of components 1 & 3, gauge #428 as leaking occurred.

Table 3-6. USBM gauge leak test summary

Gauge #	Test duration (Hrs)	Temperature at equilibrium (°C)	Approx. water pressure (PSIG)	Comments
402	23	120	15-20	Strain gauge lead pulled loose during test - returned to manufacturer for repairs.
410	24	120	15-20	Leak occurred, attributed to loose bleed plug. Blown dry, checked OK.
417	24	120	15-20	OK.
408	20	120	15-20	OK.
427	20	120	15-20	Leak test OK, gauge failed during temperature offset measurements.
424	17	127	20-25	Gauge failure, no water in gauge - returned to manufacturer for repairs.
410	17	127	20-25	Same as above.
414	48	125	15-20	Gauge leak due to loose bleed plug. Returned to manufacturer.
428	48	125	15-20	Gauge leak due to loose bleed plug. Blown dry-checked OK.
407	20	115	5-10	OK.
406	20	115	5-10	OK.
424	17	115	*	OK.
410	17	115	*	OK.
415	15	120	10-15	OK.
422	15	120	10-15	OK.
402	12	198	10-15	OK.
428	29	112	10-15	OK.
427	29	112	10-15	OK.
403	12	120	15-20	OK.
414	12	120	15-20	OK

*Pressure transducer connected improperly.

recognized that the use of an incorrect value for α could result in a substantial error when the borehole deformation data was converted to stress. Measurements of α would also check the method used to correct the measured displacement values for temperature effects.

To make the expansion coefficient measurement, the gauge was placed in a cylinder of material of known expansion coefficient. The gauge and material were heated uniformly while measuring the displacements as sensed by the three components. By knowing the expansion of the material and the displacement measured by the gauge, the expansion coefficient of the gauge could be determined.

Two tests were conducted in the laboratory: one with a gauge installed in a stainless steel (304) cylinder, and one in an aluminum (6061) cylinder. The physical dimensions of the test materials are given in Table 3-7.

Table 3-7. Dimensions of test cylinders used for the gauge thermal expansion measurements.

Material	Length (inches)	ID (inches)	OD (inches)
304 SS	18	1 1/2	2 1/2
6061 Al	18	1 1/2	2 1/2

The cylinders were initially cycled several times to 200°C to relieve any residual stresses. They were then strain-gauged to provide an independent measure of cylinder expansion with temperature. Figure 3-12 shows the strain gauge arrangement on each cylinder. Strain gauges were placed at 90 degress

to check for non-uniform expansion of the cylinders. Micromeasurements WK-00-500GB, 350-ohm strain gauges and M Bond 600 cement were used. To correct for gauge resistance changes with temperature, identical dummy gauges were bonded on fused quartz and wired in the bridge arrangement shown in Fig. 3-12. Since fused quartz has an expansion coefficient of approximately 1/30 to 1/40 to that of the 304 stainless steel and 6061 aluminum, the effect of quartz expansion on the bridge balance was minimal and assumed to be zero. The cylinders were temperature-cycled to approximately 150°C while strains were recorded using a Vishay strain indicator. Strain-gauge bridges on the cylinders generally read to within 20 microstrains of one another over a total range of 4500 microstrains (i.e., within 1%). There was no measurable non-uniform expansion of the cylinders due to temperature rise.

The USBM gauge (#405) used for both cylinder tests was a modified gauge which had been calibrated at temperatures and had temperature offsets measured. The use of one gauge for all measurements provided a direct comparison of results and a measure of the repeatability of the gauge performance. Table 3-8 gives the calibration and temperature offset data used in the analysis.

Table 3-8. Gauge #405 calibration information.

Component	C_c (mm/mV)	$\frac{(C_1 - C_o)}{C_o}$ (%)	V_{oo} (mV)	V_{o1} (mV)
1	.0770	8.6	1.82	1.950
2	.0787	8.2	-0.96	-1.107
3	.0787	6.5	1.34	1.321

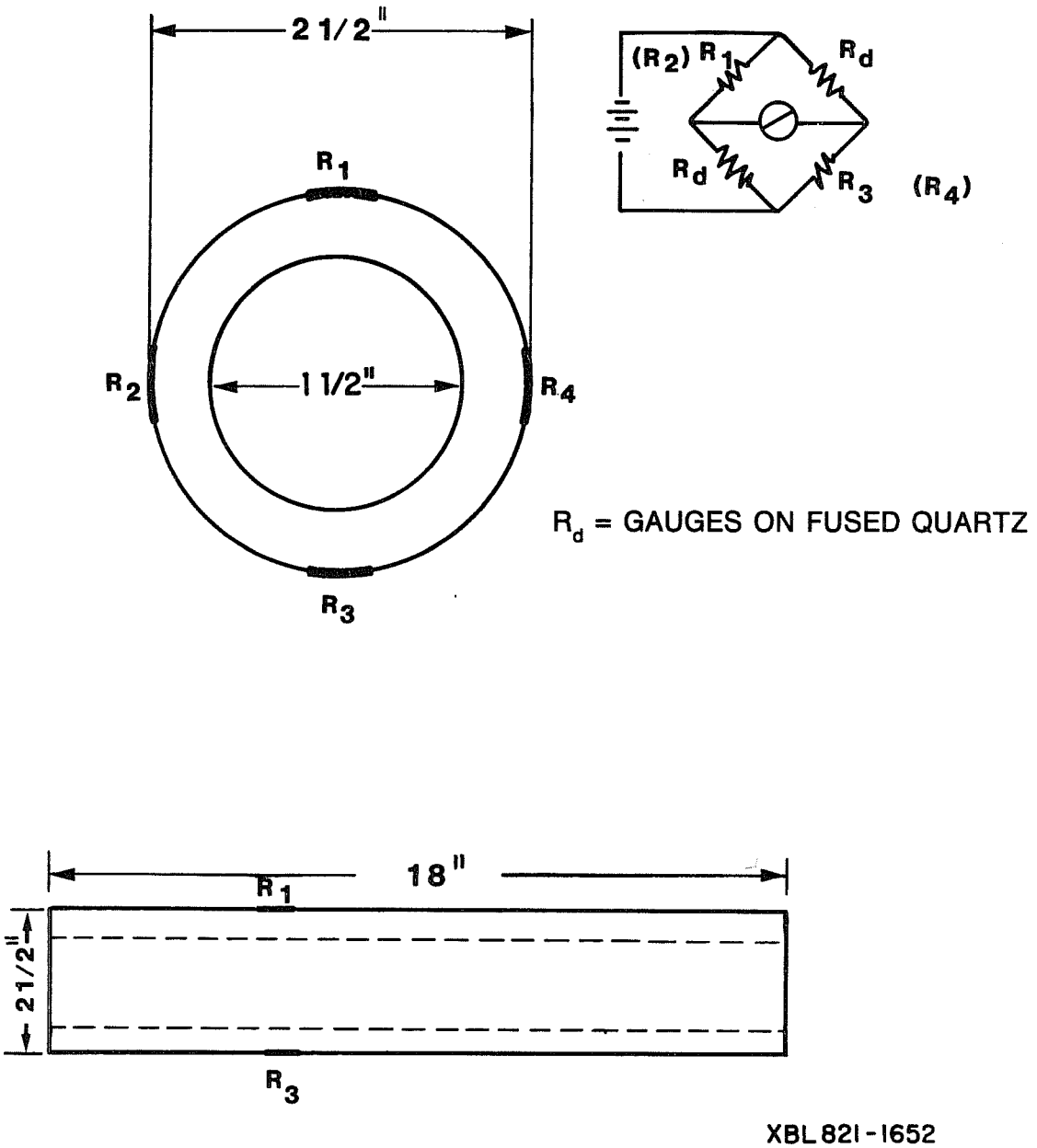

Fig. 3-12. Strain gauge arrangement for stainless steel and aluminum cylinders.

The gauge was initially placed in the stainless steel cylinder with all pistons shimmed equally. The gauge and cylinder were placed in a controlled temperature chamber and allowed to stabilize for several hours at approximately 50°C. Cylinder strains were manually read on the strain indicator with switch and balancing unit. All bridges were balanced after readings stabilized at 50°C and then the temperature was increased. The USBM gauge voltages and temperatures were recorded by a logger at 15-minute intervals. The resolution of the data logger was 1 μV and 0.1°C.

Figure 3-13 shows typical measured stainless steel cylinder strains for a temperature cycle. This plot indicates a uniform expansion of approximately 16 x 10^{-6}/°C, which is within the range of handbook values.

The identical tests were run using the aluminum cylinder; the cylinder strains plotted in Fig. 3-14 show the linear coefficient of expansion to be 22.5 x 10^{-6}/°C. The borehole displacement (ΔU_i) at each test temperature was calculated using the measured voltages and the values from Table 3-8 in Eq. (3-1). These data are shown for stainless steel cylinders in Fig. 3-15 and for aluminum in Fig. 3-16.

The expansion coefficient for the gauge (α_g) was calculated using the following equation:

$$\alpha_g = \frac{1}{d}\left(\frac{\Delta U_i}{\Delta T}\right) + \alpha_c \qquad (3\text{-}18)$$

where $\frac{\Delta U_i}{\Delta T}$ is the slope of the borehole deformation vs temperature curve, d is the borehole diameter (38 mm), and α_c is the expansion coefficient for the

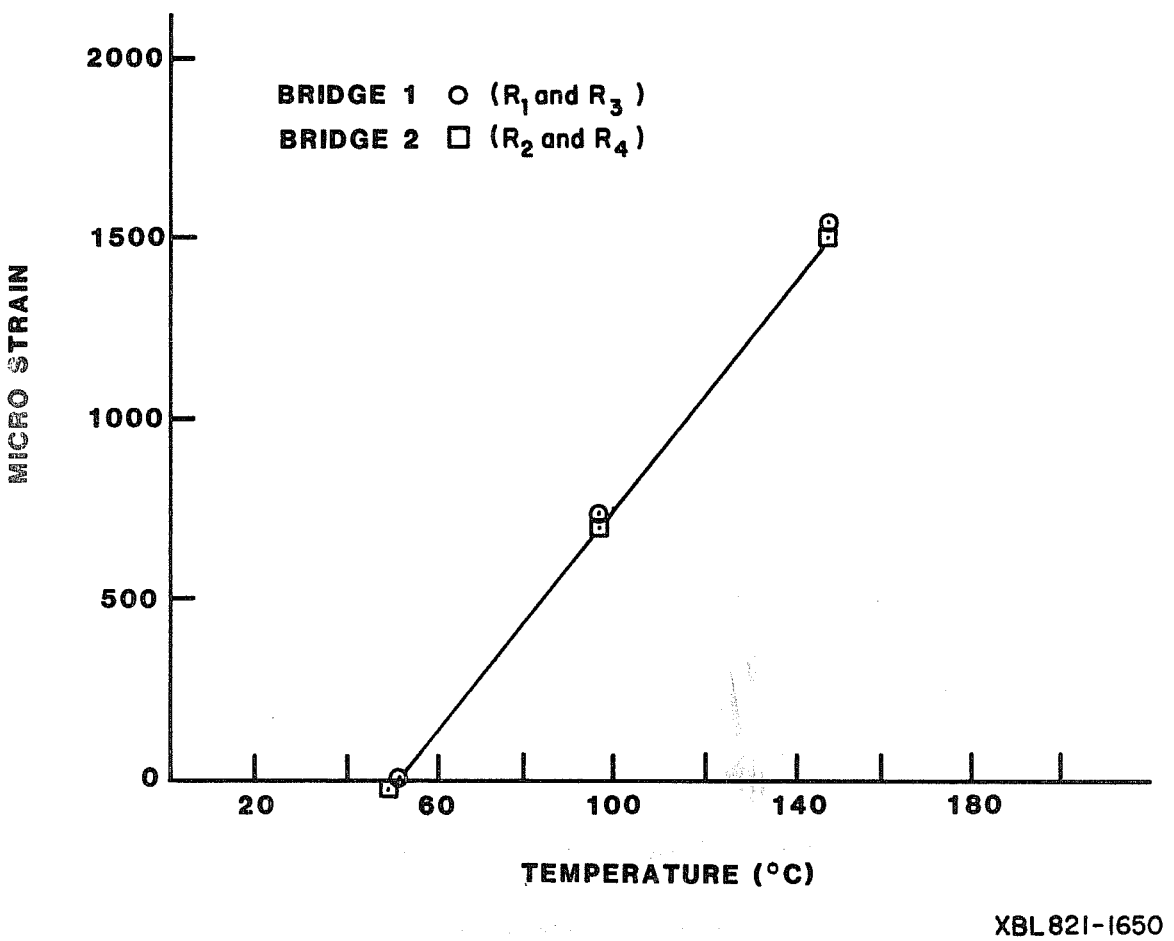

Fig. 3-13. Stainless steel cylinder strains as a function of temperature.

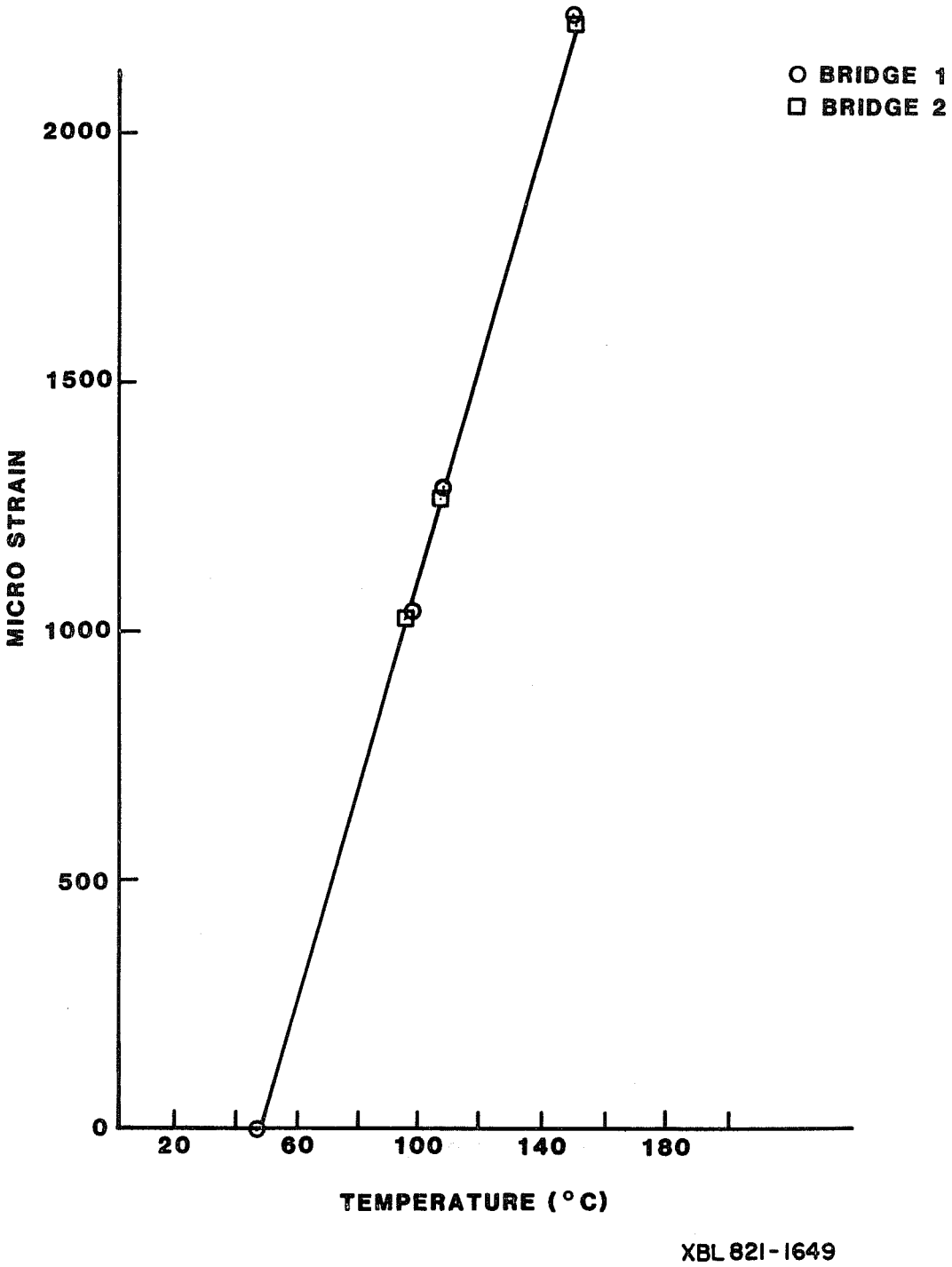

Fig. 3-14. Aluminum cylinder strains as a function of temperature.

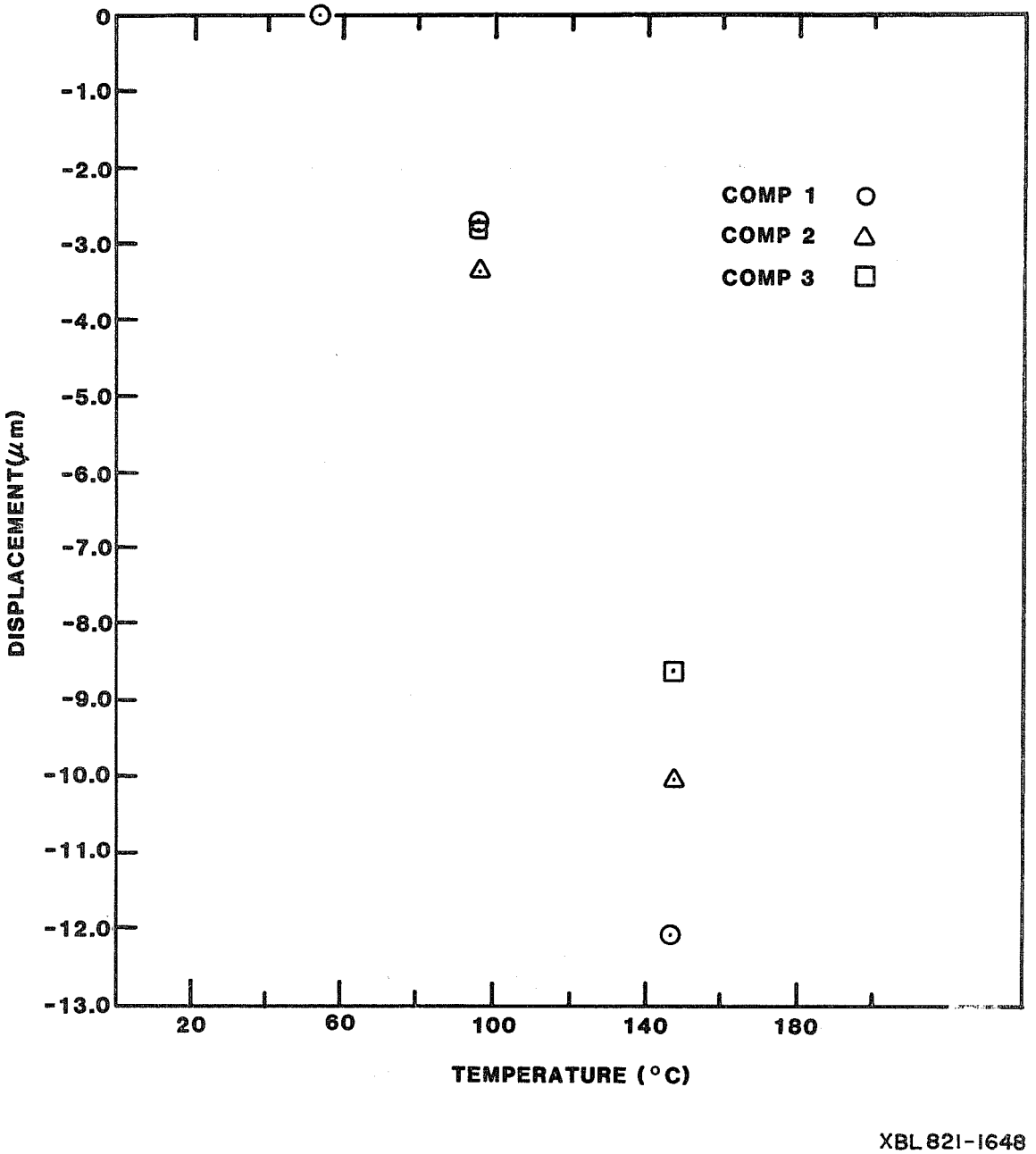

Fig. 3-15. Borehole deformation vs. temperature for stainless steel cylinder.

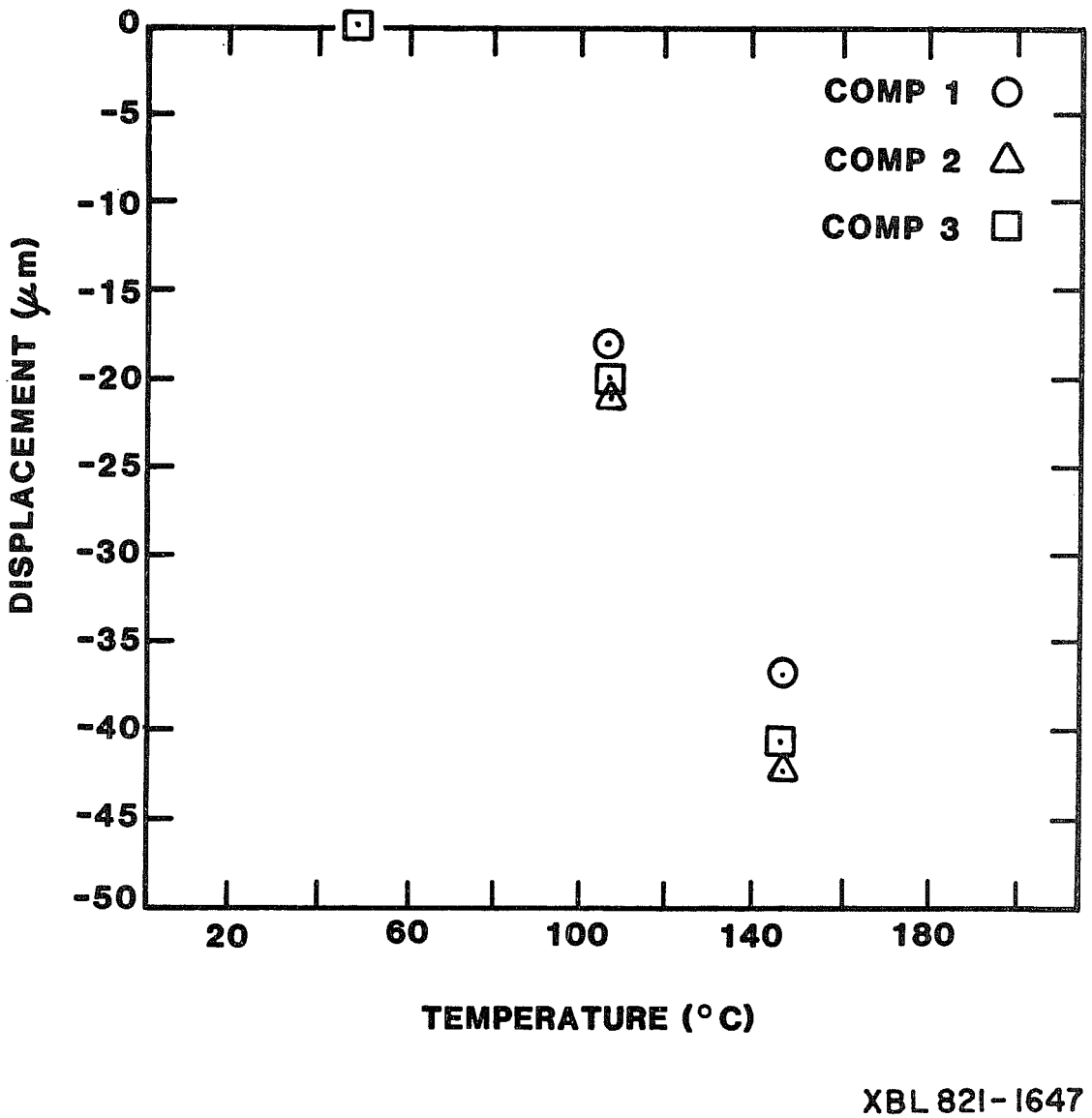

Fig. 3-16. Borehole displacement vs. temperature for aluminum cylinder.

cylinder ($16 \times 10^{-6}/°C$ for the stainless steel and $22.5 \times 10^{-6}/°C$ for aluminum). Figure 3-17 shows the calculated values for α_g using the measured data from the cylinder test. The $\frac{\Delta U_i}{\Delta T}$ values were taken as the straight line from the starting point to the value at the measured temperature. The average value for α_g from these data was $13.26 \times 10^{-6}/°C$ with a standard deviation of $\pm 0.99 \times 10^{-6}/°C$.

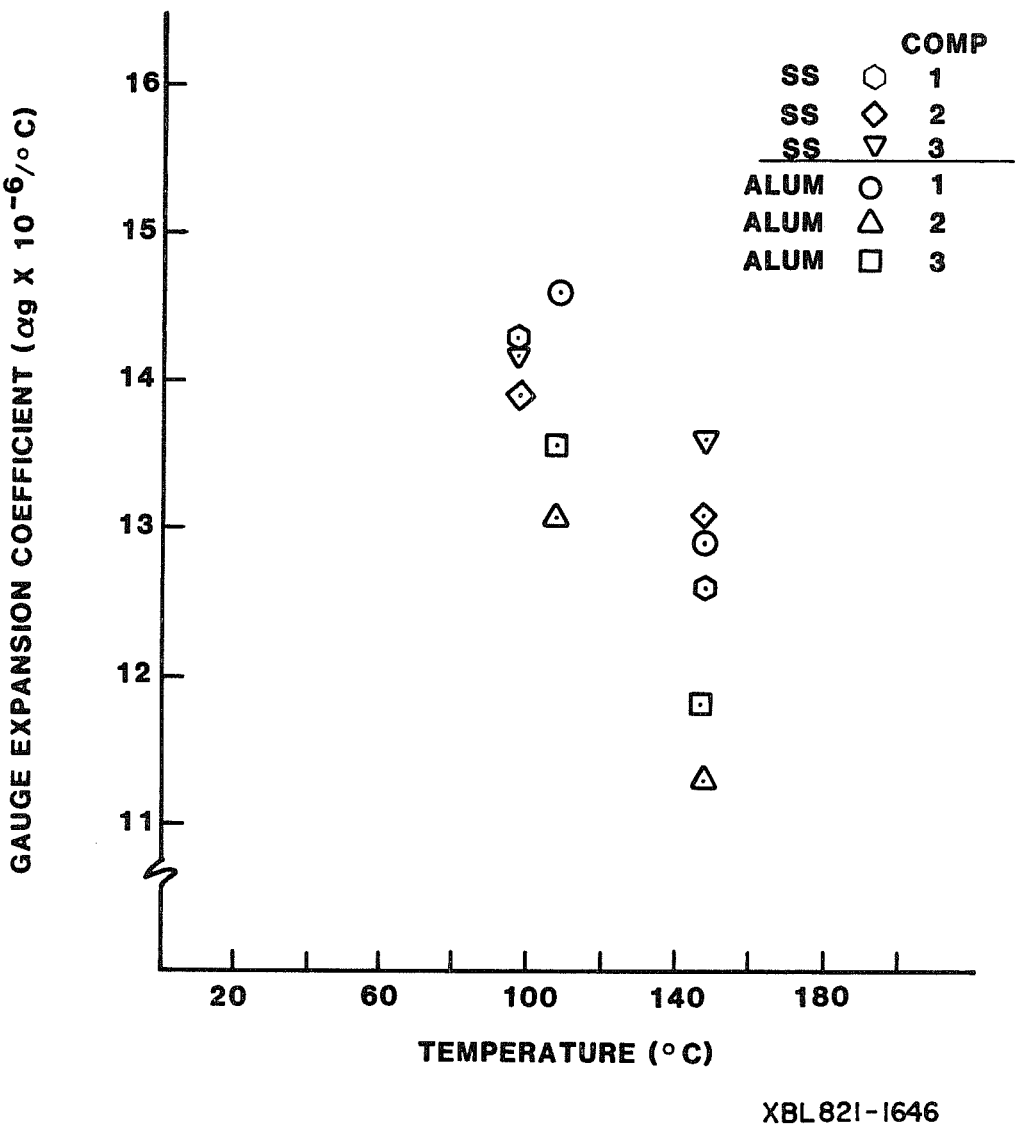

Fig. 3-17. Calculated αg from stainless steel and aluminum cylinder test.

4. SAMPLE STRESS CALCULATIONS

To illustrate the procedures for calculating stress and to compare the measured (VWS and USBM) and predicted data, a few sample calculations were made. The stress change was calculated for the cool-down period by taking values measured just before heater turn-off and before gauge deactivation. To avoid confusion from possibly conflicting sign conventions, only the magnitude of the stress change will be presented.

4.1 Stress Change Calculations from USBM Gauge Measurements

The equations used to calculate the stress changes from the corrected borehole displacement measurements are those presented by Obert and Duvall (1976) and are as follows:

$$\Delta\sigma R = \frac{E}{(1-\nu)^2}\,6d\left\{(U_1 + U_2 + U_3) + \frac{\sqrt{2}}{2}\left[(U_1 - U_2)^2 + (U_2 - U_3)^2 + (U_3 - U_1)^2\right]^{1/2}\right\} \quad (4\text{-}1)$$

$$\Delta\sigma\Theta = \frac{E}{(1-\nu)^2}\,6d\left\{(U_1 + U_2 + U_3) - \frac{\sqrt{2}}{2}\left[(U_1 - U_2)^2 + (U_2 - U_3)^2 + (U_3 - U_1)^2\right]^{1/2}\right\} \quad (4\text{-}2)$$

where $\Delta\sigma\Theta$ (minor principal stress) is the stress normal to $\Delta\sigma R$,

E = Young's modulus of the rock = 70 GPa,

ν = Poisson's ratio of the rock = 0.225,

d = borehole diameter = 38 mm, and

U_1, U_2, and U_3 are the measured borehole diametral changes. The equations were developed assuming U to be positive for increasing borehole diameter, but the data recorded at Stripa (Chan et al., 1980) were negative. Therefore, when computing the stresses it is necessary to reverse the signs of the values for the borehole deformation change.

The indicated diameter change must be corrected for the thermal expansion of the rock (α_r); in these examples, 9 x 10^{-6}/°C was used. The computed displacements and stress changes from the USBM gauge measurements during cool-down are listed in Table 4-1 and Table 4-2. Because the thermal expansion correction for the rock is of the same magnitude as the measured diameter change, uncertainty in α_r is clearly significant in the final stress calculation.

4.2 Stress-Change Calculations from VWS Measurements

The VWSs were installed in pairs. One member was mounted (in both vertical and horizontal boreholes) perpendicular to the plane that extended from the gauge itself through the heater (Θ). The other was mounted in one of two ways: in vertical boreholes, in a plane that passed through the heater borehole hole (R); in horizontal horeholes, in a plane parallel to the heater borehole (Z). The sample calculations presented here are only for gauges mounted in vertical boreholes (Θ and R).

Equation (2-9) (Section 2.1) was used to calculate the stress change from the recorded data (gauge period measurements). The equation is:

$$\Delta\sigma = C_1 \left(\frac{1}{R^2} - \frac{1}{R_s^2}\right) \quad ,$$

where R is the final gauge reading, R_s is the starting or reference reading, and C_1 = 0.44 x 10^9 (the average value for C_1). The starting and final reading are identical in time to those used in the USBM gauge sample calculations.

The values of $\Delta\sigma$ for the two gauges (Θ and R) obtained with the above equation are the apparent uniaxial stress changes, but the true values are somewhat larger because of the mutual interaction of the stress field at the

Table 4-1. Calculated stress changes in USBM gauges for H9 experiment.

Gauge ID	Gauge component	Y (meters)	Z (meters)	Diameter change (μ meters)	Temperature change (°C)	α_r corrections (μ meters)	Diameter change corrected	ΔσR (MPa)	ΔσR (MPa)
U1	A	1.51	0.85	6.279	-32.3	-11.047	- 4.768		
U1	B	1.51	0.85	-2.854	-32.3	-11.047	-13.901	13.6	7.6
U1	C	1.51	0.85	-3.134	-32.3	-11.047	-14.181		
U2	A	2.49	-0.65	1.000	-20.0	- 6.840	- 5.840		
U2	B	2.49	-0.65	-7.000	-20.0	- 6.840	-13.840	13.0	8.7
U2	C	2.49	-0.65	-6.000	-20.0	- 6.840	-12.840		
U4	A	2.25	0.85	0.897	-20.5	- 7.011	- 6.114		
U4	B	2.25	0.85	-2.760	-20.5	- 7.011	-11.196*	10.9	7.6
U4	C	2.25	0.85	-5.609	-20.5	- 7.011	-11.196*		
U5	A	3.27	-0.65	0.622	-13.1	- 4.480	- 3.858		
U5	B	3.27	-0.65	-5.006	-13.1	- 4.480	- 9.486	10.0	5.8
U5	C	3.27	-0.65	-6.560	-13.1	- 4.480	-11.040		
U6	A	1.48	-0.65	10.341	-35.6	-12.175	- 1.834		
U6	B	1.48	-0.65	-8.239	-35.6	-12.175	-20.424	29.9	7.8
U6	C	1.48	-0.65	-8.476	-35.6	-12.175	-20.651		
U7	A	2.00	-0.65	4.461	-25.2	- 8.618	- 4.157		
U7	B	2.00	-0.65	-7.208	-25.2	- 8.618	-15.826	15.4	7.8
U9	A	2.28	0.85	1.064	-20.2	- 6.908	- 5.844		
U9	B	2.28	0.85	-	-20.2	-	-12.929	12.5	8.0
U9	C	2.28	0.85	-6.021	-20.2	- 6.908	-12.929		
U10	A	3.25	0.85	-0.904	-12.3	-4.207	- 5.111		
U10	B	3.25	0.85	-	-12.3	-	- 6.155	6.0	5.3
U10	C	3.25	0.85	-1.948	-12.3	-4.207	- 6.155		

Y = radial distance to the heater.
Z = vertical distance to the heater center line (positive is above).
* = average value used.

Table 4-2. Calculated stress changes in USBM gauges for H10 experiment.

Gauge ID	Gauge component	Y (meters)	Z (meters)	Diameter change (μ meters)	Temperature change (°C)	α_r corrections (μ meters)	Diameter change corrected	ΔσR (MPa)	ΔσΘ (MPa)
U11	A	1.51	0.85	2.096	- 98.8	-33.790	-31.694		
V11	B	1.51	0.85	-36.366	- 98.8	-33.790	-70.156	68.1	43.2
U11	C	1.51	0.85	-	- 98.8	-33.790	-70.156		
U12	A	3.48	-0.65	18.314	- 35.6	-12.175	6.139		
U12	B	3.48	-0.65	-13.085	- 35.6	-12.175	-31.258*	30.3	6.1
U12	C	3.48	-0.65	-25.081	- 35.6	-12.175	-31.258*		
U14	A	3.22	-0.65	6.000	- 40.4	-13.817	- 7.817		
U14	B	3.22	-0.65	-17.326	- 40.4	-13.817	-31.143	28.7	14.5
U14	C	3.22	-0.65	-14.063	- 40.4	-13.817	-27.880		
U15	A	1.59	-0.53	6.669	-108.7	-37.175	-30.506		
U15	B	1.59	-0.53	-29.558	-108.7	-37.175	-59.974*	58.2	39.1
U15	C	1.59	-0.53	-16.039	-108.7	-37.175	-59.974*		
U17	A	2.50	-0.57	13.407	- 57.5	-19.665	- 6.258		
U17	B	2.50	-0.57	-23.980	- 57.5	-19.665	-43.645	39.2	16.9
U17	C	2.50	-0.57	-17.270	- 57.5	-19.665	-36.935		
U19	A	3.00	0.85	6.628	- 41.8	-14.296	- 7.668		
U19	B	3.00	0.85	- 6.641	- 41.8	-14.296	-27.207*	26.4	13.8
U19	C	3.00	0.85	-19.182	-41.8	-14.296	-27.207*		

Y = radial distance to the heater.
Z = vertical distance to the heater center line (positive in above).
* = average value used.

gauge location. The solution to this problem has been worked out by Hawkes and Bailey (1973), and the true principal uniaxial stress change $\delta\sigma R$ and $\delta\sigma\Theta$ are computed as follows:

$$\delta\sigma R = 9/8\Delta\sigma R + 3/8\Delta\sigma R \ , \tag{4-3}$$

and

$$\delta\sigma\Theta = 9/8\Delta\sigma\Theta + 3/8\Delta\sigma\Theta \ . \tag{4-4}$$

Table 4-3 shows the stresses calculated from the VWS readings during cool-down at the Stripa experiments.

4.3 Comparison of Stress Data

The calculated stress changes from the USBM gauges and the VWSs are plotted in Fig. 4-1 for experiment H9 and H10; predicted stresses from Chan and Cook (1979) are also shown. The input parameters for the USBM gauge conversion were the latest available at the time of this report, whereas those used in the model were the best available data at an earlier phase of the project. These values are listed in Table 4-4. The stresses can be approximately scaled by the factor $\alpha E/(1-\nu)$, according to Cook and Witherspoon (1978). This factor is also given in Table 4-4. The use of different input quantities by the model and the gauge data results in a difference in this factor (and therefore in the stress) of less than 10%.

If the theoretical stress results were recomputed using the higher value of $\alpha E/(1-\nu)$, they would increase, and the discrepancy between measured and predicted would increase by about 10%. Even so, the correspondence between stress values derived from the USBM gauges and predicted values appears reasonable in terms of the decline of stress with increasing distance from the heater; but, for some reason, the magnitude of the data from the radial

Table 4-3. Stress change calculated from VWS reading from the H9 and H10 experiments.

Gauge ID	Gauge orientation	Y (meters)	Z (meters)	R	R_s	$\delta\sigma R$ (MPa)	$\delta\sigma\Theta$ (MPa)
*C1	R	0.99	0.85	2008	2320	44.4	51.0
C1	Θ	0.99	0.85	2207	2850		
*C3	R	1.71	-0.65	2200	2353	18.3	20.7
C3	Θ	1.71	-0.65	2290	2520		
C4	R	2.46	-0.65	2174	2394	21.0	14.0
C4	Θ	2.46	-0.65	2211	2302		
C5	R	1.51	0.85	2090	2349	26.6	16.7
C5	Θ	1.51	0.85	2259	2370		
C9	R	3.49	0.85	1998	2060	8.0	4.5
C9	Θ	3.49	0.85	2183	2205		

*questionable data, change in σΘ greater than σR.

Y = radial distance to the heater.

Z = vertical distance to heater centerline (positive is above).

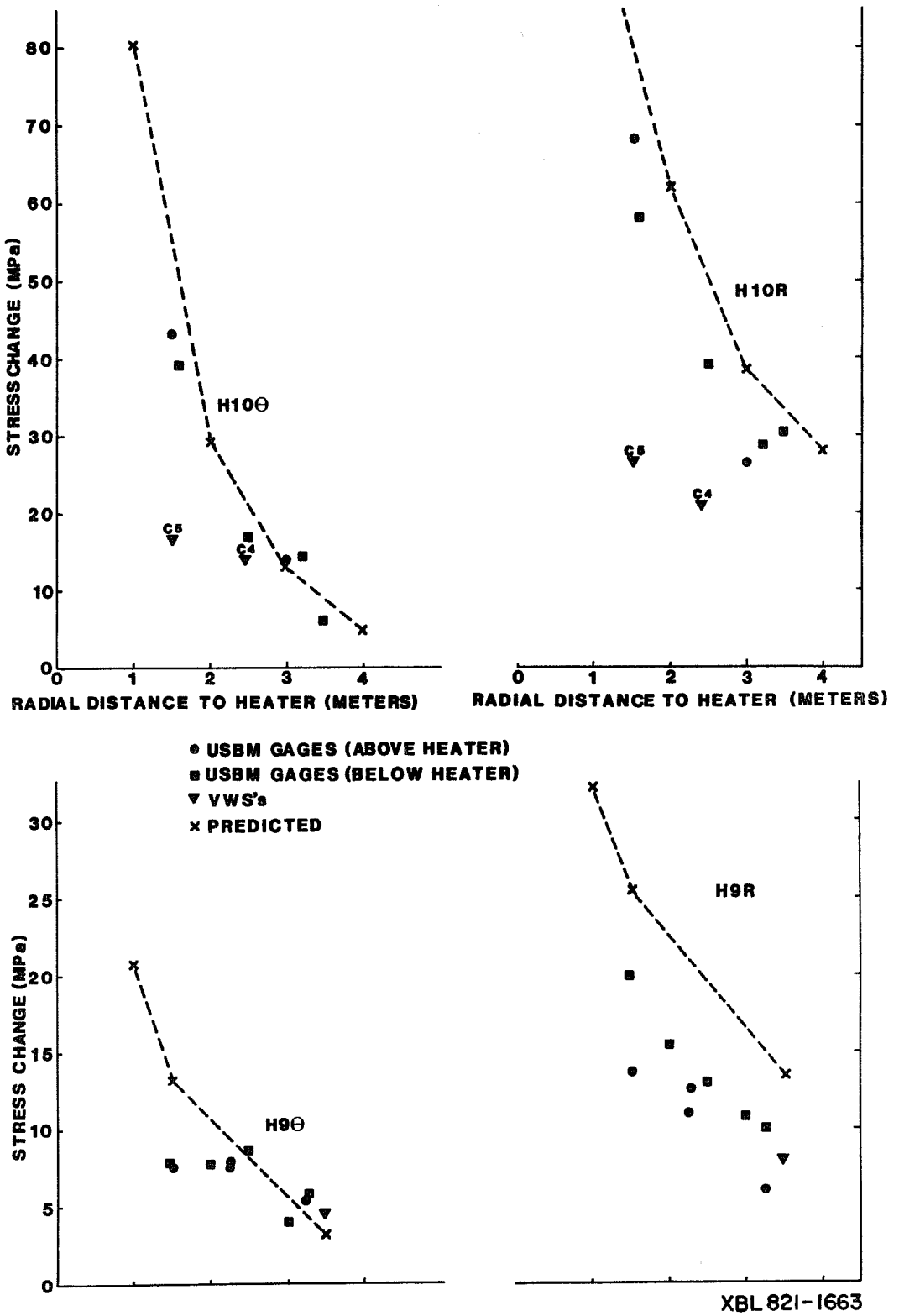

Fig. 4-1. Comparison of stress change from measurements with predicted results from Chan and Cook (1979).

Table 4-4. Input data for stress calculations.

Input	Model	USBM gauge data
Young's modulus, E (GPa)	51.3	70
Coefficient of linear thermal expansion of the rock, α_r ($^\circ C^{-1}$)	11.1×10^{-6}	9.0×10^{-6}
Poisson's ratio, ν	0.23	0.225
$\alpha E/(1-\nu)$	7.4×10^{-4}	8.1×10^{-4}

gauges are consistently lower than the predicted values. The comparison is better in the H10 area than in the H9.

Not enough VWS values are available to warrant comment.

5. SUMMARY AND CONCLUSIONS

5.1 Summary

Two types of instruments were employed during the heating experiments at Stripa in an attempt to determine the thermally induced stress changes in the rock mass. During the course of the experiment, vibrating wire stress-meters (VWSs) were installed in 15 boreholes (two per borehole), and USBM gauges were placed in 30 boreholes (one per borehole). The problems encountered with both types are summarized below.

5.1.1 Vibrating Wire Stressmeters

Of the 36 VWSs employed at Stripa, 6 failed, 16 operated for the full 550-day operating period, and another 14 operated satisfactorily, although installed for less than the full term. Failures were attributed to corrosion of the vibrating wire by moisture entering the gauge body. Despite external corrosion of some gauges, long-term stability was quite good, as determined by comparing the unloaded period before and after the heater experiments. Only four gauges changed in period by more than 20 counts.

VWS calibration posed the most serious problem. Three factors that appear to be interrelated affected the calibration of the VWSs:

1. Seating variability,
2. Elastic modulus dependence, and
3. Temperature dependence.

These three effects combined to produce an error band for the Stripa VWS data that is judged to be $\pm$33% of the indicated stress.

5.1.2 USBM Gauges

The operating performance record of the USBM gauges used at Stripa was very dismal; in all, 73% (22 of 30) of the gauges installed at the beginning

of the experiments failed. All of these failures were a direct result of water entering the gauge body. Attempted field repairs were not successful in improving the performance of the gauges.

Prior to cool-down (heater turn-off), all available gauges (15) were returned to the manufacturer for extensive modifications, including filling of the gauge body with silicone fluid. The modified gauges were subjected to a water submersion test at elevated temperature and pressure before they were returned to Stripa. Six of the modified gauges failed after installation, but these failures were all traced to breakage of internal hookup leads.

Sample calculations of stress change made from the USBM gauge data are consistent with theoretical results, but an offset in the magnitude of the maximum principal stresses remains unaccounted for.

5.2 Conclusions

An extensive test effort was made to isolate the factors that affect the sensitivity of the vibrating wire stressmeter (VWS). However, little was learned to improve the accuracy of, or confidence in, the data obtained. The chief source of uncertainty appears to be the seating of the gauge. Seating effects, manifested as variations due to alignment, slippage, or installation pressure, are closely coupled with the dependence upon rock modulus and temperature. Moreover, seating problems encountered in the laboratory cannot be expected to improve when a gauge is installed in the field. Because of these uncertainties and problems, it was not possible to reduce the combined uncertainty in the gauge readings and stress calculations.

The efforts expended to improve the reliability of the borehole deformation gauge (USBM) were considered successful in preventing infiltration for operating times of at least six months. The borehole deformation data recorded in vertical boreholes during cool-down--and, in some cases, at other times during the experiments--can be quantified to an accuracy on the order of ±10%. The stress changes derived from the borehole deformation data are subject to additional errors as a result of the uncertainty in the elastic properties and the coefficient of thermal expansion of the rock in situ. The stress data derived from gauges in horizontal boreholes are subject to further error because the deformation along the axis of maximum principal stress was unknown (not measured). Only three USBM gauges other than those in horizontal boreholes provided continuous data throughout the entire experiment, and these were on the single heater experiment (H9).

As a result of the experience gained from the heating experiments at Stripa, it is concluded that off-the-shelf instrumentation for measuring in situ stress change is not yet at the point of being able to provide long-term data in a nuclear waste repository environment. If such data will be required in a future repository licensing process or for model validation, a concerted effort among funding agencies, users, and manufacturers will be needed to advance the state of the art.

6. ACKNOWLEDGMENTS

We are grateful to Gene Binnall for helping to sort out inconsistencies in the data, assisting with measurement problems, and contributing the failure analyses for the stressmeters. Cara Coad compiled much of the data presented in this report. Mark Board, Robert Clayton, and Todd Schrauf are also acknowledged for their support in conducting laboratory tests at Terra Tek. Special thanks go to H. Carlsson and P.-A. Halén for their tireless efforts in coordinating the support activities for the project at the Stripa mine.

7. REFERENCES

Becker, R.M., 1968. "An Anisotropic Elastic Solution for Testing Stress Relief Core Solution," USBM R.I. No. 7143.

Becker, R.M. and V.E. Hooker, 1969. "A Method of Determining In Situ Stress in Anisotropic Rock," Trans. ASME, AIME, Dec. 1969, Vol. 244.

Binnall, E.P. and M. McEvoy, 1981. "Assessment of Thermocouple Temperature Measurements During In Situ Heater Experiments at Stripa, Sweden," Lawrence Berkeley Laboratory report LBL-12670, SAC-53, Berkeley, California.

Chan, T. and N.G.W. Cook, 1979. "Calculated Thermally Induced Displacements and Stresses for Heater Experiments at Stripa," Lawrence Berkeley Laboratory report LBL-7061, SAC-22, Berkeley, California.

Chan, T. et al., 1980. "Thermal and Thermomechanical Data from In Situ Heater Experiments at Stripa, Sweden," Lawrence Berkeley Laboratory report LBL-11477, SAC-29, Berkeley, California.

Cook, N.G.W. and P.A. Witherspoon, 1978. "Mechanical and Thermal Design Considerations for Radioactive Waste Repositories in Hard Rock," Lawrence Berkeley Laboratory report LBL-7073, SAC-10, Berkeley, California.

DuBois, A., M. Hood, E.P. Binnall and L. Andersson, 1981. "Extensometer Performance During Heater Experiments at Stripa," Lawrence Berkeley Laboratory report LBL-43531, SAC-50, Berkeley, California.

Dutta, P.K., R.W., Hatfield and P.W. Runstadler, Jr., 1980. "Room and High Temperature Calibration Characteristics of IRAD Gauge Vibrating Wire Stressmeter." IRAD Report, TR 80-2.

Fossum, A.F., J.E. Russell and F.D. Hansen, 1977. "Analysis of a Vibrating Wire Stress Gauge in Soft Rock," Exp. Mech. 17(7):261-264.

Hawkes, I. and W.V. Bailey, 1973. "Design, Develop, Fabricate, Test, and Demonstrate Permissible Low Cost Cylindrical Stress Gauges and Associated Components Capable of Measuring Change of Stress as a Function of Time in Underground Coal Mines," U.S. Bureau of Mines Contract Report (H0220050), Washington, D.C.

IRAD Gauge, Inc., 1977. Vibrating Wire Stress Meter Instruction Manual. Lebanon, New Hampshire.

Myer, L. and R. Rachiele, 1981. "Stripa Material Properties Investigation," Lawrence Berkeley Laboratory report LBL-13435, SAC-40, Berkeley, California.

Obert, L. and W.I. Duvall, 1967. Rock Mechanics and the Design of Structures in Rock. New York, John Wiley and Sons.

Schrauf, T., H. Pratt, E. Simonson and W. Hustrulid, 1979. "Instrument Evaluation, Calibration, and Installation for the Heater Experiments at Stripa." Lawrence Berkeley Laboratory report LBL-8313, SAC-25, Berkeley, California.

Swan, G., 1978. "The Mechanical Properties of Stripa Granite," Lawrence Berkeley Laboratory report LBL-7074, SAC-03, Berkeley, California.

APPENDIX A: IRAD GAUGE (VWS) FIELD RECORDS

IRAD GAUGE FIELD RECORD

Full Scale
Experiment H-9

Gauge C1 θ
Hole C1

Term of Gauge Usage	
Entire Experiment: [x]	Partial Experiment including... (calendar dates) / / / - / / / (y) (m) (d) (experiment days) ___ - ___

[x] vert. [ ] horiz.

r= .99
θ= 22.1
z= .85

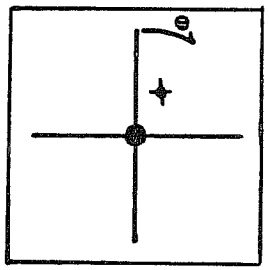

	Label	Mfg. Serial No.	Sensor No. (on disc file)	Logger Channel	R_o (pre-exp.)	R_o (post-exp.)	R_s (set)	ΔR_s ($R_s - R_o$)		
IRAD Gauge	C1A	3-20	272	1	1926	1909	2082	156		
Corresponding Thermocouple	TC1		77	100						

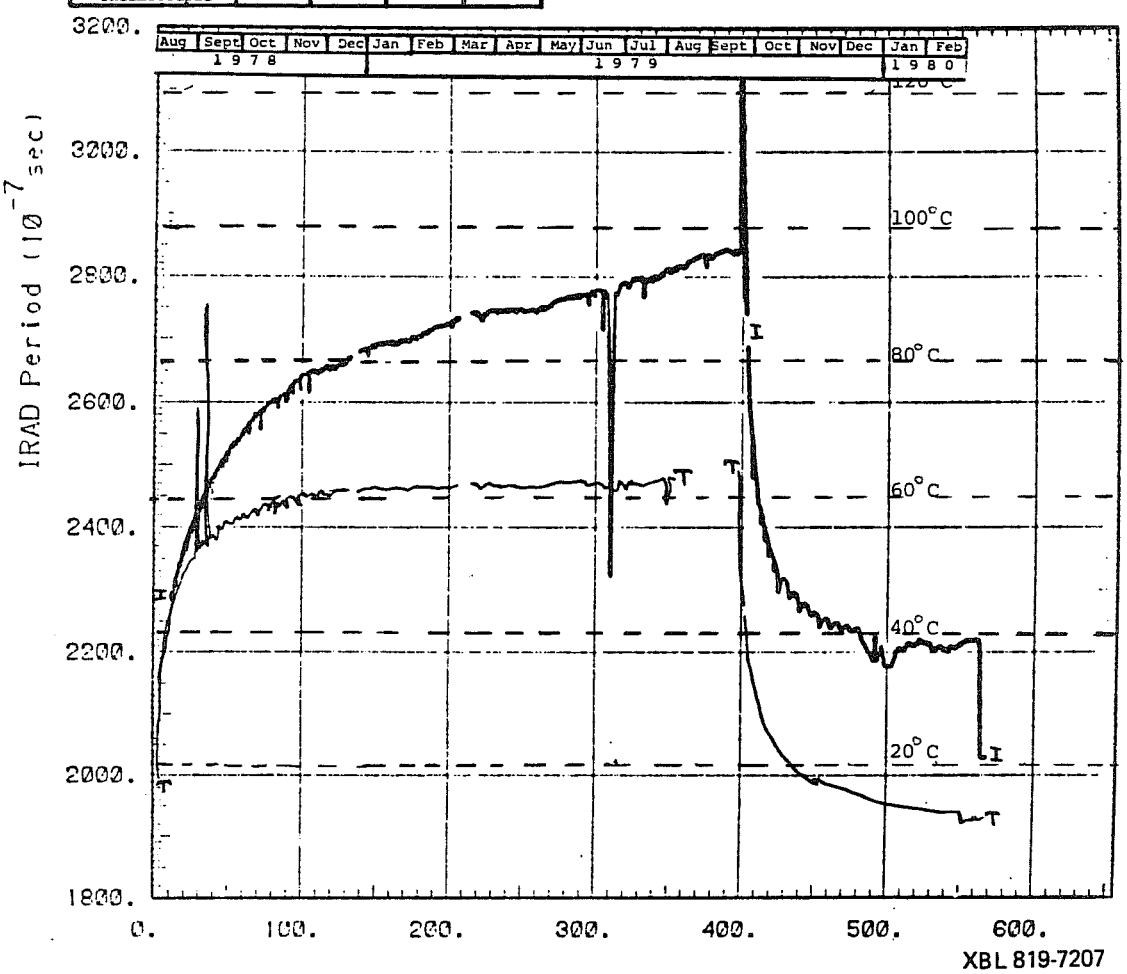

XBL 819-7207

IRAD GAUGE FIELD RECORD

Full Scale
Experiment H-9

Gauge C1R
Hole C1

Term of Gauge Usage	
Entire Experiment	Partial Experiment including...
[x]	(calendar dates) / / / (y) (m) (d) - / / /
	(experiment days) ____ - ____

[x] vert. [ ] horiz.

r= .99
θ= 22.1
z= .85

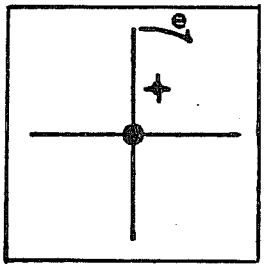

	Label	Mfg. Serial No.	Sensor No. on disc file	Logger Channel	R_o (pre-exp.)	R_o (post-exp.)	R_s (set)	ΔR_s ($R_s - R_o$)		
IRAD Gauge	C1B	3-22	271	0	1926	1940	2053	127		
Corresponding Thermocouple	TC1		77	100						

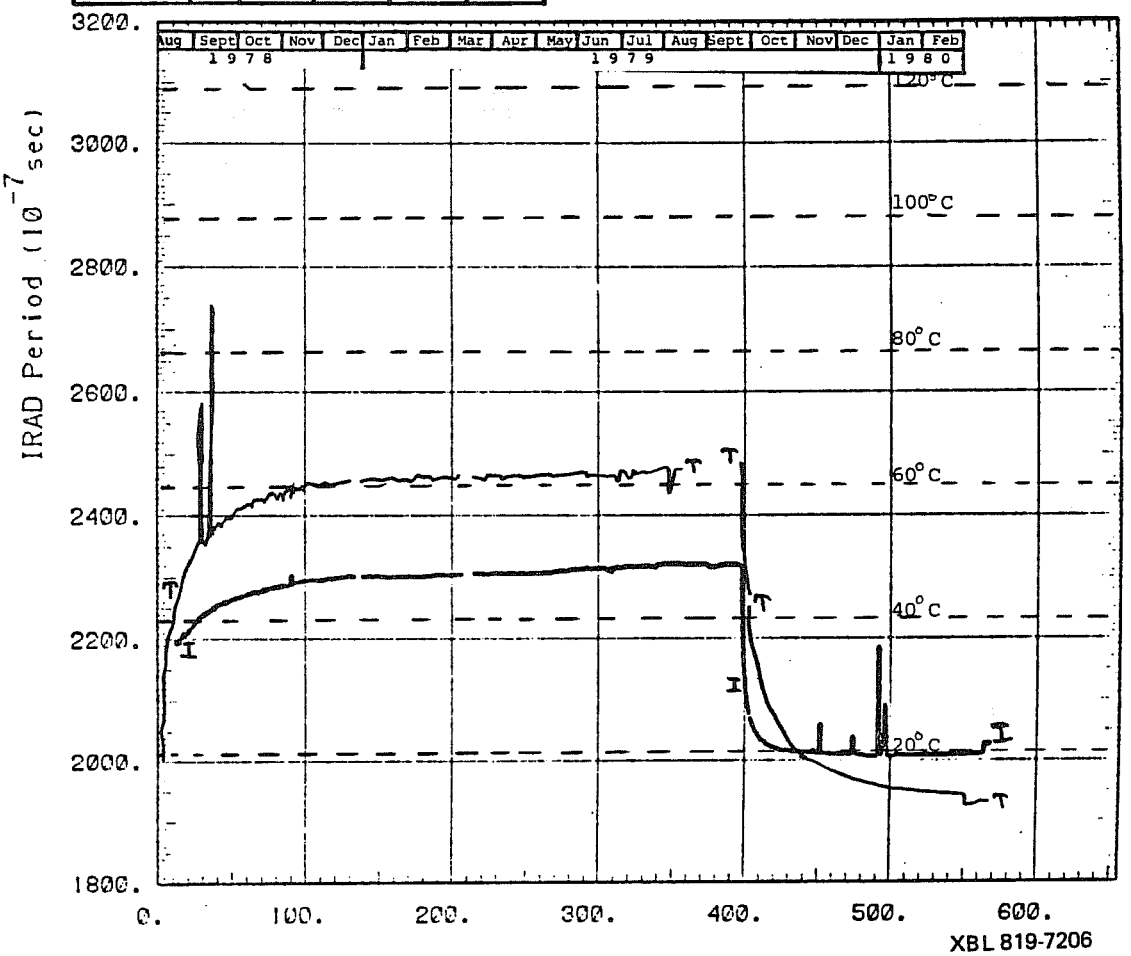

XBL 819-7206

IRAD GAUGE FIELD RECORD

Full Scale
Experiment H-9

Gauge C2θ
Hole U6

Term of Gauge Usage	
Entire Experiment ☐	Partial Experiment including... (calendar dates) / / (y) (m) (d) - / / (experiment days) 0 - ?

☒ vert. ☐ horiz.

r= 1.01
θ= 314.8
z= -.65

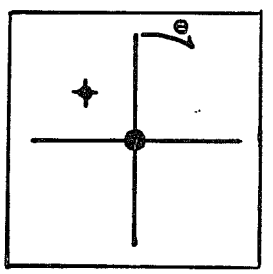

	Label	Mfg. Serial No.	Sensor No. (on disc file)	Logger Channel	R_O (pre-exp.)	R_O (post-exp.)	R_S (set)	ΔR_S (R_S-R_O)		
IRAD Gauge	C2B	3-16	274	3	1937		2131	194		
Corresponding Thermocouple	TC2		78	101						

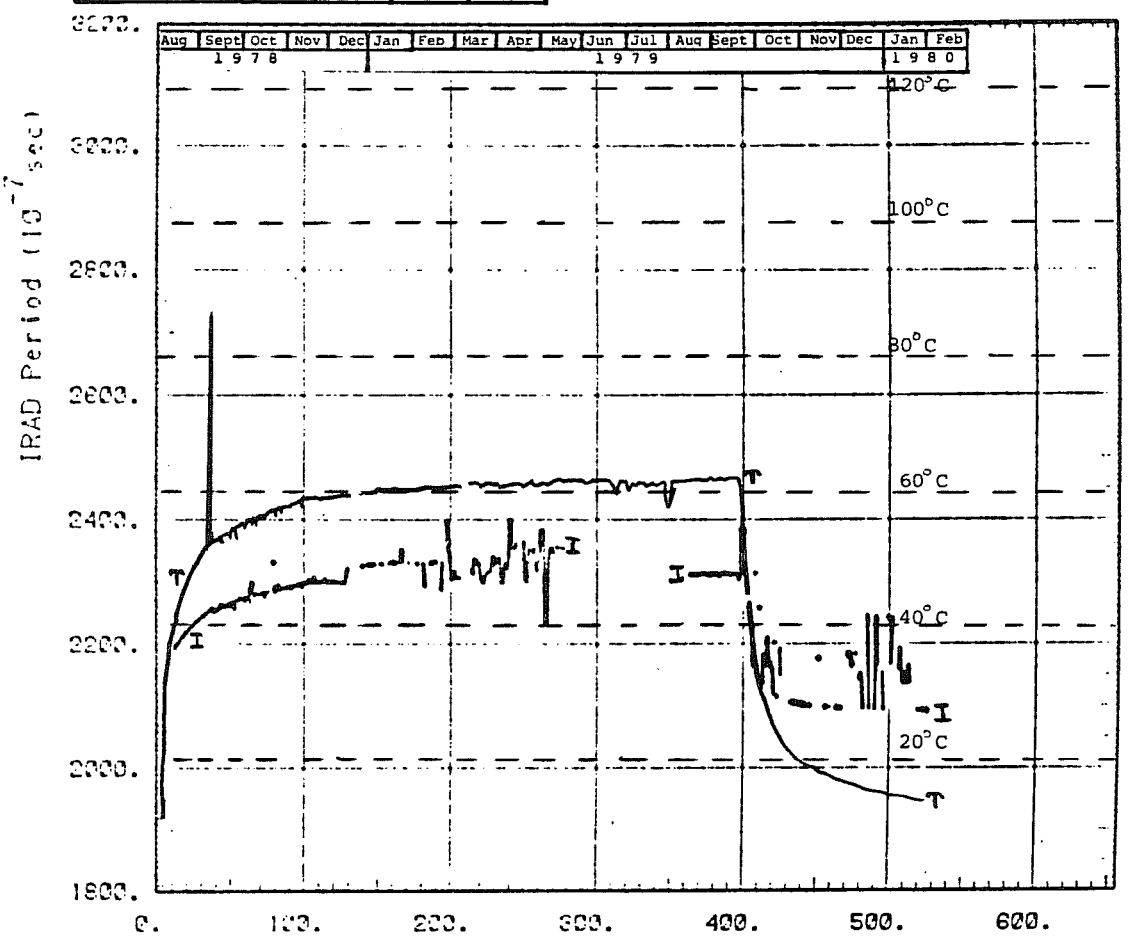

IRAD GAUGE FIELD RECORD

Full Scale Experiment H-9

Gauge C2R

Hole U6

Term of Gauge Usage	
Entire Experiment	Partial Experiment including... (calendar dates) / / (y) (m) (d) - / / (experiment days) ___ - ___
[x]	

[x] vert. [ ] horiz.

r= 1.01

θ= 314.8

z= -.65

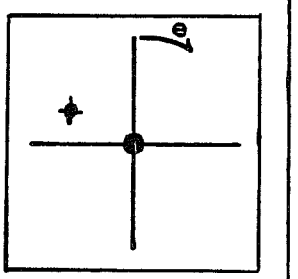

	Label	Mfg. Serial No.	Sensor No. on disc file	Logger Channel	R_O (pre-exp.)	R_O (post-exp.)	R_S (set)	ΔR_S (R_S-R_O)		
IRAD Gauge	C2A	3-18	273	2	1958		2091	133		
Corresponding Thermocouple	TC2		78	101						

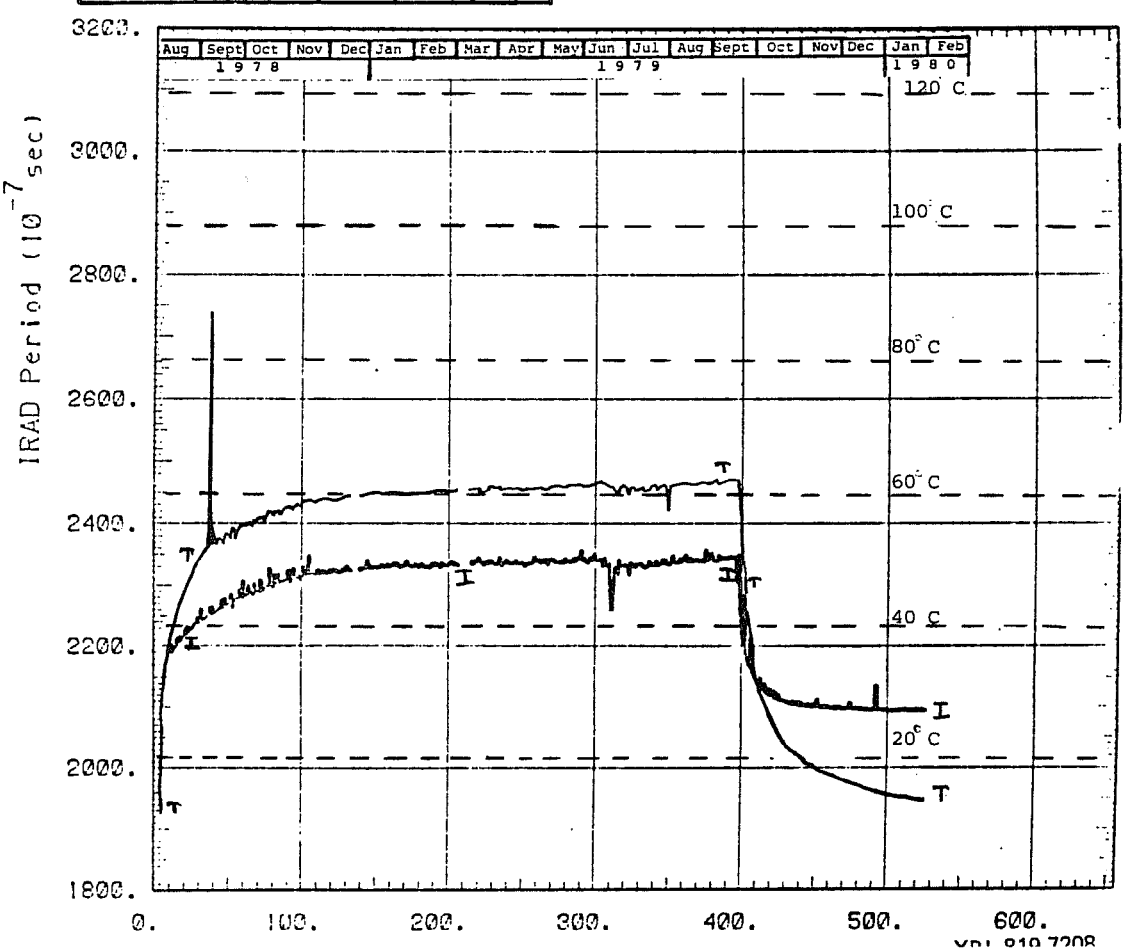

IRAD GAUGE FIELD RECORD

Full Scale
Experiment H-9

Gauge C9 θ
Hole U3

Term of Gauge Usage	
Entire Experiment ☐	Partial Experiment including... (calendar dates) 79/09/22 (y) (m) (d) - 80/02/26 (experiment days) 394 - 551

☒ vert. ☐ horiz.

r= 3.49
θ= 0
z= 0.85

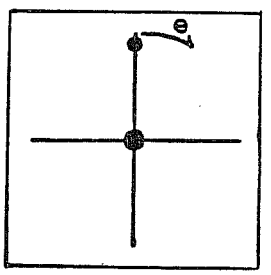

	Label	Mfg. Serial No.	Sensor No. on disc file	Logger Channel	R_o (pre-exp.)	R_o (post-exp.)	R_s (set)	ΔR_s ($R_s - R_o$)		
IRAD Gauge	C9B	J-40	286	17	1907	1901	2061	154		
Corresponding Thermocouple			4	117						

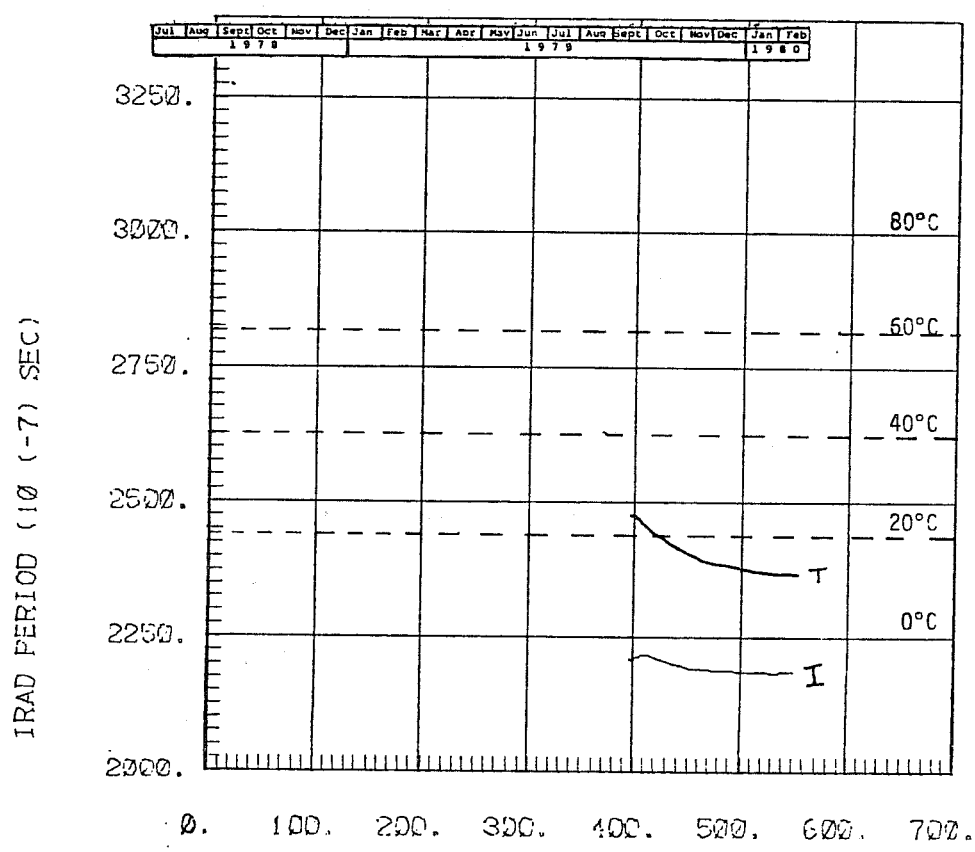

XBL 819-11515

IRAD GAUGE FIELD RECORD

Full Scale Experiment H-9

Gauge C9 R

Hole U3

Term of Gauge Usage	
Entire Experiment ☐	Partial Experiment including... (calendar dates) 79/09/22 (y) (m) (d) - 80 2/26 (experiment days) 394 - 551

X vert. ☐ horiz.

r= 3.49

θ= 0

z= 0.85

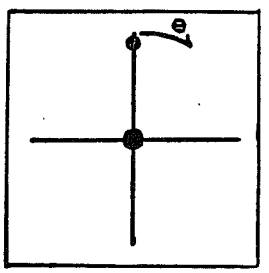

	Label	Mfg. Serial No.	Sensor No. on disc file	Logger Channel	R_o (pre-exp.)	R_o (post-exp.)	R_s (set)	ΔR_s ($R_s - R_o$)		
IRAD Gauge	C9A	K-2	285	16	2009	2007	2209	200		
Corresponding Thermocouple			4	117						

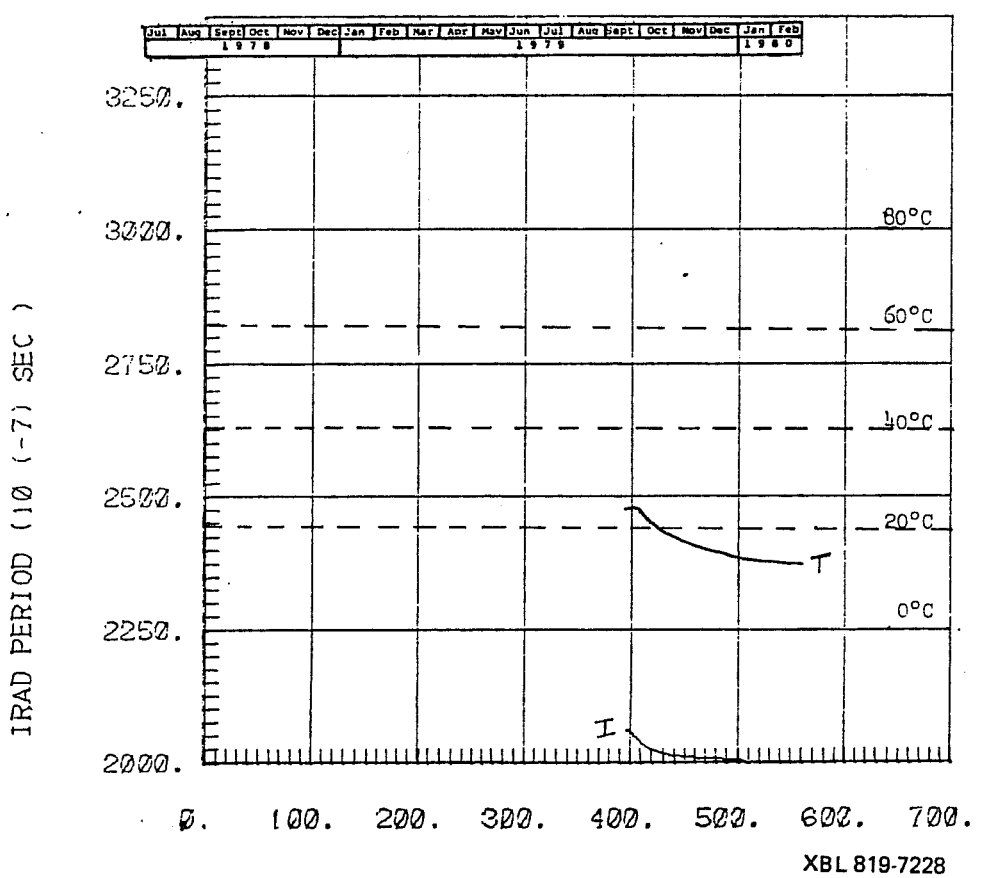

XBL 819-7228

IRAD GAUGE FIELD RECORD

Full Scale
Experiment H-9

Gauge C6θ
Hole C6

Term of Gauge Usage	
Entire Experiment	Partial Experiment including... (calendar dates) / / - / / (y) (m) (d) (experiment days) ____ - ____
x	

☐ vert. ☒ horiz.

r= 2.50
θ=47.5
z= .65

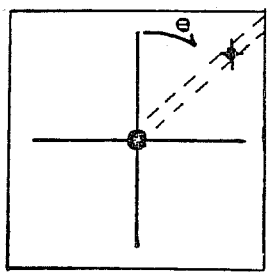

	Label	Mfg. Serial No.	Sensor No. on disc file	Logger Channel	R_o (pre-exp.)	R_o (post-exp.)	R_s (set)	ΔR_s (R_s-P_c)		
IRAD Gauge	C6A	3-55	275	10	2044	2028	2276	232		
Corresponding Thermocouple	TC6		79	105						

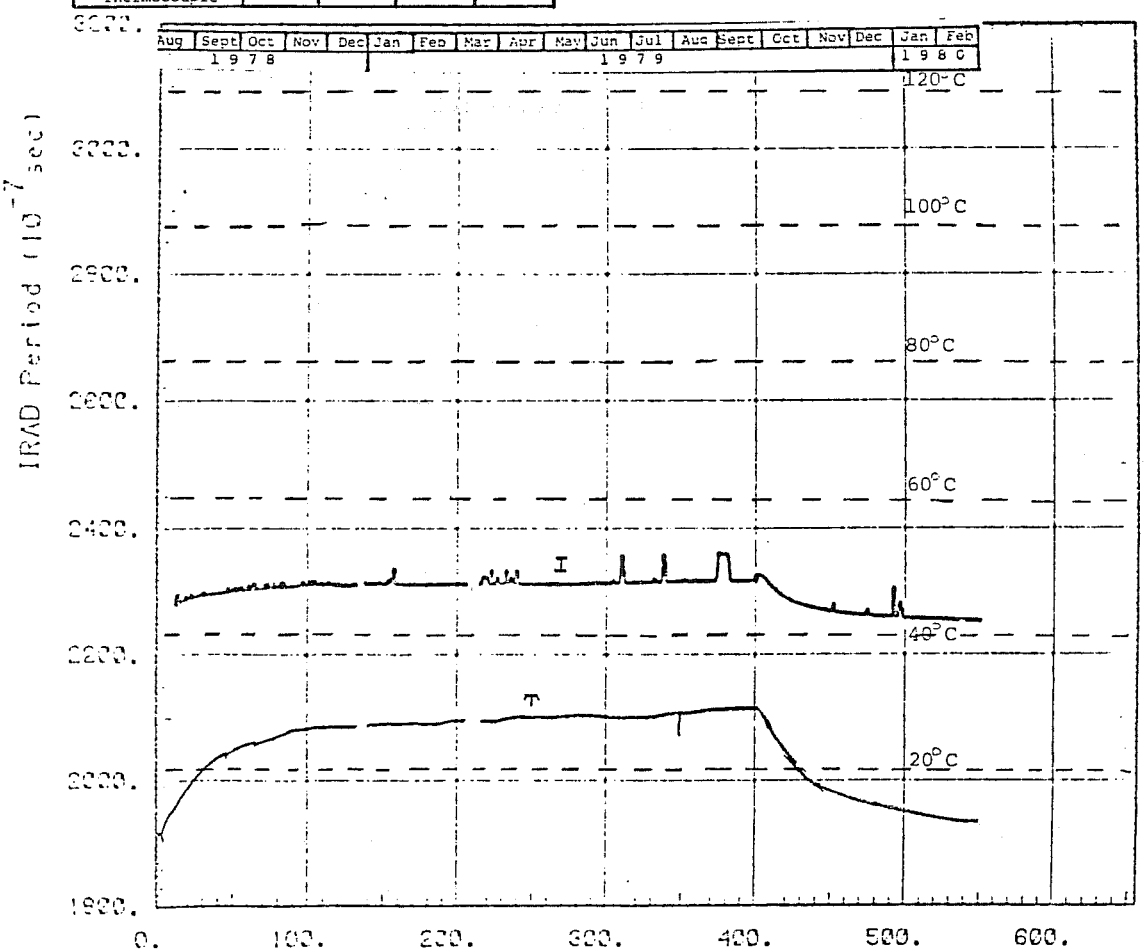

IRAD GAUGE FIELD RECORD

Full Scale
Experiment H-9

Gauge C6Z
Hole C6

Term of Gauge Usage	
Entire Experiment	Partial Experiment including...
[x]	(calendar dates) / / (y) (m) (d) - / / (experiment days) ____ - ____

[ ] vert. [x] horiz.

r= 2.50
θ= 47.5
z= .65

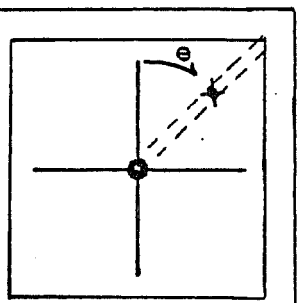

	Label	Mfg. Serial No.	Sensor No. on disc file	Logger Channel	R_O (pre-exp.)	R_O (post-exp.)	R_S (set)	ΔR_S (R_S-R_O)		
IRAD Gauge	C6B	3-68	276	11	2044	2027	2277	233		
Corresponding Thermocouple	TC6		79	105						

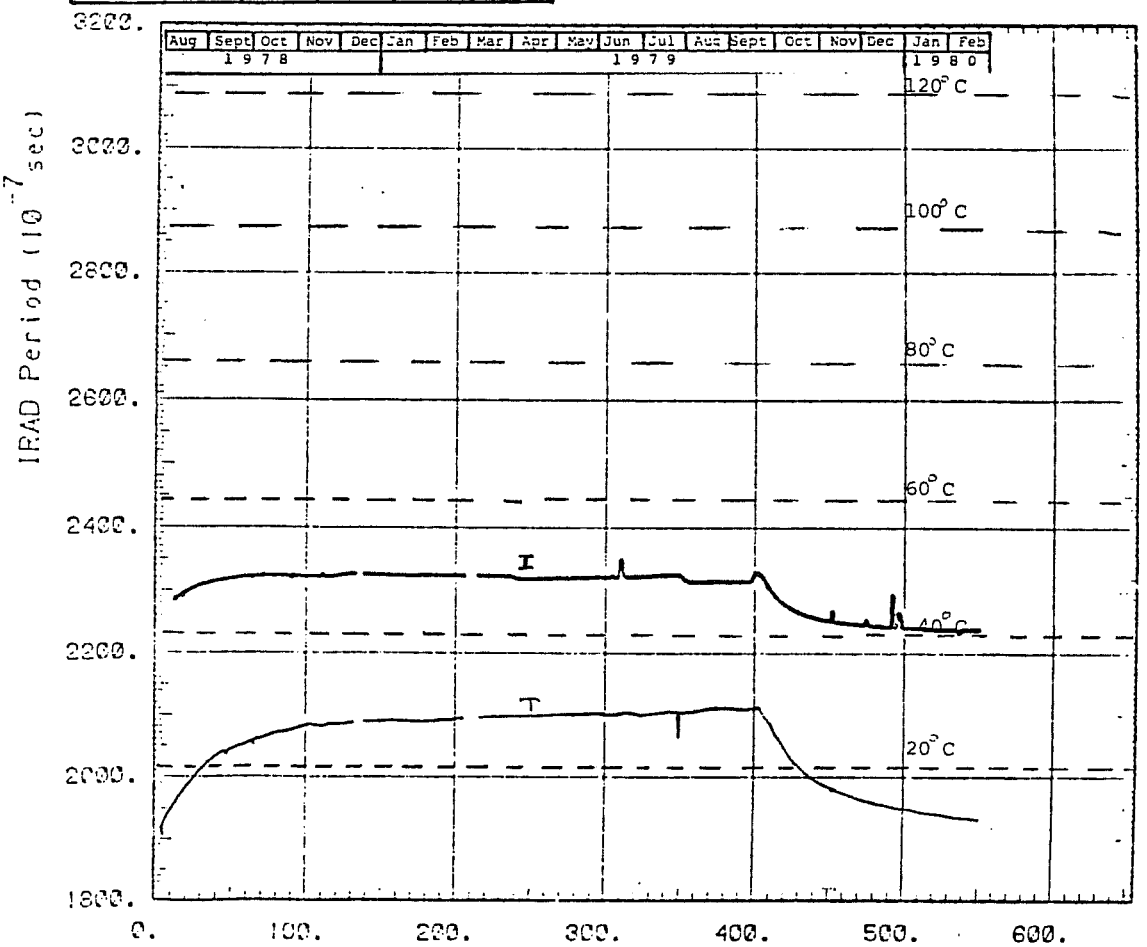

IRAD GAUGE FIELD RECORD

Full Scale Experiment H-9

Gauge C7θ

Hole C7

Term of Gauge Usage	
Entire Experiment	Partial Experiment including...
x	(calendar dates) / / - / / (y) (m) (d)
	(experiment days) ___ - ___

vert. [ ] horiz. [x]

r= 2.00

θ= 90.1

z= .66

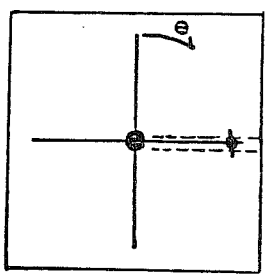

	Label	Mfg. Serial No.	Sensor No. on disc file	Logger Channel	R_O (pre-exp.)	R_O (post-exp.)	R_S (set)	ΔR_S (R_S-R_O)		
IRAD Gauge	C7A	3-92	277	12	1974	1975	2161	187		
Corresponding Thermocouple	TC7		80	106						

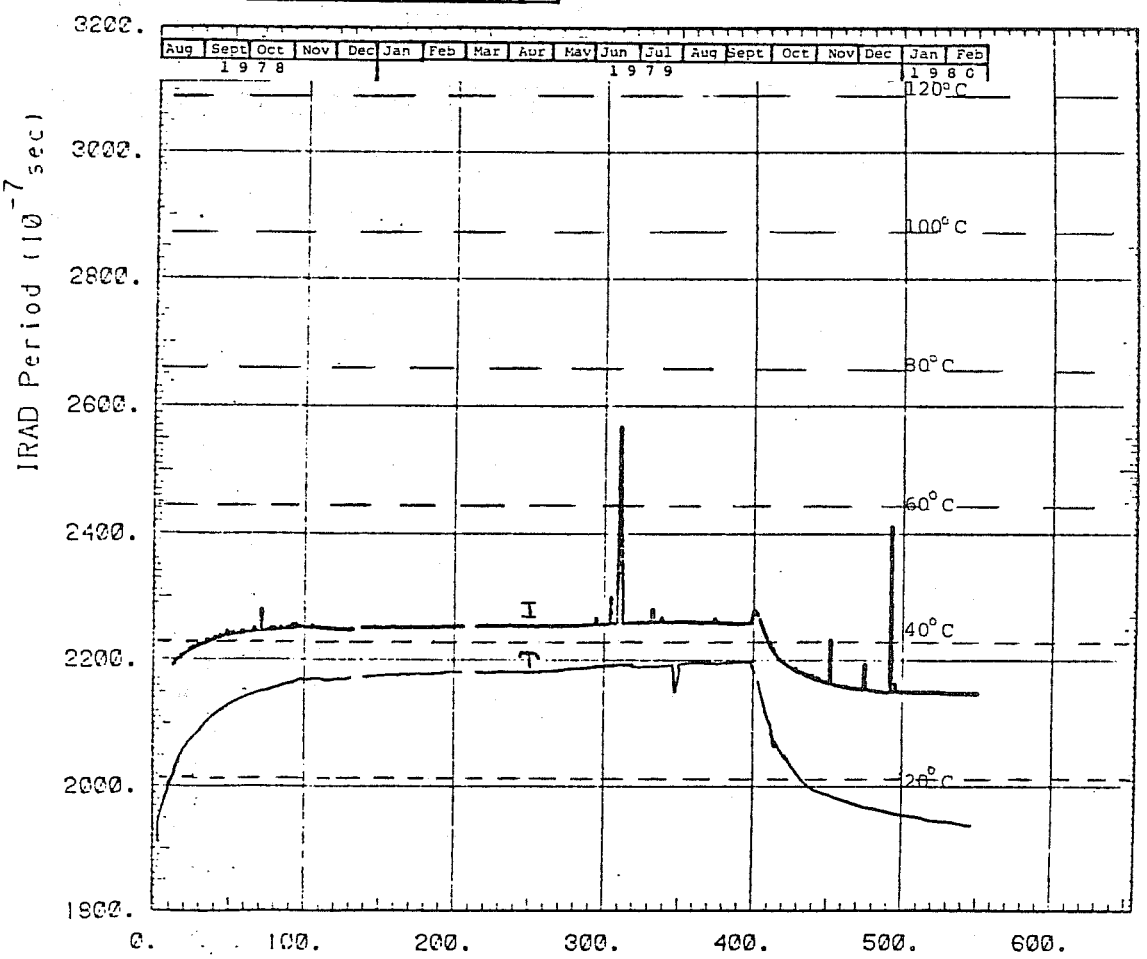

IRAD GAUGE FIELD RECORD

Full Scale
Experiment H-9

Gauge C7Z
Hole C7

Term of Gauge Usage	
Entire Experiment	Partial Experiment including...
[x]	(calendar dates)
	/ / (y) (m) (d) - / /
	(experiment days)
	___ - ___

[ ] vert. [x] horiz.

r= 2.00
θ= 90.1
z= .66

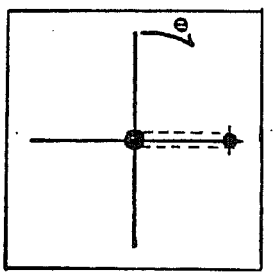

	Label	Mfg. Serial No.	Sensor No. on disc file	Logger Channel	R_o (pre-exp.)	R_o (post-exp.)	R_s (set)	ΔR_s ($R_s - R_o$)		
IRAD Gauge	C7B	3-74	278	13	1985	1979	2195	210		
Corresponding Thermocouple	TC7		80	106						

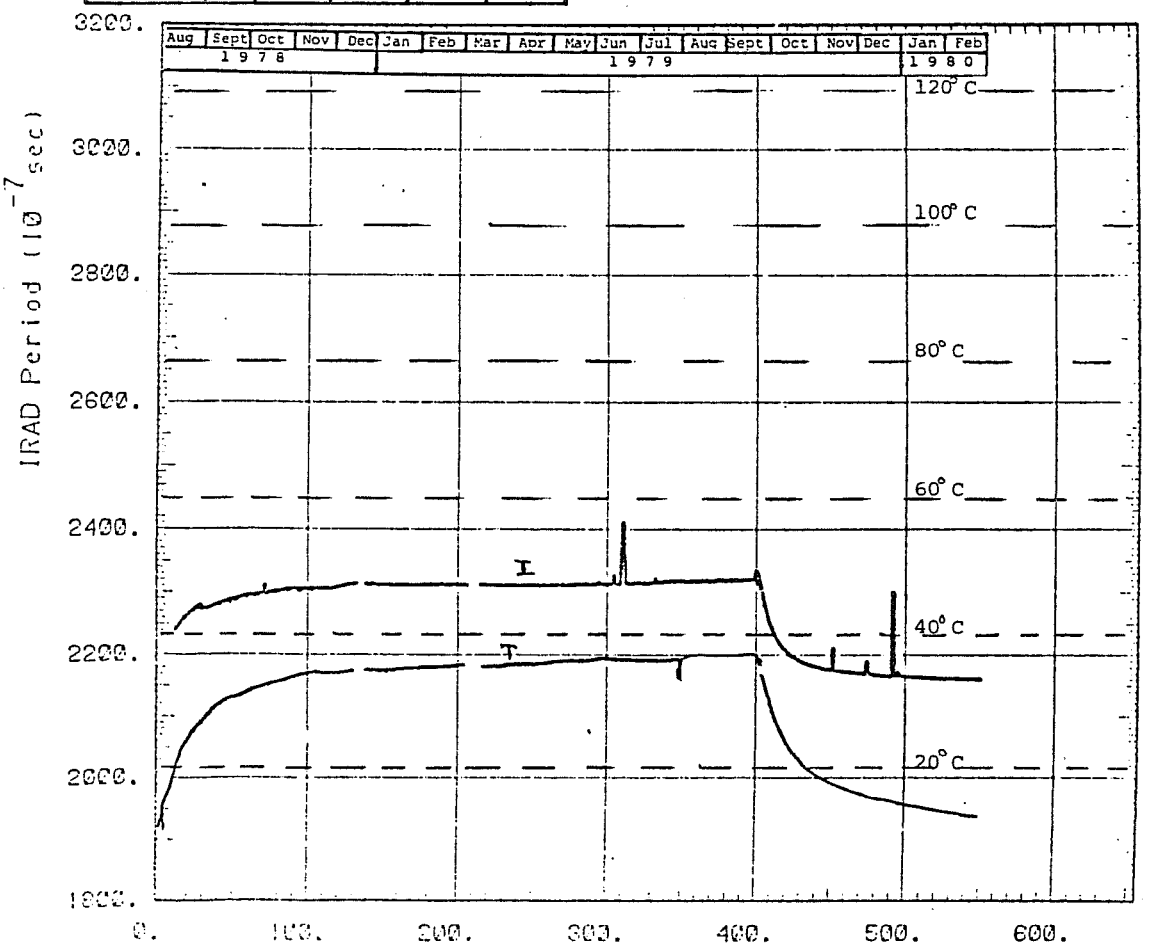

IRAD GAUGE FIELD RECORD

Full Scale
Experiment H-9

Gauge C8θ
Hole C8

Term of Gauge Usage	
Entire Experiment	Partial Experiment including...
x	(calendar dates) / / - / / (y) (m) (d)
	(experiment days) ___ - ___

vert. [ ] horiz. [x]

r= 3.01
θ= 134.8
z= .70

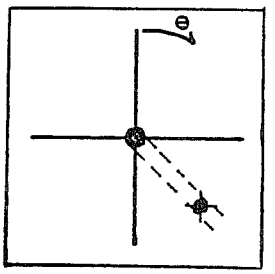

	Label	Mfg. Serial No.	Sensor No. on disc file	Logger Channel	R_o (pre-exp.)	R_o (post-exp.)	R_s (set)	ΔR_s (R_s-R_o)		
IRAD Gauge	C8A	3-90	279	14	2072	2053	2276	204		
Corresponding Thermocouple	TC8		81	107						

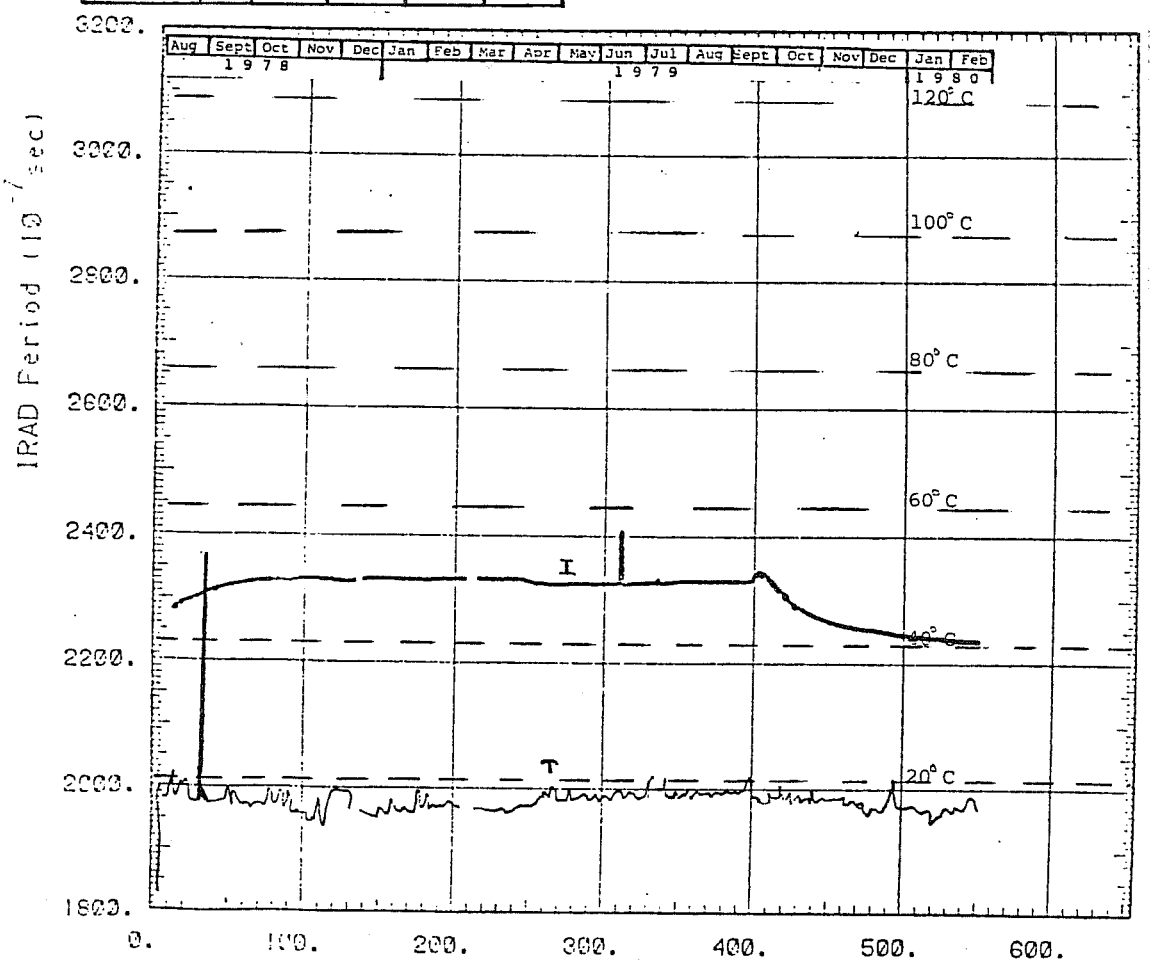

IRAD GAUGE FIELD RECORD

Full Scale
Experiment H-9

Gauge C8Z
Hole C8

Term of Gauge Usage	
Entire Experiment	Partial Experiment including...
[x]	(calendar dates)
	/ / - / /
	(y) (m) (d)
	(experiment days)
	___ - ___

[ ] vert. [x] horiz.

r= 3.01
θ= 134.8
z= .70

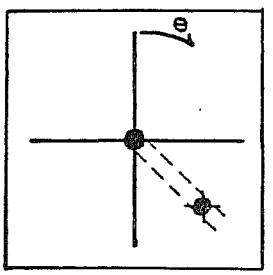

	Label	Mfg. Serial No.	Sensor No. on disc file	Logger Channel	R_o (pre-exp.)	R_o (post-exp.)	R_s (set)	ΔR_s (R_s-R_o)		
IRAD Gauge	C8B	3-58	280	15	2051	2056	2249	198		
Corresponding Thermocouple	TC8		81	107						

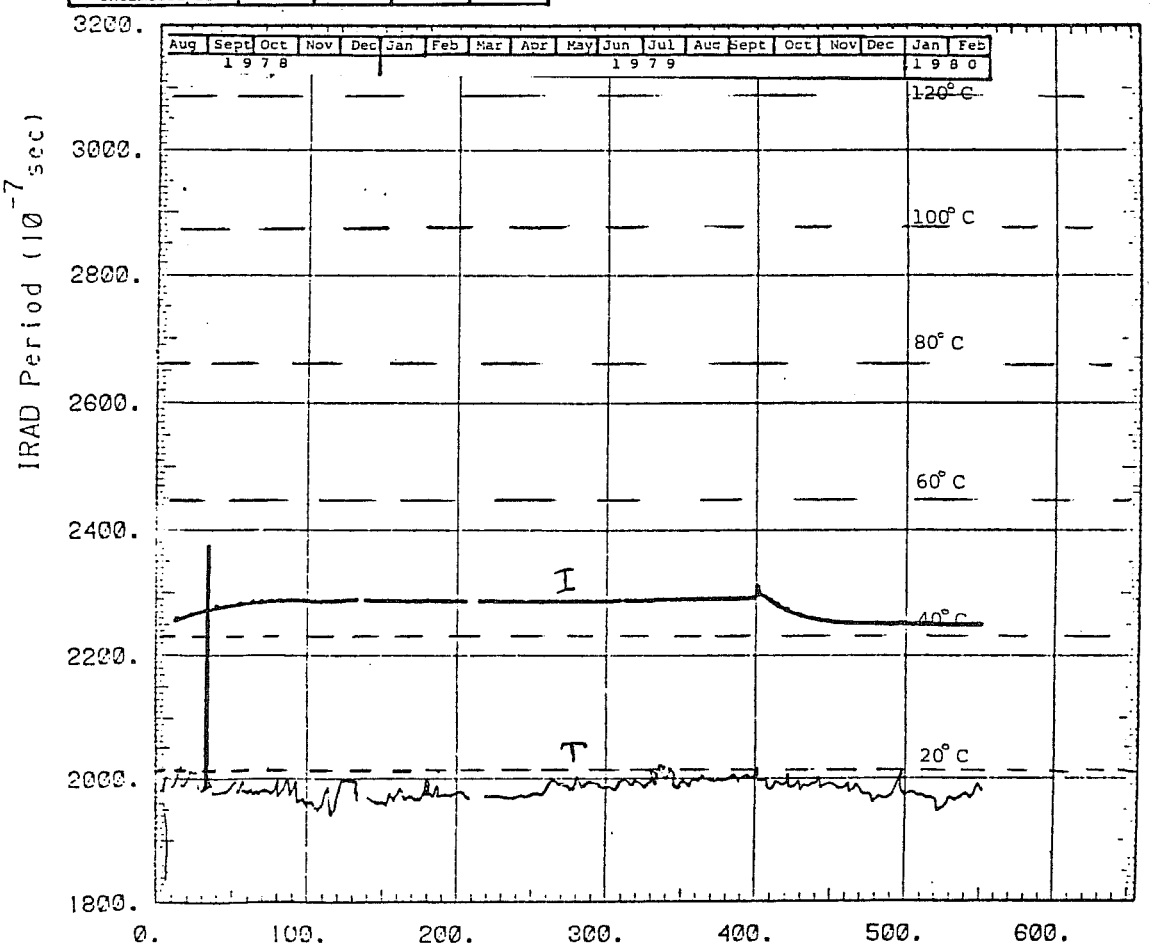

IRAD GAUGE FIELD RECORD

Full Scale Experiment H-9

Gauge C90

Hole U3

Term of Gauge Usage	
Entire Experiment ☐	Partial Experiment including... (calendar dates) 79/09/22 - 80 2 /26 (y) (m) (d) (experiment days) 394 - 551

[X] vert. [ ] horiz.

r= 3.49

e= 0

z= 0.85

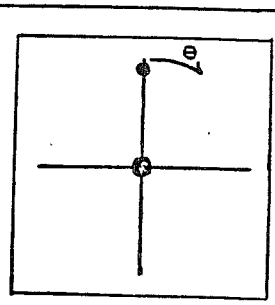

	Label	Mfg. Serial No.	Sensor No. on disc file	Logger Channel	R_o (pre-exp.)	R_o (post-exp.)	R_s (set)	ΔR_s ($R_s - R_o$)		
IRAD Gauge	C9A	K-2	285	16	2009	2007	2209	200		
Corresponding Thermocouple			4	117						

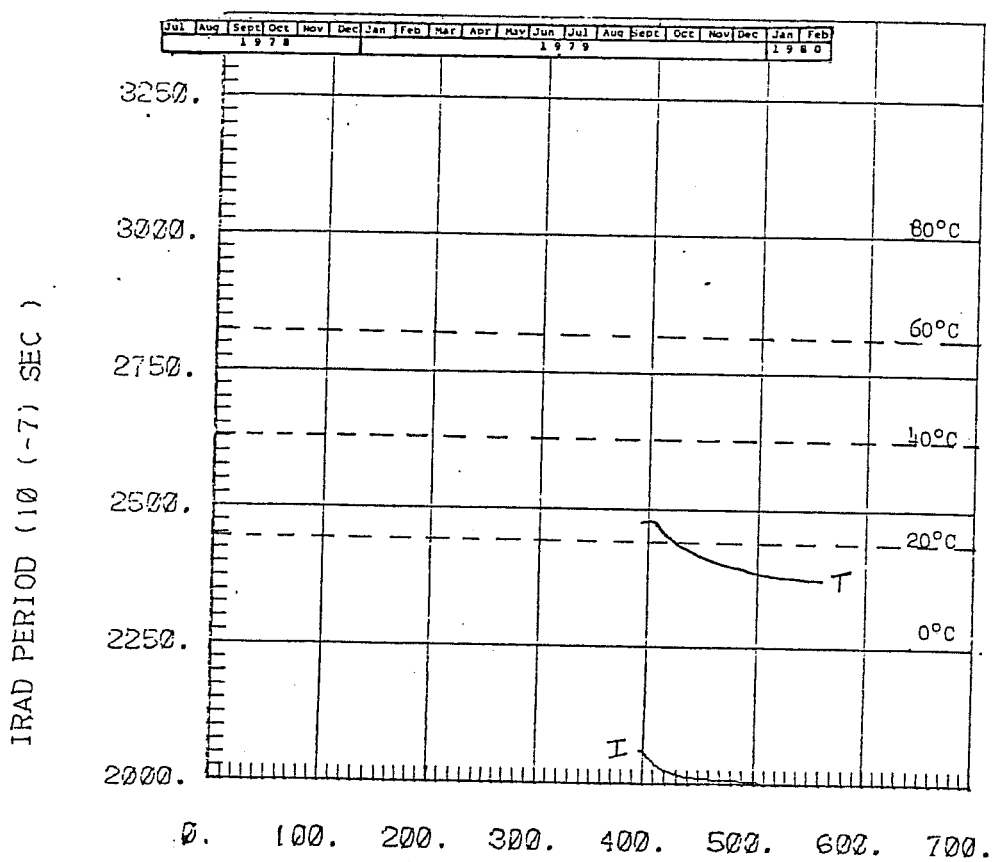

IRAD GAUGE FIELD RECORD

Full Scale
Experiment H-9

Gauge C9 R
Hole U3

Term of Gauge Usage	
Entire Experiment ☐	Partial Experiment including... (calendar dates) 79/09/22 (y) (m) (d) - 80/02/26 (experiment days) 394 - 551

☒ vert. ☐ horiz.

r= 3.49
e= 0
z= 0.85

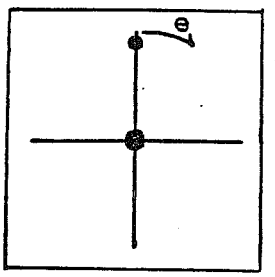

	Label	Mfg. Serial No.	Sensor No. on disc file	Logger Channel	R_o (pre-exp.)	R_o (post-exp.)	R_s (set)	ΔR_s ($R_s - R_o$)		
IRAD Gauge	C9B	J-40	286	17	1907	1901	2061	154		
Corresponding Thermocouple			4	117						

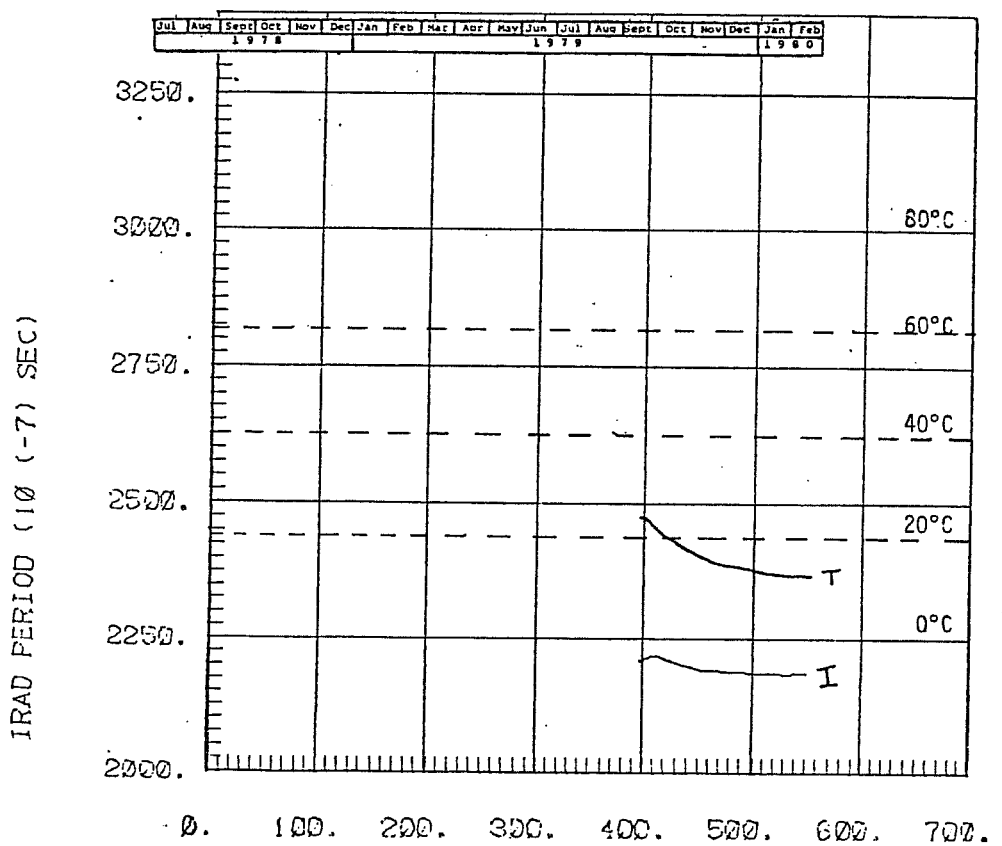

IRAD GAUGE FIELD RECORD

Full Scale Experiment H-9

Gauge C11e

Hole C11

Term of Gauge Usage	
Entire Experiment	Partial Experiment including...
[x]	(calendar dates) / / (y) (m) (d) - / / (experiment days) ____ - ____

[ ] vert. [x] horiz.

r= 3.99

θ= 67.8

z= -.85

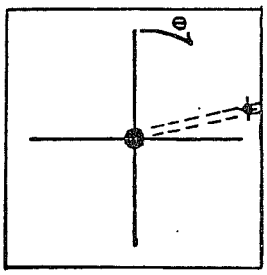

	Label	Mfg. Serial No.	Sensor No. on disc file	Logger Channel	R_o (pre-exp.)	R_o (post-exp.)	R_s (set)	ΔR_s ($R_s - R_o$)		
IRAD Gauge	C11A	3-1	281	20	2131	2137	2318	187		
Corresponding Thermocouple	TC11		82	110						

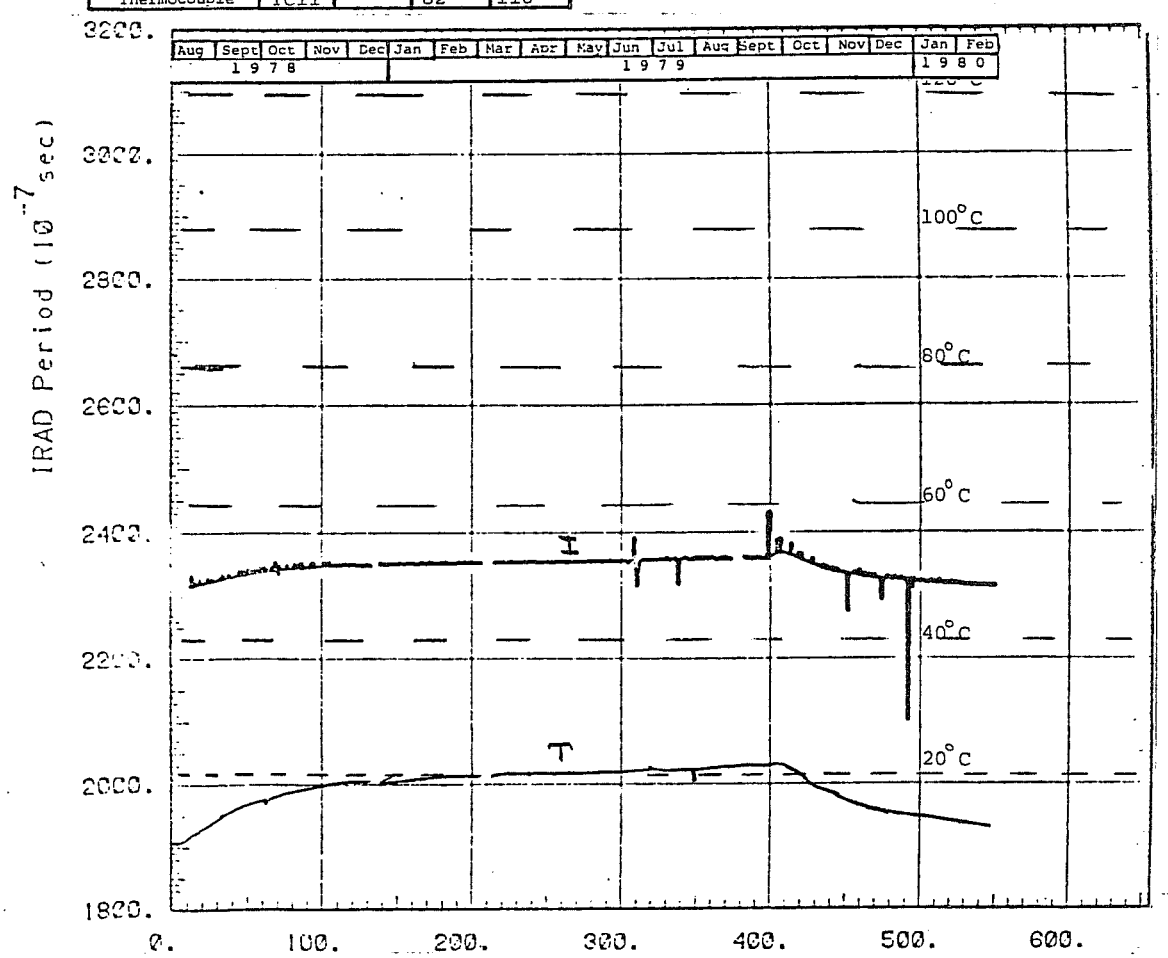

IRAD GAUGE FIELD RECORD

Full Scale
Experiment H-9

Gauge C11Z
Hole C11

Term of Gauge Usage	
Entire Experiment	Partial Experiment including...
X	(calendar dates) / / (y) (m) (d) - / /
	(experiment days) ____ - ____

☐ vert. ☒ horiz.

r= 3.99
θ=67.8
z= -.05

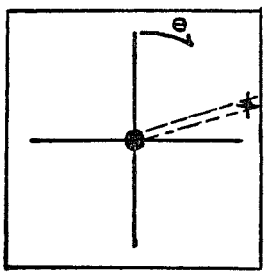

	Label	Mfg. Serial No.	Sensor No. on disc file	Logger Channel	R_o (pre-exp.)	R_o (post-exp.)	R_s (set)	ΔR_s ($R_s - R_o$)		
IRAD Gauge	C11B	3-37	282	21	2139	2127	2324	185		
Corresponding Thermocouple	TC11		82	110						

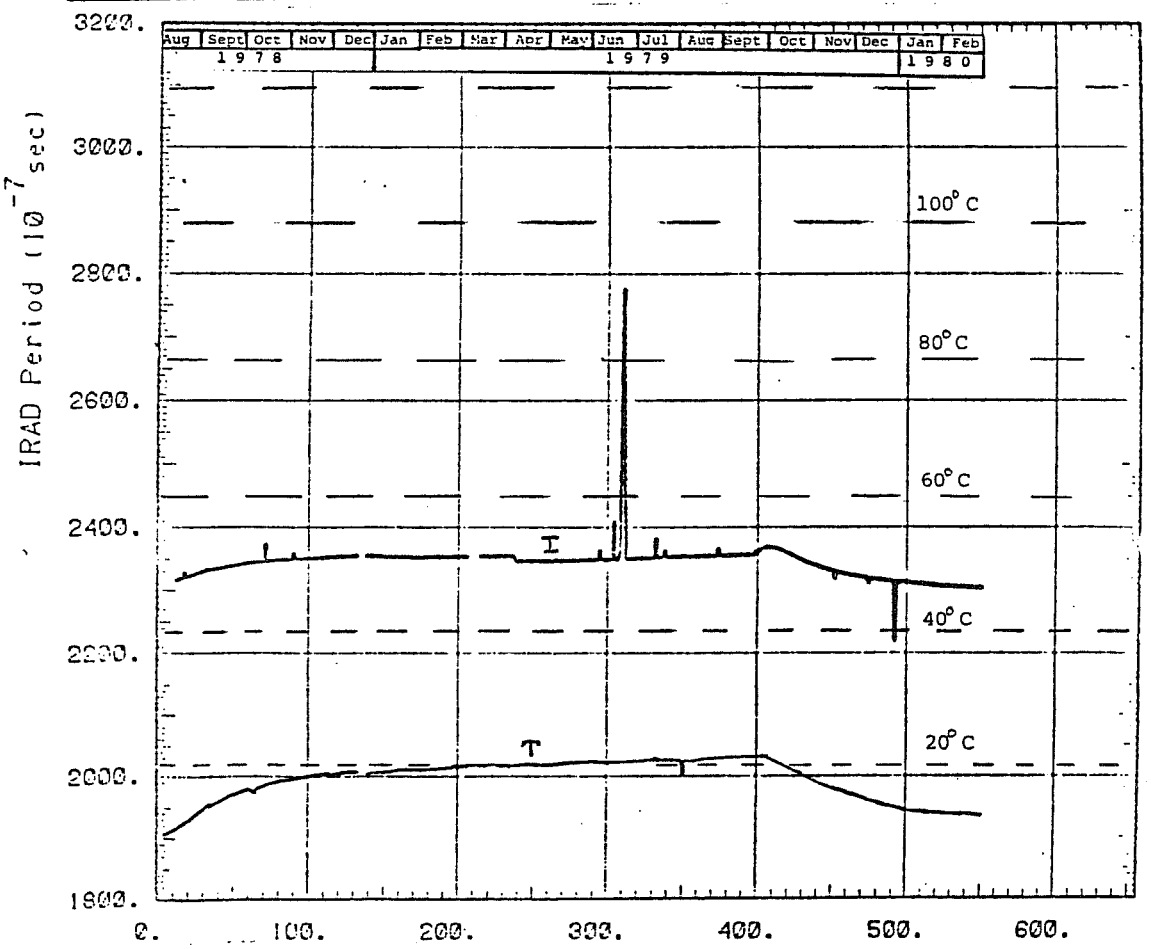

IRAD GAUGE FIELD RECORD

Full Scale Experiment H-9

Gauge C12θ
Hole C12

Term of Gauge Usage	
Entire Experiment	Partial Experiment including... (calendar dates) / / - / / (y) (m) (d) (experiment days) ___ - ___
[x]	

[ ] vert. [x] horiz.

r= 3.48
θ= 112.7
z= -.87

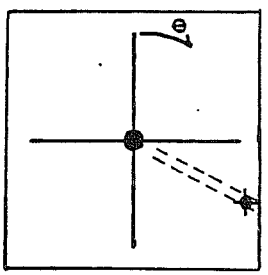

	Label	Mfg. Serial No.	Sensor No. on disc file	Logger Channel	R_o (pre-exp.)	R_o (post-exp.)	R_s (set)	ΔR_s (R_s-R_o)		
IRAD Gauge	C12A	3-48	283	22	2285	2299	2515	230		
Corresponding Thermocouple	TC12		83	111						

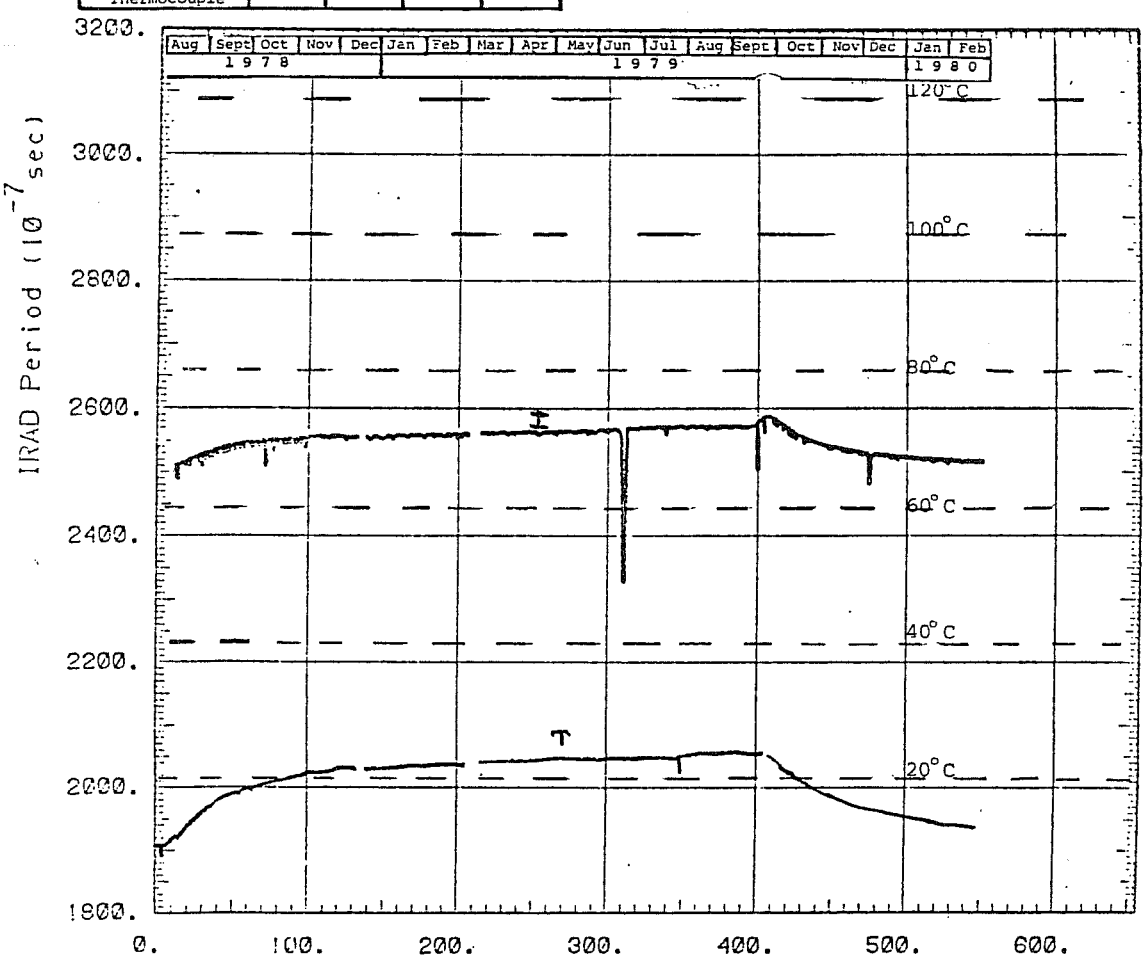

IRAD GAUGE FIELD RECORD

Full Scale
Experiment H-9

Gauge C12Z
Hole C12

Term of Gauge Usage	
Entire Experiment	Partial Experiment including...
[x]	(calendar dates)
	/ / - / /
	(y) (m) (d)
	(experiment days)
	___ - ___

[ ] vert. [x] horiz.

r= 3.48
θ= 112.7
z= - .87

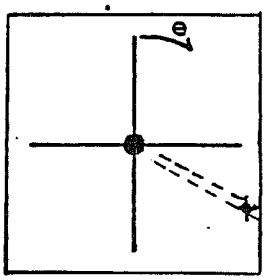

	Label	Mfg. Serial No.	Sensor No. (on disc file)	Logger Channel	R_o (pre-exp.)	R_o (post-exp.)	R_s (set)	ΔR_s ($R_s - R_o$)		
IRAD Gauge	C12B	3-43	284	23	2195	2182	2376	181		
Corresponding Thermocouple	TC12		83	111						

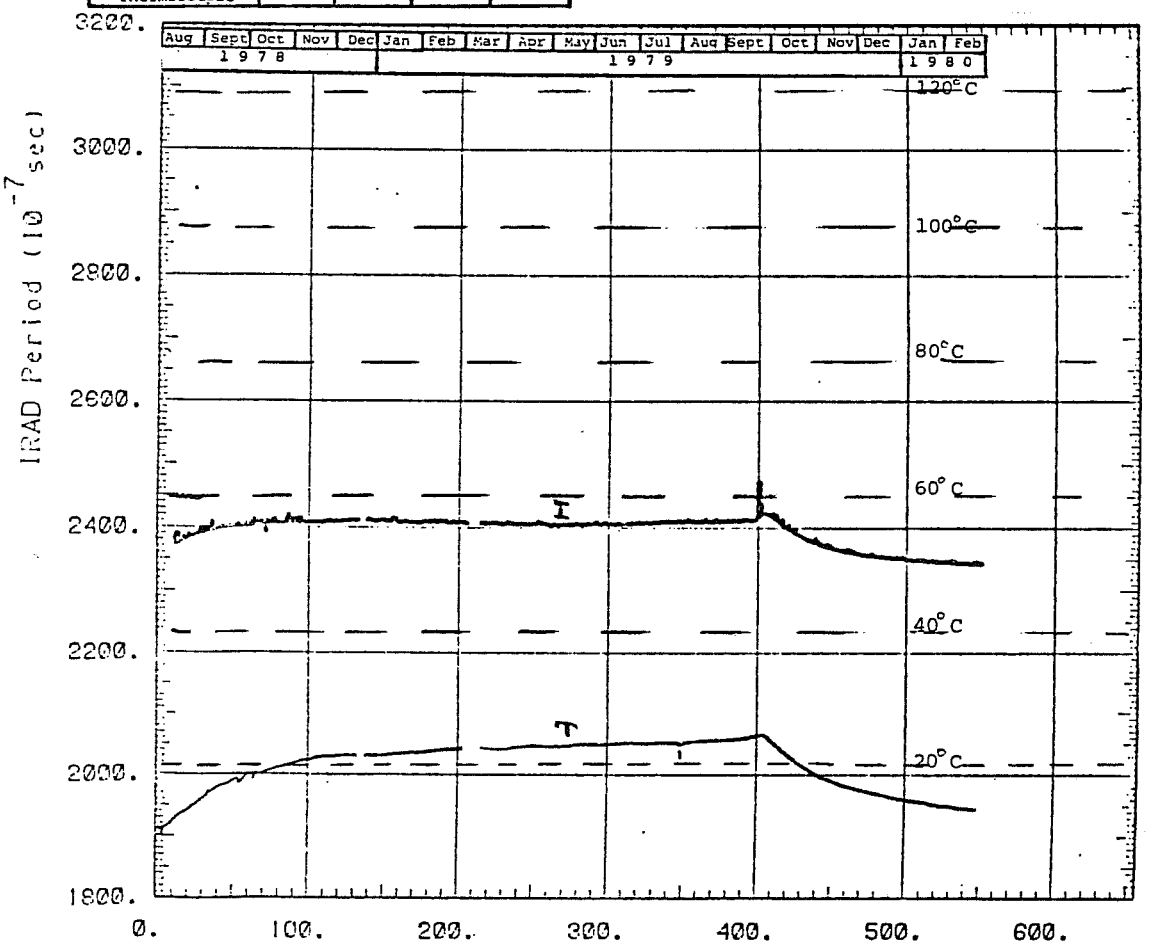

IRAD GAUGE FIELD RECORD

Full Scale Experiment H-10

Gauge C30 (1st)
Hole U15

Term of Gauge Usage	
Entire Experiment ☐	Partial Experiment including... (calendar dates) 78/ 7/2 - 79/7 /7 (y) (m) (d) (experiment days) 0 - 369

[X] vert. [ ] horiz.

r= 1.71
θ= 225.6
z= -.65

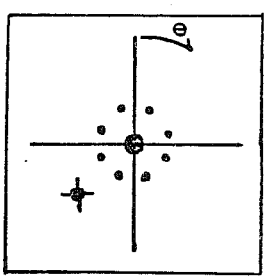

	Label	Mfg. Serial No.	Sensor No. on disc file	Logger Channel	R_o (pre-exp.)	R_o (post-exp.)	R_s (set)	ΔR_s ($R_s - R_o$)		
IRAD Gauge	C3A	3-77	861	4	1969		2167	198		
Corresponding Thermocouple	TC3		502	102						

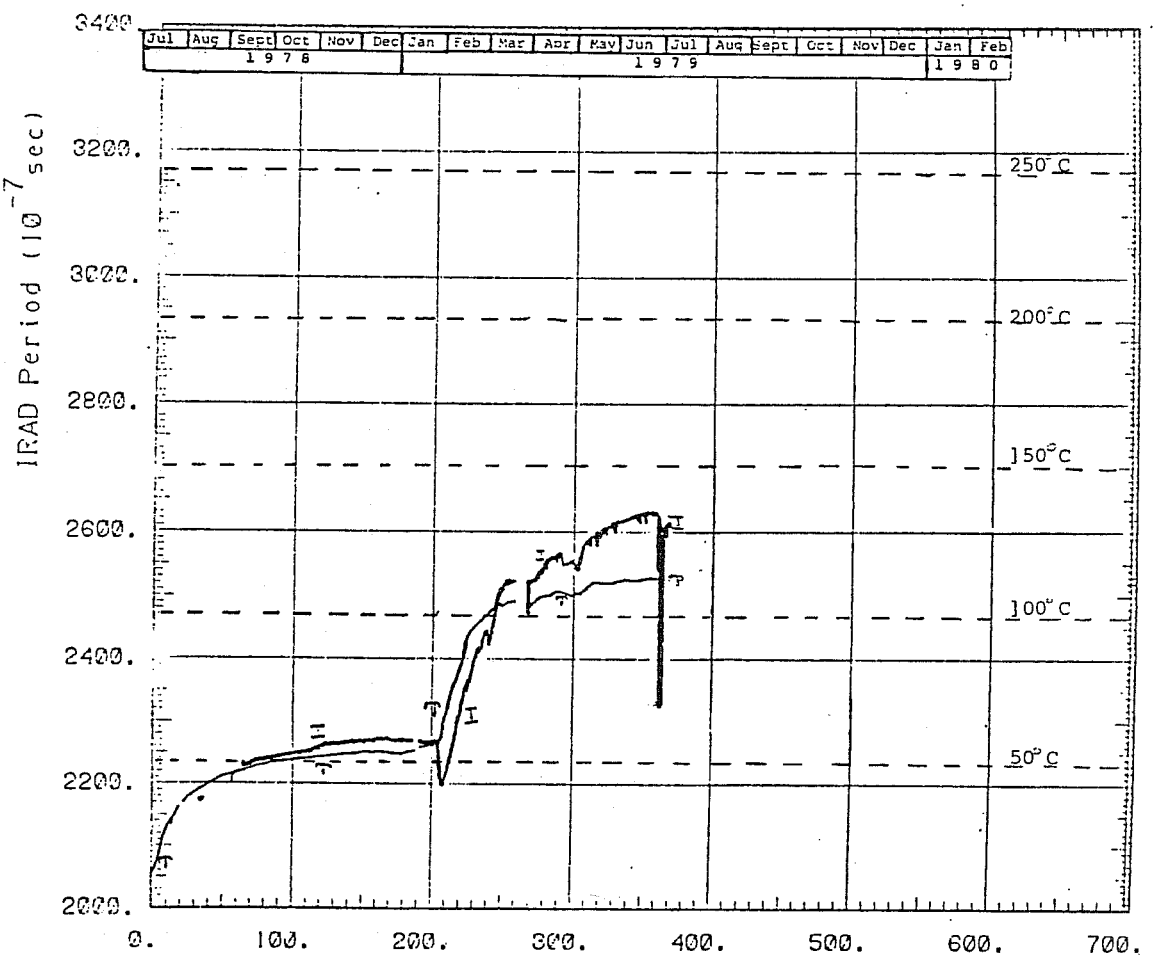

IRAD GAUGE FIELD RECORD

Full Scale
Experiment H-10

Gauge C30 (2nd)
Hole U15

Term of Gauge Usage	
Entire Experiment ☐	Partial Experiment including... (calendar dates) 79/7/26-80/2/8 (y) (m) (d) (experiment days) 388 - 585

☒ vert. ☐ horiz.

r= 1.71
θ= 225.6
z= -.65

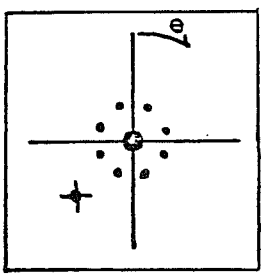

	Label	Mfg. Serial No.	Sensor No. on disc file	Logger Channel	R_o (pre-exp.)	R_o (post-exp.)	R_s (set)	ΔR_s ($R_s - R_o$)		
IRAD Gauge	C3A	E-56	861	4	2151	2160	2531	380		
Corresponding Thermocouple	TC3		502	102						

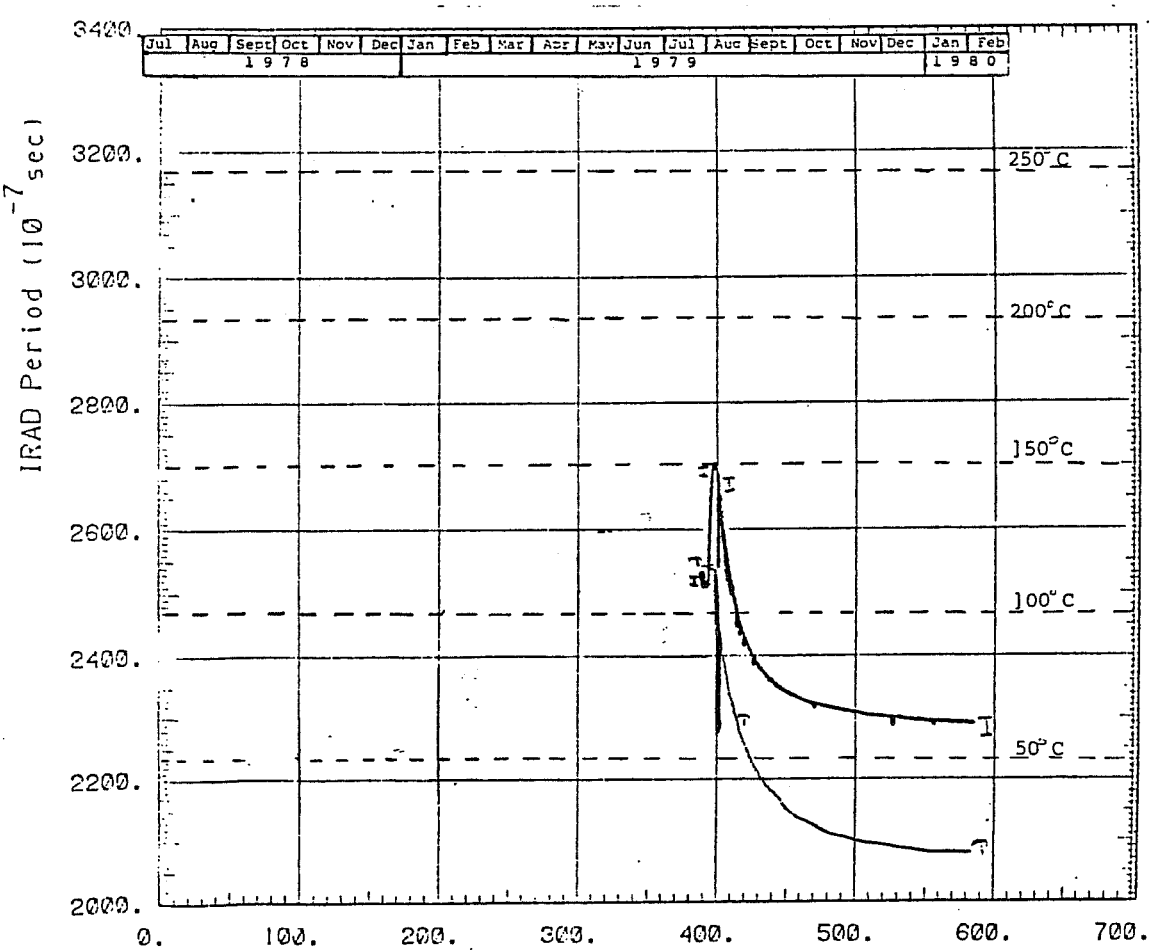

IRAD GAUGE FIELD RECORD

Full Scale
Experiment H-10

Gauge C3R (1st)
Hole U15

Term of Gauge Usage	
Entire Experiment ☐	Partial Experiment including... (calendar dates) 78/7/2 - 79/7/7 (y) (m) (d) (experiment days) 0 - 317 ~~369~~

☒ vert. ☐ horiz.

r= 1.71
θ= 225.6
z= -.65

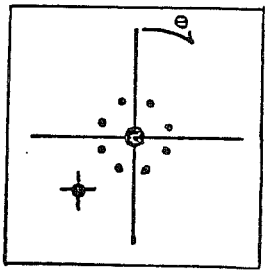

	Label	Mfg. Serial No.	Sensor No. on disc file	Logger Channel	R_o (pre-exp.)	R_o (post-exp.)	R_s (set)	ΔR_s ($R_s - R_o$)		
IRAD Gauge	C3B	3-73	862	5	1961		2180	219		
Corresponding Thermocouple	TC3		502	102						

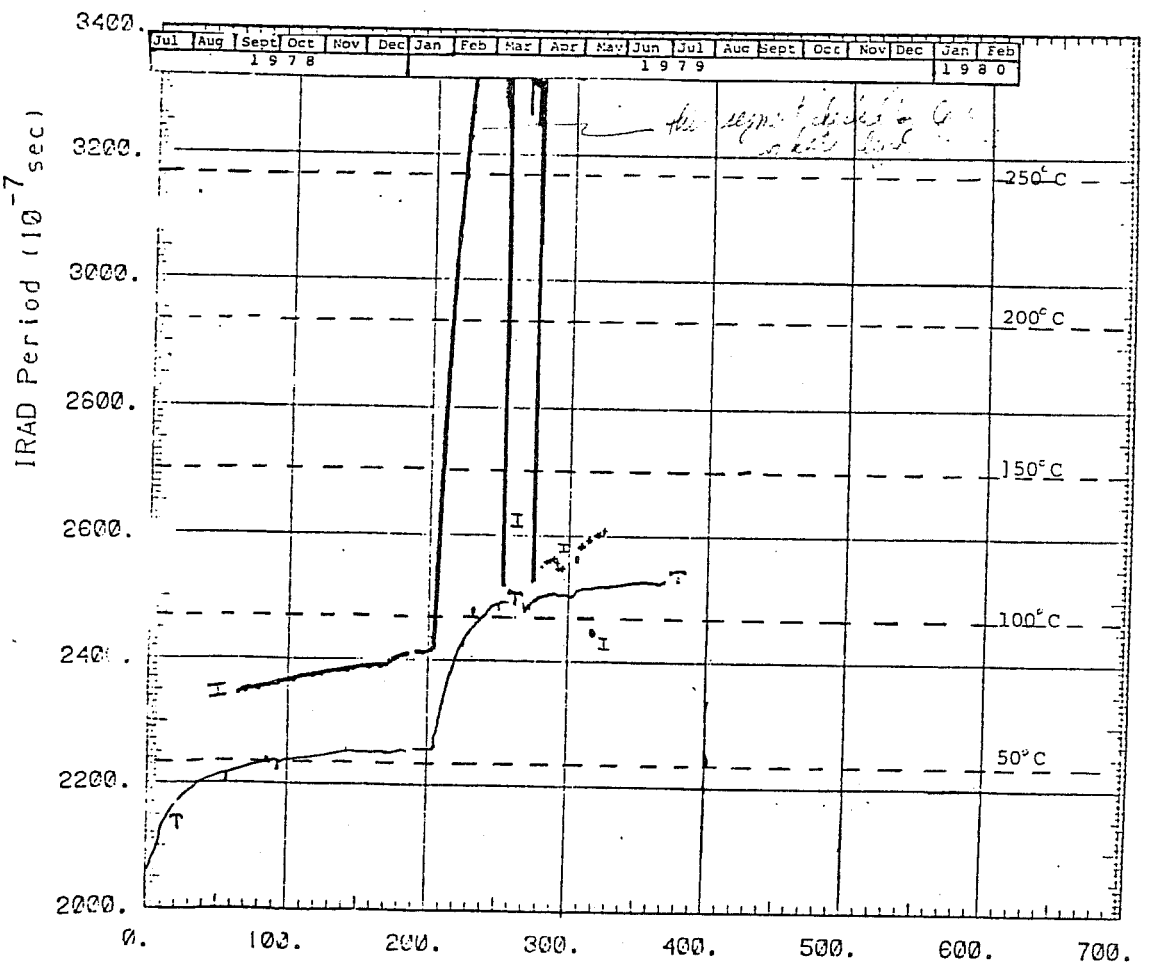

IRAD GAUGE FIELD RECORD

Full Scale
Experiment H-10

Gauge C3R (2nd)
Hole U15

Term of Gauge Usage	
Entire Experiment ☐	Partial Experiment including... (calendar dates) 79 / 7 / 26 80 / 2 / 8 (y) (m) (d) (experiment days) 388 - 585

☒ vert. ☐ horiz.

r= 1.71
θ= 225.6
z= -.65

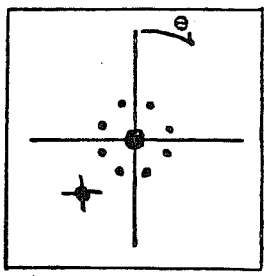

	Label	Mfg. Serial No.	Sensor No. on disc file	Logger Channel	R_o (pre-exp.)	R_o (post-exp.)	R_s (set)	ΔR_s ($R_s - R_o$)		
IRAD Gauge	C3B	E-73	862	5	2143	2143	2359	216		
Corresponding Thermocouple	TC3		502	102						

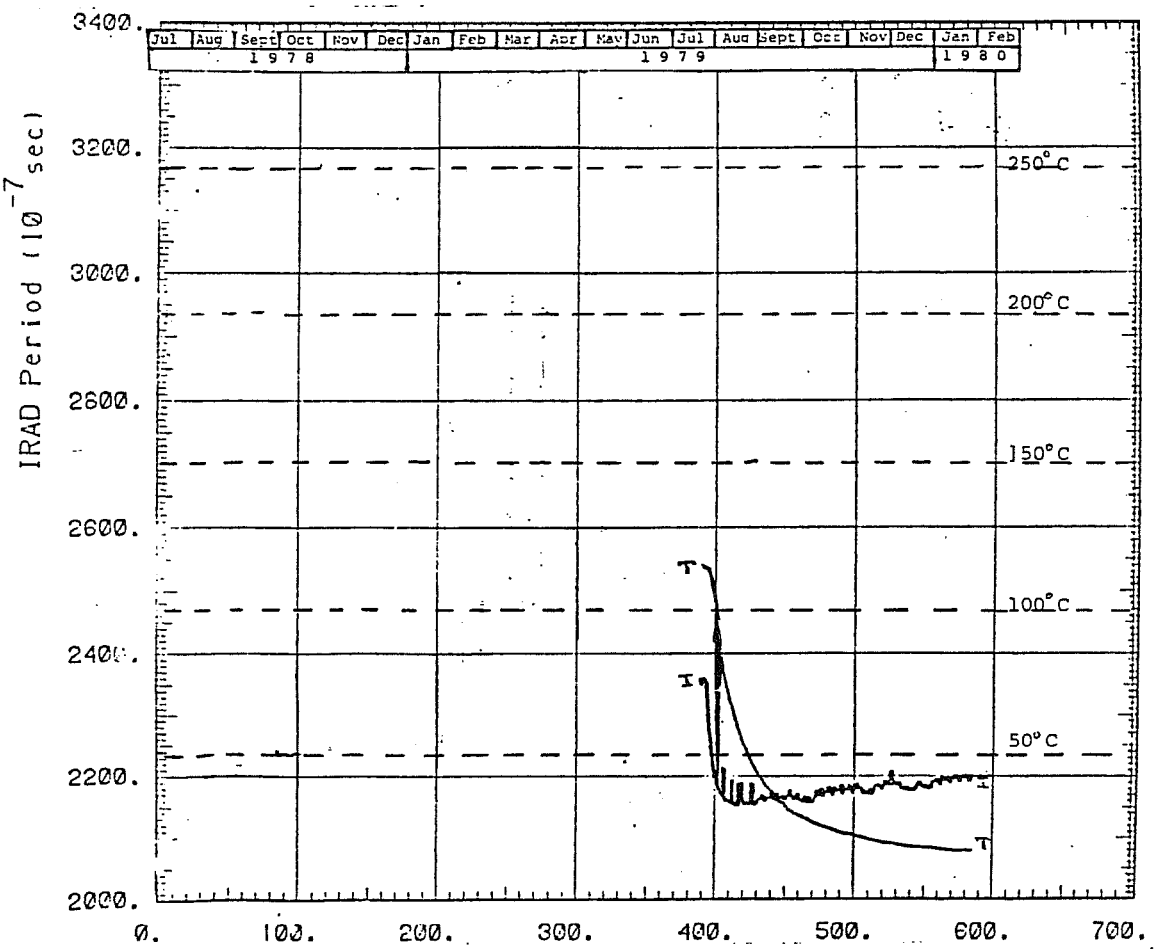

IRAD GAUGE FIELD RECORD

Full Scale Experiment H-10

Gauge C4θ (1st)
Hole U17

Term of Gauge Usage	
Entire Experiment ☐	Partial Experiment including... (calendar dates) 78/7/2 - 79/7/7 (y) (m) (d) (experiment days) 0 - 369

☒ vert. ☐ horiz.

r= 2.46
θ= 292.7
z= -.65

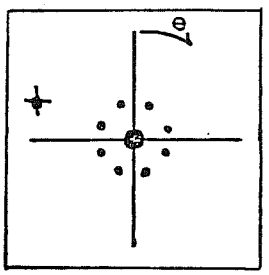

	Label	Mfg. Serial No.	Sensor No. on disc file	Logger Channel	R_O (pre-exp.)	R_O (post-exp.)	R_S (set)	ΔR_S ($R_S - R_O$)		
IRAD Gauge	C4A	3-8	863	6	1868		2047	179		
Corresponding Thermocouple	TC4		503	103						

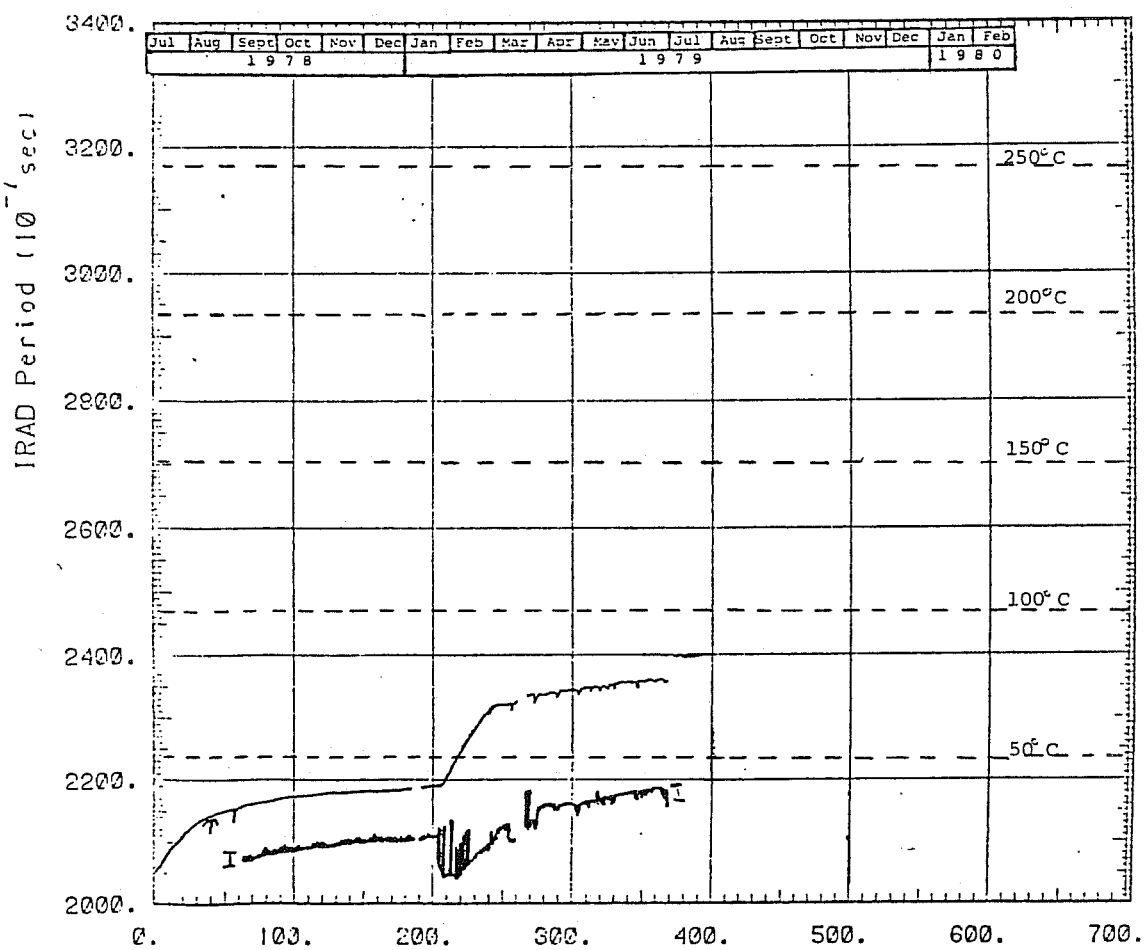

IRAD GAUGE FIELD RECORD

Full Scale Experiment H-10

Gauge C4R (1st)

Hole U17

Term of Gauge Usage	
Entire Experiment ☐	Partial Experiment including... (calendar dates) 78/7/2 (y) (m) (d) - 79/7/7 (experiment days) 0 - 369

☒ vert. ☐ horiz.

r= 2.46

θ= 292.7

z= -.65

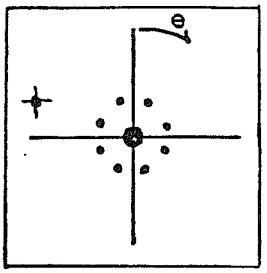

	Label	Mfg. Serial No.	Sensor No. on disc file	Logger Channel	R_o (pre-exp.)	R_o (post-exp.)	R_s (set)	ΔR_s ($R_s - R_o$)		
IRAD Gauge	C4B	3-63	864	7	2036		2165	129		
Corresponding Thermocouple	TC4		503	103						

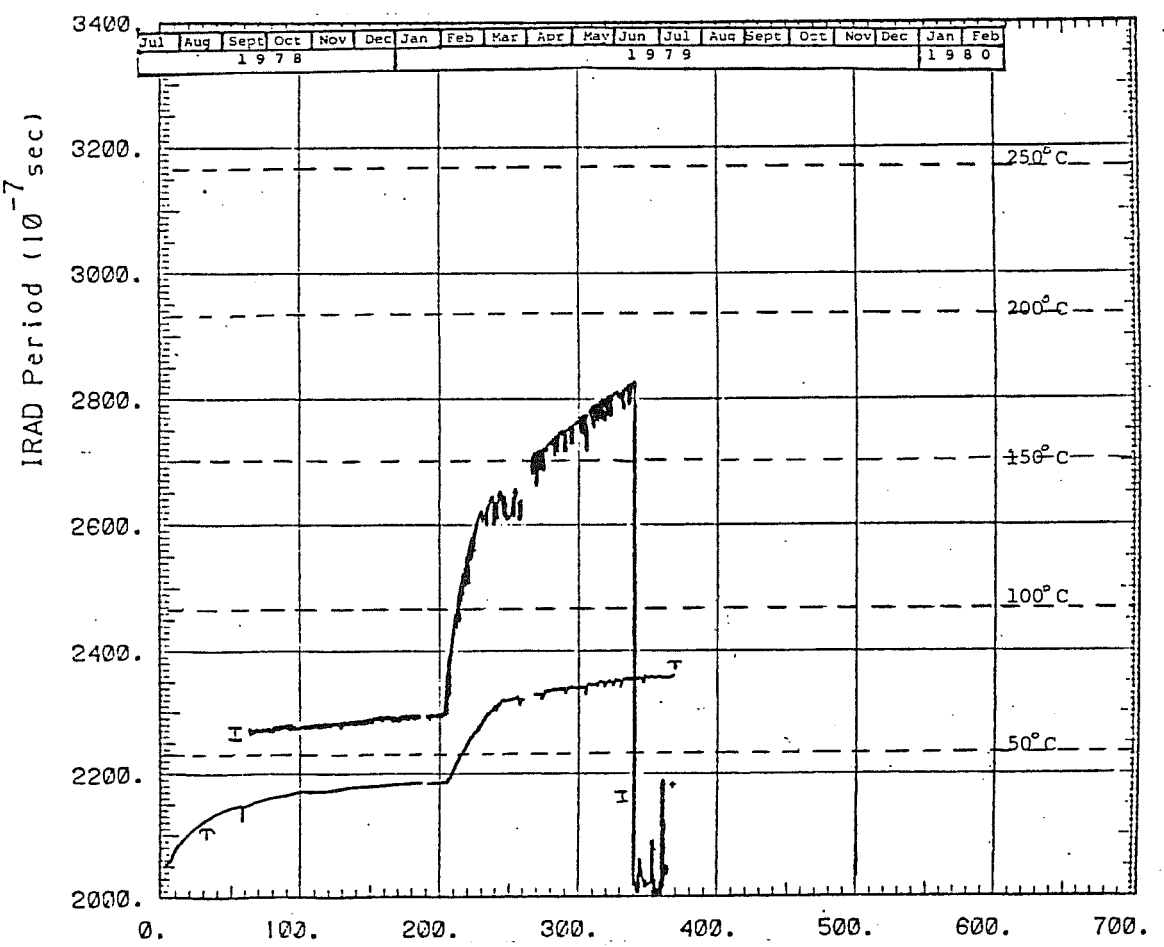

IRAD GAUGE FIELD RECORD

Full Scale Experiment H-10

Gauge C4θ (2nd)
Hole U17

Term of Gauge Usage	
Entire Experiment ☐	Partial Experiment including... (calendar dates) 79/7/11 - 80/2/6 (y) (m) (d) (experiment days) 373 - 583

☒ vert. ☐ horiz.

r= 2.46
θ= 292.7
z= -.65

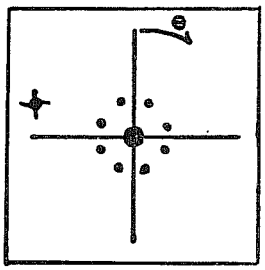

	Label	Mfg. Serial No.	Sensor No. (on disc file)	Logger Channel	R_O (pre-exp.)	R_O (post-exp.)	R_S (set)	ΔR_S ($R_S - R_O$)		
IRAD Gauge	C4B	E-62	864	7	2178	2163	2308	130		
Corresponding Thermocouple	TC4		503	103						

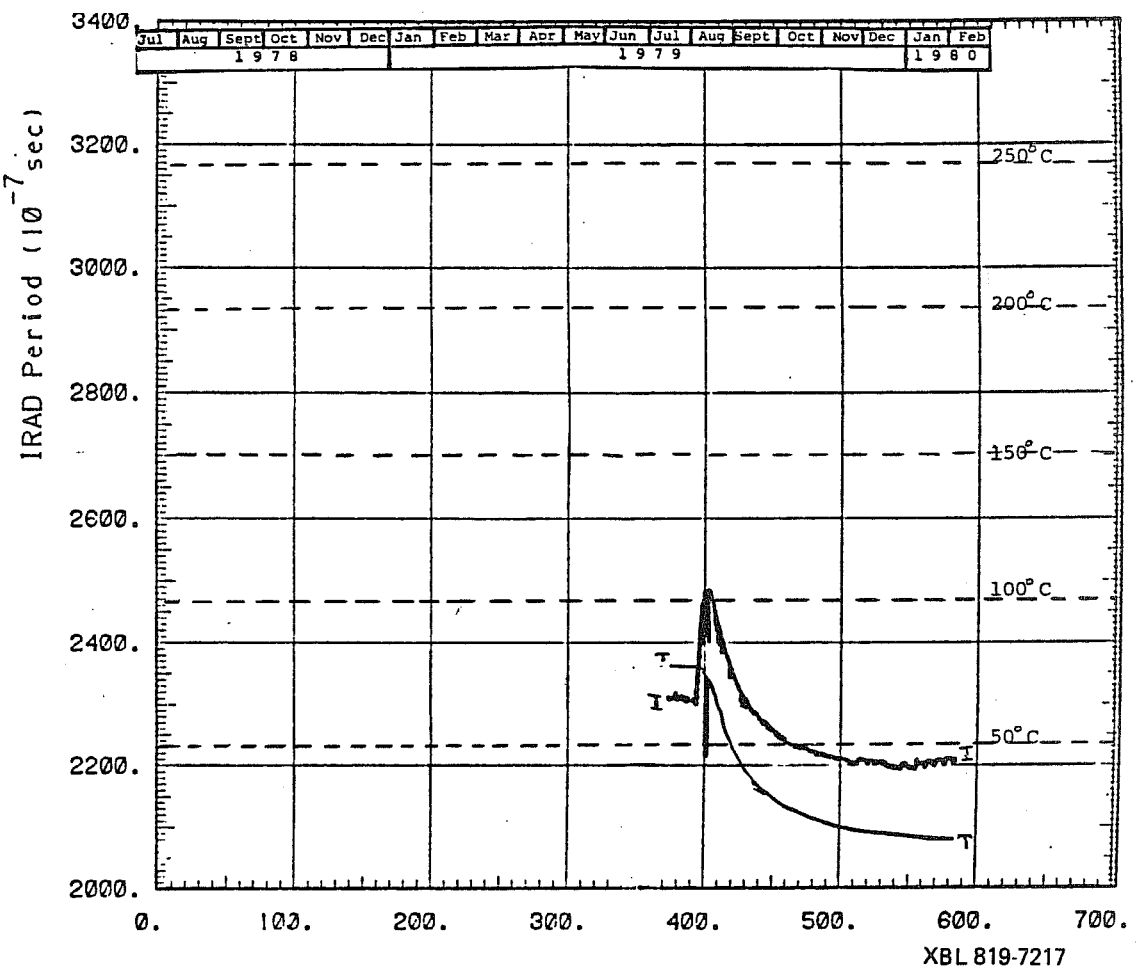

XBL 819-7217

IRAD GAUGE FIELD RECORD

Full Scale Experiment H-10

Gauge C4R (2nd)

Hole 117

Term of Gauge Usage	
Entire Experiment ☐	Partial Experiment including... (calendar dates) 79/7/11 - 80/2/6 (y) (m) (d) (experiment days) 373 - 583

☒ vert. ☐ horiz.

r= 2.46

θ= 292.7

z= -.65

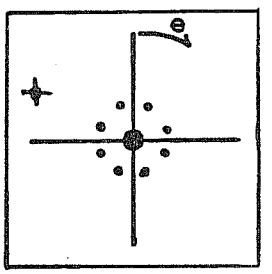

	Label	Mfg. Serial No.	Sensor No. (on disc file)	Logger Channel	R_o (pre-exp.)	R_o (post-exp.)	R_s (set)	ΔR_s (R_s-R_o)		
IRAD Gauge	C4A	E-58	863	6	2025	2021	2398	373		
Corresponding Thermocouple	TC4		503	103						

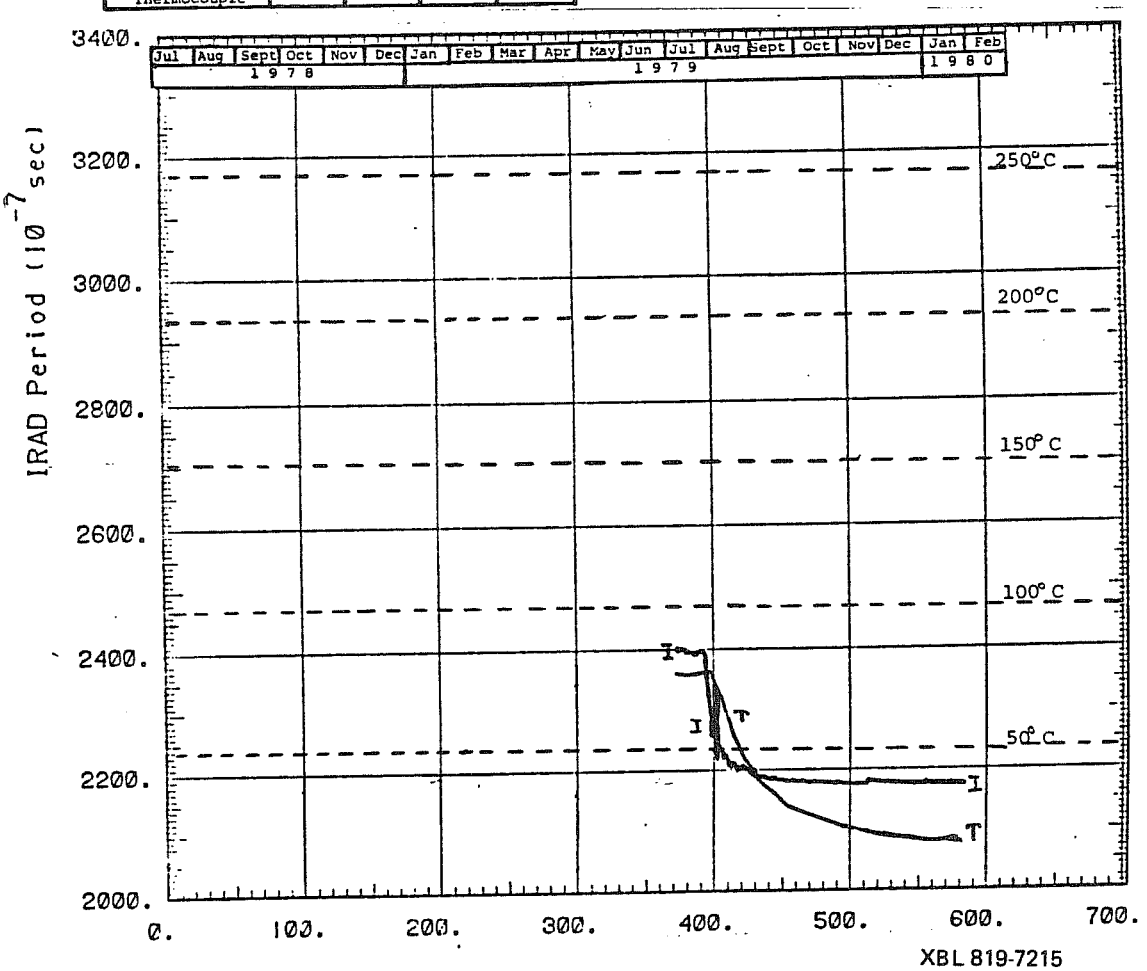

XBL 819-7215

IRAD GAUCE FIELD RECORD

Full Scale Experiment H-10

Gauge C5θ (1st)

Hole C5

Term of Gauge Usage	
Entire Experiment ☐	Partial Experiment including... (calendar dates) 78/7/2 - 79/4/27 (y) (m) (d) (experiment days) 0 - 298

[X] vert. [ ] horiz.

r= 1.51

θ= 247.9

z= .85

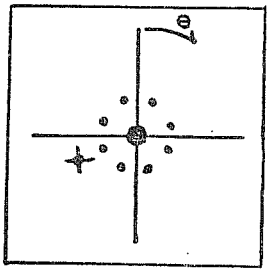

	Label	Mfg. Serial No.	Sensor No. on disc file	Logger Channal	R_o (pre-exp.)	R_o (post-exp.)	R_s (set)	ΔR_s ($R_s - R_o$)		
IRAD Gauge	C5A	3-82	865	8	1980		2151	171		
Corresponding Thermocouple	TC5		504	104						

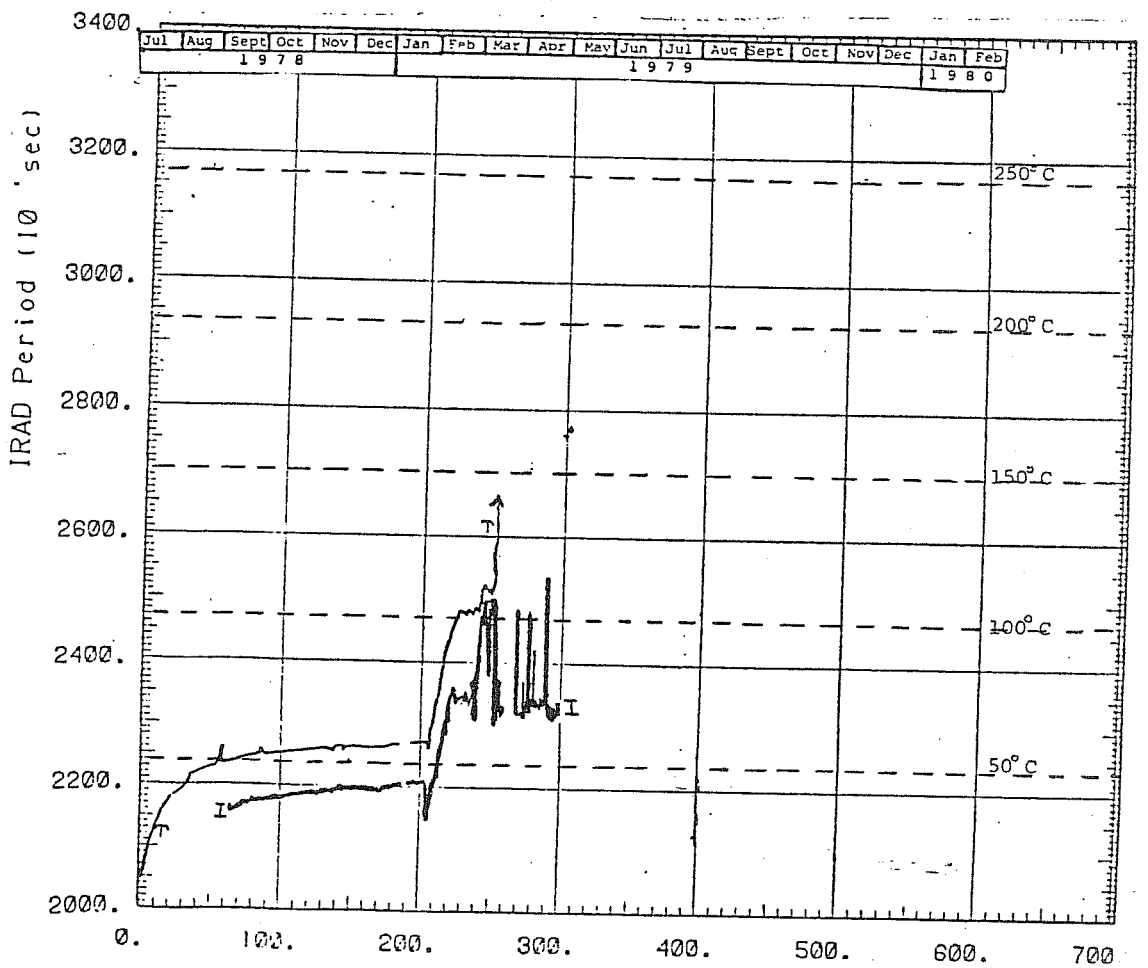

IRAD GAUGE FIELD RECORD

Full Scale
Experiment H-10

Gauge C5R (1st)
Hole C5

Term of Gauge Usage	
Entire Experiment ☐	Partial Experiment including... (calendar dates) 78/0703 (y) (m) (d) - 79/ 2/3 (experiment days) 0 - 215

☒ vert. ☐ horiz.

r= 1.51
θ= 247.9
z= .85

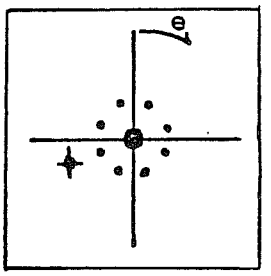

	Label	Mfg. Serial No.	Sensor No. on disc file	Logger Channel	R_o (pre-exp.)	R_o (post-exp.)	R_s (set)	ΔR_s ($R_s - R_o$)		
IRAD Gauge	C5B	3-35	866	9	1907		2086	179		
Corresponding Thermocouple	TC5		504	104						

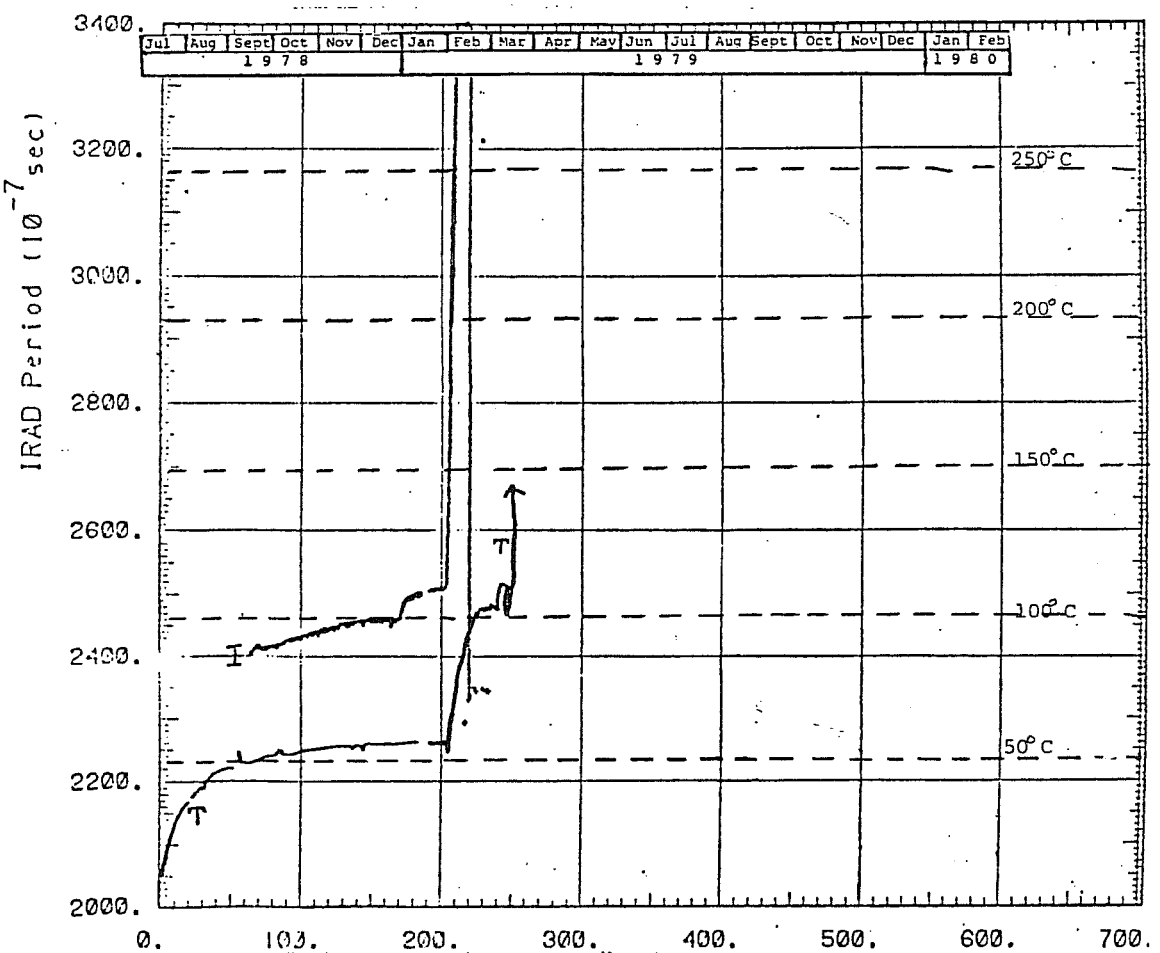

IRAD GAUGE FIELD RECORD

Full Scale Experiment H-10

Gauge C5θ (2nd)

Hole C5

Term of Gauge Usage	
Entire Experiment ☐	Partial Experiment including... (calendar dates) 79 07 11 - 80/02/8 (y) (m) (d) (experiment days) 374 – 585

☒ vert. ☐ horiz.

r= 1.51

θ= 247.9

z= .85

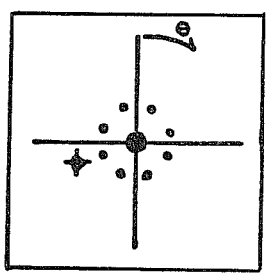

	Label	Mfg. Serial No.	Sensor No. on disc file	Logger Channel	R_o (pre-exp.)	R_o (post-exp.)	R_s (set)	ΔR_s ($R_s - R_o$)		
IRAD Gauge	C5B	E-50	866	9	2097	2088	2374	277		
Corresponding Thermocouple	TC5		504	104						

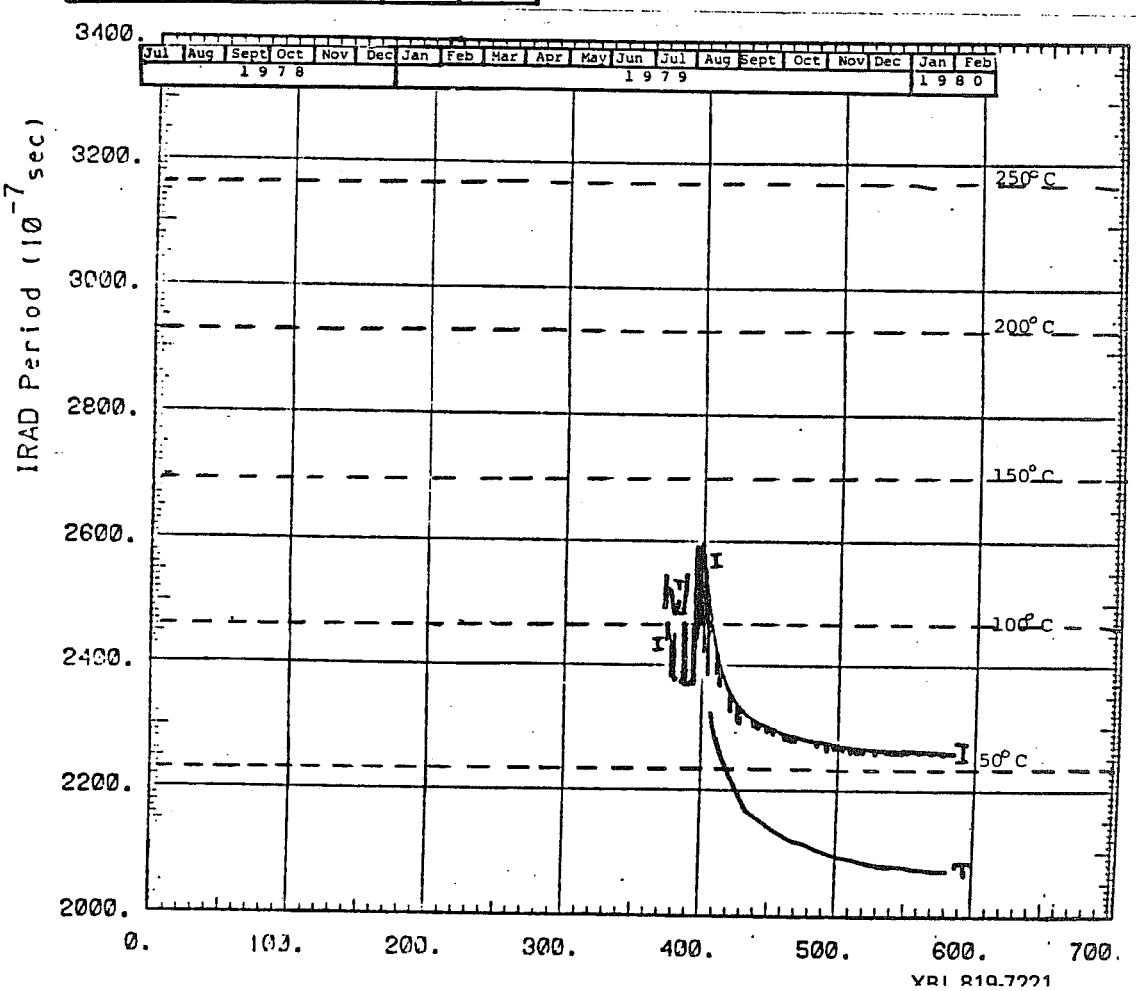

IRAD GAUGE FIELD RECORD

Full Scale
Experiment H-10

Gauge C5R (2nd)
Hole C5

Term of Gauge Usage	
Entire Experiment ☐	Partial Experiment including... (calendar dates) 79/ 7/11 - 80/ 2/ 8 (y) (m) (d) (experiment days) 374 - 585

☒ vert. ☐ horiz.

r= 1.51
θ= 247.9
z= .85

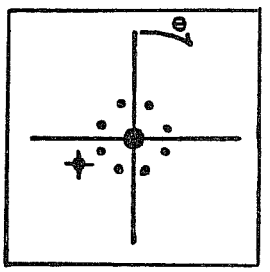

	Label	Mfg. Serial No.	Sensor No. (on disc file)	Logger Channel	R_o (pre-exp.)	R_o (post-exp.)	R_s (set)	ΔR_s ($R_s - R_o$)		
IRAD Gauge	C5A	E-51	865	8	2137	2131	2345	208		
Corresponding Thermocouple	TC5		504	104						

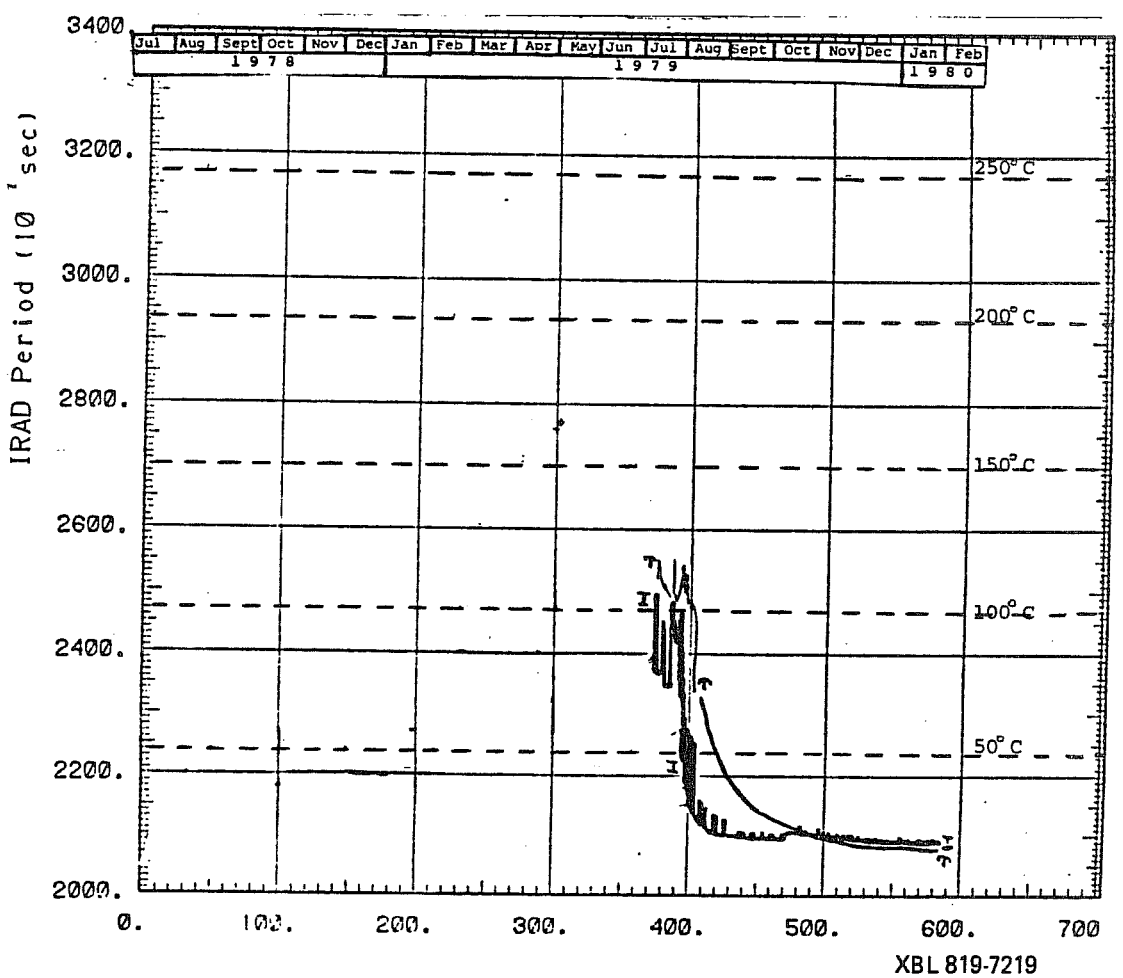

XBL 819-7219

IRAD GAUGE FIELD RECORD

Full Scale Experiment H-10

Gauge C10θ (1st)

Hole C10

Term of Gauge Usage	
Entire Experiment	Partial Experiment including... (calendar dates) 78/7 /2 -79/ 3/13 (y) (m) (d) (experiment days) 0 - 253

vert. ☐ horiz. ☒

r= 4.02

θ= 112.5

z= .65

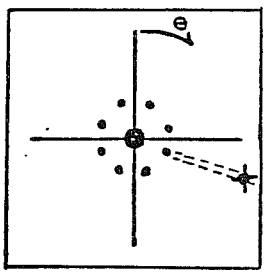

	Label	Mfg. Serial No.	Sensor No. on disc file	Logger Channel	R_o (pre-exp.)	R_o (post-exp.)	R_s (set)	ΔR_s (R_s-R_o)		
IRAD Gauge	C10A	3-14	869	18	2244	2231	2476	232		
Corresponding Thermocouple	TC10		506	109						

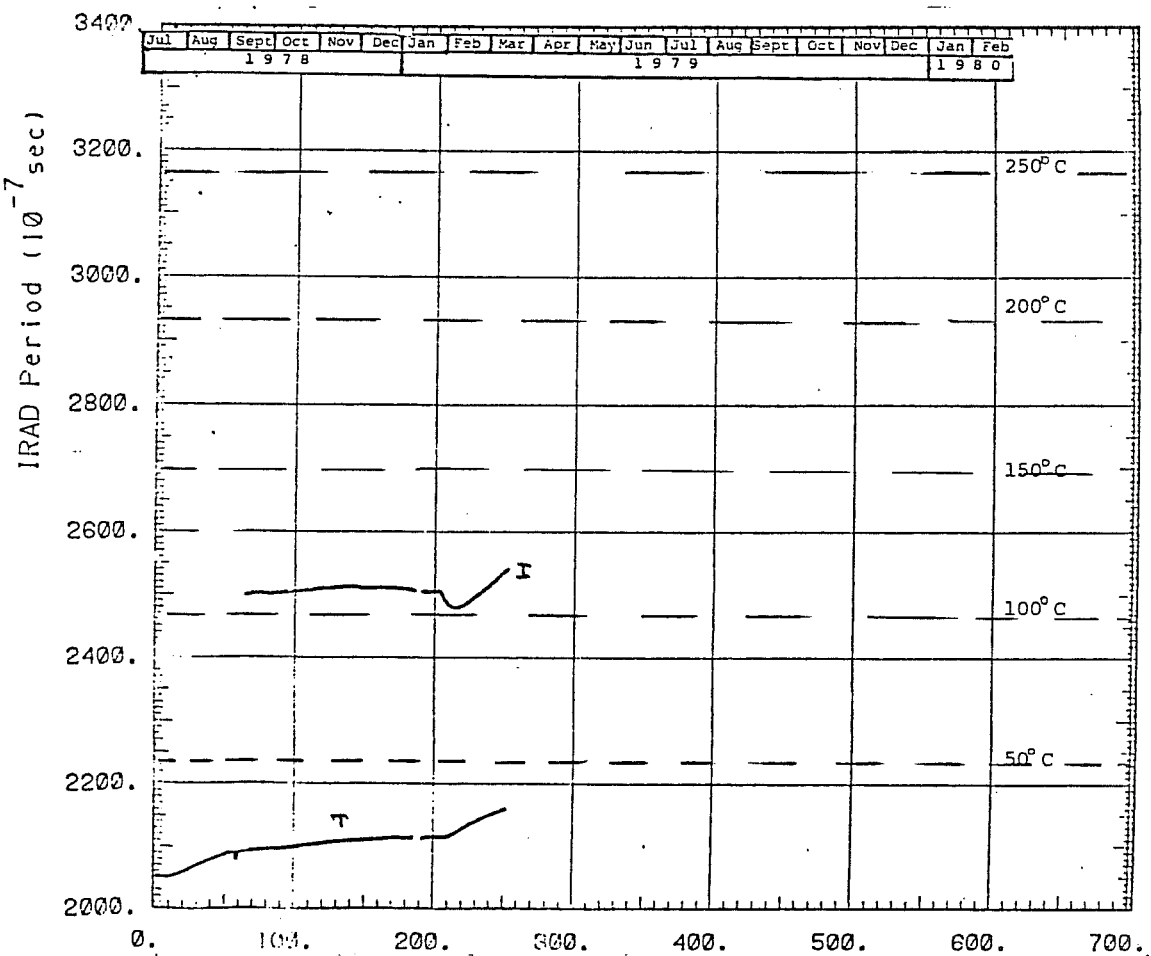

IRAD GAUGE FIELD RECORD

Full Scale
Experiment H-10

Gauge C107 (1st)
Hole C10

Term of Gauge Usage	
Entire Experiment	Partial Experiment including... (calendar dates) 78/7/2 - 79/3/13 (y) (m) (d) (experiment days) 0 - 253

☐ vert. ☒ horiz.

r= 4.02
θ=112.5
z= .65

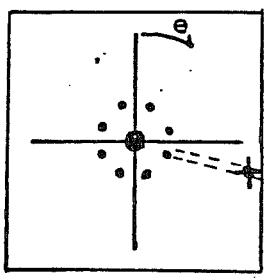

	Label	Mfg. Serial No.	Sensor No. on disc file	Logger Channel	R_o (pre-exp.)	R_o (post-exp.)	R_s (set)	ΔR_s ($R_s - R_o$)		
IRAD Gauge	C10B	3-45	870	19	2204	2198	2431	227		
Corresponding Thermocouple	TC10		506	109						

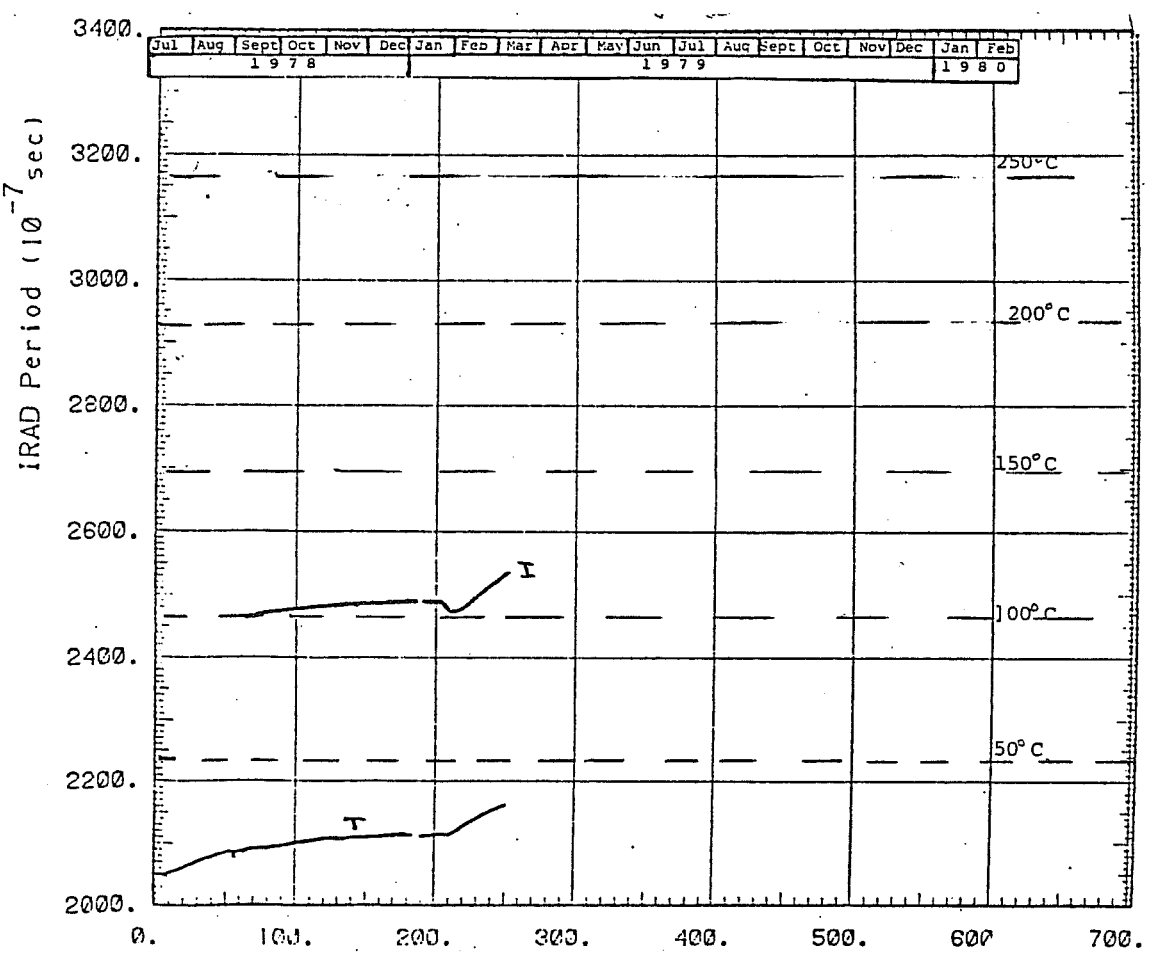

IRAD GAUGE FIELD RECORD

Full Scale Experiment H-10

Gauge C10θ (2nd)
Hole U23

Term of Gauge Usage	
Entire Experiment ☐	Partial Experiment including... (calendar dates) 79/7/20 - 80/2/13 (y) (m) (d) (experiment days) 382 - 590

☐ vert. ☒ horiz.

r= 4.02
θ= 112.5
z= .65

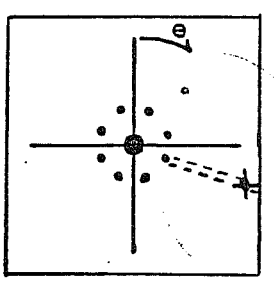

corrected by Cara.

	Label	Mfg. Serial No.	Sensor No. on disc file	Logger Channel	R_O (pre-exp.)	R_O (post-exp.)	R_S (set)	ΔR_S ($R_S - R_O$)		
IRAD Gauge	C10A	E-69	869	18	2218	2218	2480	262		
Corresponding Thermocouple	TC10		437	137						

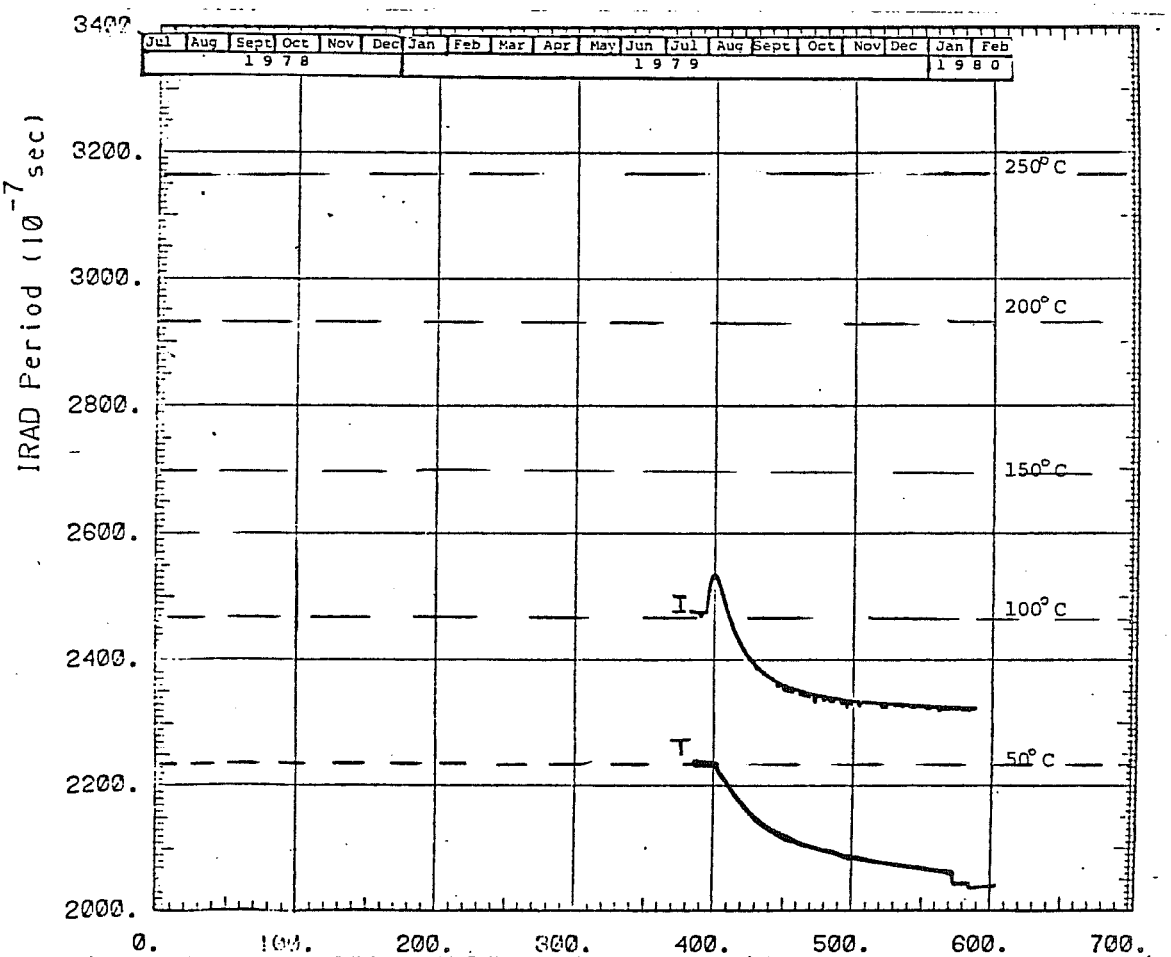

IRAD GAUGE FIELD RECORD

Full Scale Experiment H-10

Gauge C10Z (2nd)

Hole U23

Term of Gauge Usage	
Entire Experiment ☐	Partial Experiment including... (calendar dates) 79/ 7/20-80/ 2/13 (y) (m) (d) (experiment days) 382 - 590

☐ vert. ☒ horiz.

r= 4.02
θ= N2.5
z= .65

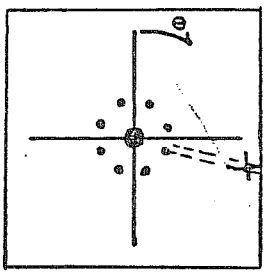

	Label	Mfg. Serial No.	Sensor No. on disc file	Logger Channel	R_o (pre-exp.)	R_o (post-exp.)	R_s (set)	ΔR_s (R_s-R_o)		
IRAD Gauge	C10B	3-42	870	19	2444	2417	2662	218		
Corresponding Thermocouple	TC10		437	137						

corrected by cara.

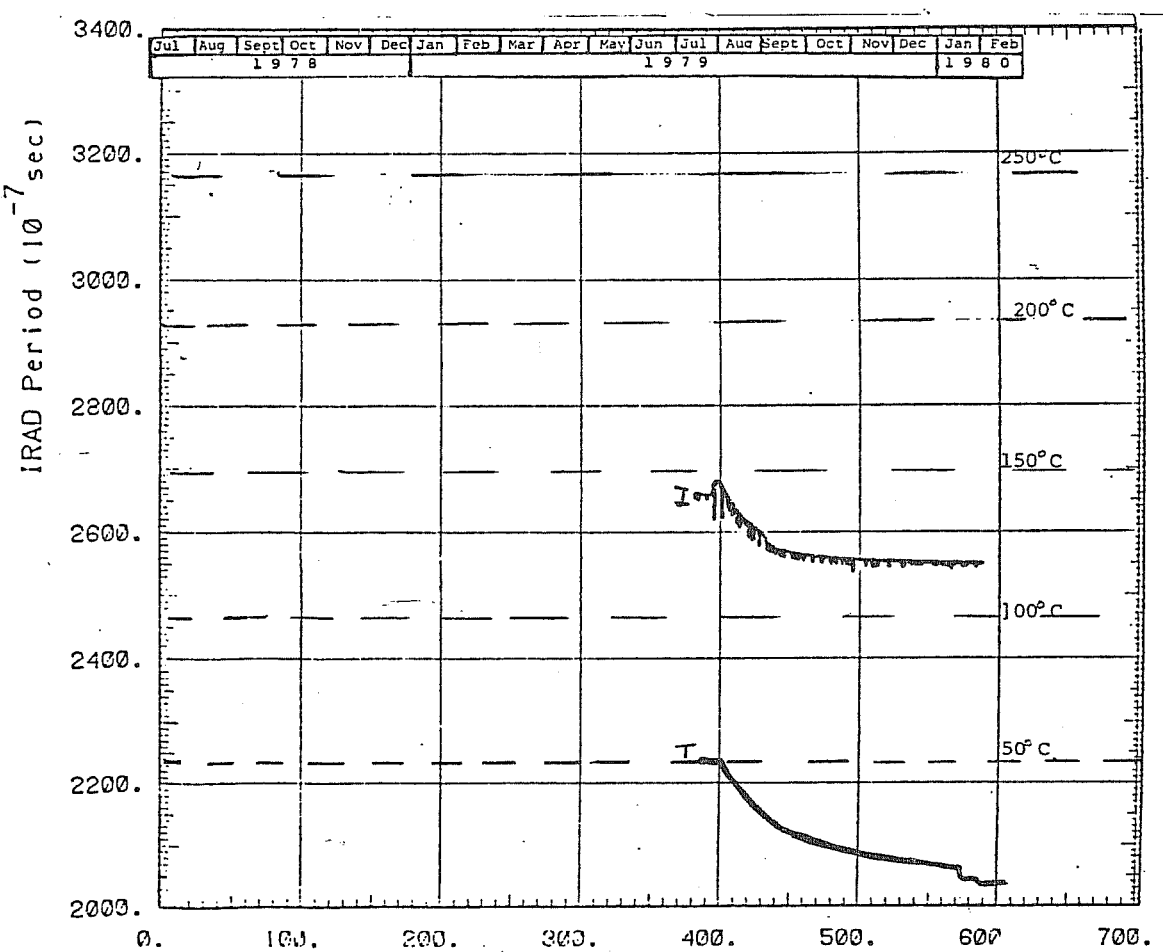

IRAD GAUGE FIELD RECORD

Full Scale Experiment H-10

Gauge C14A
Hole C14

Term of Gauge Usage	
Entire Experiment	Partial Experiment including...
X	(calendar dates) / / - / / (y) (m) (d)
	(experiment days) ___ - ___

☐ vert. ☒ horiz.

r= 1.50
θ= 90.9
z= -.82

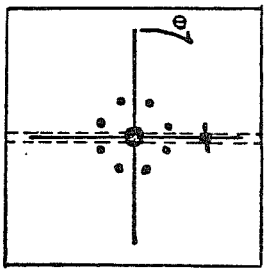

	Label	Mfg. Serial No.	Sensor No. on disc file	Logger Channel	R_O (pre-exp.)	R_O (post-exp.)	R_S (set)	ΔR_S ($R_S - R_O$)		
IRAD Gauge	C14A	3-9	873	26	2005	2004	2194	189		
Corresponding Thermocouple	TC14		508	113						

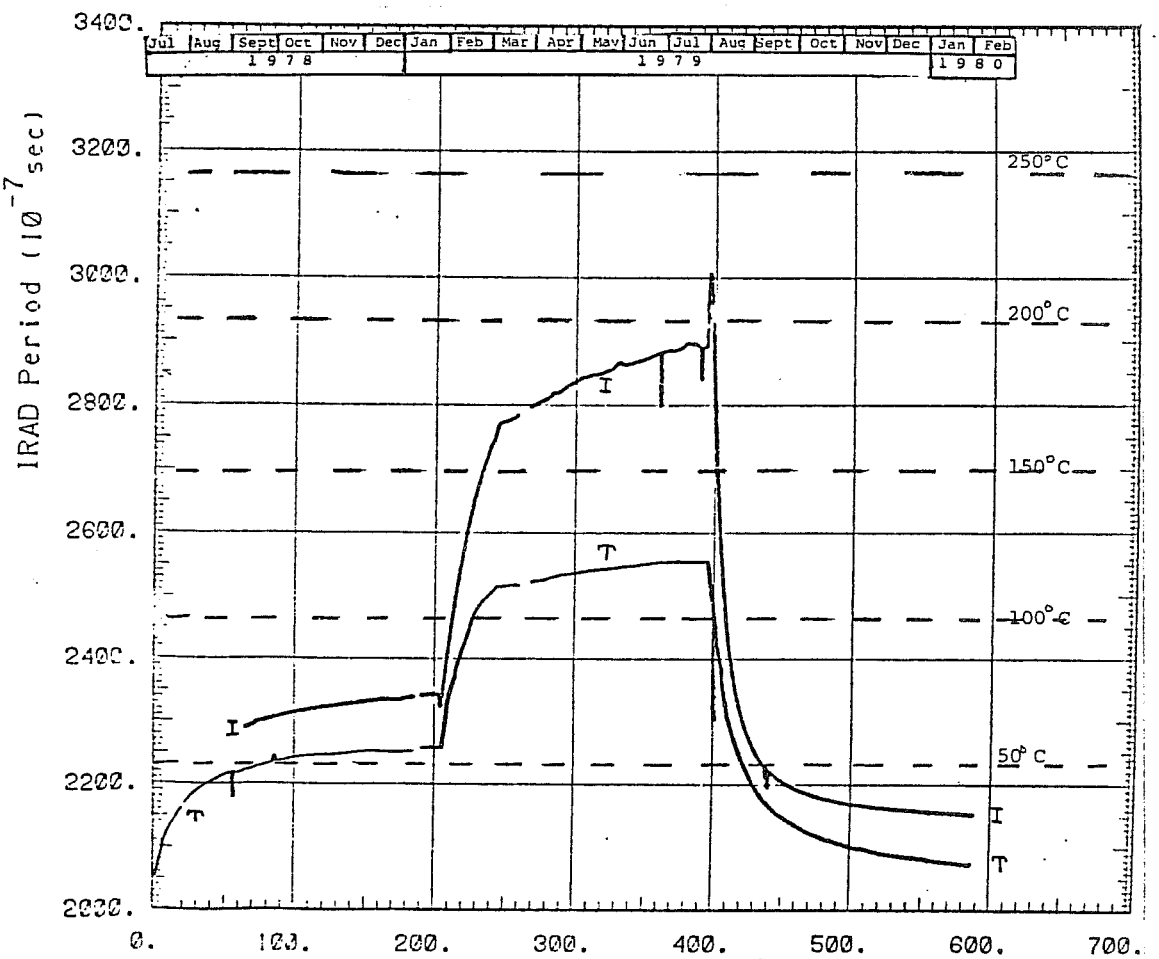

IRAD GAUGE FIELD RECORD

Full Scale Experiment H-10

Gauge C14Z
Hole C14

Term of Gauge Usage	
Entire Experiment	Partial Experiment including...
X	(calendar dates) / / - / / (y) (m) (d)
	(experiment days) ____ - ____

vert. [ ] horiz. [X]

r= 1.50
θ= 90.9
z= -.82

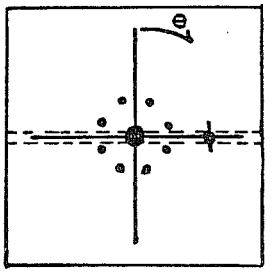

	Label	Mfg. Serial No.	Sensor No. (on disc file)	Logger Channel	R_o (pre-exp.)	R_o (post-exp.)	R_s (set)	ΔR_s (R_s-R_o)		
IRAD Gauge	C14B	3-29	874	27	2010	1980	2166	156		
Corresponding Thermocouple	TC14		508	113						

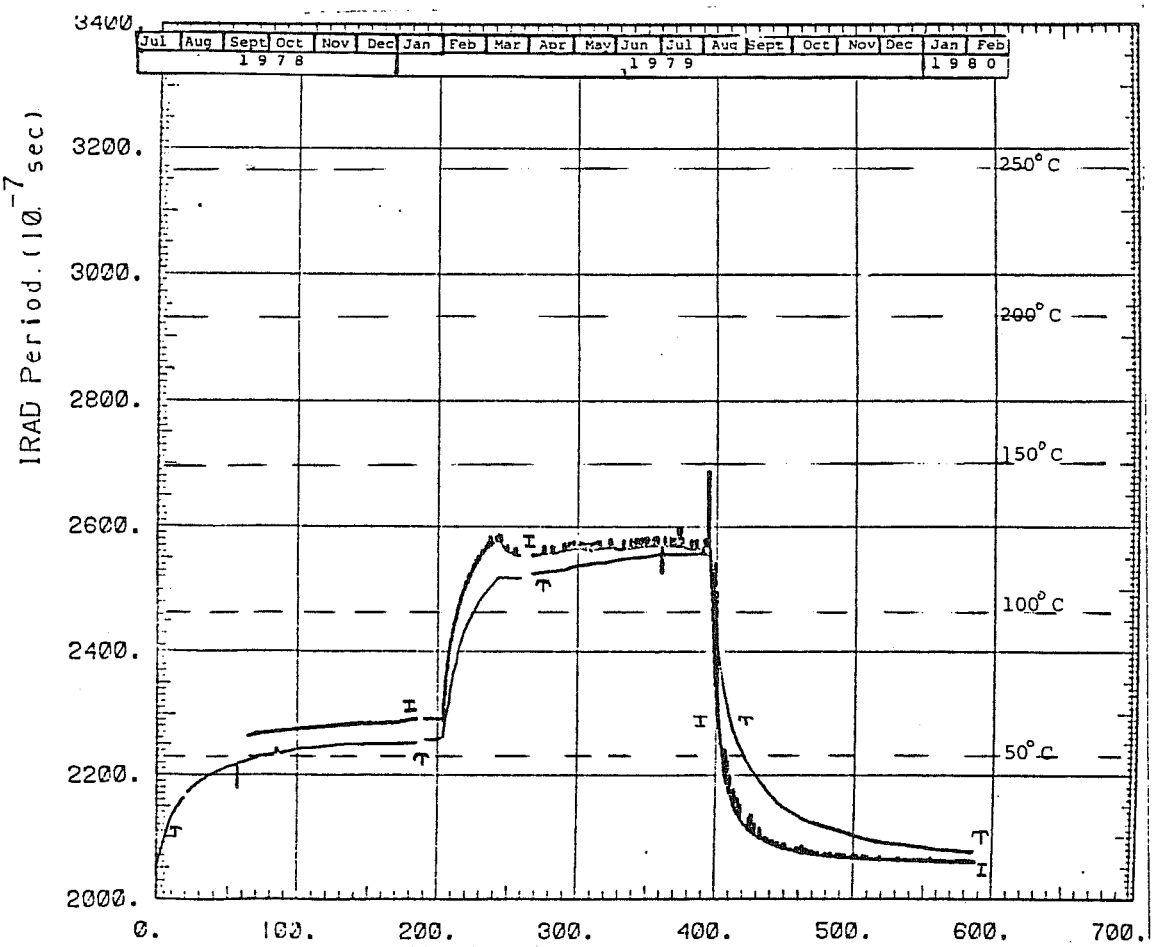

IRAD GAUGE FIELD RECORD

Full Scale
Experiment H-10

Gauge C15θ
Hole C15

Term of Gauge Usage	
Entire Experiment	Partial Experiment including...
X	(calendar dates) / / - / / (y) (m) (d)
	(experiment days) ___ - ___

vert. ☐ horiz. X

r= 3.00
θ= 135.2
z= -.81

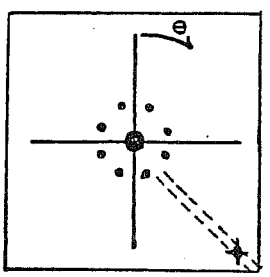

	Label	Mfg. Serial No.	Sensor No. on disc file	Logger Channel	R_o (pre-exp.)	R_o (post-exp.)	R_s (set)	ΔR_s (R_s-R_o)		
IRAD Gauge	C15A	3-50	875	28	2161	2116	2371	210		
Corresponding Thermocouple	TC15		509	114						

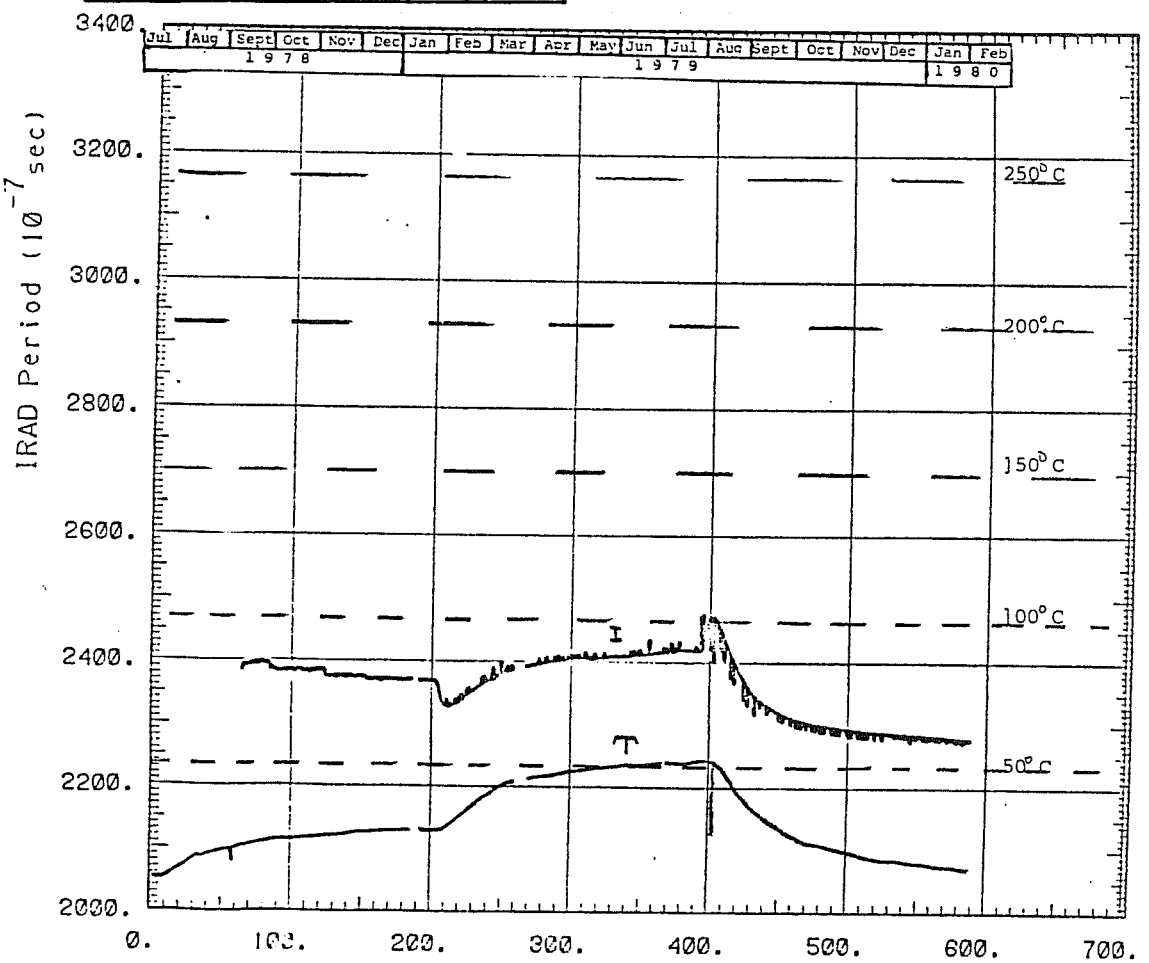

IRAD GAUGE FIELD RECORD

Full Scale
Experiment H-10

Gauge C15Z
Hole C15

Term of Gauge Usage	
Entire Experiment	Partial Experiment including...
X	(calendar dates) / / - / / (y) (m) (d)
	(experiment days) ____ - ____

vert. ☐ horiz. X

r= 3.00
θ=135.2
z= -.81

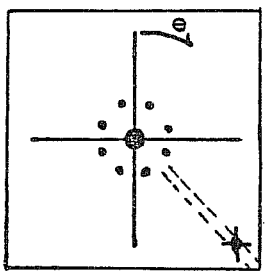

	Label	Mfg. Serial No.	Sensor No. on disc file	Logger Channel	R_o (pre-exp.)	R_o (post-exp.)	R_s (set)	ΔR_s (R_s-R_o)		
IRAD Gauge	C15B	3-36	876	29	2165	2129	2350	185		
Corresponding Thermocouple	TC15		509	114						

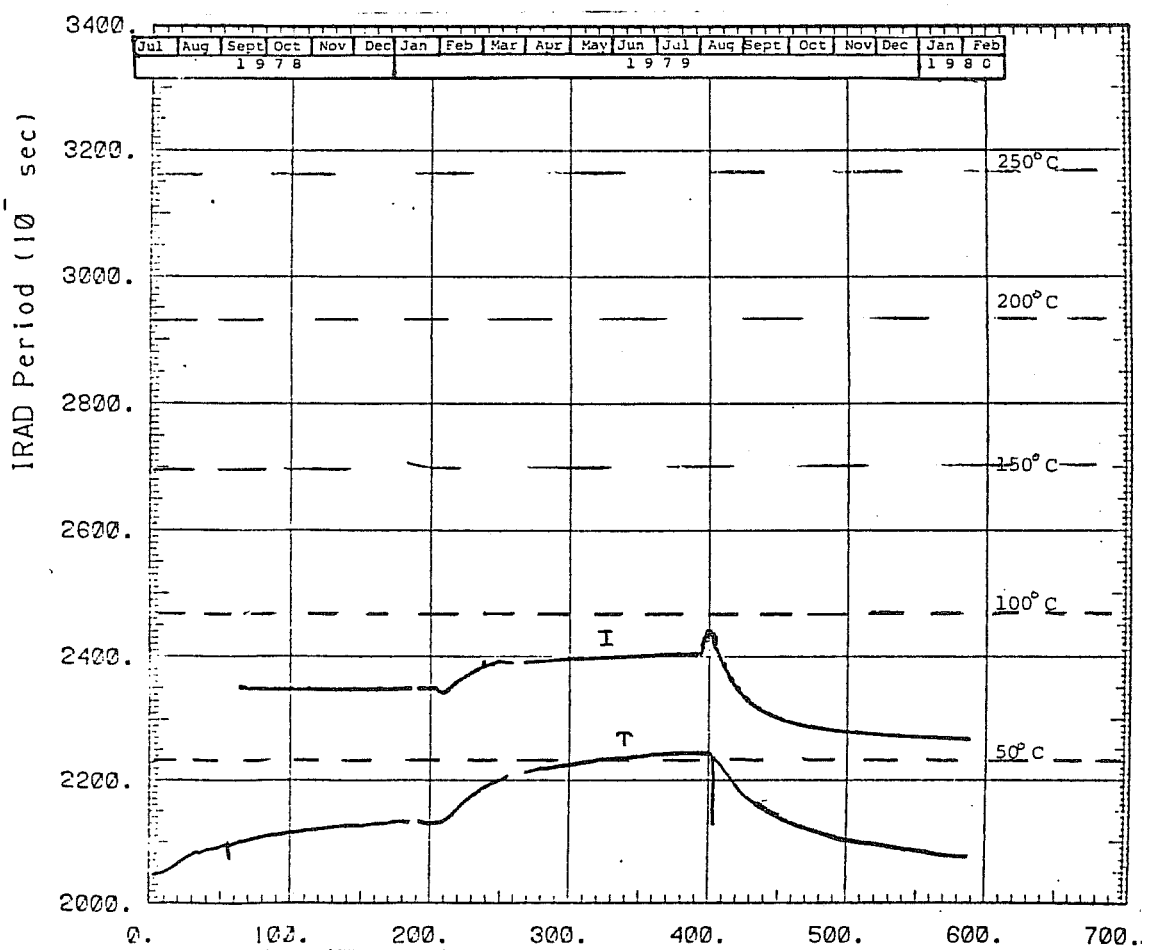

APPENDIX B: USBM GAUGE FIELD RECORDS

USBM GAUGE FIELD RECORD

Full Scale Experiment H9 Gauge U1 Hole U1

	Label	Sensor No.	Logger Channel	V_{ss} Voltage	V_{oo} Rezero	C_o Slope	V_{oi}-V_{oo} Temp. Const.	T_s Start Temp.	
USBM Gauge	U1A	201	0	7.471	0.106	0.0686	-0.320	11.12	
USBM Gauge	U1B	202	1	7.578	-0.038	0.0665	-0.140	11.12	
USBM Gauge	U1C	203	2	10.732	2.445	0.0662	0.090	11.12	
Corresponding Thermocouple		2	115						

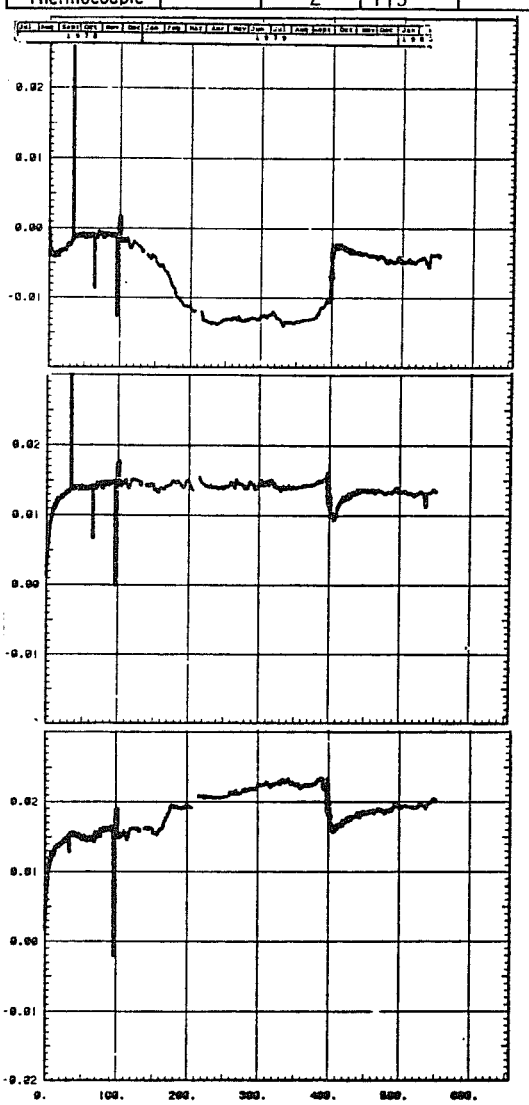

USBM displacement (mv)

[X] vert. [ ] horiz.

r = 1.51
θ = 0
z = 0.85

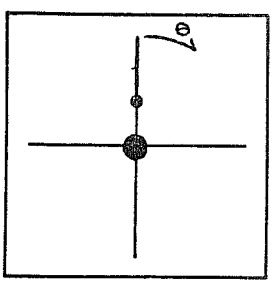

Entire Experiment [X]

Partial Experiment Including (Calendar dates)

____ – ____

(Experiment days)

____ – ____

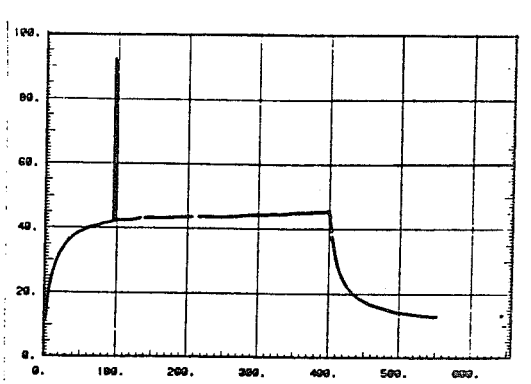

Temp (°C)

XBL 817-3279

USBM GAUGE FIELD RECORD

Full Scale Experiment H9 Gauge U2 (1st) Hole U2

	Label	Sensor No.	Logger Channel	V_{ss} Voltage	V_{oo} Rezero	C_o Slope	V_{01}-V_{oo} Temp. Const.	T_s Start Temp.	
USBM Gauge	U2A	204	3	5.571	0.207	0.0658	0.012	10.44	
USBM Gauge	U2B	205	4	5.947	0.188	0.0657	-0.054	10.44	
USBM Gauge	U2C	206	5	6.772	0.445	0.0649	0.012	10.44	
Corresponding Thermocouple		3	116						

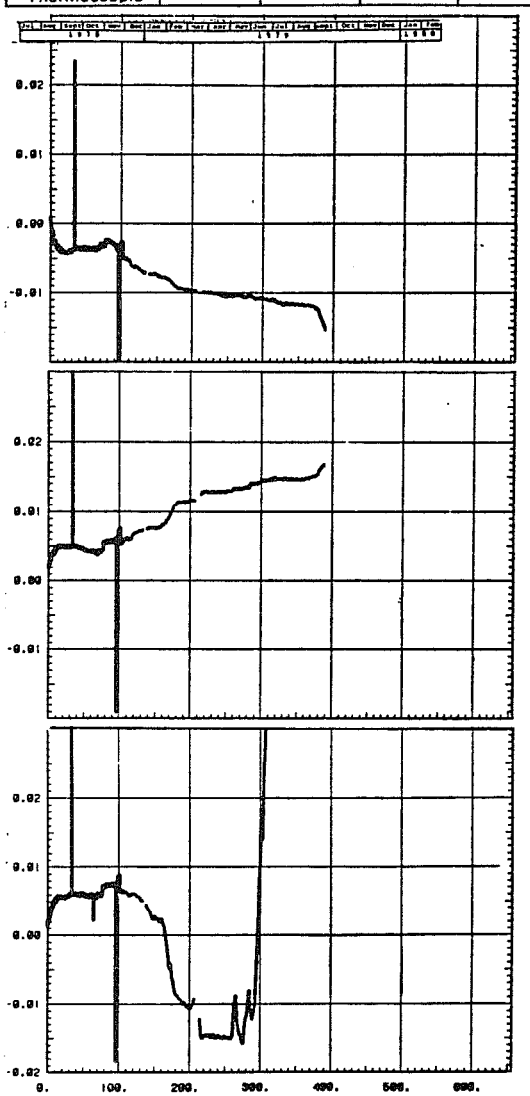

USBM displacement (mv)

[X] vert. [ ] horiz.

r = 2.49

θ = 0

z = -0.65

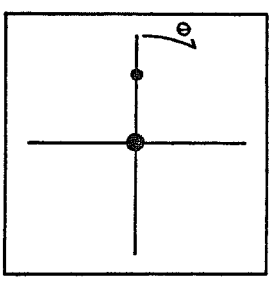

[ ] Entire Experiment

Partial Experiment Including (Calendar dates)

8/24/78 – 9/17/79

(Experiment days)

0 – 389

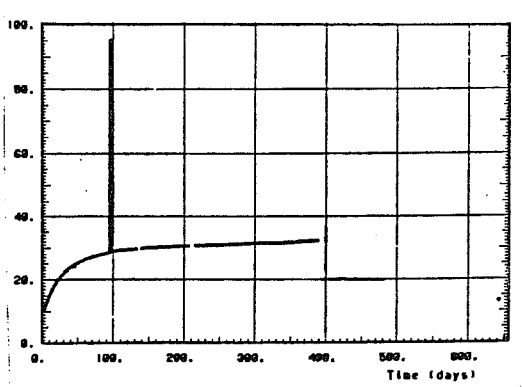

Temp (°C)

XBL 817-3279

USBM GAUGE FIELD RECORD

Full Scale Experiment H9 Gauge U2 (2nd) Hole U2

	Label	Sensor No.	Logger Channel	V_{ss} Voltage	V_{oo} Rezero	C_o Slope	$V_{oi}-V_{oo}$ Temp. Const.	T_s Start Temp.	
USBM Gauge	U2A	204	3	8.770	-0.109	0.0647	-0.172	32.28	
USBM Gauge	U2B	205	4	8.535	-0.028	0.0645	0.013	32.28	
USBM Gauge	U2C	206	5	7.295	-0.275	0.0656	0.085	32.28	
Corresponding Thermocouple		3	116						

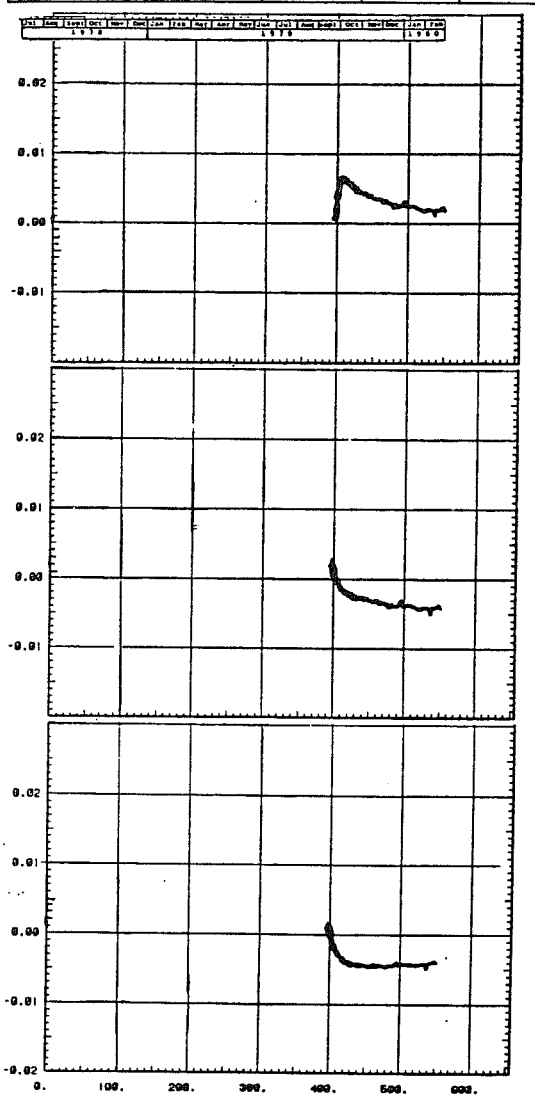

USBM displacement (mv)

[X] vert. [ ] horiz.

r = 2.49

θ = 0

z = -0.65

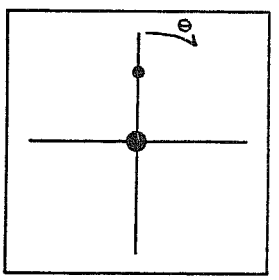

Entire Experiment [ ]

Partial Experiment Including (Calendar dates)

9/22/79 – 2/27/80

(Experiment days)

394 – 552

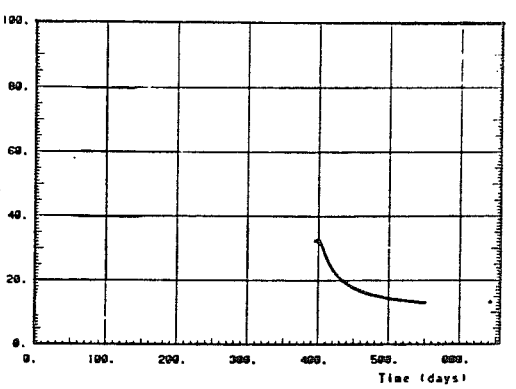

Temp (°C)

XBL 817-3279

USBM GAUGE FIELD RECORD

Full Scale Experiment H9 Gauge U3 Hole U3

	Label	Sensor No.	Logger Channel	V_{ss} Voltage	V_{oo} Rezero	C_o Slope	$V_{oi}-V_{oo}$ Temp. Const.	T_s Start Temp.	
USBM Gauge	U3A	207	6	7.041	-0.110	0.0645	0.076	10.79	
USBM Gauge	U3B	208	7	7.627	2.140	0.0656	-0.047	10.79	
USBM Gauge	U3C	209	8	8.603	-0.264	0.0646	-0.067	10.79	
Corresponding Thermocouple		4	117						

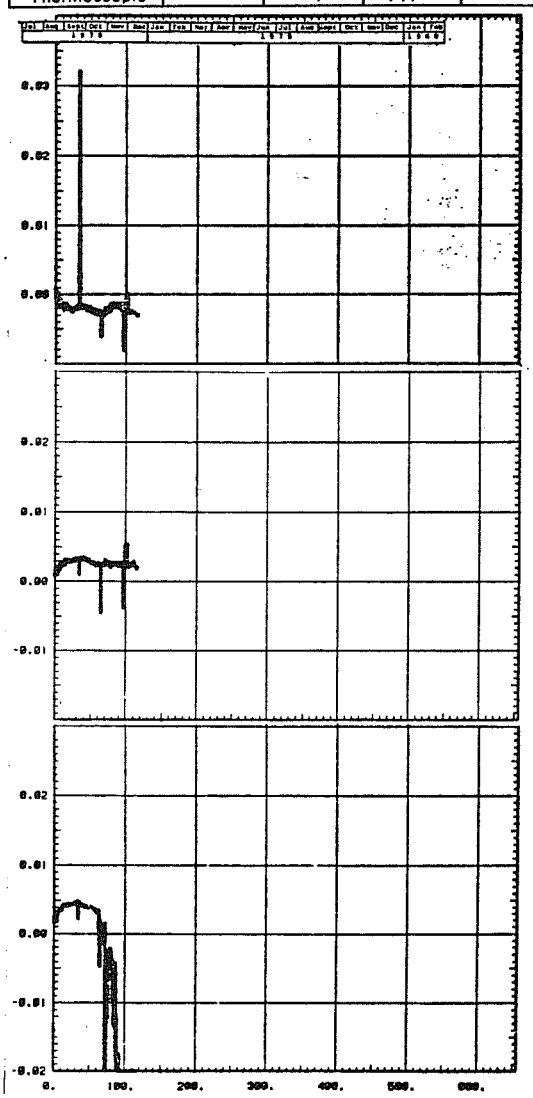

USBM displacement (mv)

[X] vert. [ ] horiz.

$r = 3.49$

$\theta = 0$

$z = 0.85$

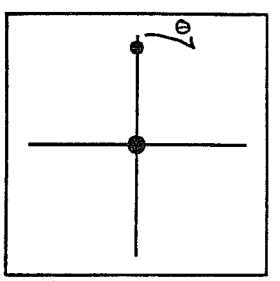

[ ] Entire Experiment

Partial Experiment Including (Calendar dates)

8/24/78 – 12/20/78

(Experiment days)

0 – 118

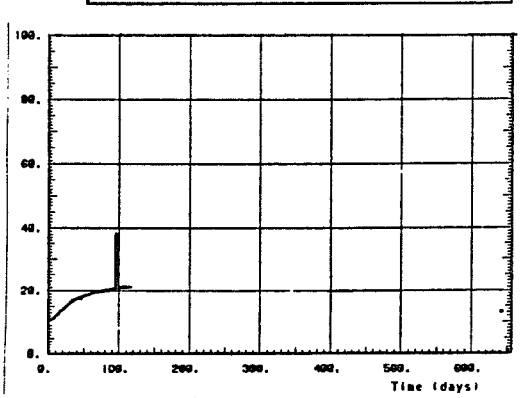

Temp (°C)

XBL 817-3279

USBM GAUGE FIELD RECORD

Full Scale Experiment H9 Gauge U4 Hole U4

	Label	Sensor No.	Logger Channel	V_{ss} Voltage	V_{oo} Rezero	C_o Slope	V_{oi}-V_{oo} Temp. Const.	T_s Start Temp.	
USBM Gauge	U4A	210	9	7.666	0.197	0.0642	0.242	11.55	
USBM Gauge	U4B	211	10	4.946	-0.252	0.0659	0.231	11.55	
USBM Gauge	U4C	212	11	4.894	0.397	0.0655	0.0	11.55	
Corresponding Thermocouple		5	118						

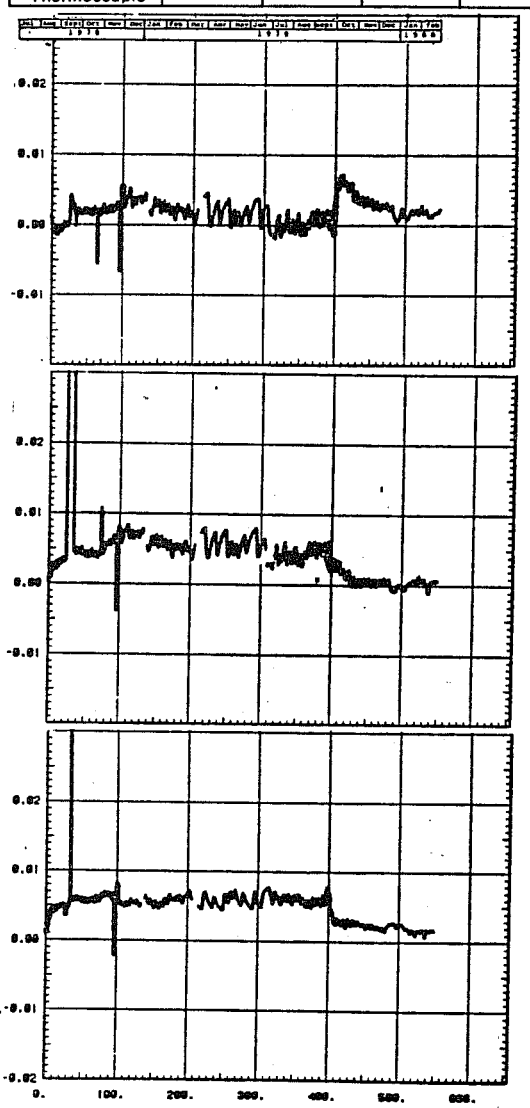

USBM displacement (mv)

[X] vert. [ ] horiz.

r = 2.25

θ = 202.6

z = 0.85

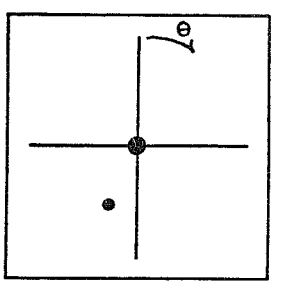

Entire Experiment [X]

Partial Experiment Including (Calendar dates)

_____ – _____

(Experiment days)

_____ – _____

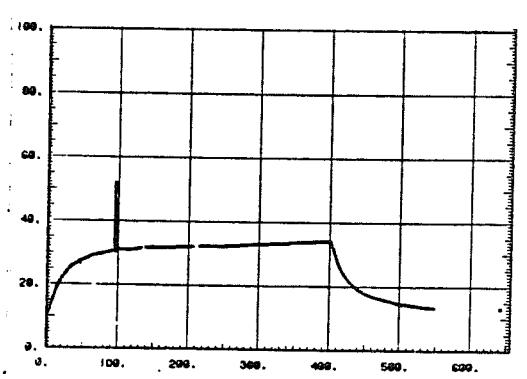

Temp (°C)

XBL 817-3279

USBM GAUGE FIELD RECORD

Full Scale Experiment H9 Gauge U5 (1st) Hole U5

	Label	Sensor No.	Logger Channel	V_{ss} Voltage	V_{oo} Rezero	C_o Slope	V_{oi}-V_{oo} Temp. Const.	T_s Start Temp.	
USBM Gauge	U5A	213	12	5.947	0.299	0.0651	0.006	11.12	
USBM Gauge	U5B	214	13	5.561	-0.235	0.0658	0.042	11.12	
USBM Gauge	U5C	215	14	7.891	2.750	0.0637	0.043	11.12	
Corresponding Thermocouple		6	119						

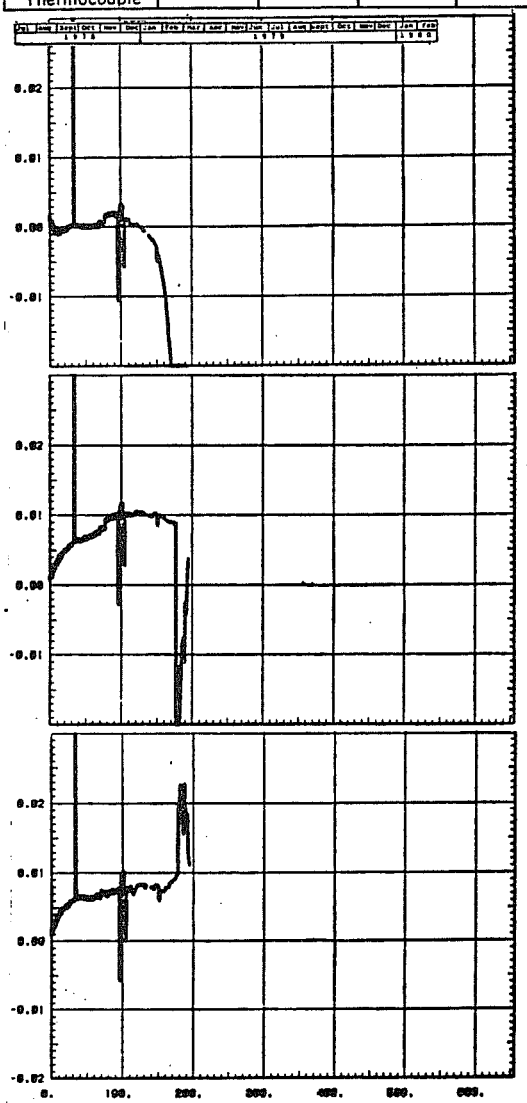

USBM displacement (mv)

[X] vert. [ ] horiz.

r = 3.27

θ = 202.8

z = -0.65

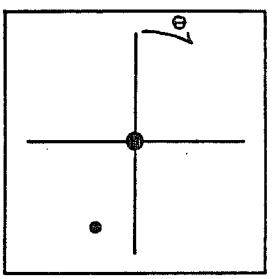

Entire Experiment [ ]

Partial Experiment Including (Calendar dates)

8/24/78 – 3/7/79

(Experiment days)

0 – 195

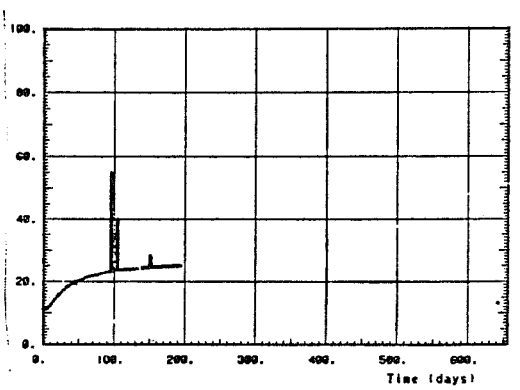

Temp (°C)

XBL 817-3279

USBM GAUGE FIELD RECORD

Full Scale Experiment H9 Gauge U5 (2nd) Hole U5

	Label	Sensor No.	Logger Channel	V_{ss} Voltage	V_{oo} Rezero	C_o Slope	V_{01}-V_{oo} Temp. Const.	T_s Start Temp.	
USBM Gauge	U5A	213	12	7.715	0.539	0.0679	-0.221	26.91	
USBM Gauge	U5B	214	13	8.672	-0.641	0.0672	-0.142	26.91	
USBM Gauge	U5 C	215	14	7.305	-0.083	0.0653	-0.065	26.91	
Corresponding Thermocouple		6	119						

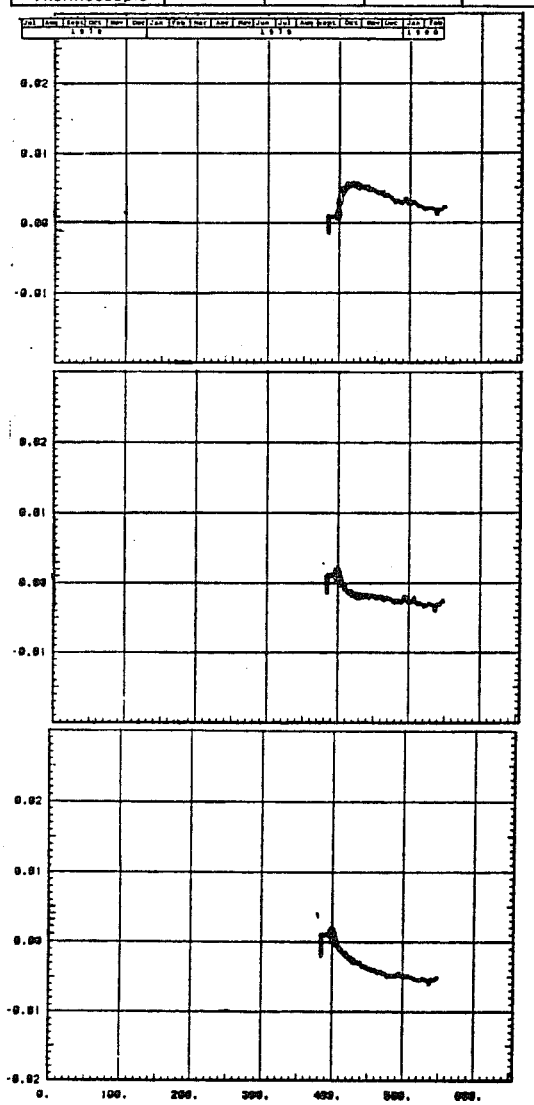

USBM displacement (mv)

[X] vert. [ ] horiz.

r = 3.27

θ = 202.8

z = -0.65

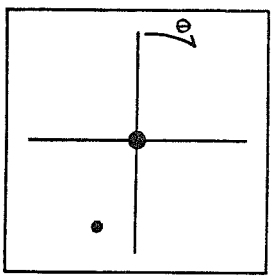

Entire Experiment [ ]

Partial Experiment Including (Calendar dates)

9/11/79 – 2/25/80

(Experiment days)

383 – 550

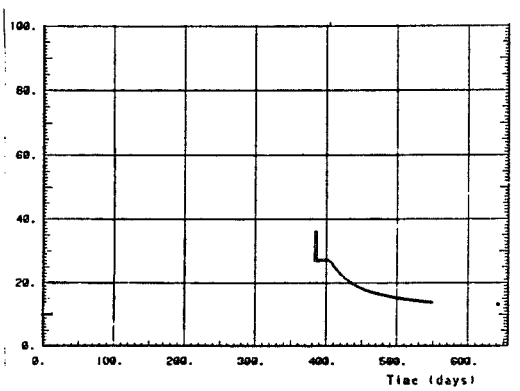

Temp (°C)

XBL 817-3279

USBM GAUGE FIELD RECORD

Full Scale Experiment H9 Gauge U6 (1st) Hole C2

	Label	Sensor No.	Logger Channel	V_{ss} Voltage	V_{oo} Rezero	C_o Slope	$V_{oi}-V_{oo}$ Temp. Const.	T_s Start Temp.	
USBM Gauge	U6A	216	15	6.143	0.046	0.0682	0.029	11.22	
USBM Gauge	U6B	217	16	6.895	0.362	0.0661	-0.017	11.22	
USBM Gauge	U6C	218	17	7.334	0.304	0.0653	0.165	11.22	
Corresponding Thermocouple		7	120						

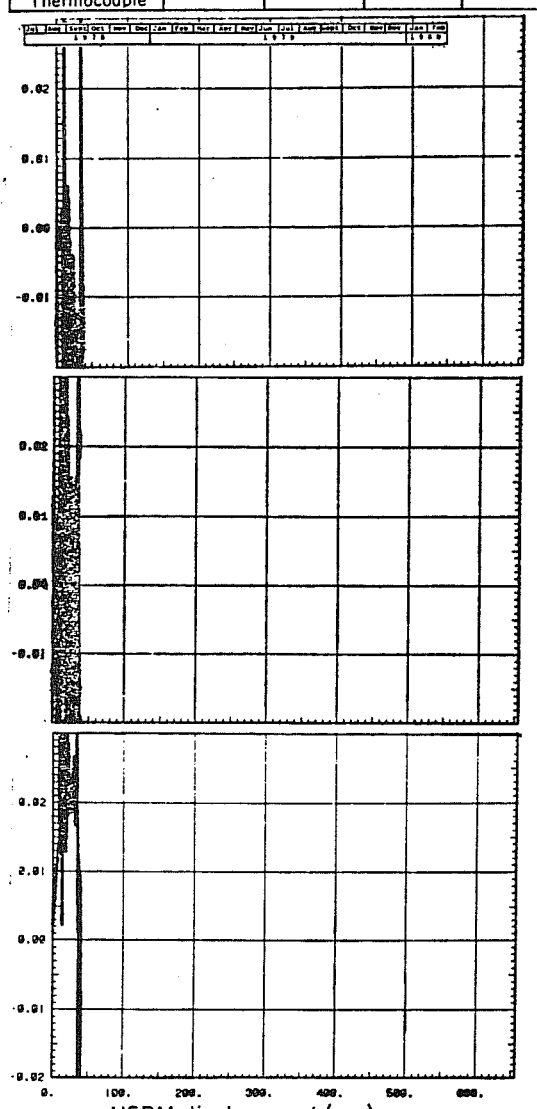

USBM displacement (mv)

[X] vert. [ ] horiz.

r = 1.48

θ = 157.6

z = -0.65

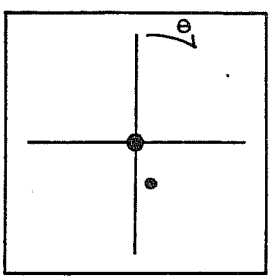

Entire Experiment [ ]

Partial Experiment Including (Calendar dates)

8/24/78 – 10/4/78

(Experiment days)

0 – 41

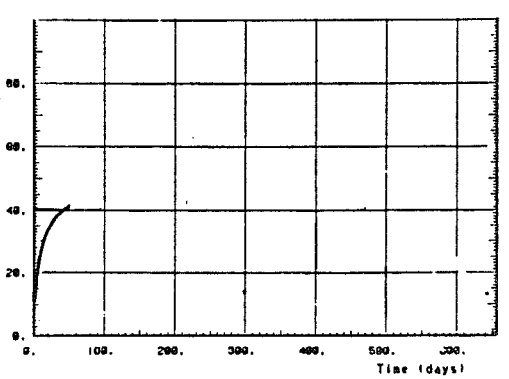

Temp (°C)

XBL 817-3279

USBM GAUGE FIELD RECORD

Full Scale Experiment H9 Gauge U6 (2nd) Hole C2

	Label	Sensor No.	Logger Channel	V_{ss} Voltage	V_{oo} Rezero	C_o Slope	V_{oi}-V_{oo} Temp. Const.	T_s Start Temp.	
USBM Gauge	U6A	216	15	8.984	1.111	0.0658	0.022	48.57	
USBM Gauge	U6B	217	16	6.680	-0.043	0.0648	-0.060	48.57	
USBM Gauge	U6C	218	17	9.336	-0.068	0.0646	0.011	48.57	
Corresponding Thermocouple		7	120						

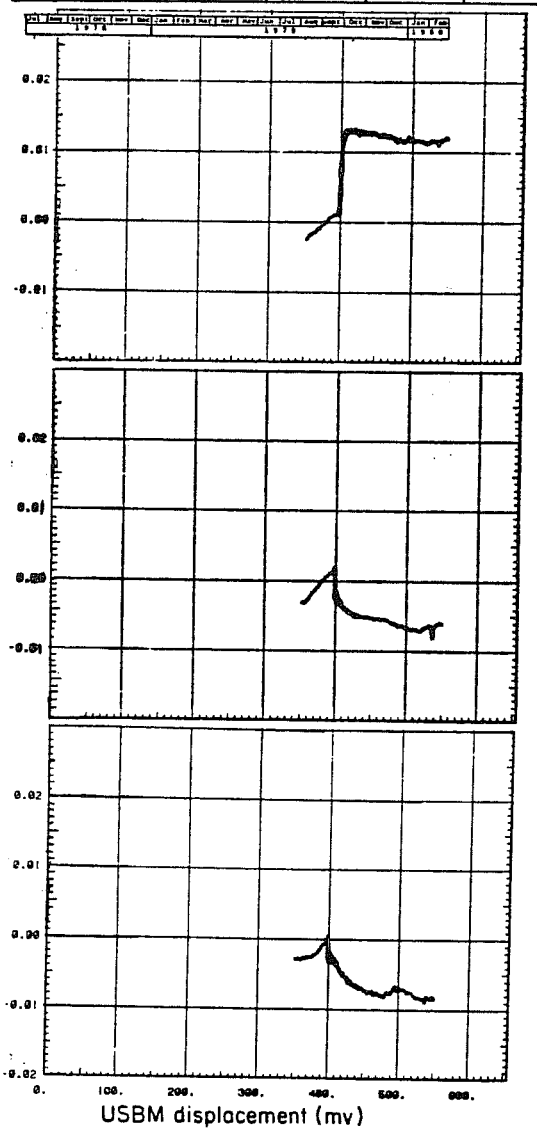

[X] vert. [ ] horiz.

r = 1.48

θ = 157.6

z = -0.65

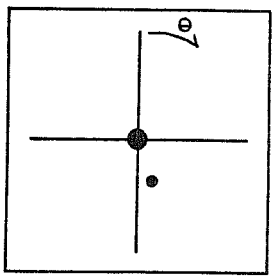

Entire Experiment [ ]

Partial Experiment Including (Calendar dates)

8/10/79 – 2/26/80

(Experiment days)

351 – 551

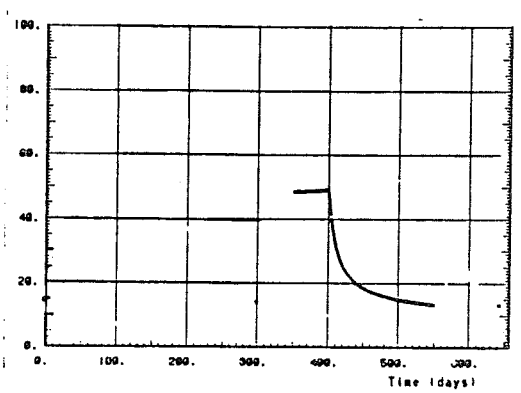

Temp (°C)

XBL 817-3279

USBM GAUGE FIELD RECORD

Full Scale Experiment H9 Gauge U7 (1st) Hole U7

	Label	Sensor No.	Logger Channel	V_{ss} Voltage	V_{oo} Rezero	C_o Slope	$V_{oi}-V_{oo}$ Temp. Const.	T_s Start Temp.	
USBM Gauge	U7A	219	18	7.227	-0.233	0.0697	-0.124	10.49	
USBM Gauge	U7B	220	19	8.193	-0.038	0.0632	-0.208	10.49	
USBM Gauge	U7C	221	20	6.602	0.631	0.0668	-0.039	10.49	
Corresponding Thermocouple		8	121						

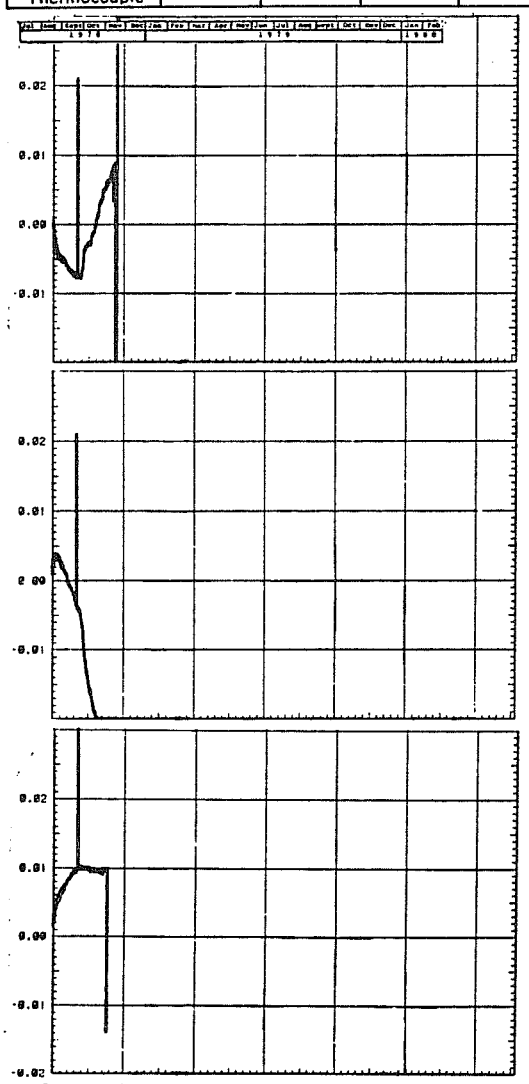

USBM displacement (mv)

[X] vert. [ ] horiz.

r = 2.00

θ = 314.6

z = -0.65

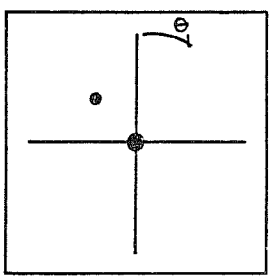

Entire Experiment [ ]

Partial Experiment Including (Calendar dates)

8/24/78 – 11/24/78

(Experiment days)

0 – 92

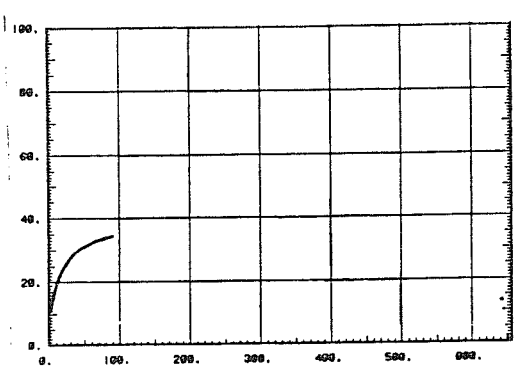

Temp (°C)

XBL 817-3279

USBM GAUGE FIELD RECORD

Full Scale Experiment H9 Gauge U7 (2nd) Hole U7

	Label	Sensor No.	Logger Channel	V_{ss} Voltage	V_{oo} Rezero	C_o Slope	$V_{oi}-V_{oo}$ Temp. Const.	T_s Start Temp.	
USBM Gauge	U7A	219	18	10.176	-0.221	0.0621	-0.028	38.27	
USBM Gauge	U7B	220	19	9.346	-0.049	0.0650	-0.122	38.27	
USBM Gauge	U7C	221	20	8.623	0.636	0.0677	0.071	38.27	
Corresponding Thermocouple		8	121						

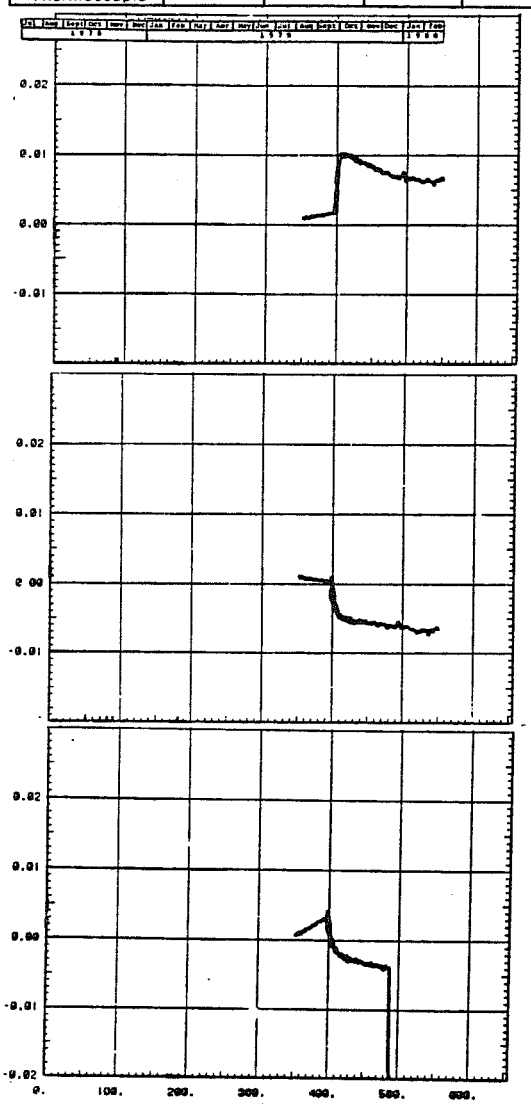

USBM displacement (mv)

[X] vert. [ ] horiz.

r = 2.00

θ = 314.6

z = -0.65

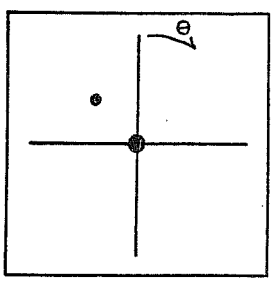

Entire Experiment [ ]

Partial Experiment Including (Calendar dates)

8/10/79 – 2/26/80

(Experiment days)

351 – 551

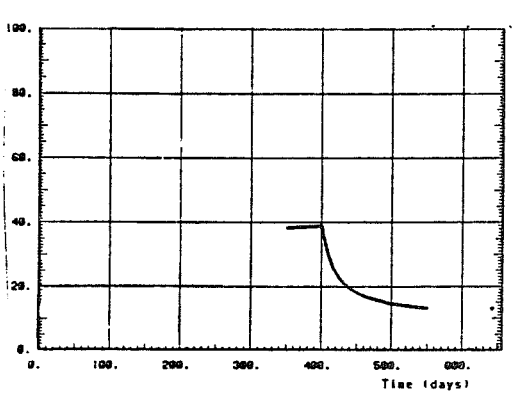

Temp (°C)

XBL 817-3279

USBM GAUGE FIELD RECORD

Full Scale Experiment H9 Gauge U8 (1st) Hole U8

	Label	Sensor No.	Logger Channel	V_{ss} Voltage	V_{oo} Rezero	C_o Slope	V_{oi}-V_{oo} Temp. Const.	T_s Start Temp.	
USBM Gauge	U8A	222	21	8.281	0.073	0.0649	-0.061	10.44	
USBM Gauge	U8B	223	22	8.623	0.216	0.0641	0.058	10.44	
USBM Gauge	U8C	224	23	8.125	-0.040	0.0639	0.048	10.44	
Corresponding Thermocouple		9	122						

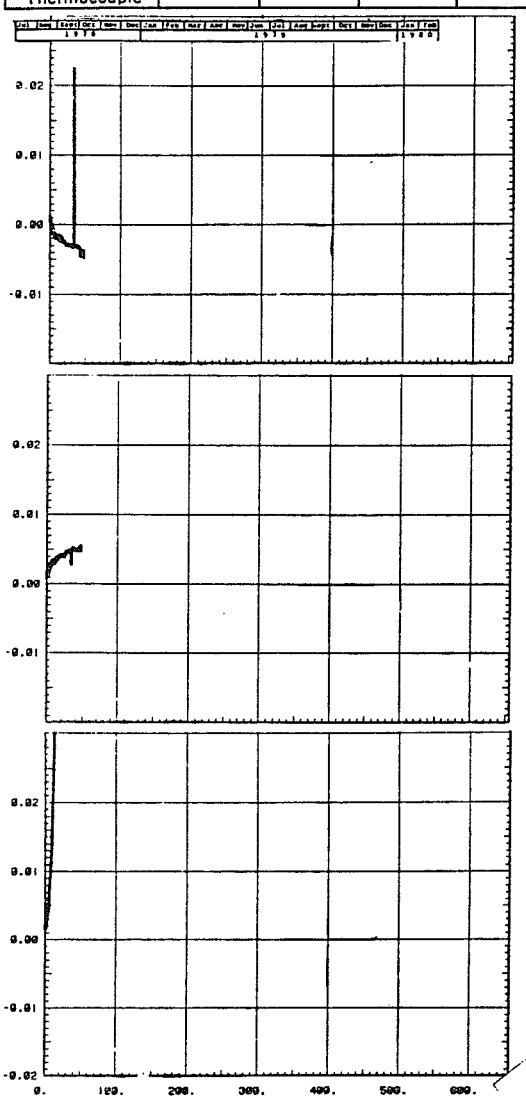

USBM displacement (mv)

[X] vert. [ ] horiz.

r = 3.01

θ = 314.7

z = -0.65

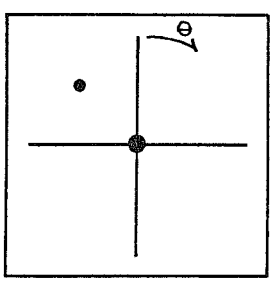

Entire Experiment [ ]

Partial Experiment Including (Calendar dates)

8/24/78 – 10/11/78

(Experiment days)

0 – 48

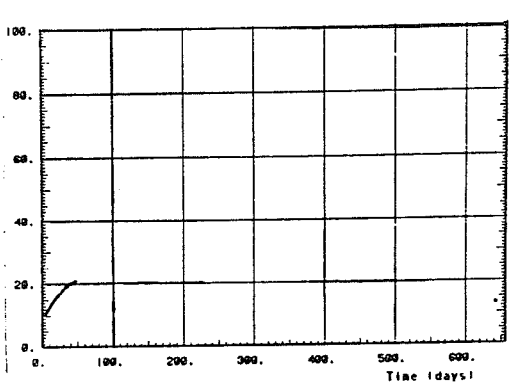

Temp (°C)

XBL 817-3279

USBM GAUGE FIELD RECORD

Full Scale Experiment H9 Gauge U8 (2nd) Hole U8

	Label	Sensor No.	Logger Channel	V_{ss} Voltage	V_{oo} Rezero	C_o Slope	V_{01}-V_{oo} Temp. Const.	T_s Start Temp.	
USBM Gauge	U8A	222	21	10.557	-0.517	0.0650	0.090	27.75	
USBM Gauge	U8B	223	22	8.350	-0.562	0.0654	0.003	27.75	
USBM Gauge	U8C	224	23	9.316	-1.617	0.0647	0.033	27.75	
Corresponding Thermocouple		9	122						

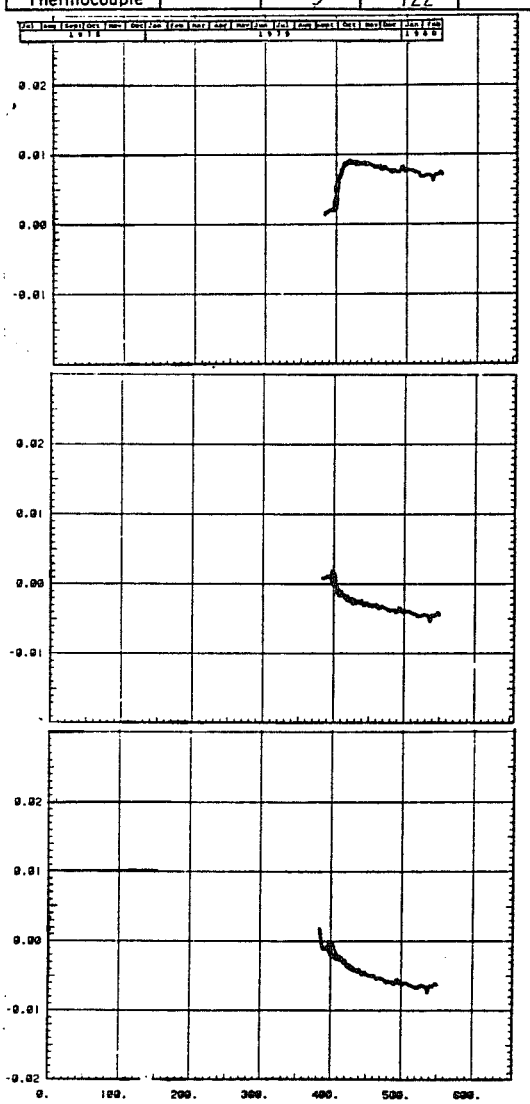

USBM displacement (mv)

[X] vert. [ ] horiz.

r = 3.01

θ = 314.7

z = -0.65

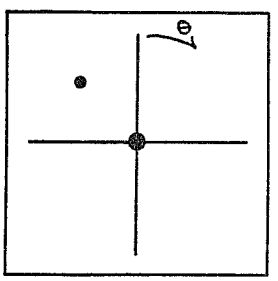

Entire Experiment [ ]

Partial Experiment Including (Calendar dates)

9/11/79 – 2/26/80

(Experiment days)

383 – 551

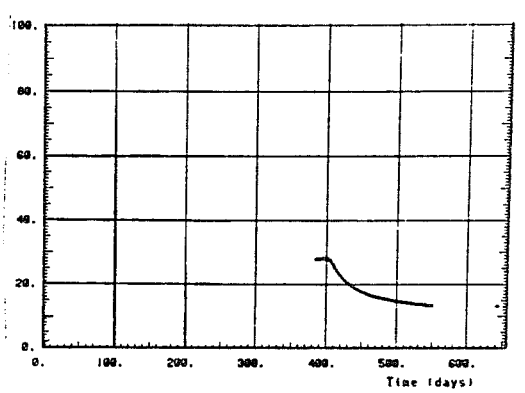

Temp (°C)

XBL 817-3279

USBM GAUGE FIELD RECORD

Full Scale Experiment H9 Gauge U9 (1st) Hole U9

	Label	Sensor No.	Logger Channel	V_{ss} Voltage	V_{oo} Rezero	C_o Slope	$V_{01}-V_{oo}$ Temp. Const.	T_s Start Temp.	
USBM Gauge	U9A	225	24	5.244	-0.463	0.0581	0.200	11.05	
USBM Gauge	U9B	226	25	7.334	-0.033	0.0695	0.008	11.05	
USBM Gauge	U9C	227	26	7.529	0.630	0.0671	0.093	11.05	
Corresponding Thermocouple		10	123						

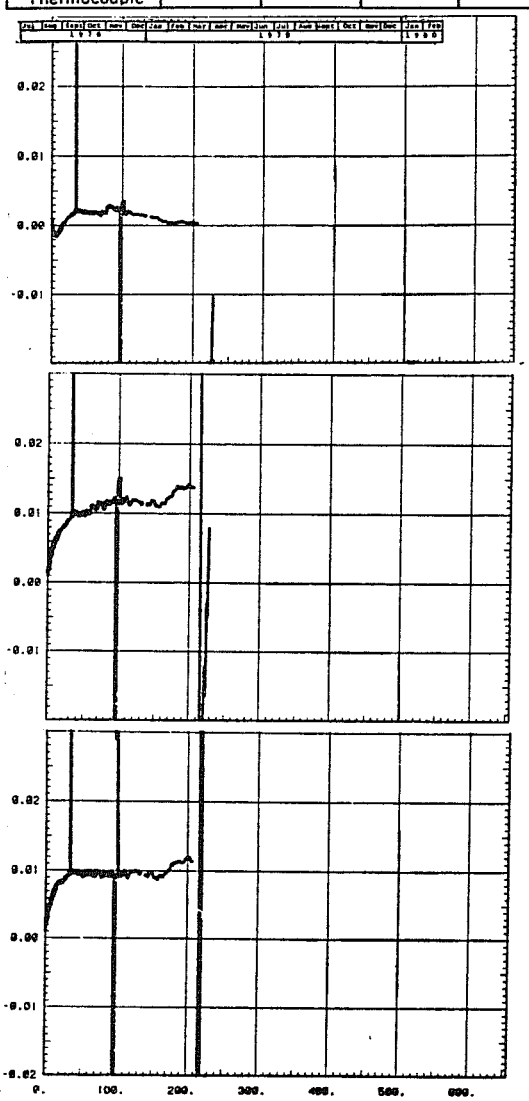

USBM displacement (mv)

[X] vert. [ ] horiz.

r = 2.28

θ = 337.1

z = 0.85

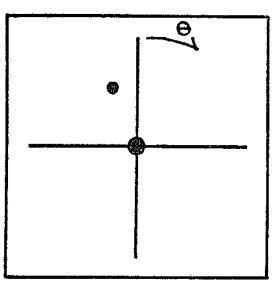

Entire Experiment [ ]

Partial Experiment Including (Calendar dates)

8/25/78 – 4/10/79

(Experiment days)

1 – 229

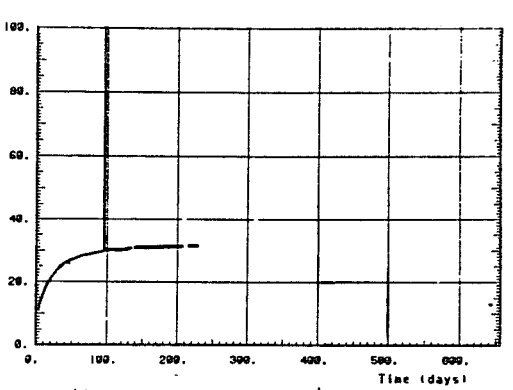

Temp (°C)

XBL 817-3279

USBM GAUGE FIELD RECORD

Full Scale Experiment H9 Gauge U9 (2nd) Hole U9

	Label	Sensor No.	Logger Channel	V_{ss} Voltage	V_{oo} Rezero	C_o Slope	V_{oi}-V_{oo} Temp. Const.	T_s Start Temp.	
USBM Gauge	U9A	225	24	11.318	0.421	0.0570	0.039	32.94	
USBM Gauge	U9B	226	25	9.092	-0.230	0.0646	-0.130	32.94	
USBM Gauge	U9C	227	26	8.428	0.049	0.0655	0.102	32.94	
Corresponding Thermocouple		10	123						

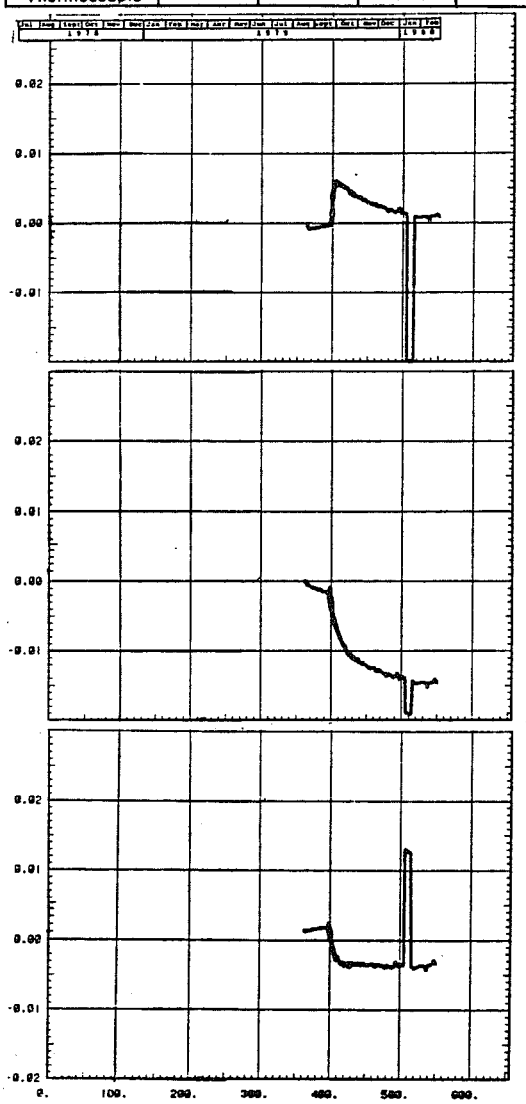

[X] vert. [ ] horiz.

r = 2.28

θ = 337.1

z = 0.85

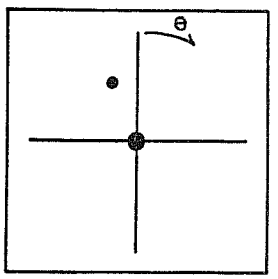

Entire Experiment [ ]

Partial Experiment Including (Calendar dates)

8/22/79 2/27/80

(Experiment days)

363 – 552

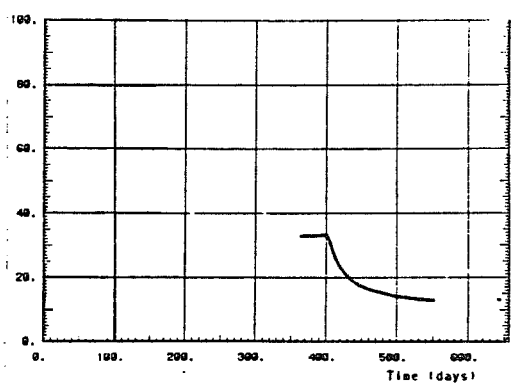

XBL 817-3279

USBM GAUGE FIELD RECORD

Full Scale Experiment H9 Gauge U10 Hole U10

	Label	Sensor No.	Logger Channel	V_{ss} Voltage	V_{oo} Rezero	C_o Slope	$V_{oi}-V_{oo}$ Temp. Const.	T_s Start Temp.	
USBM Gauge	U10A	228	27	4.844	0.057	0.0651	-0.026	10.92	
USBM Gauge	U10B	229	28	5.020	-0.154	0.0662	0.091	10.92	
USBM Gauge	U10C		29	6.563	0.097	0.0658	0.0	10.92	
Corresponding Thermocouple		11	124						

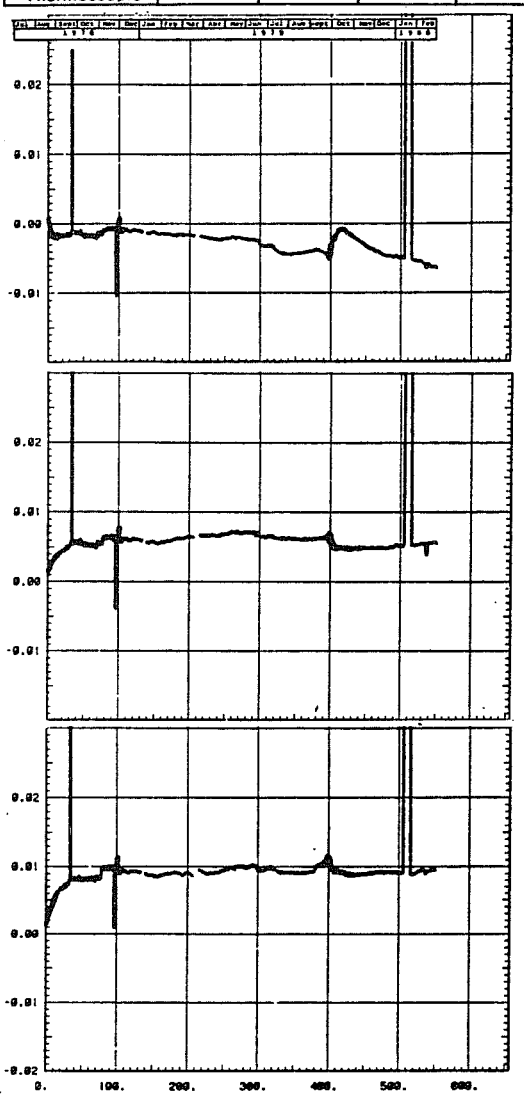

USBM displacement (mv)

[X] vert. [ ] horiz.

r = 3.25

θ = 337.2

z = 0.95

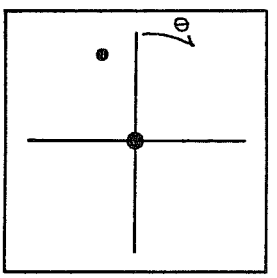

Entire Experiment [X]

Partial Experiment Including (Calendar dates)

_____ – _____

(Experiment days)

_____ – _____

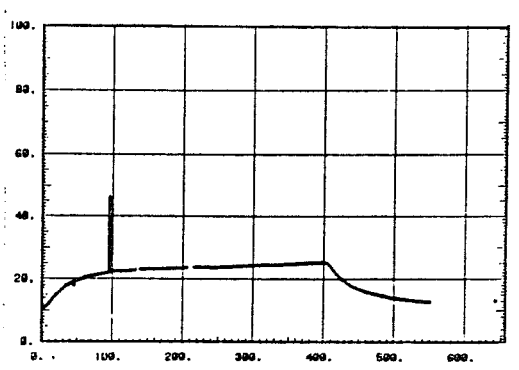

Temp (°C)

XBL 817-3279

USBM GAUGE FIELD RECORD

Full Scale Experiment H10 Gauge U11 (1st) Hole U11

	Label	Sensor No.	Logger Channel	V_{ss} Voltage	V_{oo} Rezero	C_o Slope	V_{oi}-V_{oo} Temp. Const.	T_s Start Temp.	
USBM Gauge	U11A	711	30	7.617	0.177	0.0645	0.033	11.75	
USBM Gauge	U11B	712	31	6.336	0.262	0.0656	-0.058	11.75	
USBM Gauge	U11C	713	32	6.049	1.765	0.0657	-0.070	11.75	
Corresponding Thermocouple		427	125						

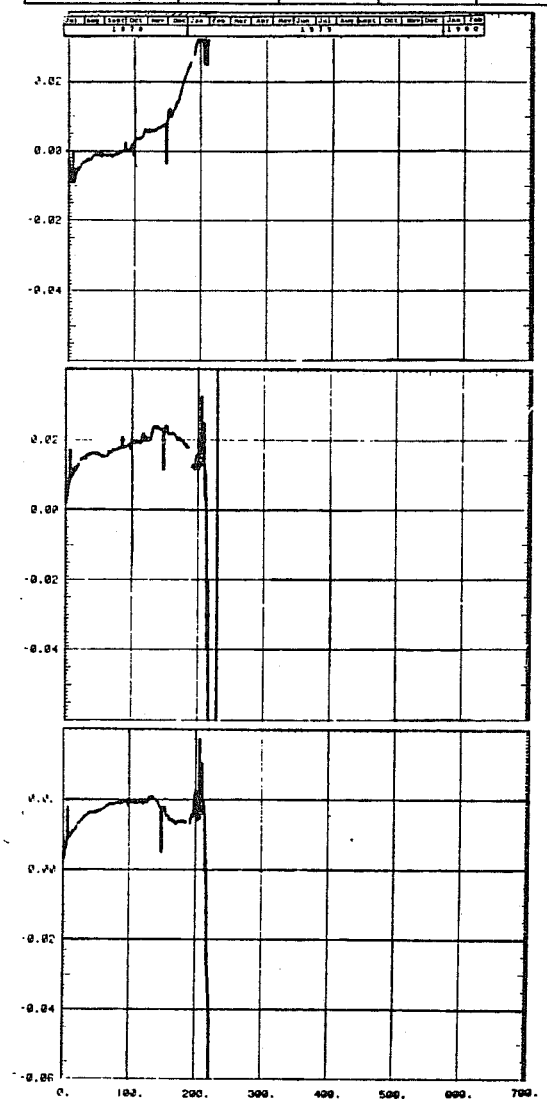

USBM displacement (mv)

[X] vert. [ ] horiz.

r = 1.51
θ = 180.1
z = 0.85

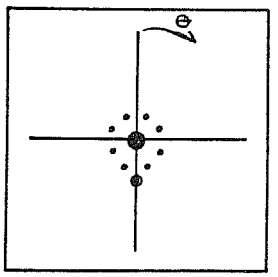

Entire Experiment [ ]

Partial Experiment Including (Calendar dates)

7/3/78 – 2/20/79

(Experiment days)

0 – 232

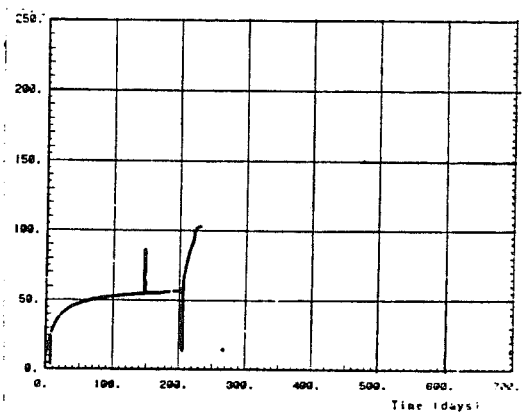

Temp (°C)

XBL 817-3279

USBM GAUGE FIELD RECORD

Full Scale Experiment H10 Gauge U11 (2nd) Hole U11

	Label	Sensor No.	Logger Channel	V_{ss} Voltage	V_{oo} Rezero	C_o Slope	V_{oi}-V_{oo} Temp. Const.	T_s Start Temp.	
USBM Gauge	U11A	711	30	10.342	-1.178	0.0638	0.059	116.14	
USBM Gauge	U11B	712	31	9.727	1.146	0.0652	-0.038	116.14	
USBM Gauge	U11C	713	32	9.863	0.906	0.0639	-0.113	116.14	
Corresponding Thermocouple		427	125						

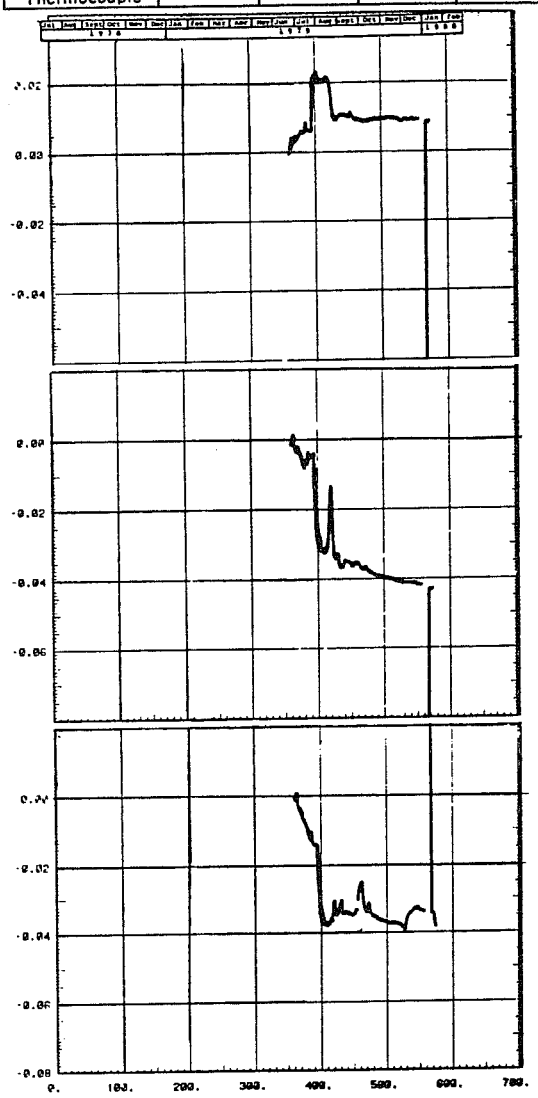

USBM displacement (mv)

X vert. ☐ horiz.

r = 1.51

θ = 180.1

z = 0.85

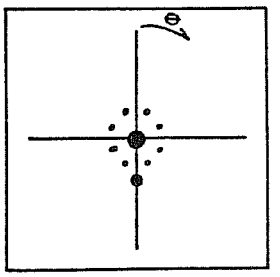

Entire Experiment ☐

Partial Experiment Including (Calendar dates)

6/27/79 – 1/28/80

(Experiment days)

359 – 574

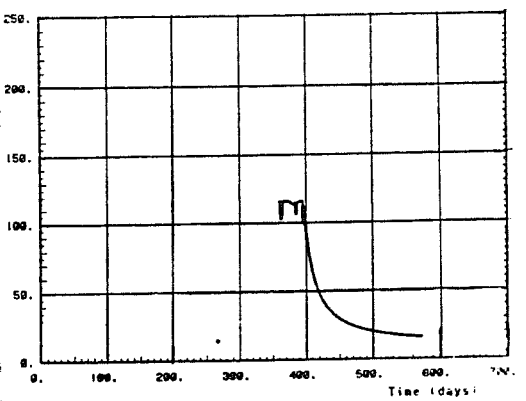

Temp (°C)

XBL 817-3279

USBM GAUGE FIELD RECORD

Full Scale Experiment H10 Gauge U12 (1st) Hole U12

	Label	Sensor No.	Logger Channel	V_{ss} Voltage	V_{oo} Rezero	C_o Slope	V_{oi}-V_{oo} Temp. Const.	T_s Start Temp.	
USBM Gauge	U12A	714	33	4.585	-0.040	0.0666	0.057	11.01	
USBM Gauge	U12B	715	34	4.406	0.118	0.0650	-0.214	11.01	
USBM Gauge	U12C	716	35	5.884	0.021	0.0675	-0.171	11.01	
Corresponding Thermocouple		428	126						

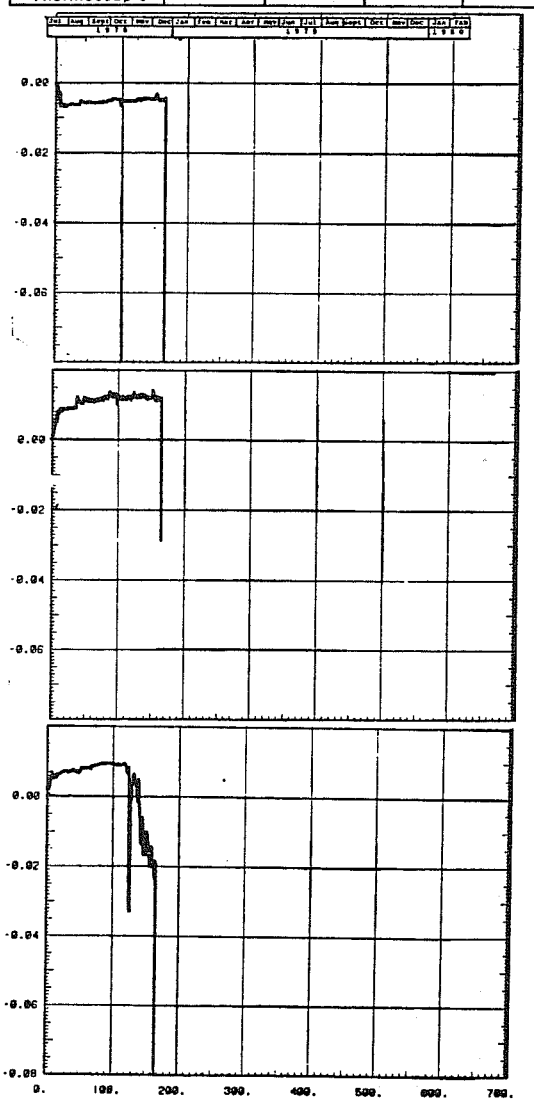

[X] vert. [ ] horiz.

r = 3.48

θ = 180.2

z = -0.65

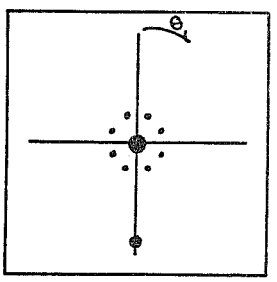

Entire Experiment [ ]

Partial Experiment Including (Calendar dates)

7/3/78 – 12/18/78

(Experiment days)

0 – 168

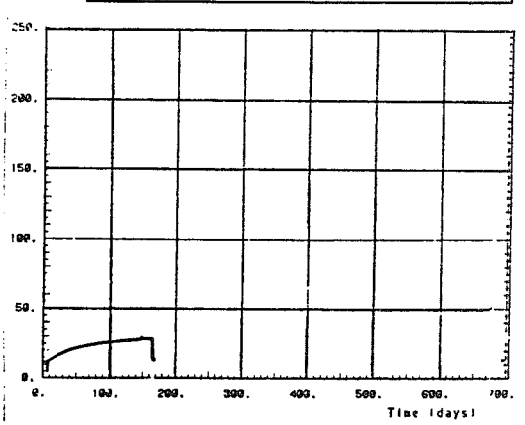

XBL 817-3279

USBM GAUGE FIELD RECORD

Full Scale Experiment H10 Gauge U12 (2nd) Hole U12

	Label	Sensor No.	Logger Channel	V_{ss} Voltage	V_{oo} Rezero	C_o Slope	$V_{01}-V_{oo}$ Temp. Const.	T_s Start Temp.	
USBM Gauge	U12A	714	33	5.493	0.075	0.0676	0.075	29.19	
USBM Gauge	U12B	715	34	6.489	0.275	0.0653	-0.150	29.19	
USBM Gauge	U12C	716	35	7.207	0.075	0.0690	-0.175	29.19	
Corresponding Thermocouple		428	126						

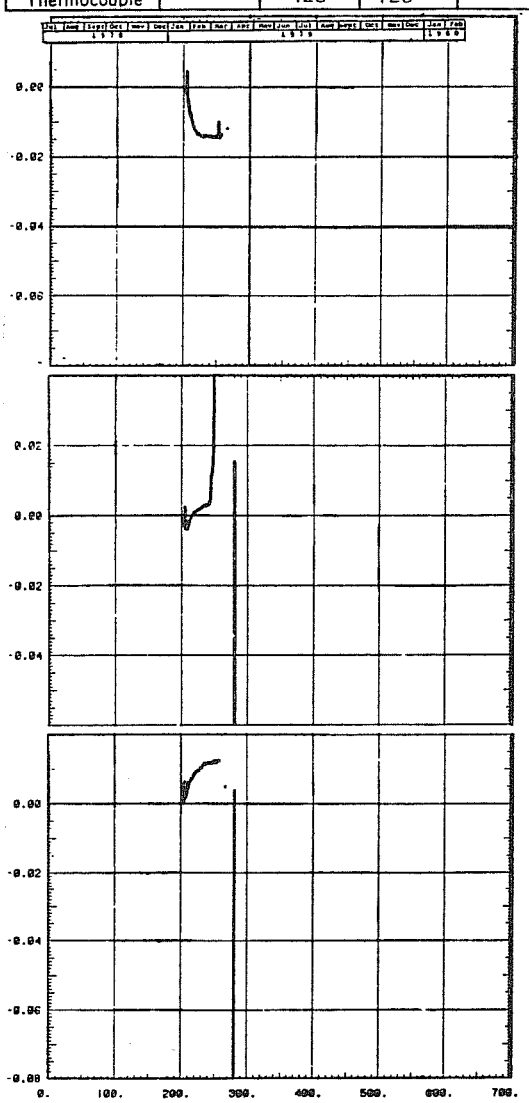

USBM displacement (mv)

X vert. ☐ horiz.

r = 3.48

θ = 180.2

z = -0.65

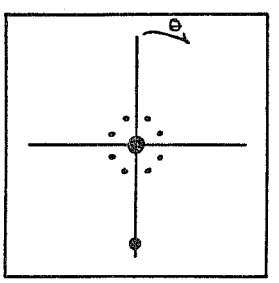

☐ Entire Experiment

Partial Experiment Including (Calendar dates)

1/20/79 – 4/10/79

(Experiment days)

201 – 281

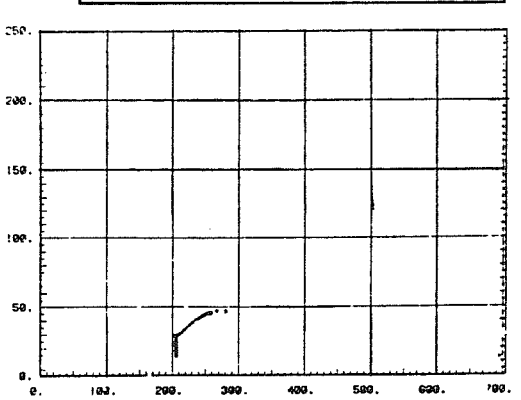

Temp (°C)

XBL 817-3279

USBM GAUGE FIELD RECORD

Full Scale Experiment H10 Gauge U12 (3rd) Hole U12

	Label	Sensor No.	Logger Channel	V_{ss} Voltage	V_{oo} Rezero	C_o Slope	V_{oi}-V_{oo} Temp. Const.	T_s Start Temp.	
USBM Gauge	U12A	714	33	8.623	0.109	0.0643	-0.018	53.68	
USBM Gauge	U12B	715	34	8.926	-0.595	0.0653	0.153	53.68	
USBM Gauge	U12C	716	35	7.246	-0.308	0.0696	-0.114	53.68	
Corresponding Thermocouple		428	126						

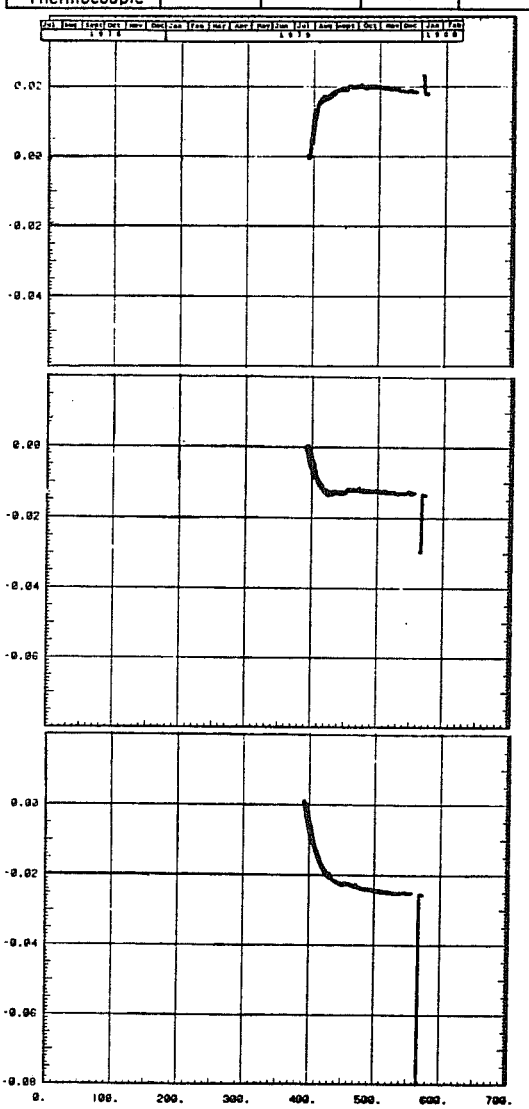

USBM displacement (mv)

[X] vert. [ ] horiz.

r = 3.48

θ = 180.2

z = -0.65

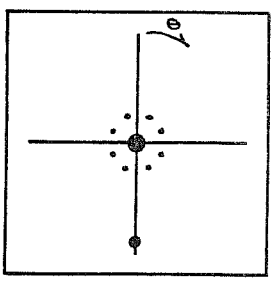

Entire Experiment [ ]

Partial Experiment Including (Calendar dates)

7/29/79 – 1/28/80

(Experiment days)

391 – 574

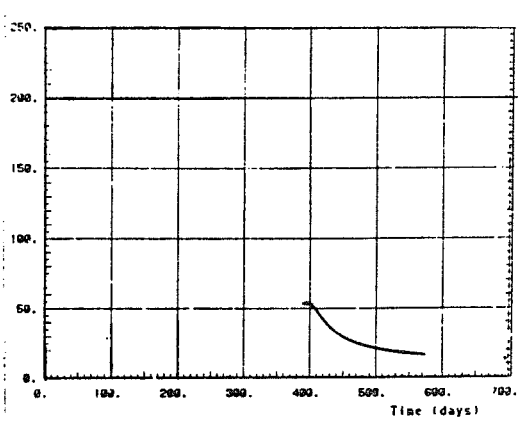

Temp (°C)

XBL 817-3279

USBM GAUGE FIELD RECORD

Full Scale Experiment H10 Gauge U13 (1st) Hole U13

	Label	Sensor No.	Logger Channel	V_{ss} Voltage	V_{oo} Rezero	C_o Slope	V_{oi}-V_{oo} Temp. Const.	T_s Start Temp.	
USBM Gauge	U13A	717	36	6.680	0.113	0.0650	0.146	11.07	
USBM Gauge	U13B	718	37	9.170	-0.010	0.0645	-0.650	11.07	
USBM Gauge	U13C	719	38	8.640	-0.183	0.0638	-0.045	11.07	
Corresponding Thermocouple		429	127						

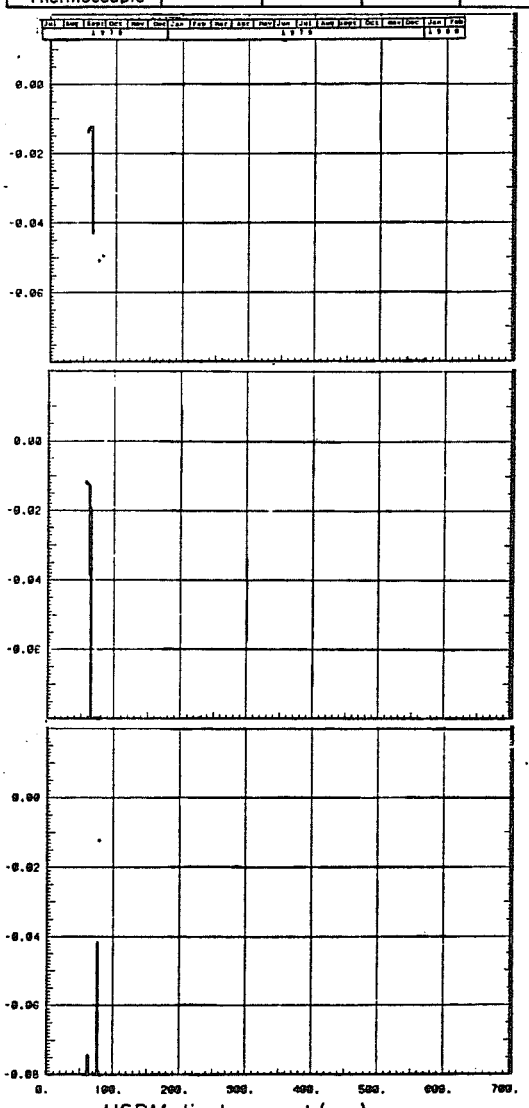

USBM displacement (mv)

X vert. ☐ horiz.

r = 2.26

θ = 202.0

z = -0.65

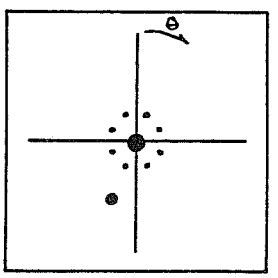

Entire Experiment ☐

Partial Experiment including (Calendar dates)

7/3/78 – 9/26/78

(Experiment days)

0 – 85

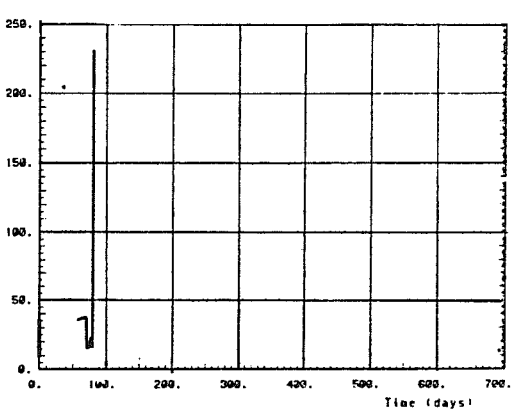

Temp (°C)

XBL 817-3279

USBM GAUGE FIELD RECORD

Full Scale Experiment H10 Gauge U13 (2nd) Hole U13

	Label	Sensor No.	Logger Channel	V_{ss} Voltage	V_{oo} Rezero	C_o Slope	V_{oi}-V_{oo} Temp. Const.	T_s Start Temp.	
USBM Gauge	U13A	717	36	4.873	0.100	0.0622	-0.075	43.64	
USBM Gauge	U13B	718	37	6.123	-1.250	0.0650	0.0	43.64	
USBM Gauge	U13C	719	38	5.396	-1.250	0.0647	-0.125	43.64	
Corresponding Thermocouple		429	127						

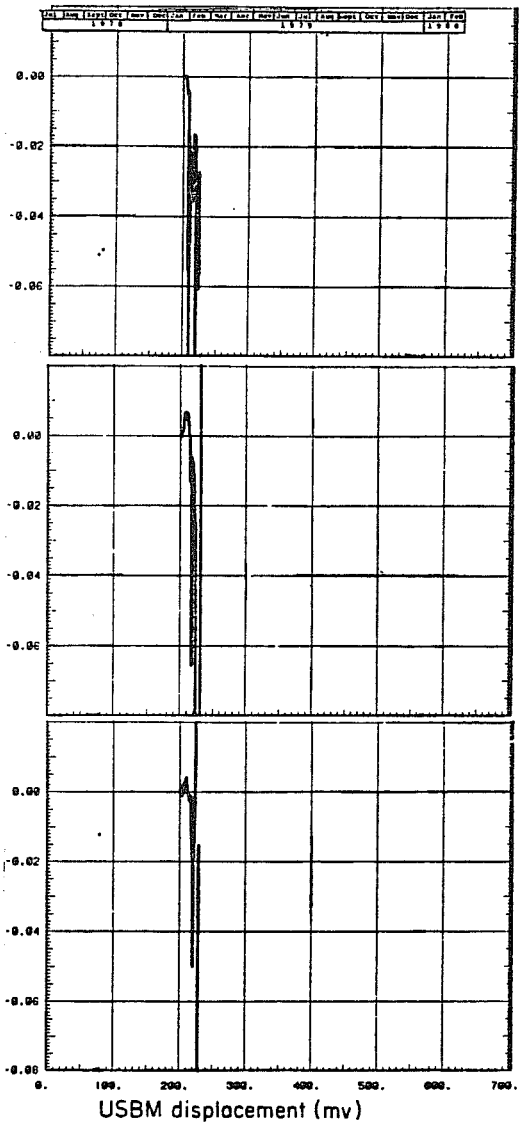

USBM displacement (mv)

[X] vert. [ ] horiz.

r = 2.26

θ = 202.0

z = -0.65

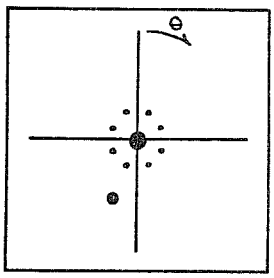

Entire Experiment [ ]

Partial Experiment Including (Calendar dates)

1/20/79 – 2/20/79

(Experiment days)

201 – 232

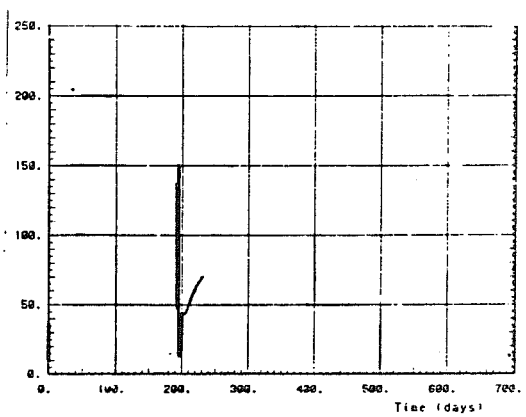

Temp (°C)

XBL 817-3279

USBM GAUGE FIELD RECORD

Full Scale Experiment H10 Gauge U13 (3rd) Hole U13

	Label	Sensor No.	Logger Channel	V_{ss} Voltage	V_{oo} Rezero	C_o Slope	V_{oi}-V_{oo} Temp. Const.	T_s Start Temp.	
USBM Gauge	U13A	717	36	8.760	0.032	0.0676	-0.098	86.41	
USBM Gauge	U13B	718	37	9.150	1.113	0.0641	-0.022	86.41	
USBM Gauge	U13C	719	38	8.164	-1.107	0.0657	0.096	86.41	
Corresponding Thermocouple		429	127						

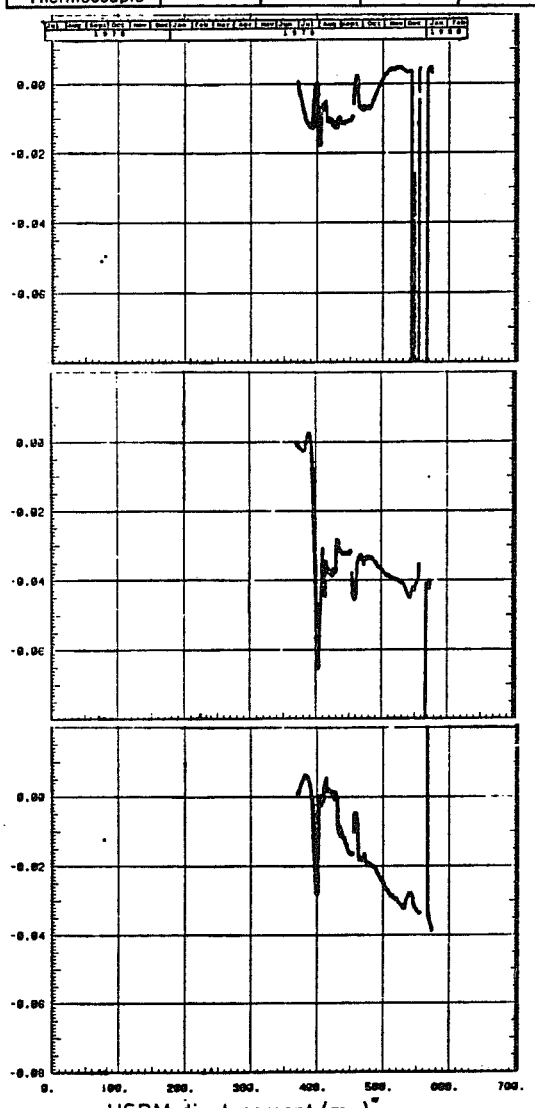

USBM displacement (mv)

[X] vert. [ ] horiz.

r = 2.26

θ = 202.0

z = -0.65

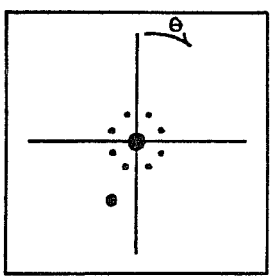

Entire Experiment [ ]

Partial Experiment Including (Calendar dates)

7/9/79 – 1/28/80

(Experiment days)

371 – 574

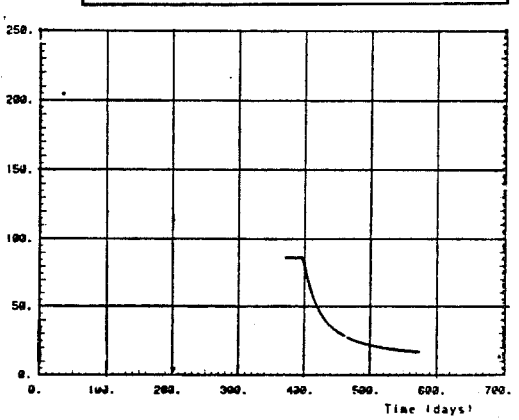

Temp (°C)

XBL 817-3279

USBM GAUGE FIELD RECORD

Full Scale Experiment H10 Gauge U14 (1st) Hole U14

	Label	Sensor No.	Logger Channel	V_{ss} Voltage	V_{oo} Rezero	C_o Slope	$V_{oi}-V_{oo}$ Temp. Const.	T_s Start Temp.	
USBM Gauge	U14A	720	39	5.629	0.128	0.0645	0.136	11.07	
USBM Gauge	U14B	721	40	6.406	-0.152	0.0644	-0.183	11.07	
USBM Gauge	U14C	722	41	6.712	-0.190	0.0643	-0.025	11.07	
Corresponding Thermocouple		430	128						

☒ vert. ☐ horiz.

r = 3.22

θ = 202.0

z = -0.65

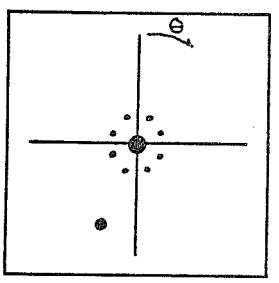

Entire Experiment ☐

Partial Experiment Including (Calendar dates)

7/3/78 – 7/3/78

(Experiment days)

0 – 0

USBM displacement (mv)

Temp (°C)

XBL 817-3279

USBM GAUGE FIELD RECORD

Full Scale Experiment H10 Gauge U14 (2nd) Hole U14

	Label	Sensor No.	Logger Channel	V_{ss} Voltage	V_{oo} Rezero	C_o Slope	V_{oi}-V_{oo} Temp. Const.	T_s Start Temp.	
USBM Gauge	U14A	720	39	5.439	0.405	0.0629	-0.156	25.42	
USBM Gauge	U14B	721	40	10.664	1.538	0.0627	0.087	25.42	
USBM Gauge	U14C	722	41	5.630	0.237	0.0638	-0.042	25.42	
Corresponding Thermocouple		430	128						

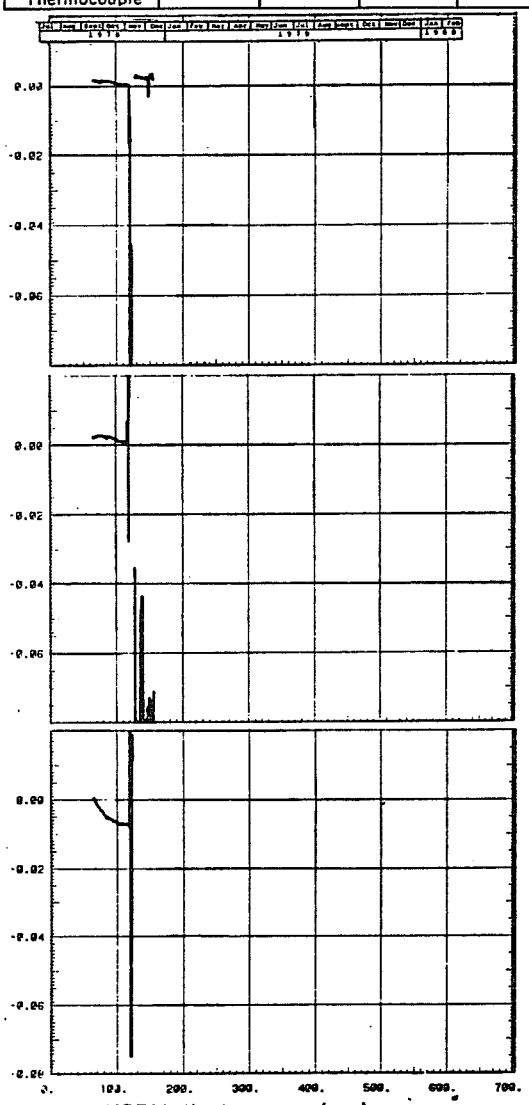

USBM displacement (mv)

X vert. ☐ horiz.

r = 3.22

θ = 202.0

z = -0.65

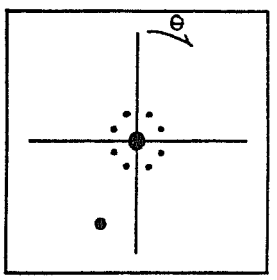

Entire Experiment ☐

Partial Experiment Including (Calendar dates)

9/6/78 – 12/6/78

(Experiment days)

65 – 156

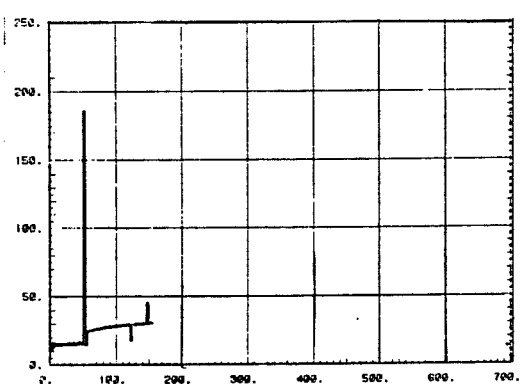

Temp (°C)

XBL 817-3279

USBM GAUGE FIELD RECORD

Full Scale Experiment H10 Gauge U14 (3rd) Hole U14

	Label	Sensor No.	Logger Channel	V_{ss} Voltage	V_{oo} Rezero	C_o Slope	V_{oi}-V_{oo} Temp. Const.	T_s Start Temp.	
USBM Gauge	U14A	720	39	5.439	0.110	0.0643	-0.160	31.49	
USBM Gauge	U14B	721	40	7.422	-0.010	0.0631	0.060	31.49	
USBM Gauge	U14C	722	41	5.020	-0.020	0.0641	0.150	31.49	
Corresponding Thermocouple		430	128						

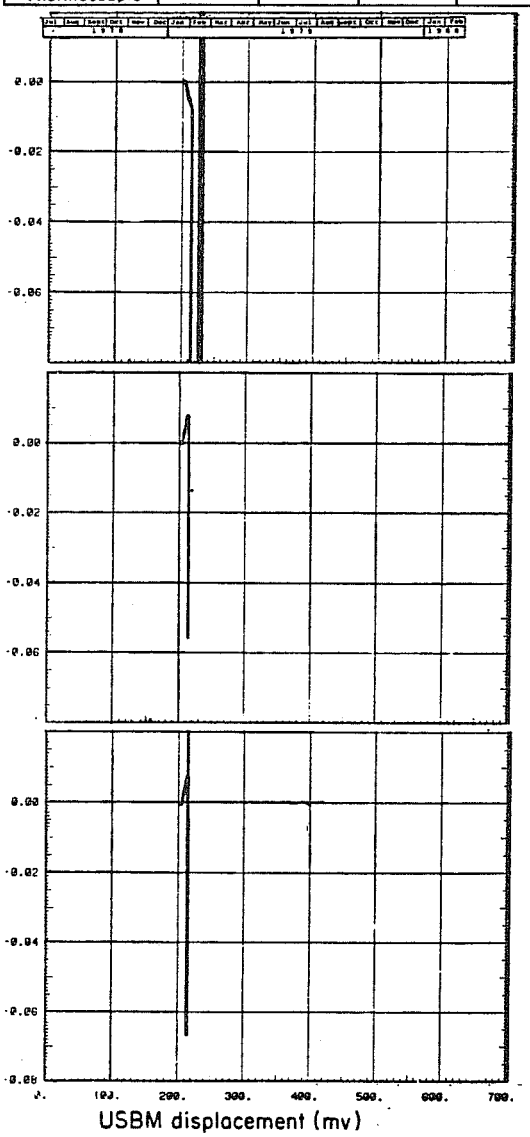

USBM displacement (mv)

[X] vert. [ ] horiz.

r = 3.22

θ = 202.0

z = -0.65

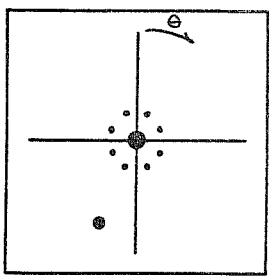

Entire Experiment [ ]

Partial Experiment Including (Calendar dates)

1/20/79 – 2/20/79

(Experiment days)

201 – 232

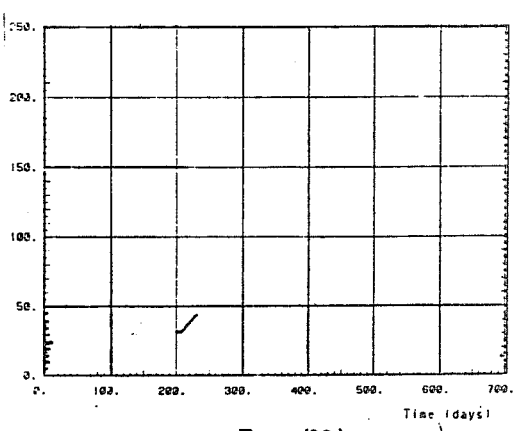

Temp (°C)

XBL 817-3279

USBM GAUGE FIELD RECORD

Full Scale Experiment H10 Gauge U14 (4th) Hole U14

	Label	Sensor No.	Logger Channel	V_{ss} Voltage	V_{oo} Rezero	C_o Slope	V_{oi}-V_{oo} Temp. Const.	T_s Start Temp.	
USBM Gauge	U14A	720	39	6.880	-0.441	0.0675	-0.043	58.57	
USBM Gauge	U14B	721	40	10.147	-0.496	0.0645	0.193	58.57	
USBM Gauge	U14C	722	41	9.395	0.429	0.0670	-0.064	58.57	
Corresponding Thermocouple		430	128						

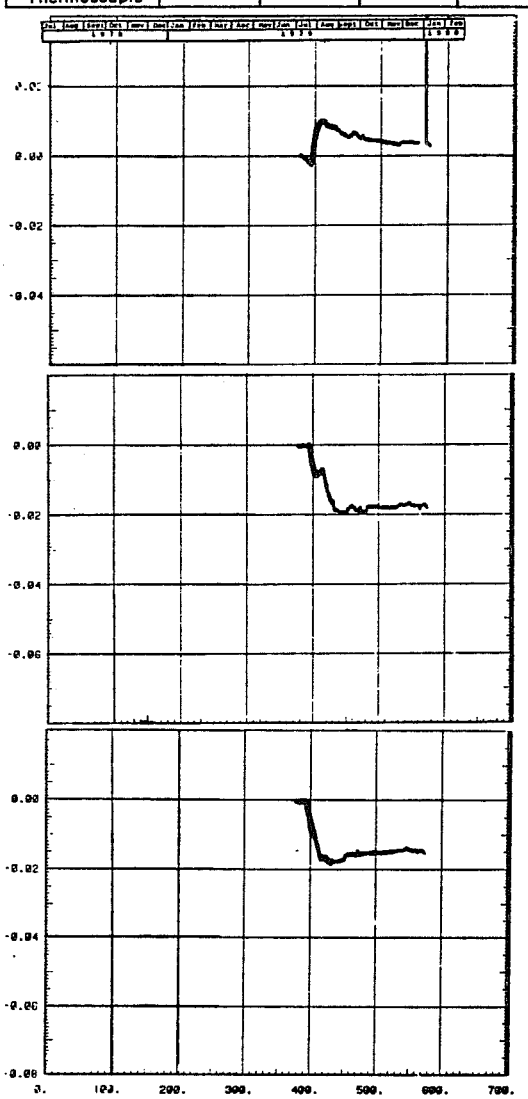

USBM displacement (mv)

[X] vert. [ ] horiz.

r = 3.22

θ = 202.0

z = -0.65

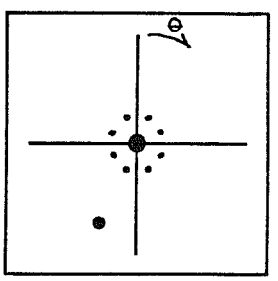

Entire Experiment [ ]

Partial Experiment Including (Calendar dates)

7/13/79 – 1/28/80

(Experiment days)

375 – 574

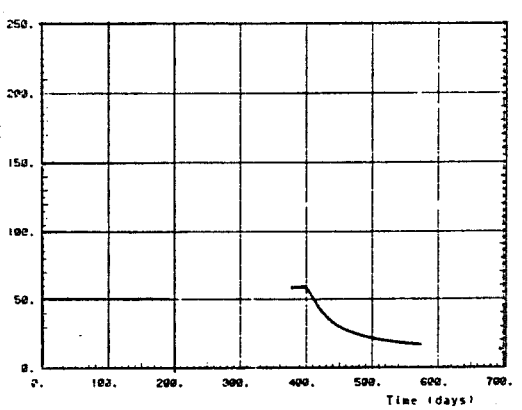

Temp (°C)

XBL 817-3279

USBM GAUGE FIELD RECORD

Full Scale Experiment H10 Gauge U15 (1st) Hole C3

	Label	Sensor No.	Logger Channel	V_{ss} Voltage	V_{oo} Rezero	C_o Slope	V_{ot}-V_{oo} Temp. Const.	T_s Start Temp.	
USBM Gauge	U15A	723	42	4.671	-0.190	0.0666	-0.086	11.12	
USBM Gauge	U15B	724	43	5.323	0.105	0.0683	0.022	11.12	
USBM Gauge	U15C	725	44	6.703	0.081	0.0692	0.208	11.12	
Corresponding Thermocouple		431	129						

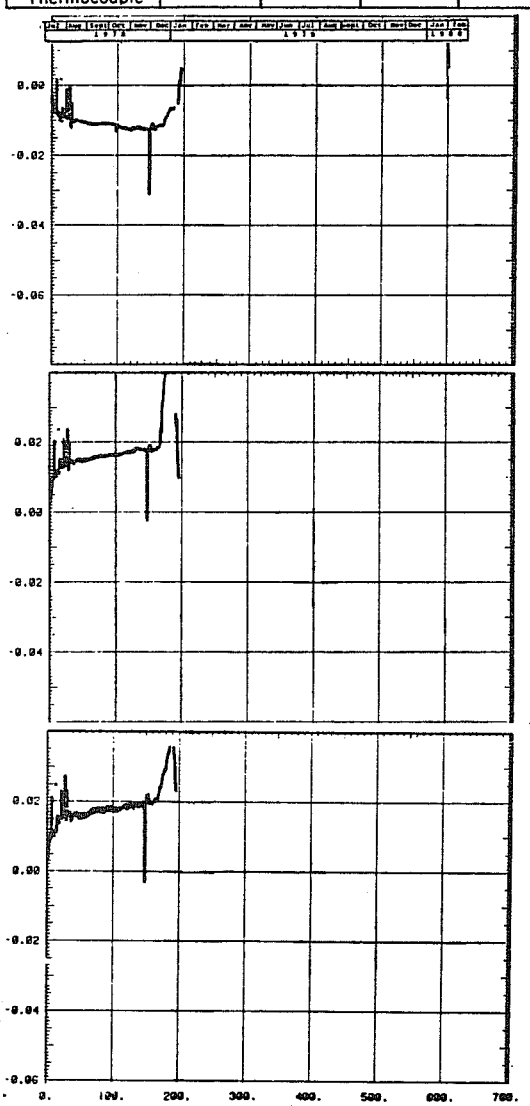

USBM displacement (mv)

[X] vert. [ ] horiz.

r = 1.59

θ = 21.6

z = -0.53

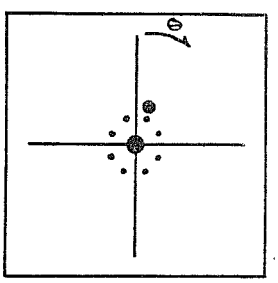

Entire Experiment [ ]

Partial Experiment Including (Calendar dates)

7/3/78 – 1/15/79

(Experiment days)

0 – 196

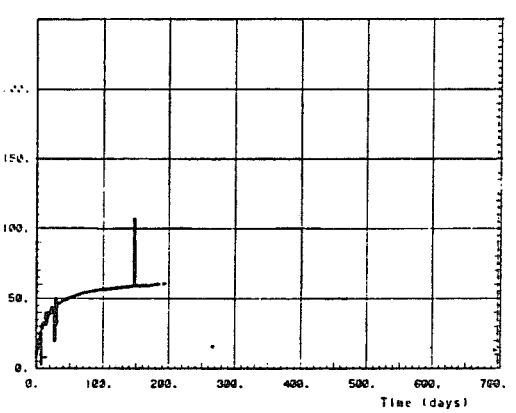

Temp (°C)

XBL 817-3279

USBM GAUGE FIELD RECORD

Full Scale Experiment H10 Gauge U15 (2nd) Hole C3

	Label	Sensor No.	Logger Channel	V_{ss} Voltage	V_{oo} Rezero	C_o Slope	V_{oi}-V_{oo} Temp. Const.	T_s Start Temp.	
USBM Gauge	U15A	723	42	10.215	0.158	0.0647	-0.050	125.97	
USBM Gauge	U15B	724	43	10.488	0.070	0.0648	0.035	125.97	
USBM Gauge	U15C	725	44	9.805	-0.001	0.0616	-0.037	125.97	
Corresponding Thermocouple		431	129						

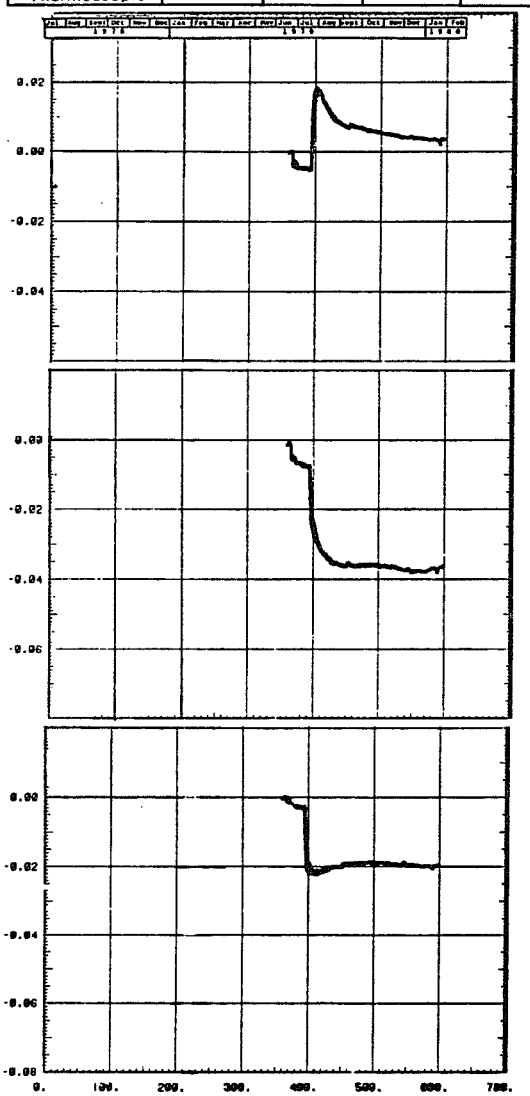

USBM displacement (mv)

[X] vert. [ ] horiz.

r = 1.59

θ = 21.6

z = -0.53

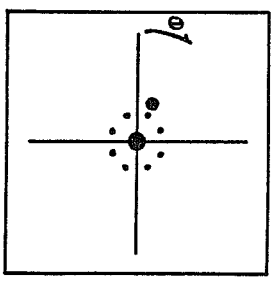

Entire Experiment [ ]

Partial Experiment Including (Calendar dates)

6/27/79 – 2/22/80

(Experiment days)

359 – 599

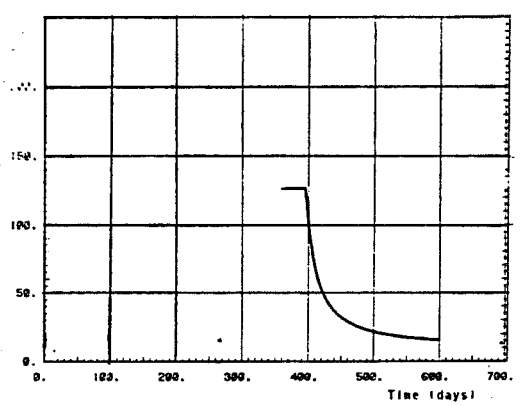

Temp (°C)

XBL 817-3279

USBM GAUGE FIELD RECORD

Full Scale Experiment H10 Gauge U16 (1st) Hole U16

	Label	Sensor No.	Logger Channel	V_{ss} Voltage	V_{oo} Rezero	C_o Slope	V_{oi}-V_{oo} Temp. Const.	T_s Start Temp.	
USBM Gauge	U16A	726	45	4.803	-1.345	0.0657	-0.146	11.24	
USBM Gauge	U16B	727	46	7.027	0.066	0.0691	0.034	11.24	
USBM Gauge	U16C	728	47	5.611	0.327	0.0659	-0.261	11.24	
Corresponding Thermocouple		432	130						

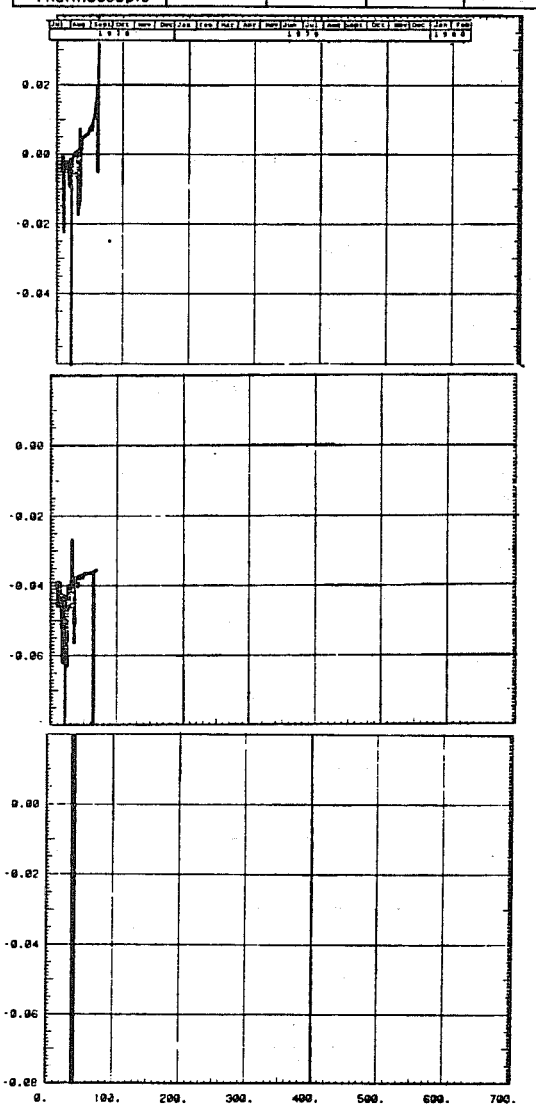

[X] vert. [ ] horiz.

r = 2.77

θ = 224.8

z = 0.85

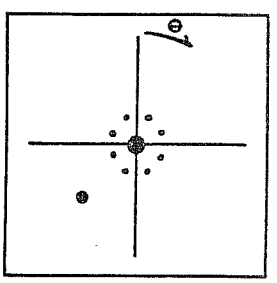

Entire Experiment [ ]

Partial Experiment Including (Calendar dates)

7/11/78 – 9/11/78

(Experiment days)

8 – 70

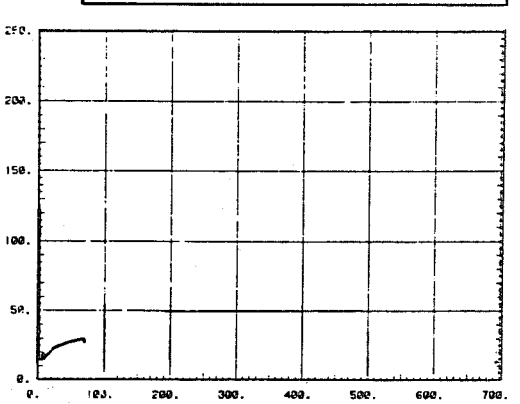

XBL 817-3279

USBM GAUGE FIELD RECORD

Full Scale Experiment H10 Gauge U16 (2nd) Hole U16

	Label	Sensor No.	Logger Channel	V_{ss} Voltage	V_{oo} Rezero	C_o Slope	V_{oi}-V_{oo} Temp. Const.	T_s Start Temp.	
USBM Gauge	U16A	726	45	9.434	0.113	0.0633	0.146	30.59	
USBM Gauge	U16B	727	46	9.404	-0.010	0.0633	-0.650	30.59	
USBM Gauge	U16C	728	47	7.588	-0.183	0.0634	-0.045	30.59	
Corresponding Thermocouple		432	130						

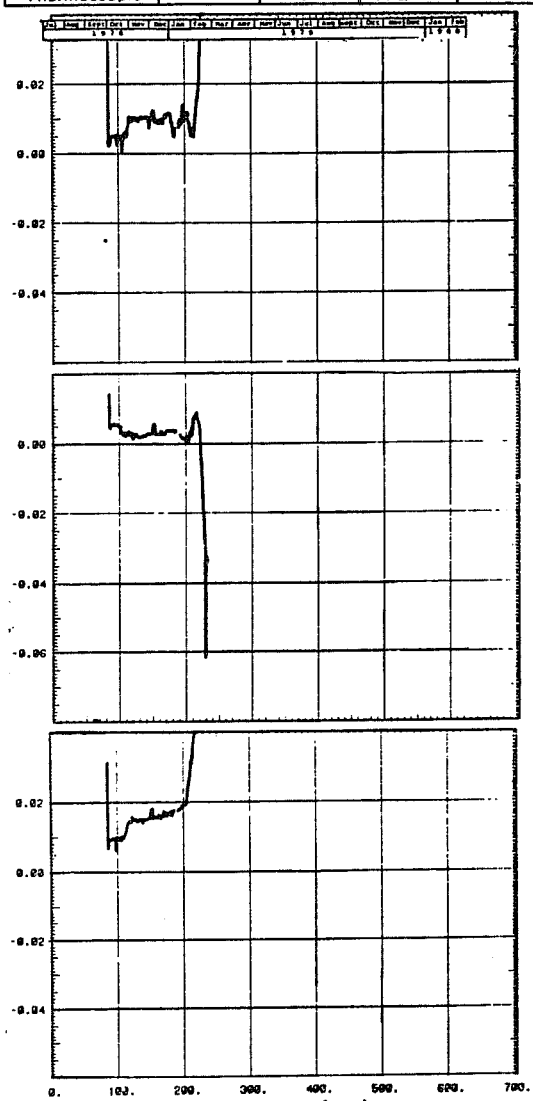

X vert. ☐ horiz.

r = 2.77

θ = 224.8

z = 0.85

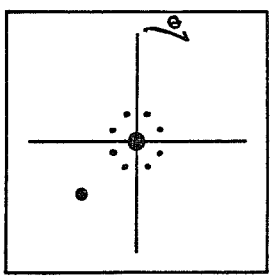

Entire Experiment ☐

Partial Experiment including (Calendar dates)

9/26/78 – 2/20/79

(Experiment days)

85 – 232

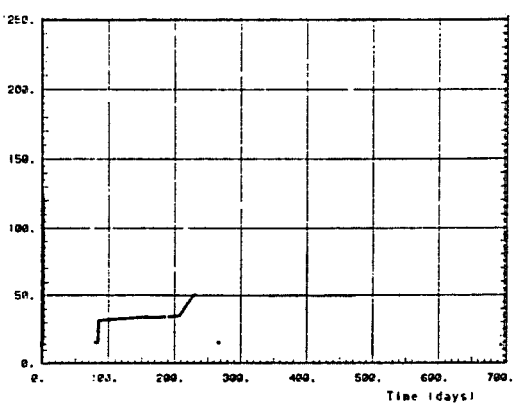

XBL 817-3279

USBM GAUGE FIELD RECORD

Full Scale Experiment H10 Gauge U16 (3rd) Hole U16

	Label	Sensor No.	Logger Channel	V_{ss} Voltage	V_{oo} Rezero	C_o Slope	$V_{oi}-V_{oo}$ Temp. Const.	T_s Start Temp.	
USBM Gauge	U16A	726	45	8.086	0.402	0.0672	0.088	64.25	
USBM Gauge	U16B	727	46	9.941	0.100	0.0653	-0.090	64.25	
USBM Gauge	U16C	728	47	10.293	0.114	0.0682	0.112	64.25	
Corresponding Thermocouple		432	130						

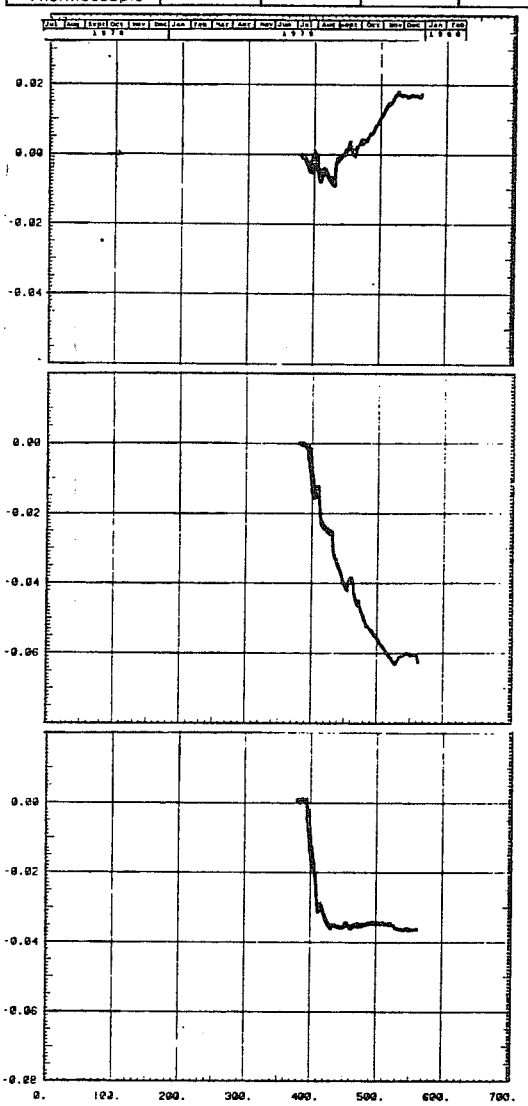

USBM displacement (mv)

[X] vert. [ ] horiz.

r = 2.77

θ = 224.8

z = 0.85

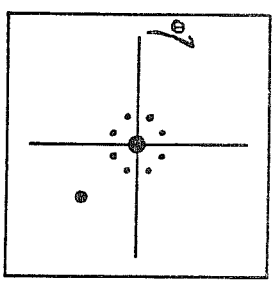

[ ] Entire Experiment

Partial Experiment Including (Calendar dates)

7/17/79 — 1/16/80

(Experiment days)

379 — 562

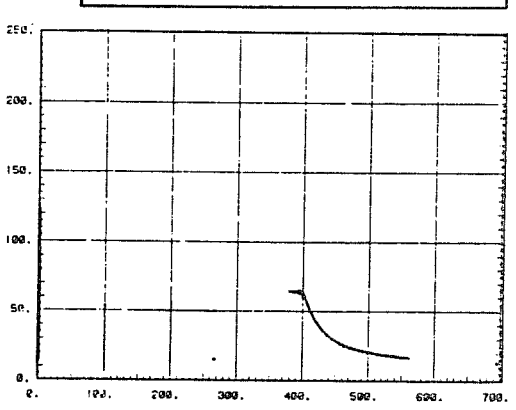

Temp (°C)

XBL 817-3279

USBM GAUGE FIELD RECORD

Full Scale Experiment H10 Gauge U17 (1st) Hole C4

	Label	Sensor No.	Logger Channel	V_{ss} Voltage	V_{oo} Rezero	C_o Slope	V_{oi}-V_{oo} Temp. Const.	T_s Start Temp.	
USBM Gauge	U17A	729	48	9.467	-0.221	0.0645	0.038	11.01	
USBM Gauge	U17B	730	49	6.653	0.117	0.0655	0.038	11.01	
USBM Gauge	U17C	731	50	7.770	-0.079	0.0635	-0.117	11.01	
Corresponding Thermocouple		433	131						

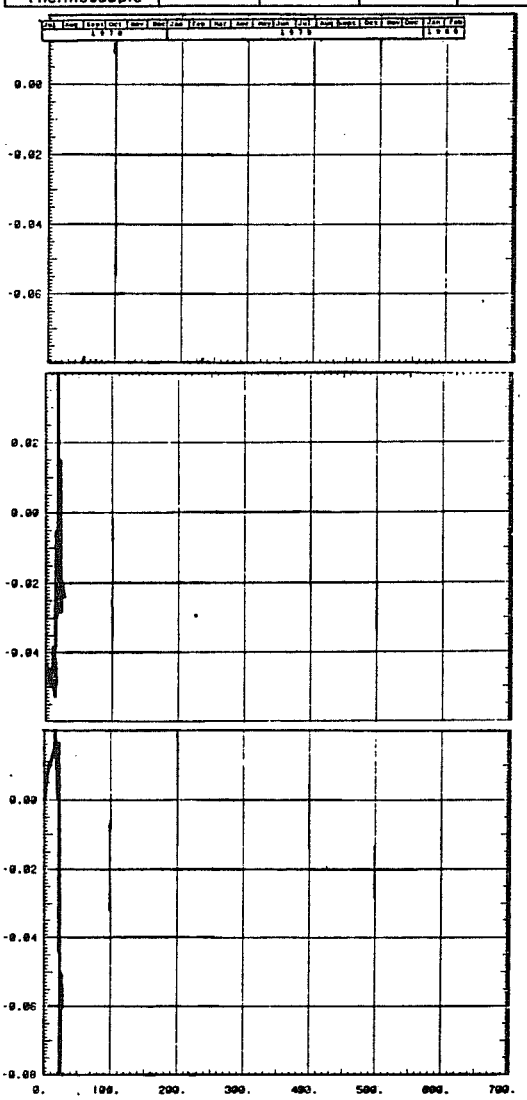

[X] vert. [ ] horiz.

r = 2.50

θ = 22.6

z = -0.57

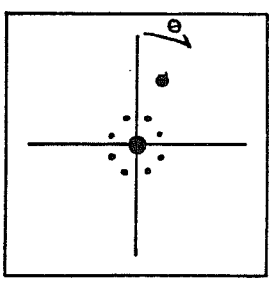

Entire Experiment [ ]

Partial Experiment Including (Calendar dates)

7/3/78 – 8/1/78

(Experiment days)

0 – 29

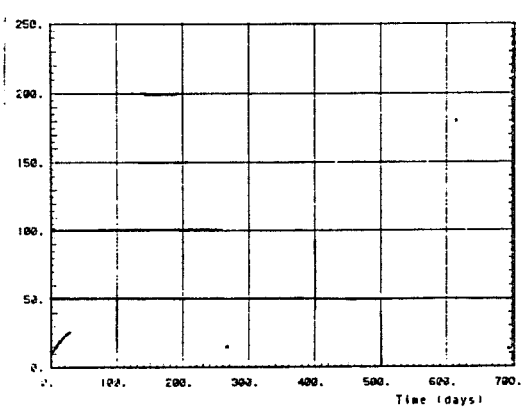

XBL 817-3279

USBM GAUGE FIELD RECORD

Full Scale Experiment H10 Gauge U17 (2nd) Hole C4

	Label	Sensor No.	Logger Channel	V_{ss} Voltage	V_{oo} Rezero	C_o Slope	$V_{oi}-V_{oo}$ Temp. Const.	T_s Start Temp.	
USBM Gauge	U15A	729	48	4.854	0.0	0.0666	0.0	39.53	
USBM Gauge	U17B	730	49	7.607	0.075	0.0649	0.050	39.53	
USBM Gauge	U17C	731	50	8.174	-0.820	0.0642	-0.105	39.53	
Corresponding Thermocouple		433	131						

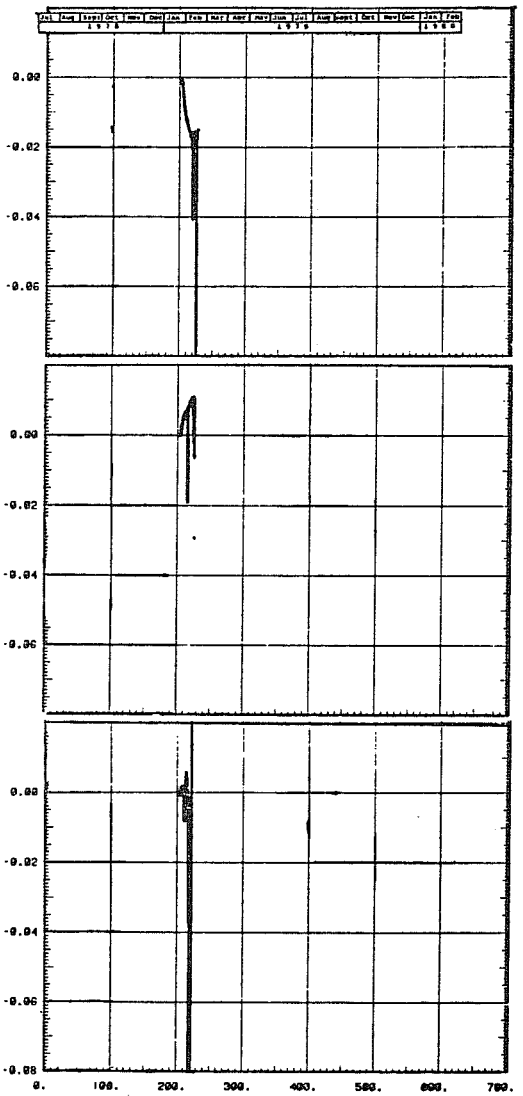

USBM displacement (mv)

[X] vert. [ ] horiz.

r = 2.50

θ = 22.6

z = -0.57

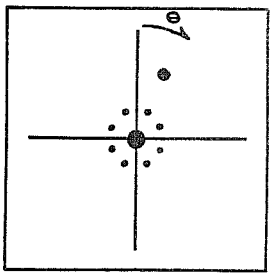

Entire Experiment [ ]

Partial Experiment Including (Calendar dates)

1/20/79 – 2/20/79

(Experiment days)

201 – 232

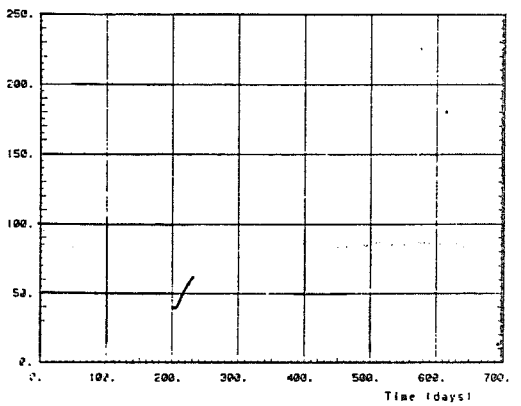

Temp (°C)

XBL 817-3279

USBM GAUGE FIELD RECORD

Full Scale Experiment H10 Gauge U17 (3rd) Hole C4

	Label	Sensor No.	Logger Channel	V_{ss} Voltage	V_{oo} Rezero	C_o Slope	V_{oi}-V_{oo} Temp. Const.	T_s Start Temp.	
USBM Gauge	U17A	729	48	8.623	0.171	0.0673	-0.087	77.95	
USBM Gauge	U17B	730	49	9.072	0.607	0.0644	0.076	77.95	
USBM Gauge	U17C	731	50	8.291	0.215	0.0677	0.144	77.95	
Corresponding Thermocouple		433	131						

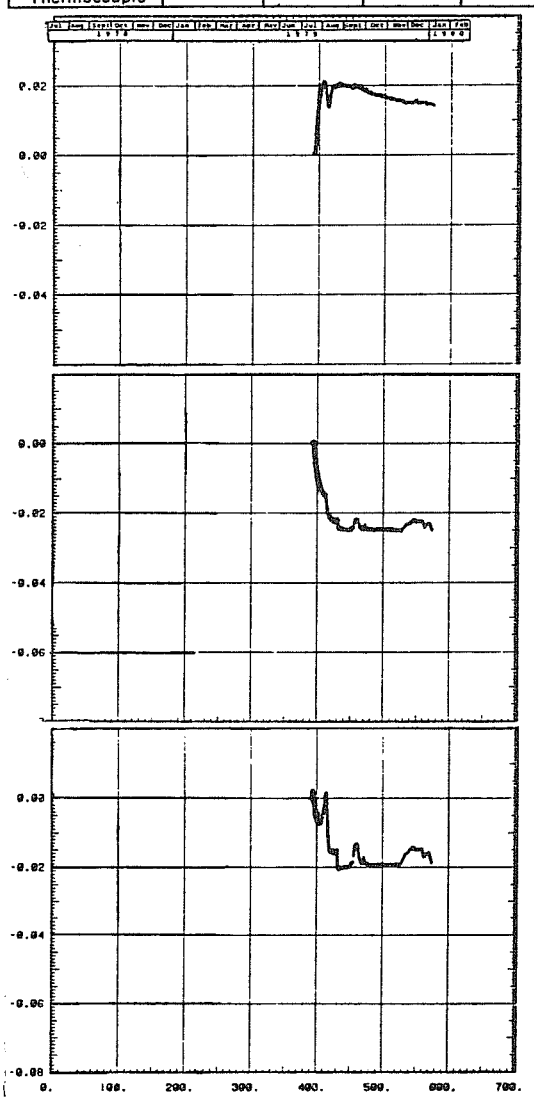

USBM displacement (mv)

[X] vert. [ ] horiz.

r = 2.50

θ = 22.6

z = -0.57

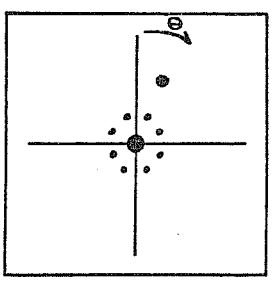

Entire Experiment [ ]

Partial Experiment Including (Calendar dates)

7/29/79 – 1/28/80

(Experiment days)

391 – 574

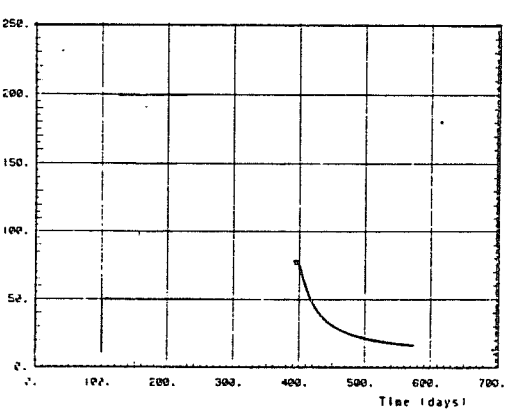

Temp (°C)

XBL 817-3279

USBM GAUGE FIELD RECORD

Full Scale Experiment H10 Gauge U18 (1st) Hole U18

	Label	Sensor No.	Logger Channel	V_{ss} Voltage	V_{oo} Rezero	C_o Slope	V_{oi}-V_{oo} Temp. Const.	T_s Start Temp.	
USBM Gauge	U18A	732	51	6.264	0.008	0.0640	-0.165	11.75	
USBM Gauge	U18B	733	52	6.360	0.049	0.0647	-0.151	11.75	
USBM Gauge	U18C	734	53	6.244	-0.485	0.0645	-0.120	11.75	
Corresponding Thermocouple		434	132						

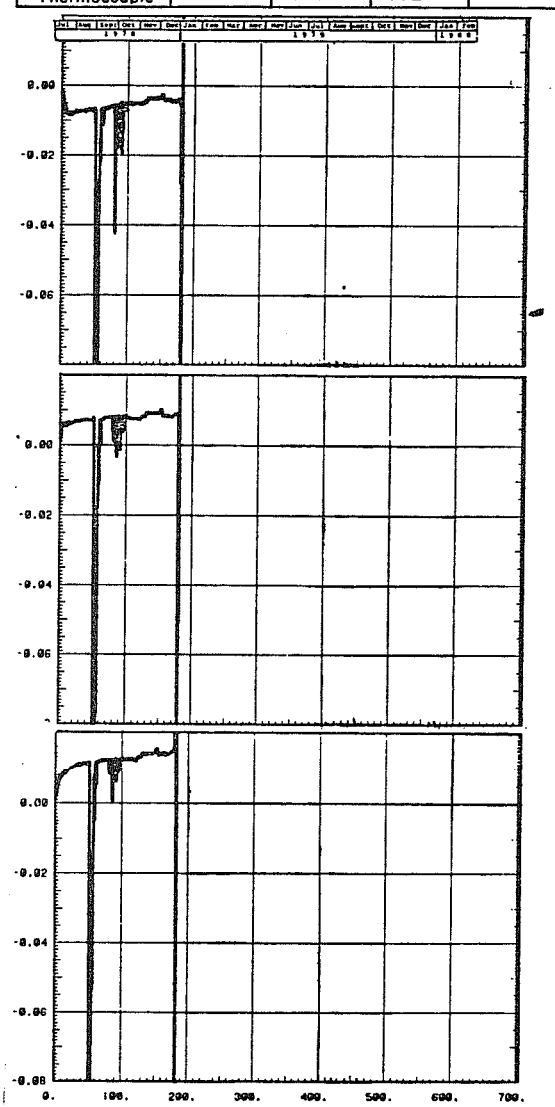

USBM displacement (mv)

[X] vert. [ ] horiz.

r = 1.99

θ = 337.9

z = 0.85

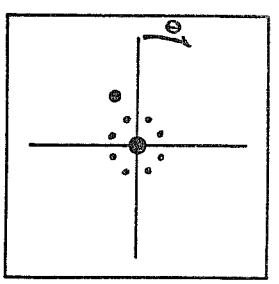

Entire Experiment [ ]

Partial Experiment Including (Calendar dates)

7/3/78 – 1/3/79

(Experiment days)

0 – 184

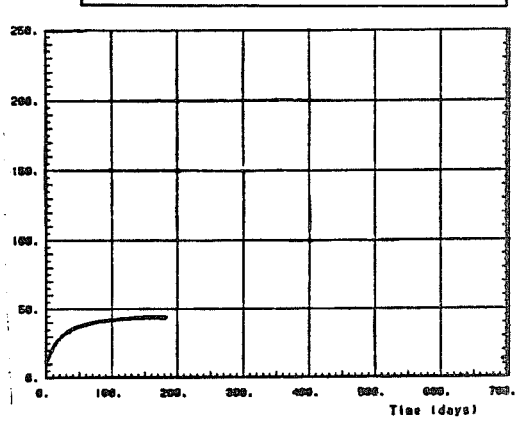

Temp (°C)

XBL 817-3279

USBM GAUGE FIELD RECORD

Full Scale Experiment H10 Gauge U18 (2nd) Hole U18

	Label	Sensor No.	Logger Channel	V_{ss} Voltage	V_{oo} Rezero	C_o Slope	$V_{oi}-V_{oo}$ Temp. Const.	T_s Start Temp.	
USBM Gauge	U18A	732	51	3.679	0.040	0.0693	-0.115	45.25	
USBM Gauge	U18B	733	52	7.656	0.110	0.0645	-0.135	45.25	
USBM Gauge	U18C	734	53	8.301	-0.200	0.0647	-0.125	45.25	
Corresponding Thermocouple		434	132						

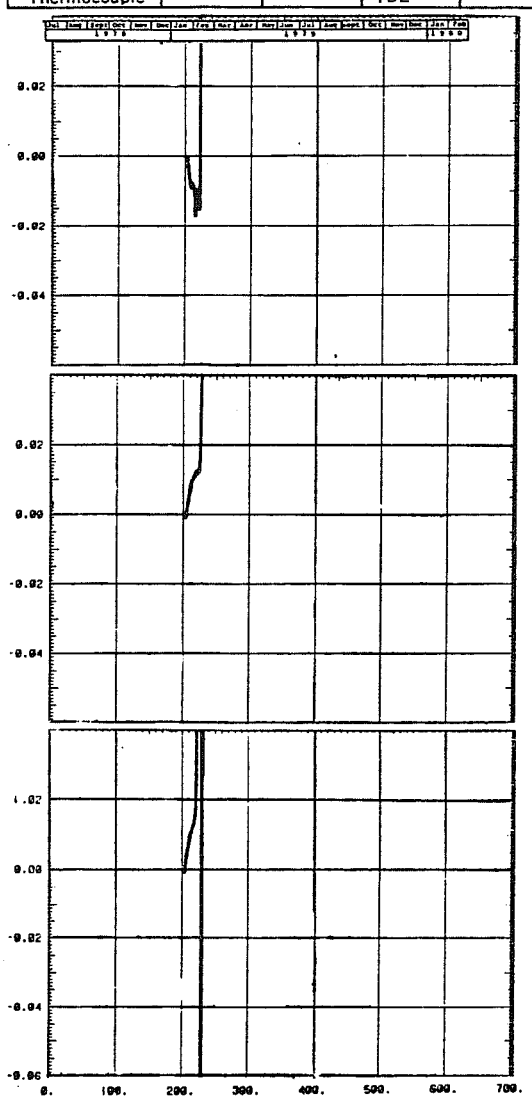

USBM displacement (mv)

X vert. ☐ horiz.

r = 1.99

θ = 337.9

z = 0.85

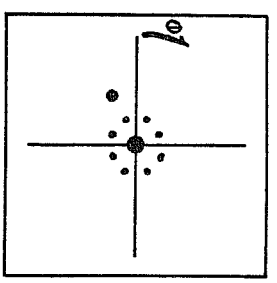

Entire Experiment ☐

Partial Experiment Including (Calendar dates)

1/20/79 – 2/20/79

(Experiment days)

201 – 232

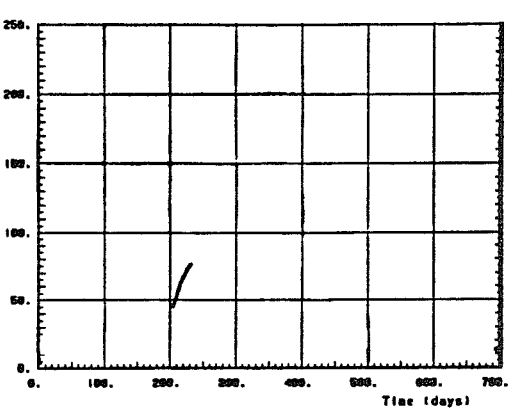

Temp (°C)

XBL 817-3279

USBM GAUGE FIELD RECORD

Full Scale Experiment H10 Gauge U18 (3rd) Hole U18

	Label	Sensor No.	Logger Channel	V_{ss} Voltage	V_{oo} Rezero	C_o Slope	$V_{oi}-V_{oo}$ Temp. Const.	T_s Start Temp.	
USBM Gauge	U18A	732	51	4.736	0.001	0.1757	-0.007	88.94	
USBM Gauge	U18B	733	52	4.531	0.120	0.1764	0.014	88.94	
USBM Gauge	U18C	734	53	4.800	0.389	0.1742	0.006	88.94	
Corresponding Thermocouple		434	132						

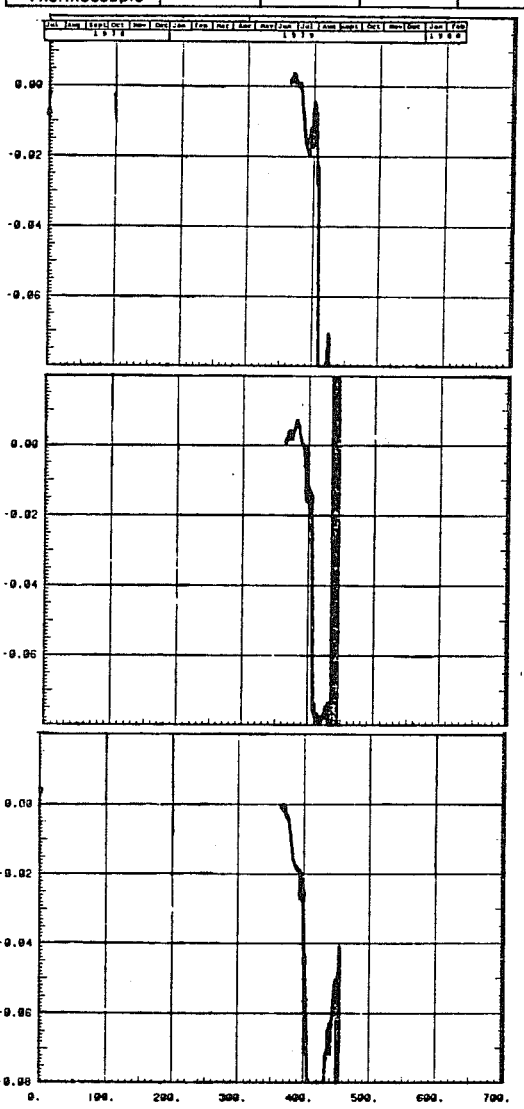

[X] vert. [ ] horiz.

r = 1.99

θ = 337.9

z = 0.85

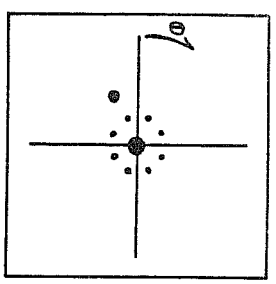

Entire Experiment [ ]

Partial Experiment Including (Calendar dates)

7/2/79 – 10/1/79

(Experiment days)

364 – 455

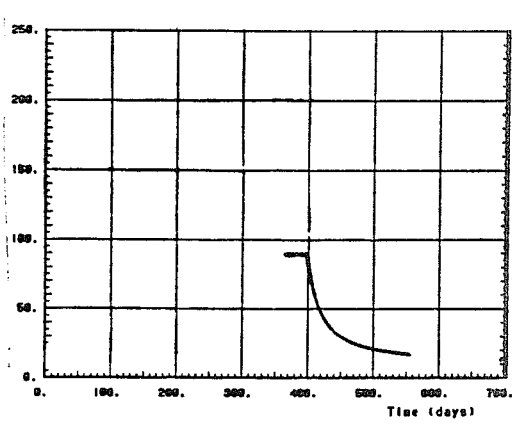

XBL 817-3279

USBM GAUGE FIELD RECORD

Full Scale Experiment H10 Gauge U19 (1st) Hole U19

	Label	Sensor No.	Logger Channel	V_{ss} Voltage	V_{oo} Rezero	C_o Slope	V_{oi}-V_{oo} Temp. Const.	T_s Start Temp.	
USBM Gauge	U19A	735	54	4.826	-0.100	0.0637	-0.049	11.75	
USBM Gauge	U19B	736	55	6.404	0.331	0.0656	-0.149	11.75	
USBM Gauge	U19C	737	56	5.089	-0.698	0.0655	-0.175	11.75	
Corresponding Thermocouple		435	133						

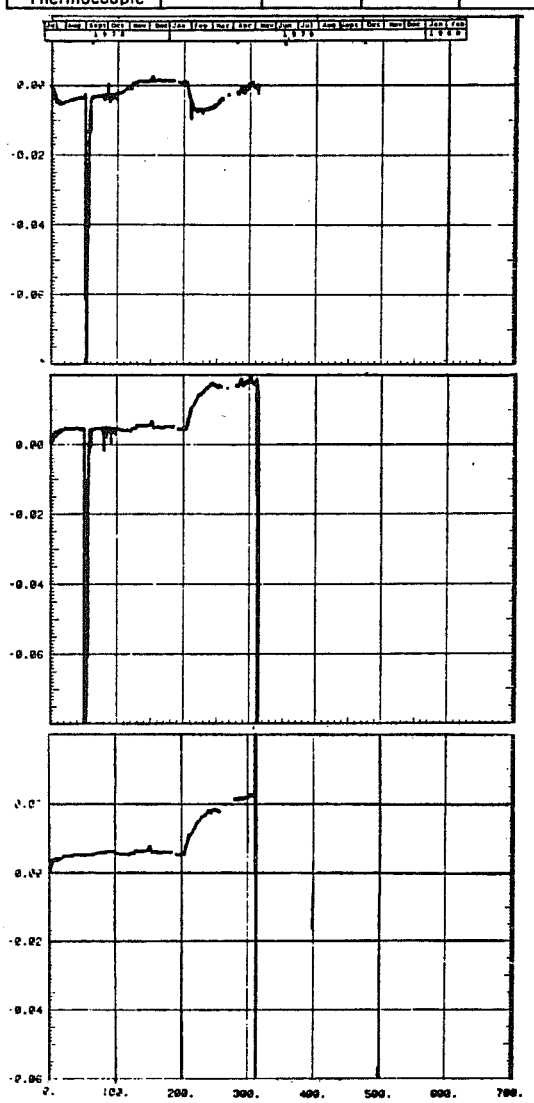

[X] vert. [ ] horiz.

r = 3.00

θ = 337.8

z = 0.85

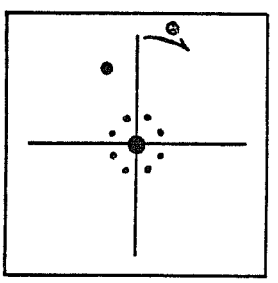

Entire Experiment [ ]

Partial Experiment Including (Calendar dates)

7/3/78 – 5/15/79

(Experiment days)

0 – 316

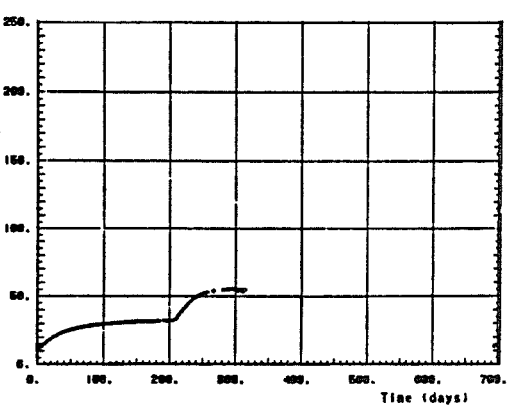

XBL 817-3279

USBM GAUGE FIELD RECORD

Full Scale Experiment H10 Gauge U19 (2nd) Hole U19

	Label	Sensor No.	Logger Channel	V_{ss} Voltage	V_{oo} Rezero	C_o Slope	V_{oi}-V_{oo} Temp. Const.	T_s Start Temp.	
USBM Gauge	U19A	735	54	7.920	-1.069	0.0681	0.008	56.16	
USBM Gauge	U19B	736	55	9.189	-0.446	0.0681	0.297	56.16	
USBM Gauge	U19C	737	56	9.150	-0.025	0.0652	0.008	56.16	
Corresponding Thermocouple		435	133						

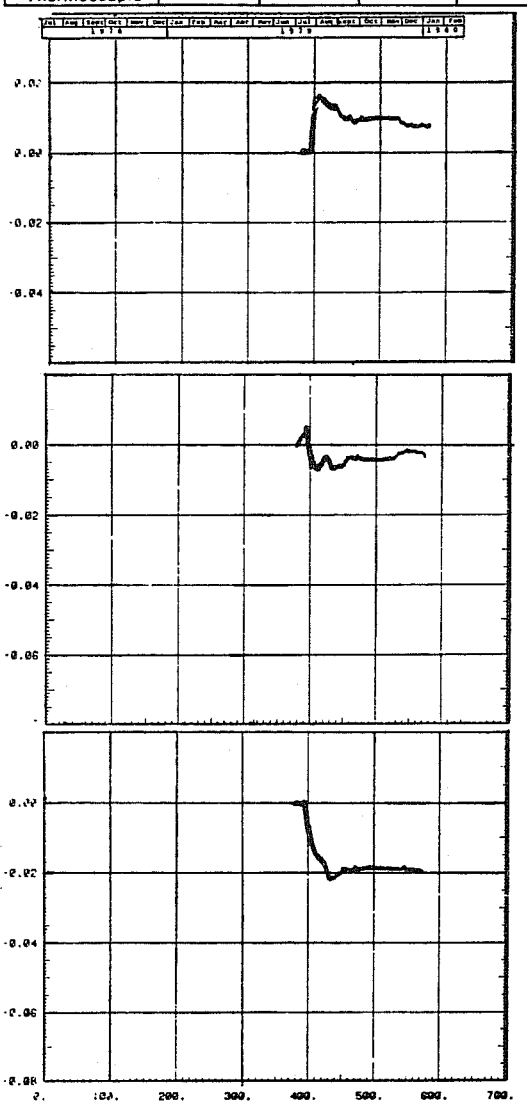

USBM displacement (mv)

☒ vert. ☐ horiz.

r = 3.00

θ = 337.8

z = 0.85

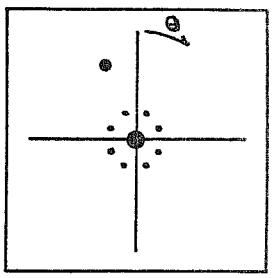

Entire Experiment ☐

Partial Experiment Including (Calendar dates)

7/17/79 – 1/28/80

(Experiment days)

379 – 574

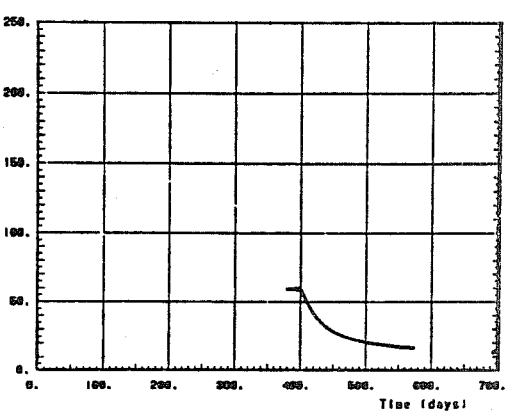

Temp (°C)

XBL 817-3279

USBM GAUGE FIELD RECORD

Full Scale Experiment H10 Gauge U20 (1st) Hole U20

	Label	Sensor No.	Logger Channel	V_{ss} Voltage	V_{oo} Rezero	C_o Slope	$V_{01}-V_{oo}$ Temp. Const.	T_s Start Temp.	
USBM Gauge	U20A	738	57	5.473	0.065	0.0655	0.008	11.01	
USBM Gauge	U20B	739	58	5.735	0.522	0.0643	0.0	11.01	
USBM Gauge	U20C	740	59	5.871	-0.052	0.0666	0.087	11.01	
Corresponding Thermocouple		436	134						

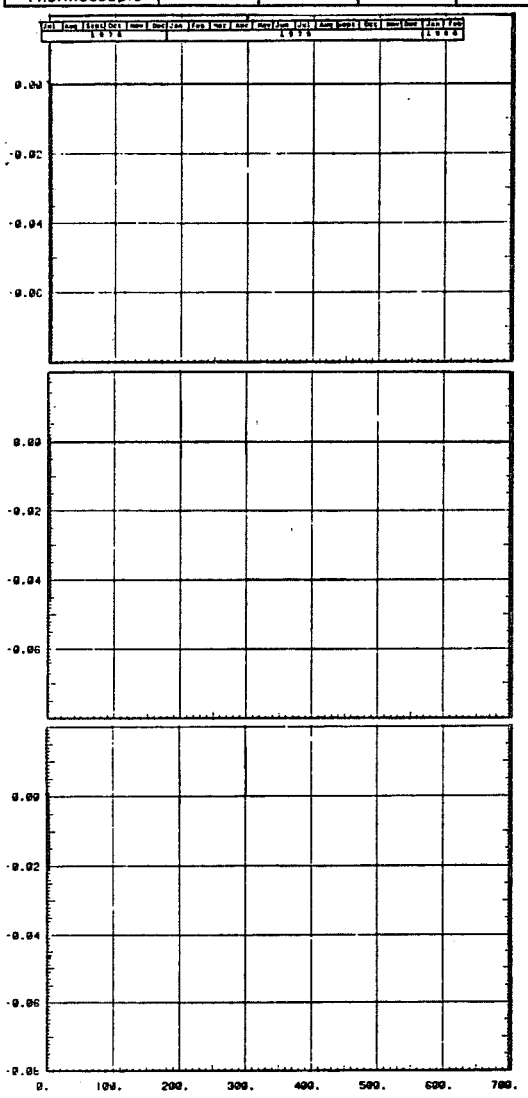

USBM displacement (mv)

[X] vert. [ ] horiz.

r = 4.01

θ = 338.2

z = -0.65

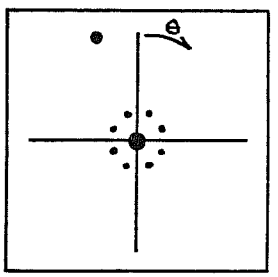

Entire Experiment [ ]

Partial Experiment Including (Calendar dates)

7/3/78 – 7/17/78

(Experiment days)

0 – 14

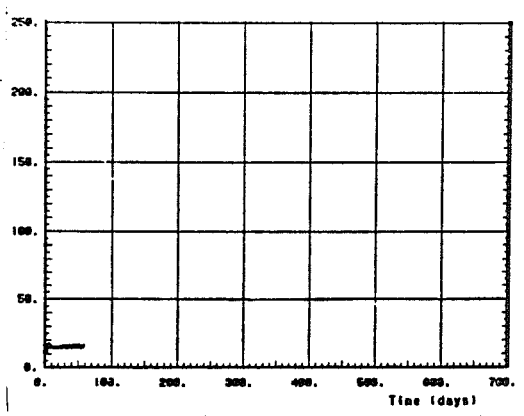

Temp (°C)

XBL 817-3279

USBM GAUGE FIELD RECORD

Full Scale Experiment H1C Gauge U20 (2nd) Hole U20

	Label	Sensor No.	Logger Channel	V_{ss} Voltage	V_{oo} Rezero	C_o Slope	$V_{oi}-V_{oo}$ Temp. Const.	T_s Start Temp.	
USBM Gauge	U20A	738	57	8.184	-0.050	0.0655	-0.300	25.68	
USBM Gauge	U20B	739	58	7.383	0.100	0.0698	0.175	25.68	
USBM Gauge	U20C	740	59	7.891	0.700	0.0666	-0.350	25.68	
Corresponding Thermocouple		436	134						

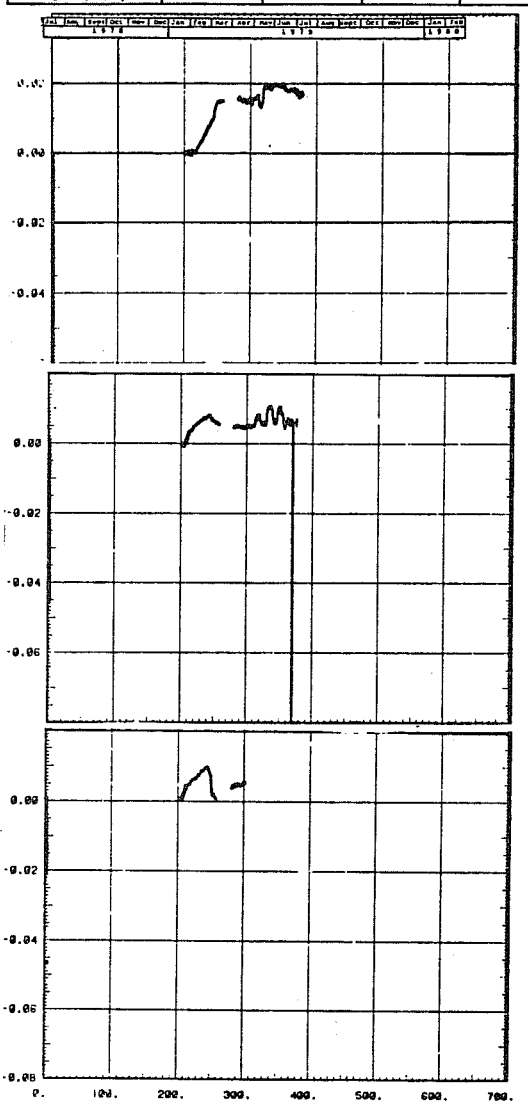

USBM displacement (mv)

X vert. ☐ horiz.

r = 4.01

θ = 338.2

z = -0.65

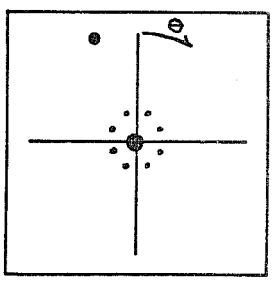

Entire Experiment ☐

Partial Experiment Including (Calendar dates)

1/20/79 – 7/17/79

(Experiment days)

201 – 379

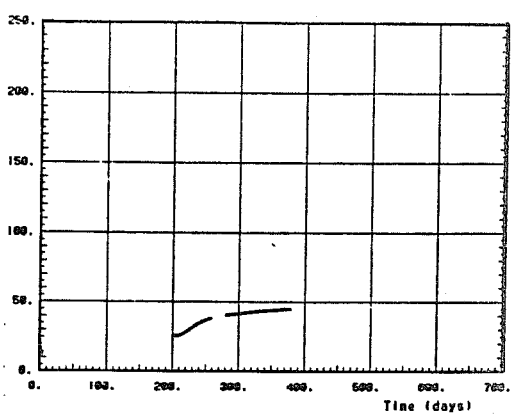

Temp (°C)

XBL 817-3279

USBM GAUGE FIELD RECORD

Full Scale Experiment H9 Gauge U21 Hole U21

	Label	Sensor No.	Logger Channel	V_{ss} Voltage	V_{oo} Rezero	C_o Slope	V_{oi}-V_{oo} Temp. Const.	T_s Start Temp.	
USBM Gauge	U21A	231	60	4.331	-0.003	0.0713	-0.054	10.74	
USBM Gauge	U21B	232	61	3.716	-0.258	0.0694	-0.074	10.74	
USBM Gauge	U21C	233	62	5.669	0.003	0.0667	-0.252	10.74	
Corresponding Thermocouple		12	135						

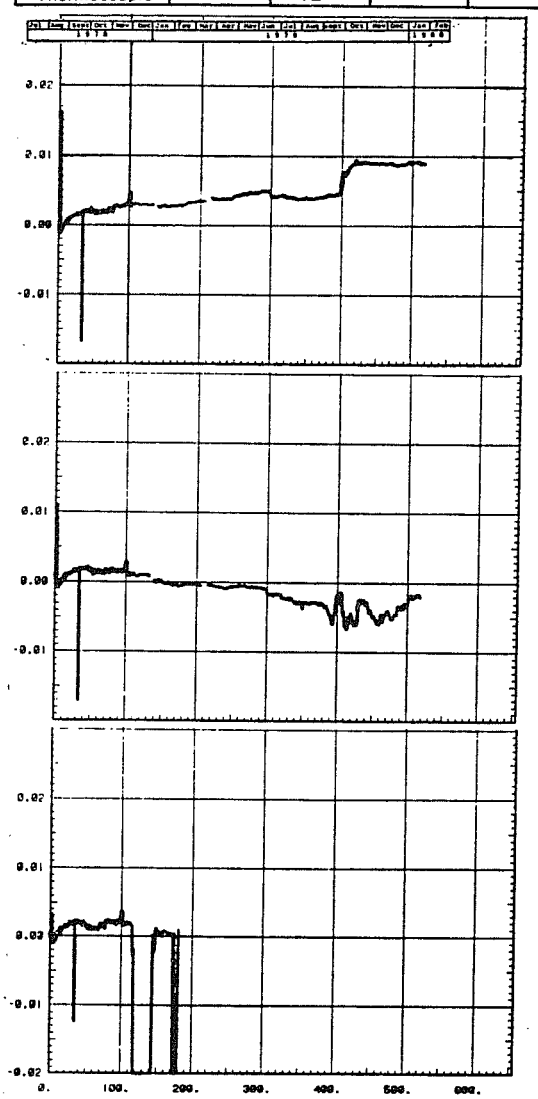

USBM displacement (mv)

☐ vert. ☒ horiz.

r = 2.49

θ = 67.9

z = 0.62

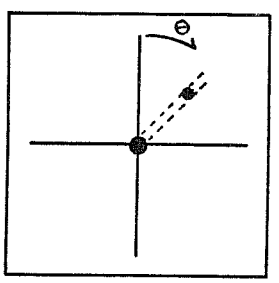

Entire Experiment ☒

Partial Experiment Including (Calendar dates)

_____ – _____

(Experiment days)

_____ – _____

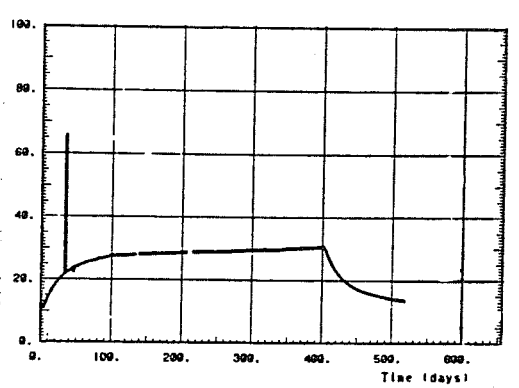

Temp (°C)

XBL 817-3279

USBM GAUGE FIELD RECORD

Full Scale Experiment H9 Gauge U22 Hole U22

	Label	Sensor No.	Logger Channel	V_{ss} Voltage	V_{oo} Rezero	C_o Slope	V_{oi}-V_{oo} Temp. Const.	T_s Start Temp.	
USBM Gauge	U22A	234	63	5.063	-0.166	0.0661	-0.085	10.74	
USBM Gauge	U22B	235	64	4.971	-0.418	0.0673	0.042	10.74	
USBM Gauge	U22C	236	65	4.248	-1.530	0.0666	-0.066	10.74	
Corresponding Thermocouple		13	136						

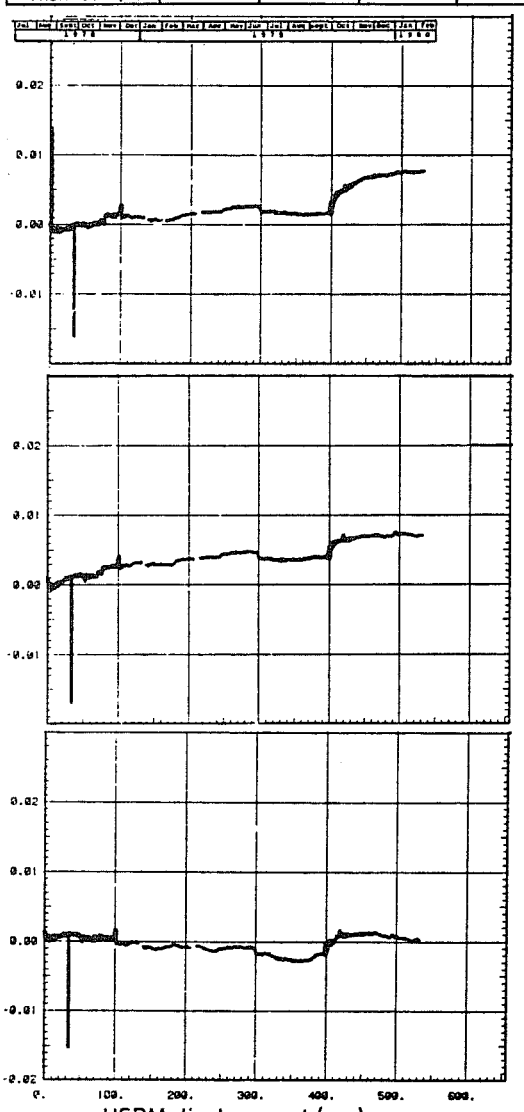

USBM displacement (mv)

☐ vert. ☒ horiz.

r = 3.49

θ = 112.7

z = 0.68

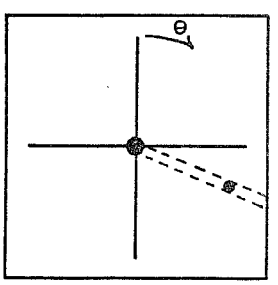

Entire Experiment ☒

Partial Experiment Including (Calendar dates)

_____ – _____

(Experiment days)

_____ – _____

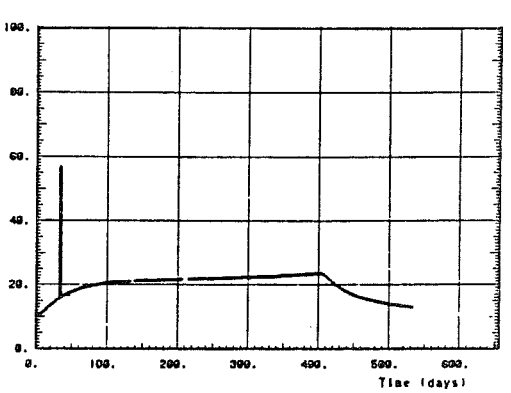

Temp (°C)

XBL 817-3279

USBM GAUGE FIELD RECORD

Full Scale Experiment H10 Gauge U23 Hole U23

	Label	Sensor No.	Logger Channel	V_{ss} Voltage	V_{oo} Rezero	C_o Slope	V_{oi}-V_{oo} Temp. Const.	T_s Start Temp.	
USBM Gauge	U23A	741	66	6.121	-0.015	0.0680	-0.195	11.24	
USBM Gauge	U23B	742	67	8.389	1.560	0.0667	0.114	11.24	
USBM Gauge	U23C	743	68	7.374	0.007	0.0678	0.020	11.24	
Corresponding Thermocouple		437	137						

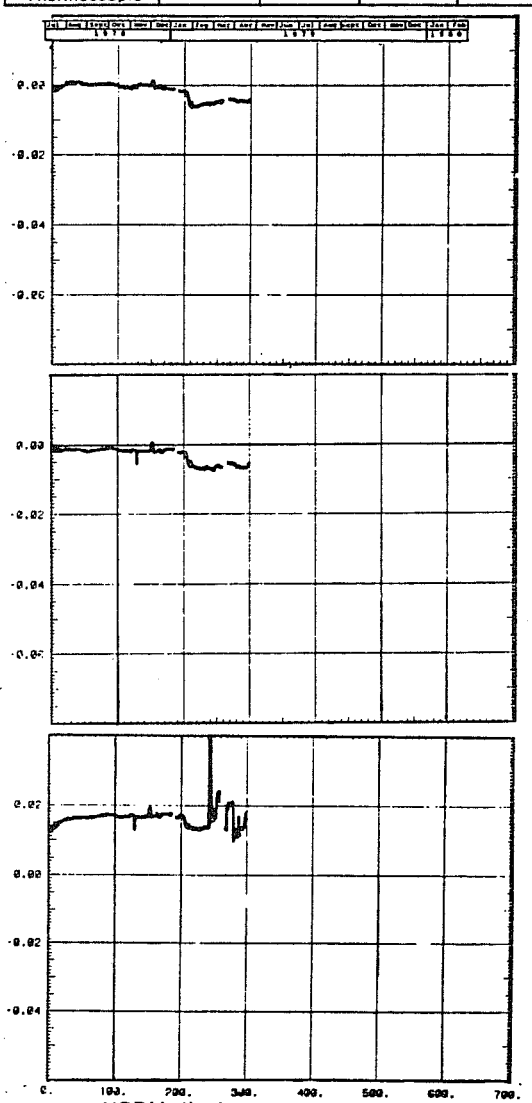

USBM displacement (mv)

☐ vert. ☒ horiz.

r = 2.50

θ = 46.6

z = 0.66

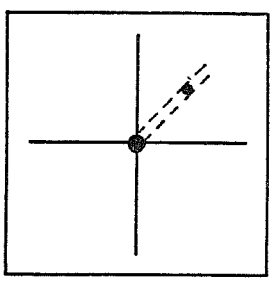

Entire Experiment ☐

Partial Experiment Including (Calendar dates)

7/3/78 – 4/27/79

(Experiment days)

0 – 298

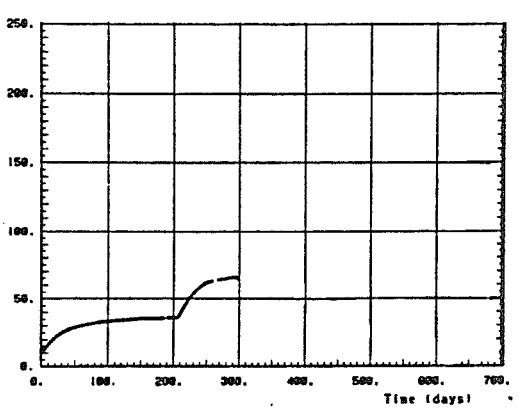

Temp (°C)

XBL 817-3279

USBM GAUGE FIELD RECORD

Full Scale Experiment H10 Gauge U24 Hole U24

	Label	Sensor No.	Logger Channel	V_{ss} Voltage	V_{oo} Rezero	C_o Slope	V_{01}-V_{oo} Temp. Const.	T_s Start Temp.	
USBM Gauge	U24A	744	69	6.806	1.714	0.0631	-0.065	11.19	
USBM Gauge	U24B	745	70	3.287	-0.283	0.0638	-0.186	11.19	
USBM Gauge	U24C	746	71	5.049	-0.298	0.0655	0.101	11.19	
Corresponding Thermocouple		438	138						

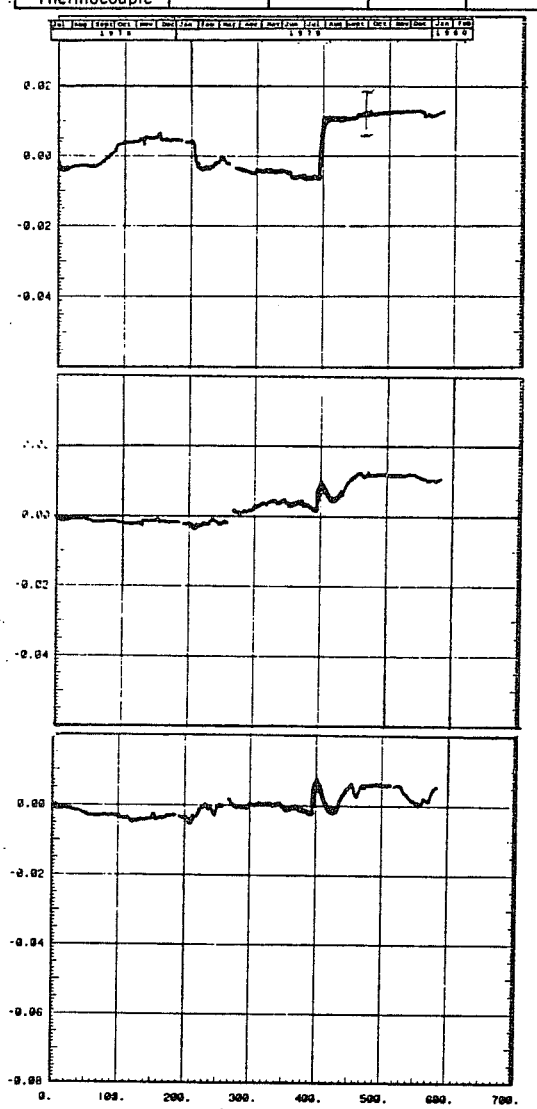

☐ vert. ☒ horiz.

r = 2.00

θ = 90.4

z = 0.66

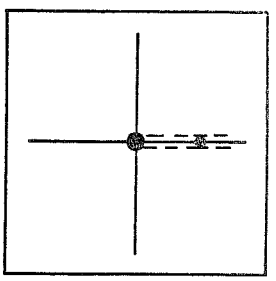

Entire Experiment ☒

Partial Experiment Including (Calendar dates)

_____ – _____

(Experiment days)

_____ – _____

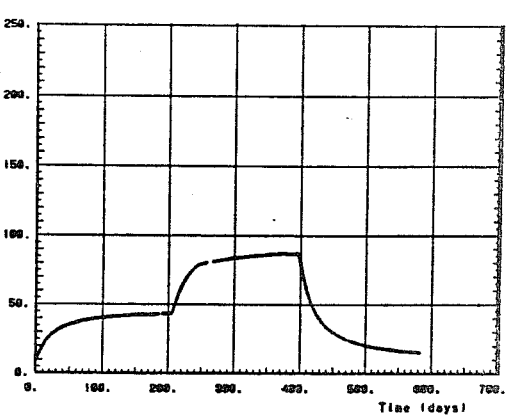

XBL 817-3279

USBM GAUGE FIELD RECORD

Full Scale Experiment H10 Gauge U25 Hole U25

	Label	Sensor No.	Logger Channel	V_{ss} Voltage	V_{oo} Rezero	C_o Slope	V_{01}-V_{oo} Temp. Const.	T_s Start Temp.	
USBM Gauge	U25A	747	72	6.118	-0.344	0.0641	-0.100	11.19	
USBM Gauge	U25B	748	73	7.169	0.153	0.0642	-0.019	11.19	
USBM Gauge	U25C	749	74	5.427	-0.898	0.0648	-0.032	11.19	
Corresponding Thermocouple		439	139						

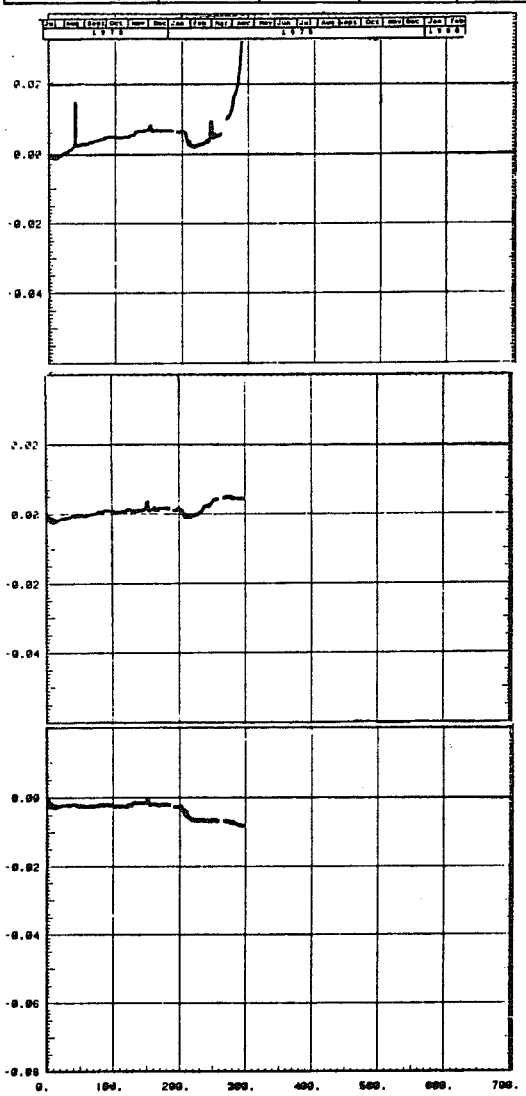

☐ vert. ☒ horiz.

r = 2.99

θ = 134.5

z = 0.62

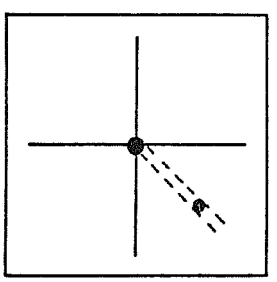

Entire Experiment ☐

Partial Experiment Including (Calendar dates)

7/3/78 – 4/26/79

(Experiment days)

0 – 297

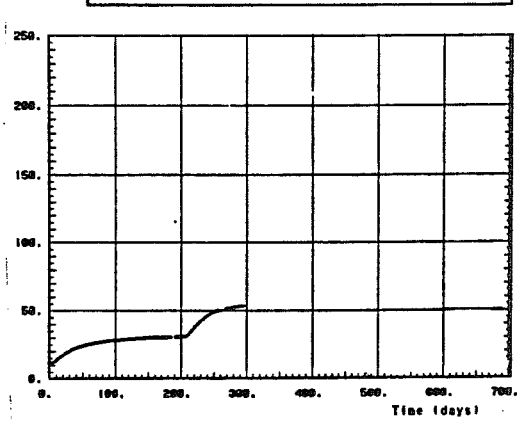

XBL 817-3279

USBM GAUGE FIELD RECORD

Full Scale Experiment H9 Gauge U26 Hole U26

	Label	Sensor No.	Logger Channel	V_{ss} Voltage	V_{oo} Rezero	C_o Slope	V_{oi}-V_{oo} Temp. Const.	T_s Start Temp.	
USBM Gauge	U26A	237	75	5.537	0.290	0.0641	0.055	10.19	
USBM Gauge	U26B	238	76	8.242	0.763	0.0655	-0.006	10.19	
USBM Gauge	U26C	239	77	6.079	0.242	0.0643	0.020	10.19	
Corresponding Thermocouple		14	140						

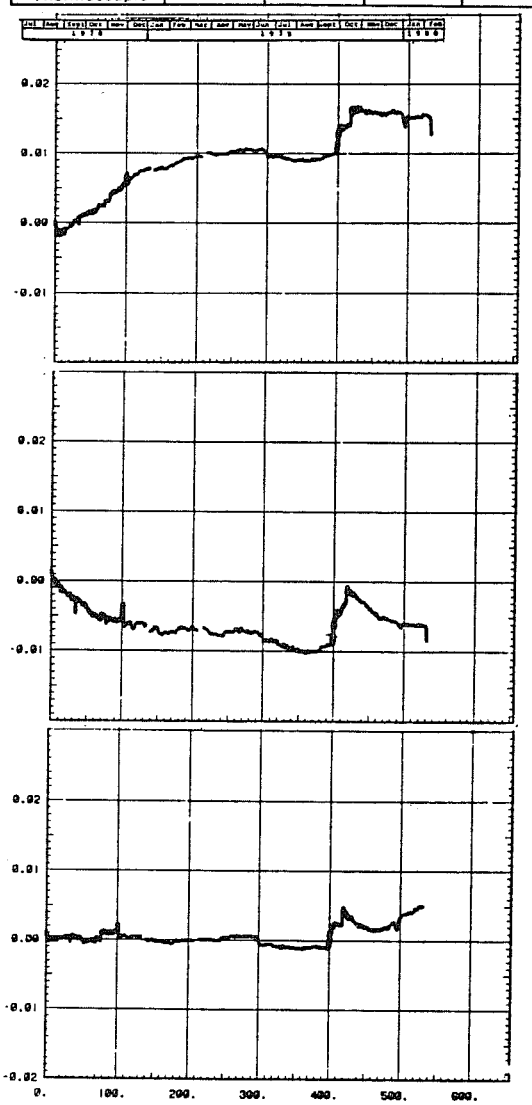

USBM displacement (mv)

☐ vert. ☒ horiz.

r = 2.48

θ = 46.2

z = -0.82

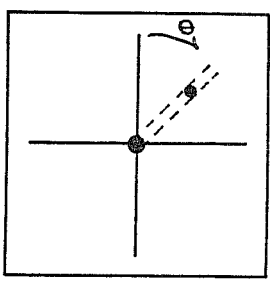

Entire Experiment ☒

Partial Experiment Including (Calendar dates)

_____ – _____

(Experiment days)

_____ – _____

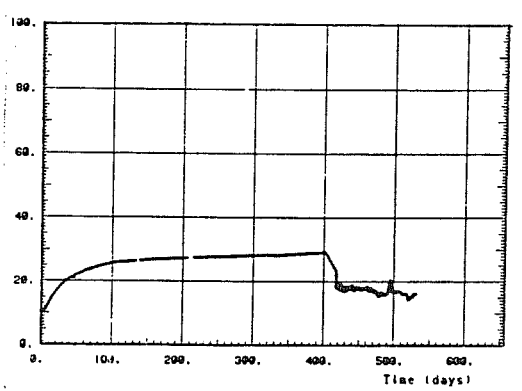

Temp (°C)

XBL 817-3279

USBM GAUGE FIELD RECORD

Full Scale Experiment H9 Gauge U27 Hole U27

	Label	Sensor No.	Logger Channel	V_{ss} Voltage	V_{oo} Rezero	C_o Slope	V_{o1}-V_{oo} Temp. Const.	T_s Start Temp.	
USBM Gauge	U27A	240	78	4.643	0.518	0.0626	-0.139	10.31	
USBM Gauge	U27B	241	79	5.337	0.454	0.0631	0.026	10.31	
USBM Gauge	U27C	242	80	6.592	-0.141	0.0650	0.130	10.31	
Corresponding Thermocouple		15	141						

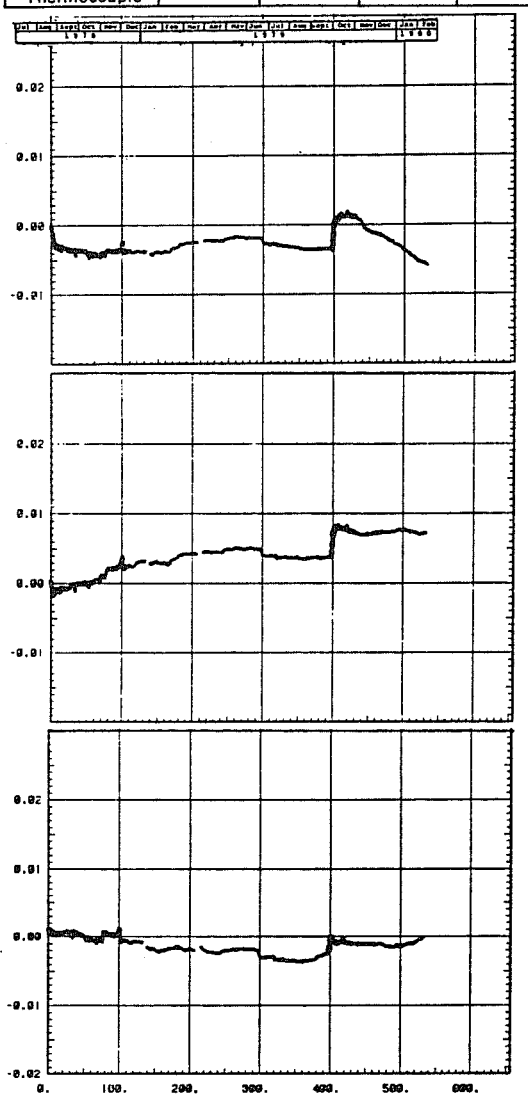

USBM displacement (mv)

☐ vert. ☒ horiz.

r = 2.00

θ = 90.9

z = -0.83

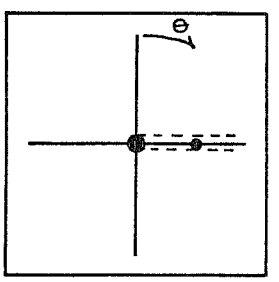

Entire Experiment ☒

Partial Experiment Including (Calendar dates)

_____ – _____

(Experiment days)

_____ – _____

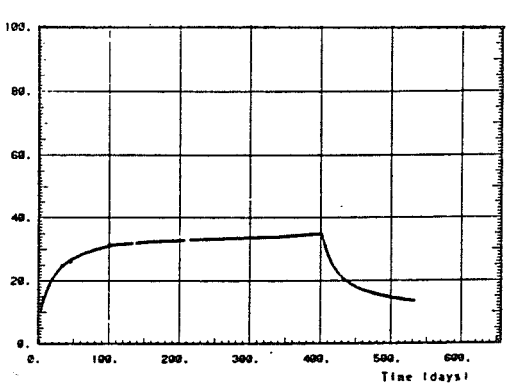

Temp (°C)

XBL 817-3279

USBM GAUGE FIELD RECORD

Full Scale Experiment H9 Gauge U28 Hole U28

	Label	Sensor No.	Logger Channel	V_{ss} Voltage	V_{oo} Rezero	C_o Slope	V_{oi}-V_{oo} Temp. Const.	T_s Start Temp.	
USBM Gauge	U28A	243	81	4.648	0.079	0.0625	-0.158	10.36	
USBM Gauge	U28B	244	82	6.772	-1.580	0.0663	-0.113	10.36	
USBM Gauge	U28C	245	83	5.898	-0.589	0.0666	0.0	10.36	
Corresponding Thermocouple		16	142						

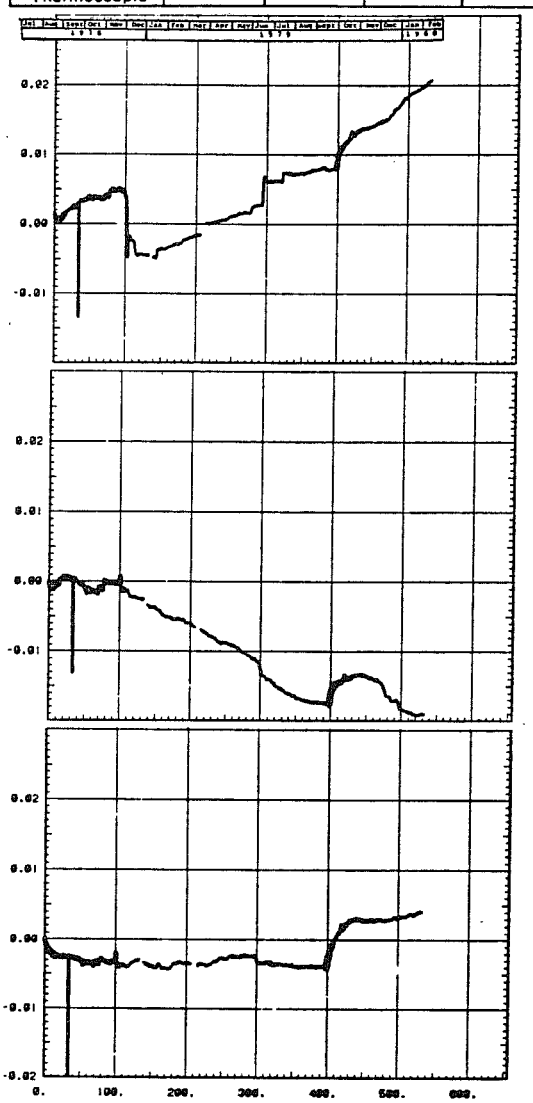

vert. [ ] horiz. [X]

r = 2.99

θ = 135.3

z = -0.84

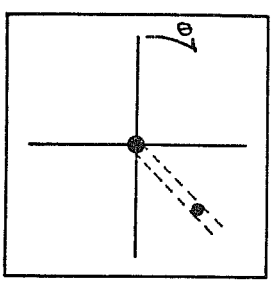

Entire Experiment [X]

Partial Experiment Including (Calendar dates)

_____ – _____

(Experiment days)

_____ – _____

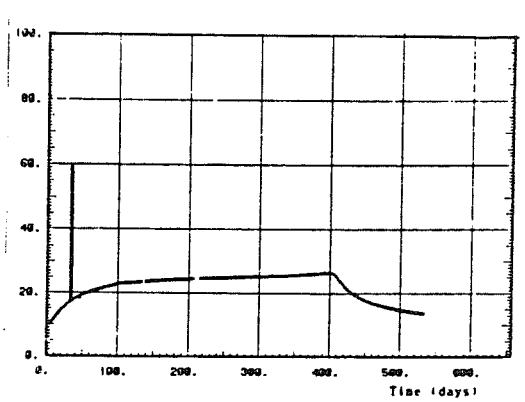

XBL 817-3279

USBM GAUGE FIELD RECORD

Full Scale Experiment H10 Gauge U29 Hole U29

	Label	Sensor No.	Logger Channel	V_{ss} Voltage	V_{oo} Rezero	C_o Slope	$V_{oi}-V_{oo}$ Temp. Const.	T_s Start Temp.	
USBM Gauge	U29A	750	84	4.991	0.369	0.0674	-0.024	10.38	
USBM Gauge	U29B	751	85	3.459	-0.237	0.0687	-0.374	10.38	
USBM Gauge	U29C	752	86	4.812	0.061	0.0660	0.205	10.38	
Corresponding Thermocouple		440	143						

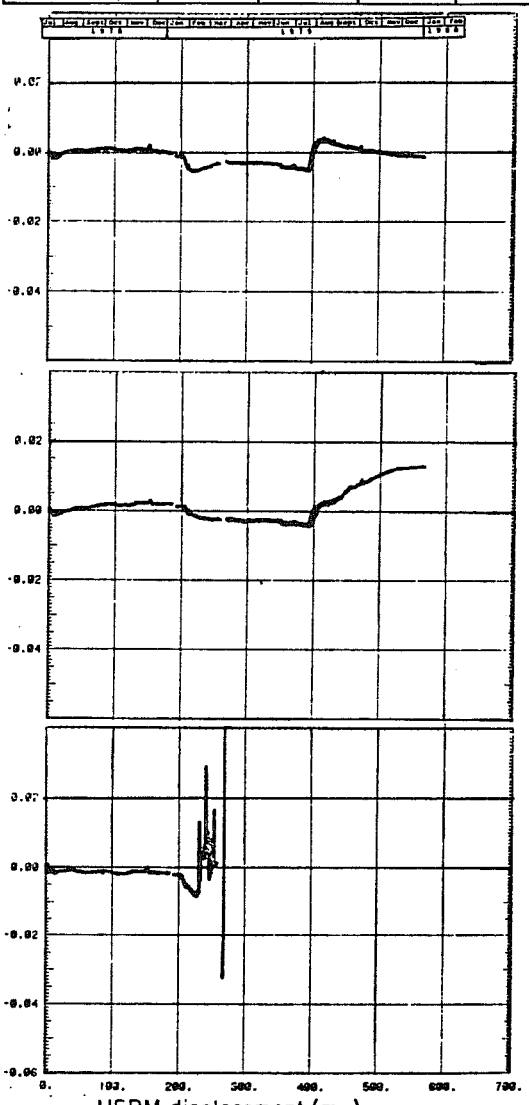

USBM displacement (mv)

vert. ☐ horiz. ☒

r = 3.50

θ = 67.7

z = -0.85

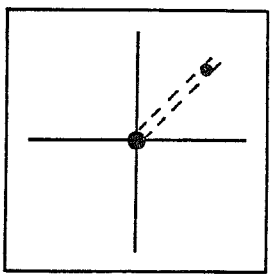

Entire Experiment ☒

Partial Experiment Including (Calendar dates)

_____ – _____

(Experiment days)

_____ – _____

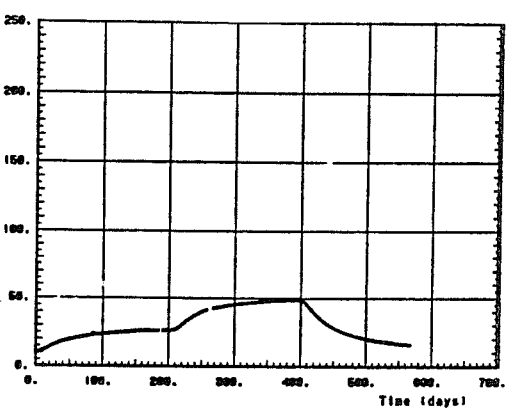

Temp (°C)

XBL 817-3279

USBM GAUGE FIELD RECORD

Full Scale Experiment H10 Gauge U30 Hole U30

	Label	Sensor No.	Logger Channel	V_{ss} Voltage	V_{oo} Rezero	C_o Slope	$V_{oi}-V_{oo}$ Temp. Const.	T_s Start Temp.	
USBM Gauge	U30A	753	87	7.156	-0.308	0.0668	0.128	10.64	
USBM Gauge	U30B	754	88	5.209	-0.085	0.0661	-0.069	10.64	
USBM Gauge	U30C	755	89	8.918	-0.347	0.0687	0.219	10.64	
Corresponding Thermocouple		441	144						

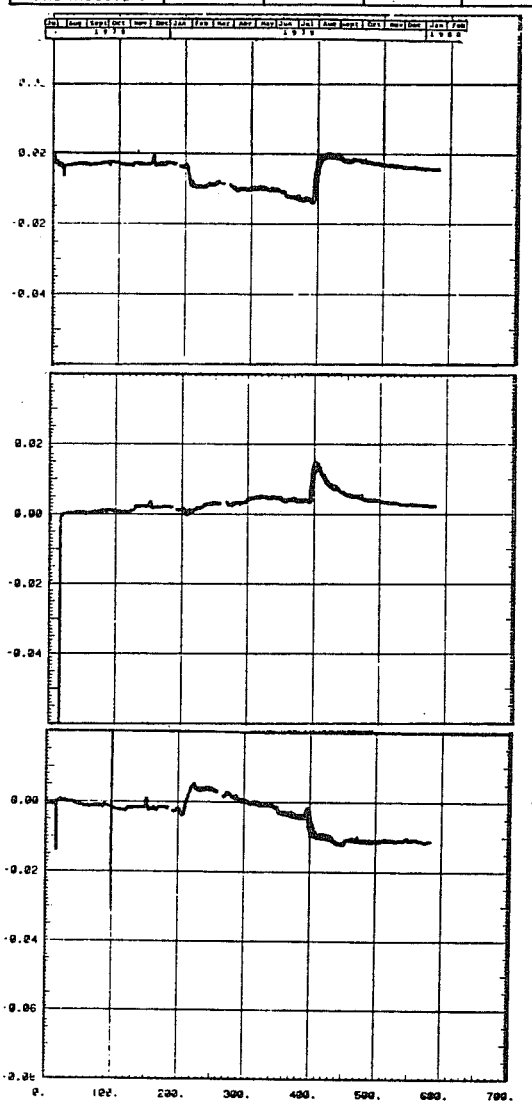

USBM displacement (mv)

☐ vert. ☒ horiz.

r = 2.26

θ = 112.4

z = -0.83

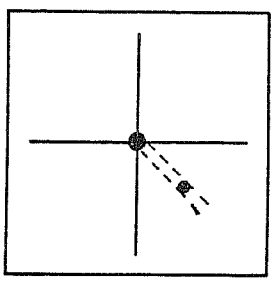

Entire Experiment ☒

Partial Experiment Including (Calendar dates)

_____ – _____

(Experiment days)

_____ – _____

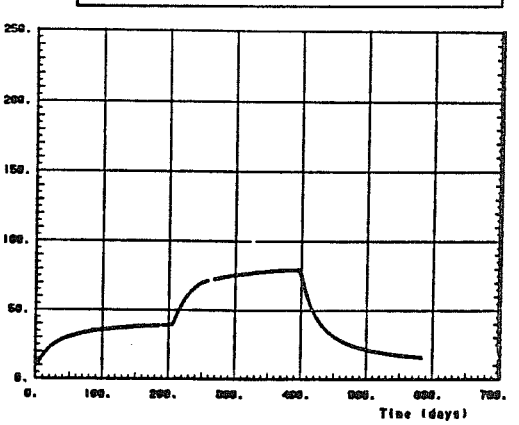

Temp (°C)

XBL 817-3279

APPENDIX C. Interchanges of Gauges in Boreholes

In most cases, gauge labels remained the same before and after reinstallation of a repaired gauge or a replacement gauge. However, in four boreholes (U3, C3, C10, and U23), gauges were interchanged. Figure C-1 illustrates the details of the changes made, and also gives the data logger channel numbers (B & F data logger for USBM gauges, IRAD for the VWS gauges), the Modcomp-based sensor number (SPF), and, where appropriate, computer input channel numbers (COMP).

A borehole-by-borehole summary of the stress gauge changes is given below:

Borehole U3. USBM gauge U3 was removed on 12/20/78 for repair. On 9/22/79, two VWSs, designated C9 (spares since borehole C9 had not been drilled), were installed in borehole U3. Note that sensor parameter file numbers differ for the two gauge types used in borehole U3.

Borehole C3. USBM gauge U15 was installed in borehole C3 and failed on 1/15/79. It could not be removed for repair, because it became wedged in the borehole. It was subsequently pushed deeper into the hole and its cable removed to allow installation of the repaired U3 gauge. This replacement gauge was installed about 1/22/79; however, sensor parameter files were not properly activated to collect valid data until 6/27/79. The replacement gauge (U3) was physically cabled to its original data logger and computer input channels, but its sensor parameter file numbers were ultimately changed to those previously used by gauge U15 in borehole C3. The results were that B & F data logger printouts for channels 6, 7, and 8 are for the U3 gauge in borehole U3 until 12/20/78,

and for the U3 gauge in borehole C3 after 1/22/79. Computer data and plots for sensor parameter file numbers 723-725 are associated only with borehole C3.

Borehole C10. VWS pair C10 was removed from borehole C10 on 3/13/79 for recalibration at Terra Tek.

Borehole U23. USBM gauge U23 was removed from borehole U23 on 4/27/79 due to failure. A new pair of VWSs using the C10 designation were installed in borehole U23 on 7/20/79. Note that the sensor parameter file numbers differ for the two instrument types used in borehole U23.

Five other sets of gauges, not shown in Fig. C-1, were installed in boreholes other than those originally assigned and remained there throughout the experiment. Table C-1 lists these additional gauge labels that differ from borehole designations.

Table C-1. Gauge labels not matching borehole labels.

Borehole	Gauge Designations
C2	U6
C4	U17
U6	C2
U15	C3
U17	C4

Some thermocouples associated with USBM gauges and VWSs were replaced with new thermocouples when gauges were repaired or changed. However, thermocouple data logger channels and sensor parameter file numbers always remained with the original borehole and location, i.e., thermocouples were not moved from one borehole to another when gauges were moved.

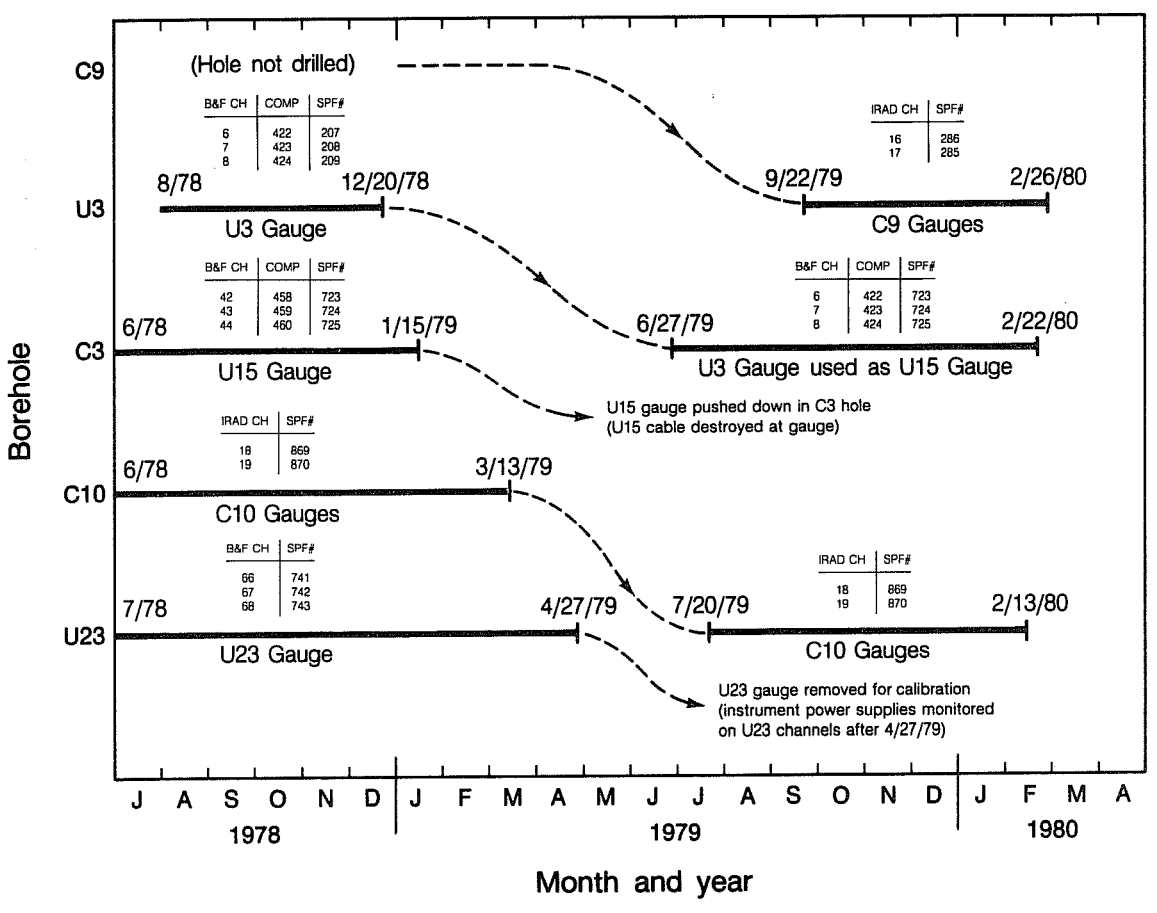

Fig. C1. USBM and IRAD gauge hole changes during heater experiments.

This report is part of a cooperative Swedish-American project supported by the U.S. Department of Energy and/or the Swedish Nuclear Fuel Supply Company. Any conclusions or opinions expressed in this report represent solely those of the author(s) and not necessarily those of The Regents of the University of California, the Lawrence Berkeley Laboratory, the Department of Energy, or the Swedish Nuclear Fuel Supply Company.

Reference to a company or product name does not imply approval or recommendation of the product by the University of California or the U.S. Department of Energy to the exclusion of others that may be suitable.

TECHNICAL INFORMATION DEPARTMENT
LAWRENCE BERKELEY LABORATORY
UNIVERSITY OF CALIFORNIA
BERKELEY, CALIFORNIA 94720